UNIVERSITÀ
DEGLI STUDI
FIRENZE

UNIVERSITÀ DEGLI STUDI DI FIRENZE

Scuola di Ingegneria

DOTTORATO DI RICERCA IN

INGEGNERIA INDUSTRIALE E DELL'AFFIDABILITÀ

CICLO XXX

COORDINATORE DEL DOTTORATO

Prof. Ing. Maurizio De Lucia

An Innovative Approach for the Energetic Optimisation of High-Speed Railway Systems

A dissertation submitted in partial fulfillment of the requirements for the degree of Doctor of Philosophy

Settore scientifico disciplinare ING-IND/13

DOTTORANDO

Amedeo Frilli

TUTORE

Prof. Ing. Benedetto Allotta

COORDINATORE

Prof. Ing. Maurizio De Lucia

ANNI ACCADEMICI 2014/2017

...what I am looking for is a little piece of love

What I have earned is the bitter taste

Of all the rotten flesh I left back seeking my revenge

I was so wrong... Remorse... Regrets...

A Benedetta

Questa tesi è il frutto di un periodo molto importante della mia vita. Vorrei dunque provare a citare la maggior parte delle persone che hanno contribuito con la loro presenza a questo lavoro ed alla mia crescita come persona.

Innanzitutto è doveroso ringraziare il Professor Allotta, il Professor Rindi e l'Ingegner Meli per avermi reso parte del loro gruppo di ricerca ed avermi inserito nel progetto di ricerca che ha portato alla stesura di questa tesi. Un particolare e sentito ringraziamento va all'Ingegner Pugi, senza il cui aiuto ed interesse questo lavoro di tesi non avrebbe potuto certamente svilupparsi, e all'Ingegner Papini, per il suo sostegno e la sua amicizia.

Un ringraziamento va ai colleghi dottorandi Boccini e Panconi, per aver contribuito alle ricerche svolte in questi anni e soprattutto per aver alleggerito il periodo passato all'Università con comuni sfoghi, lamenti e sigari; ovviamente un ringraziamento va anche a tutti coloro che hanno fatto parte del laboratorio e hanno contribuito a rendere piacevole il periodo del dottorato.

Un ringraziamento va certamente alla mia famiglia, che mi ha sostenuto durante questi anni e mi ha consentito di raggiungere questo traguardo.

Tra gli altri, un ringraziamento sentitissimo va a Camilla, Alessandro e Andrea, che mi hanno aiutato a comprendere meglio me stesso e a capire come migliorarmi.

Voglio ringraziare i Manfru, che in ogni occasione sono sempre pronti a essermi vicini, nonostante tutto. E un ringraziamento importantissimo va ai Still Jacks, che sono stati costantemente per me uno sfogo ed un supporto e che sono stati pronti a sostenermi senza bisogno di chiedere perchè.

Infine, il ringraziamento più importante va a Benedetta, che è entrata nella mia vita proprio grazie al dottorato e a Tesys Rail, che sin da subito è riuscita a rendere migliore ogni cosa e che ha

completamente cambiato la mia vita e la mia prospettiva su essa. Ho trovato la compagna migliore che potessi desiderare, e per questo devo nuovamente ringraziare tutti coloro che hanno portato la mia vita su questo binario.

Abstract

The current development trend in the railway field has led to an ever increasing interest for the energetic optimisation of railway systems (especially considering the braking phases), with a strong attention to the mutual interactions between the loads represented by railway vehicles and the electrical infrastructure, including all the sub-systems related to distribution and smart energy management such as energy storage systems. The use of regenerative braking and energy storage solutions has been investigated within light railway systems but there is a strong lack of analyses and applications in High-Speed railway systems. The main goal of this thesis is to try to partially fill this gap, trying to understand the energetic possibilities of High-Speed railway systems. In this research work, an innovative coupled modelling approach suitable for the analysis of the energetic optimisation of railway systems and based on the use of the new object oriented language MATLAB®-Simscape™ has been developed and presents several advantages with respect to conventional modelling tools. The proposed model has been validated considering an Italian Direct Current High-Speed line and the High-Speed train ETR 1000. After the experimental validation, the model has been used to perform a feasibility and an optimisation analysis, considering the use of energy storage devices. The results obtained with the developed model show that the use of energy recovery systems in High-Speed railway can provide great opportunities of energy savings.

Contents

List of Figures

List of Tables

Symbols

a	Acceleration	$\left[m/s^2\right]$
a	Vehicle motion resistance coefficient	$\left[1/\left(m \cdot s^2\right)\right]$
b	Vehicle motion resistance coefficient	$\left[1/s^2\right]$
c	Vehicle motion resistance coefficient	$\left[m/s^2\right]$
C	UIC 544-1 Constant for braking performance calculation	$[-]$
C''	Constant for braking performance calculation	$[-]$
d	Charges distance	$[m]$
d	Vehicle motion resistance coefficient	$\left[m/s^2\right]$
D	UIC 544-1 Constant for braking performance calculation	$[-]$
f	Frequency	$[Hz]$
f_0	Static friction factor	$[Hz]$
f_b	Braking frequency	$[Hz]$
g	Gravity acceleration	$\left[m/s^2\right]$
i	Current	$[A]$
i	Line slope	$[-]$
i_c	Curves resistance coefficient	$[-]$
k	Butterworth polynomial order	
k_m	Motorized weight fraction	$[-]$
k_{muller}	Muller coefficient	$[-]$

k_Φ	Motor energy conversion coefficient	$[-]$
l	Line span length	$[m]$
m	Mass	$[kg]$
n_{cell}	Energy storage device number of cells	$[-]$
r	Line curves radius	$[m]$
s	Braking distance for rapid brake applications	$[m]$
t	Time	$[s]$
u	Energy density	$\left[J/m^3\right]$
v	Velocity	$[m/s]$
x	Vehicle position	$[m]$
B	Butterworth polynomial	
C	Capacitance	$[F]$
E	Energy	$[J]$
E_g	Electromotive force	$[V]$
ESS	Electrical substation	
F	Force	$[N]$
G	Conductance	$[1/\Omega]$
H	Butterworth polynomial transfer function	
I	Current	$[A]$
L	Inductance	$[H]$
OCV	Open circuit voltage	$[V]$
P_2	Line span second substation position	$[m]$
P_m	Motor power	$[W]$
Q	Charge	$[C]$
R	Resistance	$[\Omega]$
$S.O.C.$	State of Charge	$[-]$
$S.O.H.$	State of Health	$[-]$
T_m	Motor torque	$[N \cdot m]$

T	Vehicle traction and braking force	$[N]$
V	Voltage	$[V]$
W	Power	$[W]$

Greek letters

α	Line slope	$[rad]$
Δ	Difference	
ϵ	Butterworth filter maximum pass band gain	
ϵ_0	Vacuum permittivity	$[F/m]$
η	Efficiency	$[-]$
λ	Braked weight percentage	$[-]$
μ	Adherence	$[-]$
ξ	Line receptivity	$[-]$
ρ	Line distributed impedance	$[\Omega/m]$
ϕ	Phase	$[rad]$
Ω	Angular velocity	$[rad/s]$
Ω_0	Butterworth filter cut-off frequency	$[rad/s]$
Ω_P	Butterworth filter pass band frequency	$[rad/s]$

Subscripts and superscripts

$/\!/$	Parallel connection
$-$	Series connection
$*$	Reference or limit value
0	Nominal
1	Before the vehicle
2	After the vehicle
a	Armature
aux	Auxiliary

b	Braking
$batt$	Battery
c	Collected
c	Curves
c	Pantograph
$cell$	Energy storage device cell
d	Discharge
des	Desired
$diss$	Dissipative
$dist$	Distance
DC	Direct current
e	Electrical
eq	Equivalent
ESS	Electrical substation
$gearbox$	Transmission system
i	Inertial
$init$	Initial
iso	Isopower, isotorque
kmh	km/h
$leak$	Leakage
m	Mechanical
m	Motor
mb	Pneumatic
mr	Motion resistances
max	Maximum
$mean$	Mean
$motor$	Electric motor
$motordrive$	Motor drive

nom	Nominal
off	Switched off
on	Switched on
p	Line profile
r	Regenerated
s	Storage
S	Chopper
sc	Supercapacitor
sv	On-board storage
reg	Regenerative
t	Traction
tot	Total
$wheels$	Wheel/rail contact point

1

Introduction

The fears for the future depletion of petroleum stocks, the problems connected to the climate changes due to greenhouse gases emissions and the ever growing environmental pollution in most cities worldwide, are compelling the society to reflect on the harms produced by the huge number of private vehicles and to try to investigate the possibility of more sustainable transport systems.
In this scenario, the use of electric public transport systems for the urban and extra-urban mobility can play a significant role. These systems, depending on the distance, include buses, trains, tramways and metro systems. Electric transport systems already contribute to cut down pollutant emissions but their efficiency could be greatly enhanced.
Considering passengers transport, the most important sectors are railway, airplanes and road vehicles. This thesis focuses on railway: nowadays it represents the most environmentally efficient transport method but its development tendency is very far from that of the other competitors. However, since railway can easily compete both in terms of distances and passengers volumes, the possibility to enhance its energetic efficiency are significant and must be pursued in order to make the presence of the human being in the planet more sustainable.
A significant solution to improve transport efficiency is given by the possibility to couple electric motors and feeding lines with energy storage devices in order to save and reuse energy flows otherwise dissipated: as an example, some authors [1], [2] have estimated that regenerative braking could recover up to 40% of the total braking energy.

In a railway system, the reuse of this recovered energy and its reintroduction in the feeding line bring with them the problem of losses management. In particular, in Italy, following the 440/91 European directive, which required the accounting separation between carriers and infrastructure managers, two new entities have started to operate respectively from July 2000 and July 2001: Trenitalia, which incorporated the previous *Passeggeri*, *Trasporto Regionale* and *Cargo* Departments of the former Ferrovie dello Stato, and Rete Ferroviaria Italiana (RFI), which incorporated the *Infrastruttura* Department. Both societies are holdings of the Ferrovie dello Stato Italiane Spa group.

This European directive was conceived to open railway market to free competition among the societies involved in railway transportation: in particular, in Italy, the High-Speed railway system includes a new competitor in addition to Trenitalia, i.e. NTV (Nuovo Trasporto Viaggiatori).

To allow these competitors to adequately operate, a model to estimate the energy losses due to the train and to the line is essential; furthermore, such model should allow to develop a strong synergy between carriers and infrastructure managers and to reach important efficiency goals. The use of regenerative braking goes along with the problem of losses on the line: a stationary storage device would increment line losses and the infrastructure manager would have to take into account the the balance between the recovered energy and the additional losses to evaluate the convenience of regenerative braking.

Since regenerative braking has been typically applied in light railway systems, in this thesis, its use within High-Speed railway systems has been investigated, performing a comparison among different energy storage technologies and evaluating their feasibility and trying to detect some strategies for the optimisation of a High-Speed system. These activities have been carried out through the development of a coupled vehicle-line model, which allowed to evaluate both mechanical and electrical physical quantities. The model has been developed and experimentally validated considering two different test cases: an Italian commuter train, i.e the E 464 locomotive with 4 Vivalto coaches, on the Firenze-Pisa-Livorno line and an Italian High-Speed train, i.e. the ETR 1000, on the Firenze-Roma High-Speed line. The same scenarios have been used to perform the feasibility and optimisation analyses which represented the final goals of the thesis.

This research work is part of the TESYS Rail project, an Italian research project financed by the MIUR and involving a large number of different partners.
All the activities, including the model development and validation, have been carried out in cooperation with many industrial and academic partners, including Italcertifer, which provided the technical and experimental data needed for the analyses of High-Speed systems, EnginSoft, Ansaldo STS, RFI, Te.Si.Fer., the University of Pisa and the University of Napoli Federico II.

1.1 Railway transportation and energy market

Global Warming and, more in general, the issues related to pollution are enforcing a growing interest to the increase of efficiency of transportation systems [3], which still represent in Europe and in all industrial countries about 20-30% of CO_2 pollution sources (i.e. about 23% worldwide and 30% in Europe, see Figures 1.1 and 1.2). This situation has been investigated by both the Europe Environment Office [4] and the Association of American Railroads [5]; furthermore, Fridell et al. [6] performed a number of experimental tests and found out that, in the railway sector, a significant part of emissions is due to mechanical braking. Railway transportation represents the most efficient transportation technology in terms of pollution and energetic efficiency, but the continuous technological improvements accomplished by its competitors (i.e. ground and air vehicles) are quickly reducing this gap: Figure 1.3 shows how, considering the current development trends, by the year 2050 railway would have almost lost its advantage in terms of pollutant emissions. Furthermore, the current market growth for High-Speed and freight sectors in industrialized countries with high population densities would be strongly enhanced by the improvement of the efficiency of the system. Another important aspect, which is pushing towards a strong energy optimisation of the railway system, is the liberalization process of both energy

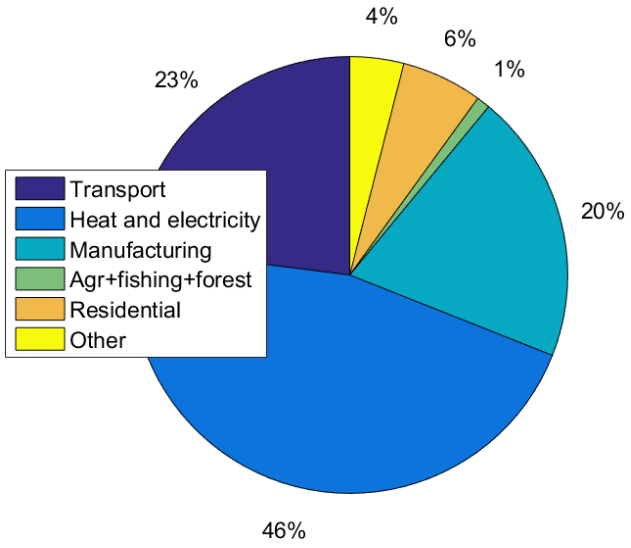

Figure 1.1: CO_2 sources worldwide.

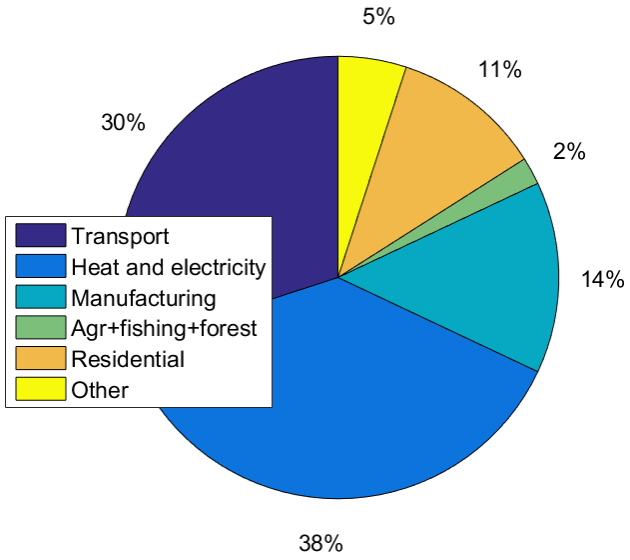

Figure 1.2: CO_2 sources in Europe.

and transportation markets: this process is stimulating all the stakeholders in the railway sector (e.g. energy infrastructures and suppliers, railway infrastructures and vectors, see Figure 1.4) to accurately measure and quantify energy consumptions and their costs. In particular, the combined liberalization of both energy and railway sectors should give to the infrastructure managers the

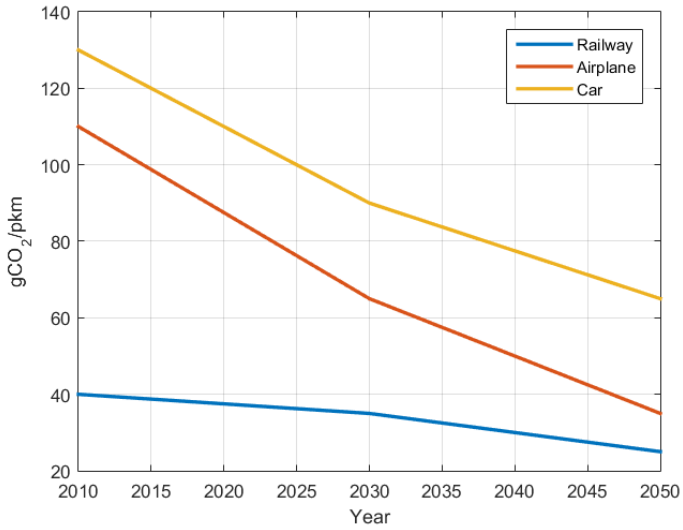

Figure 1.3: Comparison between the CO_2 emissions of different transport methods.

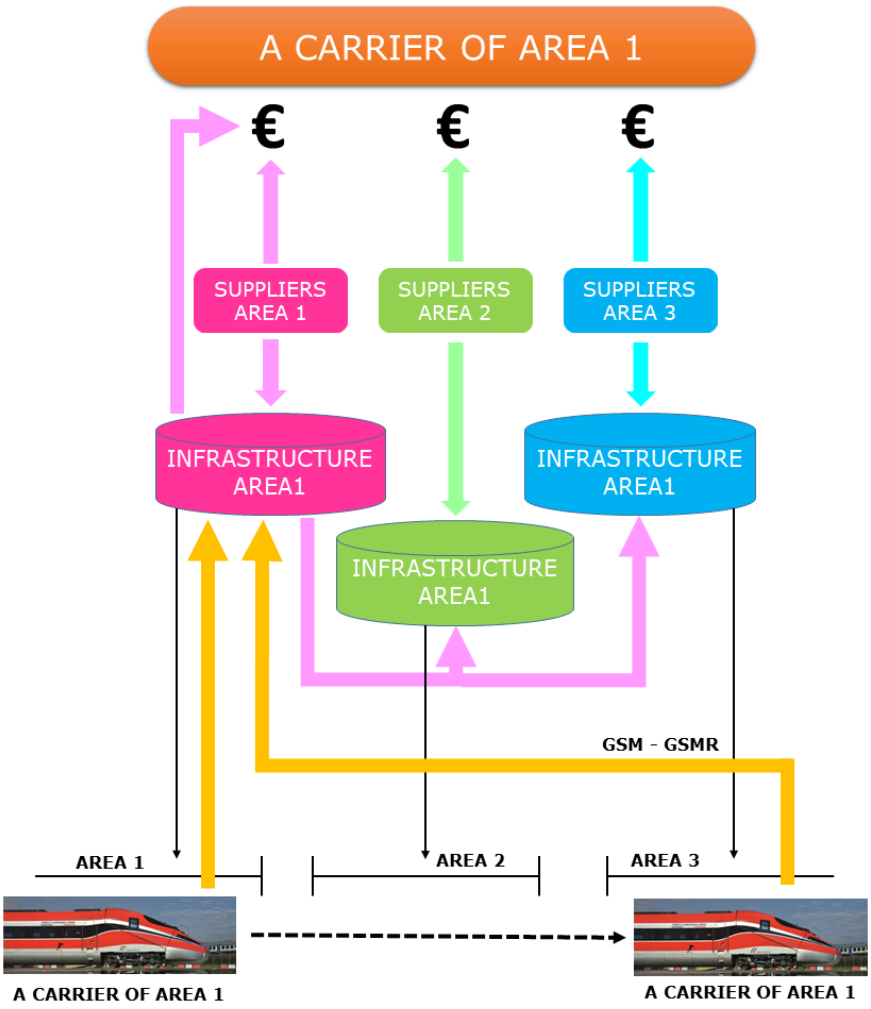

Figure 1.4: Energy billing and management.

opportunity to apply different costs to travelling trains according to the real measured energy efficiency. Furthermore, the possibility of acquiring energy from different suppliers would allow to optimise costs with respect to the line geographic location, to seasonal factors, involving the availability of different resources, and, finally, to specific requirements of railway vectors/transport managers. In this scenario, the competition between the different subjects involved in the entire railway field and the need to respect interoperability issues established by the European Railway Agency in the Technical Specifications for interoperability (TSI) [7], will further stimulate the optimisation of train energy consumptions, as reported in the analysis of different methods to

improve railway energy efficiency performed by Douglas et al. [8].

Finally, it is important to take into account the expectations from the final stakeholder of the system: the passenger. Nowadays, the customer is ever more demanding from the transport system and informed on environmental aspects, and a transport sector should try to meet the requirements of its public: environmental friendliness, reliability and efficiency and finally liveability, both within the vehicle, in the zones near the system and more in general in the planet.

Obviously, all the stakeholders involved within the railway system would push towards conflicting requirements: however, a proper energetic efficiency optimisation could be able to satisfy all of them.

1.2 State of the art and literature review

In modern railway, aside from the classic considerations that should be made concerning the traction systems and the electrical line, one of the greatest source of energy savings is the use of regenerative braking (see Bartłomiejczyk and Połom [9], who investigated the perspectives of braking energy recovery within urban electrified transports like tramways); in particular, the growing diffusion of trains with distributed traction systems has drastically increased the percentage of energy that can be recovered during the train braking phase. Using regenerative braking instead of the classical dissipative braking allows to convert a relevant part of the train kinetic energy in electric power, without dissipating it over the pneumatic brakes friction surfaces, with another important advantage in terms of brake maintenance costs. Furthermore, the reduced wear and prolonged life of pneumatic brake pads and discs can produce significant benefits in terms of pollution, since the brakes wear produce solid particles and contaminants, whose impact on the environment is still a matter of monitoring and research: Abbasi et al. [10] analysed the particles due to brake wear and proposed a comparison index to identify their impact, Gehrig et al. [11] performed experimental tests in a Switzerland railway node and Salma et al. [12] performed their experimental analyses on polluting particles near Budapest.

Figure 1.5 shows the main energy fluxes involved in a railway system, which can be classified in traction and non-traction contributions. The infrastructure losses include both electrical substations (i.e. ESSs) and catenary losses; the losses within the line are higher than the internal substation losses. They depend on the system characteristics and on the number of vehicles within the line. Auxiliary systems losses, e.g. air conditioning, are quite significant (and they would also absorb a significant part of recovered braking energy), as well as motion resistances (both aerodynamical and mechanical). In particular, since aerodynamic forces depends on the square of the velocity, they represent an important contribution in High-Speed systems. Furthermore, a part of energy is dissipated by electrical devices inefficiency, depending on speed and traction and braking efforts. Finally, the main energy loss is due to braking and this share depends on different parameters, as shown in Figure 1.6: in fact the energy globally dissipated during braking depends on the vehicle

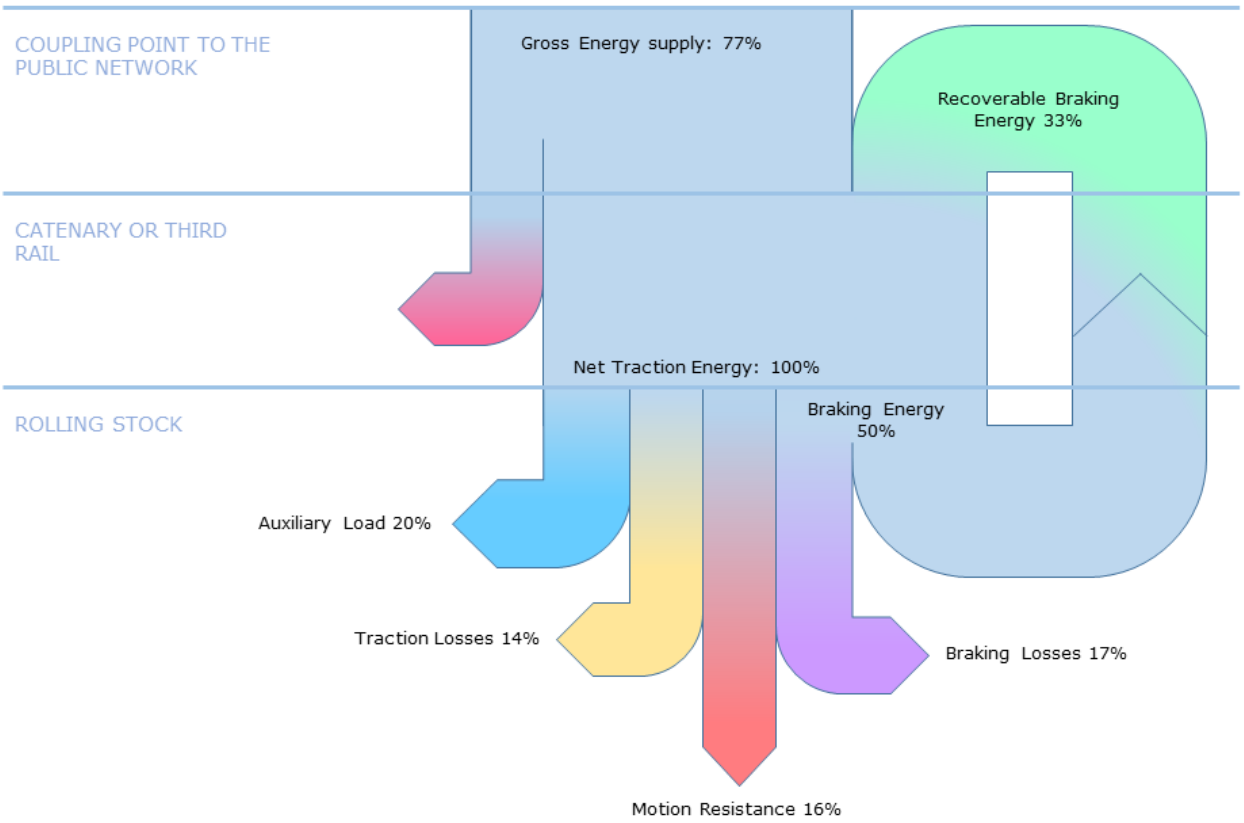

Figure 1.5: Typical energy flows in a railway system.

kinetic energy and on the number of braking phases.

The application of regenerative braking involve the availability of a load or a storage device (whose performances in electric vehicles have been investigated by Marr et al. [13]), able to manage the energy recovered from the braking phase of the train: Hillmansen et al. [14] found that a significant percentage of the railway energy consumption could be saved using proper storage devices. Another important method to recover braking energy is the transfer of a vehicle braking energy to another train which is accelerating, within the same line, as shown in Figure 1.7.

For the use of regenerative braking, it is important to consider two main indicators, i.e. the peak recovered power $W_{r,max}$ and the mean recovered power $W_{r,mean}$, which can be defined as follows:

$$W_{r,max} \propto m_i \dot{x}_{max} \ddot{x}_b, \tag{1.1}$$

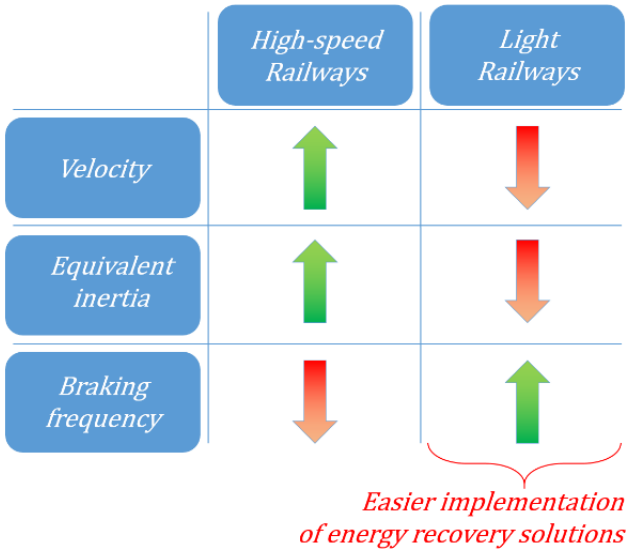

Figure 1.6: Comparison of braking energy parameters between High-Speed and light railway systems.

$$W_{r,mean} \propto m_i \dot{x}_{max}^2 f_b. \tag{1.2}$$

The peak power $W_{r,max}$ that has to be managed during regenerative braking is roughly proportional to the maximum speed reached by the train before braking $\dot{x}_{max}$, to the deceleration of the train during the braking phase $\ddot{x}_b$ and to the train equivalent inertia m_i, which takes into account also the contributions to kinetic energy due to motors, gearboxes, axles, wheels and brake discs.

On the other hand, the mean power $W_{r,mean}$ that can be regenerated depends on the kinetic energy of the train $m_i \dot{x}_{max}^2$ and on the braking occurrence f_b (i.e. defined as the number of braking events with respect to travelling time).

As shown in Figure 1.6, in tramway and light urban railway, the vehicles travelling speed and equivalent inertia are much smaller with respect to High-Speed trains, but the braking frequency f_b is much higher: therefore, the mean regenerated power $W_{r,mean}$ is relatively high with respect to the peak power $W_{r,max}$. For this reason, the power management of regenerative braking is typically easier on tramways, metro and light urban railway with respect to High-Speed lines. Furthermore, the length of metro and tramway lines is typically lower than conventional lines: hence it is easier

to implement customized innovative solutions (e.g. the synchronization of trains accelerations and decelerations, investigated by Peña-Alcaraz et al. [15]). Consequently, the application of energy storage systems on metro, tramways and, more in general, on light railway systems, has been widely recognized as an important opportunity for energy optimisation and has been extensively investigated by different authors, while the application of energy recovery systems in High-Speed trains is still an open research field: Falvo et al. analysed the energy efficiency of a metro system, comparing a Spanish and an Italian line [16] and González-Gil et al. [17] investigated the most important energy savings possibilities in urban railway. Research works available in literature can be typically classified as follows:

- Energy storage systems location: energy storage systems can be stationary or installed on-board the vehicle. Barrero et al. [18] investigated the advantages and disadvantages of on-board and stationary energy storage devices, using a simulation tool to analyse the metro line of Brussels, while Teymourfar et al. [19] investigated the use of stationary supercapacitors within the Tehran metro network. The on-board configuration allows to reduce electrical line losses and assures system autonomy with bad or discontinued current collection and even catenary free operation. On-board devices represent a good choice for brand new vehicles but they involve high encumbrances on-board and the increment of the vehicle total mass, which in turn contributes to an increased wear both of rolling stock and braking devices; furthermore, each vehicle needs its own device. On the other hand, stationary systems connected to the infrastructure, are easier to install and maintain, avoiding additional weights and encumbrances on vehicle, which can penalize performances and available payload for goods and passengers. However, stationary devices involve increased line losses and the presence of line voltage limits obliges the vehicle to cut off regenerative braking if the device is too far; furthermore, a stationary device should be properly sized to be able to manage the presence of more than one braking train in its proximity. Table 1.1, [20], shows the main characteristics of a set of on-board storage devices, which have been proposed in previous literature works, while Table 1.2, [20], shows the characteristics of stationary energy storage systems found in literature.

Table 1.1: On-board energy storage devices developed by railway manufactures.

Brand name	Company	Technology	Main features[1]	Application in urban rail	Reference
MITRAC™	Bombardier	EDLC	PC: 300kV SC: 1 kWh W: 450 kg D: 1700 x 680 x 450	Commercially available.	[21]
Sitras® MES	Siemens	EDLC	PC: 288kV SC: 0.85 kWh W: 820 kg D: 2000 x 1520 x 630	Commercially available.	[22]
ACR	CAF	EDLC	PC: N/A SC: 0.8 kWh W: 800 kg D: N/A	Commercially available.	[23]
STEEM	Alstom	EDLC	PC: N/A SC: 0.8 kWh W: 800 kg D: N/A	Prototype testes Paris tramway, tested from 2009 to 2010.	[24]
Citadis flywheel	Alstom &	Flywheel	PC: 325 kW SC: 4 kWh W: 1600 kg D: N/A	Prototype testes in Rotterdam in 2004-2005.	[25]
LRV Swimo	Kawasaki	NiMH	PC: 250 kW SC: 120 kWh W: 3200 kg D: N/A	Prototype testes in Sapporo Municipal Transport network, 2007-2008.	[26]
LFX-300 streetcar	Kinki Shayro	Li-ion	PC: N/A SC: 40 kWh W: 3200 kg D: N/A	Prototype testes in Charlotte,2010.	[27]
Sitras® HES	Siemens	EDLC + NiMH	PC: 288 + 105kV SC: 0.85+ 18 kWh W: 820 + 826 kg D: 2000 x 1520 x 630 1670 x 1025 x 517	MTS light rail system in south Lisbon, in service since 2008.	[28]

([1]) PC = Power capacity, SC = Storage capacity, W = Weight, D = Dimension (width x depth x height) in mm.

- Energy storage systems application and usage: the most typically analysed applications are tramways or metro, where energy storage systems allow to save energy, reduce line voltage fluctuations and optimise both energy and infrastructure costs. In particular, Teymourfar et

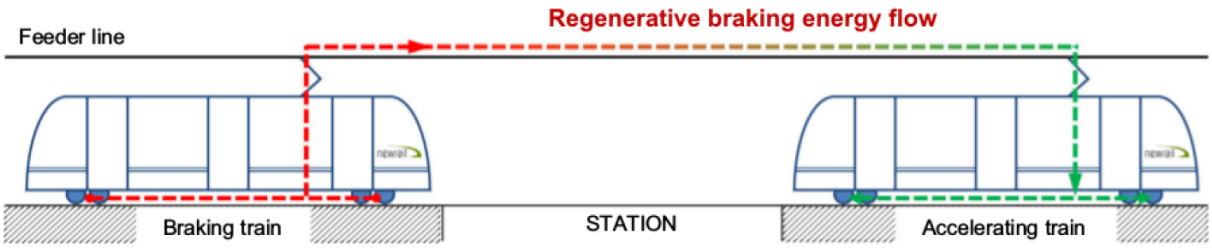

Figure 1.7: Energy flux between different trains on the same line.

al. [29] analysed the possibility to perform energy recovery within a metro network, Ceraolo and Lutzemberger [30], using the Modelica® environment, analysed and compared different configurations useful to increase the efficiency of tramways, Barrero et al. [31] analysed the energetic efficiency of light railway, investigated the sizing of supercapacitors for the Brussels tramway [32] and performed an analysis on a set of on-board supercapacitors for a tram, evaluating also the effect of power converter (Barrero et al. [33] and Van Mierlo et al. [34]), while González-Gil et al. [35], [36] analysed different strategies to enhance the energetic efficiency of urban railway systems, including regenerative braking. Furthermore, Iannuzzi et al. [37] proposed a technique to optimise the sizing of supercapacitors for light railway and Mir et al. [38] designed a supercapacitor storage system for tramways. The shortage of research works concerning energy recovery in High-Speed railway applications represents an important lack, which should be filled in order to enhance the efficiency of the entire railway system.

- Energy storage technology: Vasebi et al. [50] developed an innovative method for the calculation of batteries State Of Charge (i.e. $S.O.C.$), which is fundamental for the correct analysis of batteries behaviour; Tsang et al. [51] proposed and validated a model for the analysis of Li-ion batteries (which are the most suitable for the use in the railway field), as well as Castano et al. [52]; on the contrary Zhu et al. [53] analysed the use of Pb-acid batteries for energy storage purposes. Other researchers have studied batteries behaviour considering their use together with other storage devices, like Trovão and Antunes [54], who investigated the possibilities to use a hybrid storage system coupling batteries and

Table 1.2: Stationary energy storage devices developed by railway manufactures.

Brand name	Company	Technology	Main features[1]	Application in urban rail	Reference
Sitras® SES	Siemens	EDLC	SV: 600/750 V PC: 700 kW SC: 2.5 kWh	Madrid and Cologne, in service since 2003; Beijing metro, in service since 2007; Toronto rail transit, in service since 2011.	[39]
EnerGstor™	Bombardier	EDLC	SV: 600, 750, 1500 V PC: 650 kW SC: 1 kWh	N/A	[40]
NeoGreen® Power	Adeneo (Adetel)	EDLC	SV: 750 V PC: 300-1000 kW SC: 1-4 kWh	Lyon tramway, pilot project in 2011.	[41]
Envistore™	Envitech Energy (ABB)	EDLC	SV: 500-1850 V PC: 750-4500 kW SC: 0.8-16.5 kWh	Warsaw metro, to be implemented; Philadelphia transit system, pilot project in 2012 (battery-based).	[42]
Capapost	Meidensha	EDLC	SV: N/A PC: 2000 kW max SC: N/A	Hong Kong metro, to be delivered.	[43]
Powerbridge	Piller Power Systems	Flywheel	SV: 400, 1000 V PC: 1000 kW SC: 5 kWh	Hannover and Rennes metro systems, pilot project in 2004 and 2010, respectively.	[44]
GTR system	Kinetic Traction System	Flywheel	SV: 570-900 V PC: 200 kW SC: 1.5 kWh	London metro, pilot project in 2000; New York City transit system, pilot project in 2002; Lyon metro, pilot project in 2003-2004.	[45]
Regen® system	Vycon	Flywheel	SV: N/A PC: 500 kW SC: N/A	Los Angeles metro, to be delivered	[46]
Gigacell® BPS	Kawasaki	NiMH	SV: 600,1500 V PC: N/A SC: 150-400 kWh	New York City Transit network, pilot project in 2010; Osaka City Subway, tested in 2007.	[47]
B-CHOP	Hitachi	Li-ion	SV: 600/750, 1500 V PC: 500-2000 kW SC: N/A	Kobe transit system, pilot project in 2005 and regular service since 2007; Macau metro system, to be delivered.	[48]
Intensium Max	Saft	Li-ion	SV: 700 V PC: 900-1500 kW SC: 600-400 kWh	Philadelphia transit system, pilot project in 2012.	[49]

([1]) SV = Supply voltage, PC = Power capacity, SC = Storage capacity.

supercapacitors, or with fuel cell-powered systems, like Guo et al. [55], who analysed the use of batteries in a fuel cell-powered locomotive (the batteries are able to store braking

energy and to cover transient energy requests), Paladini et al. [56], who investigated the use of both on-board batteries and supercapacitors in a fuel cell-powered vehicle, developing a MATLAB®-Simulink® model (the use of MATLAB®-Simulink® is typical in the analysis of this kind of systems), and Thiounn-Guermeur [57], who developed a hybrid locomotive which uses two different storage systems. Supercapacitors are relatively new with respect to batteries, but it is possible to find in literature many studies concerning their behaviour, like that by Sharma and Bhatti [58], where they proposed a detailed analysis of the characteristics of supercapacitors and of their applications, or that by Steiner et al. [21], where they analysed the use of on-board supercapacitors. Supercapacitors have been greatly appreciated within light railway systems because they represent a quite good choice in presence of small braking times. Among the many possibilities to implement energy storage, researchers have analysed the different performances that a device could provide in different systems; an important work is that by Kondoh et al. [59], who performed a comparison of different energy storage systems, highlighting which technology could better suit specific applications. Finally, for a correct use of energy storage devices it is fundamental to be aware of the subsystems needed for their operation (see Fernão Pires et al. [60], who analysed the power electronics devices needed by different energy storage systems to be successfully employed in electrical systems) and also to understand the complete life cycle of the considered device; an important analysis of this last point is provided in a work by Oliveira et al. [61], where they investigated the environmental characteristics of energy storage devices, taking into account their whole life cycle. A final mention should be devoted to composite flywheels: they are characterised by a fast dynamical behaviour in terms of charge/discharge cycle, by a long operating life and by a significant power density; however, current technology is not able to safely operate them and avoid their explosion in case of system failure. Current energy storage technologies differ in terms of costs, specific energy and power densities. Therefore, the design and sizing of these systems (and of regenerative braking systems themselves) are influenced by the adopted storage technology, especially for on-board applications where the installation of energy storage systems is limited by interoperability issues and by weight and

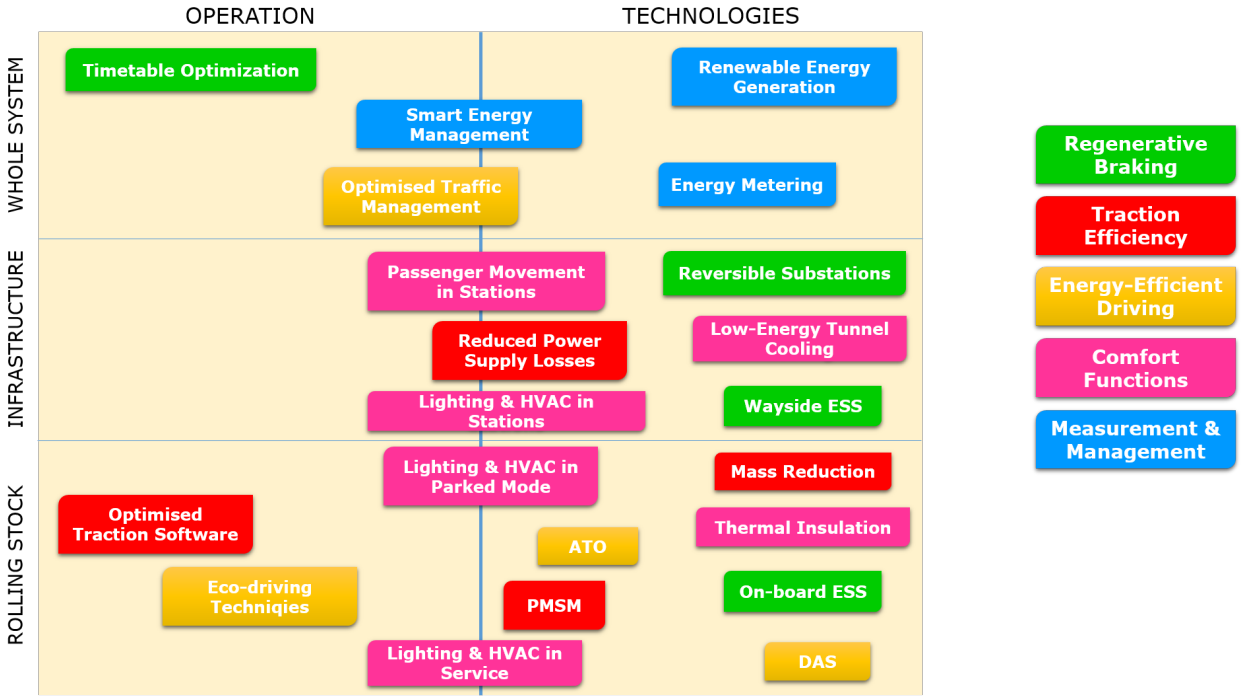

Figure 1.8: Main contributions to energy savings in railway.

encumbrance constraints.

Furthermore, it is important to underline how the use of energy storage device does not represent the only method to optimise the energetic efficiency of a railway system: as reported in Figure 1.8, [36], many possible solutions can be applied, obviously with different impacts on the system. By way of example, since line losses depend on the square of current, it useful to avoid current peaks due to the presence of a large number of accelerating vehicles, and the use of high voltage systems and low resistance materials would be preferable. Another interesting perspective is the use of Permanent Magnet Synchronous Motors, which could help reducing on-board traction losses, and, due to the possibility to operate in a direct drive configuration, also to increment the mechanical transmission efficiency. Obvious measures include the vehicle total mass reduction and the optimisation of comfort systems (e.g. air conditioning), but all these techniques have to be coupled with an accurate measurement of energy consumptions.

Finally, Figure 1.9 shows how all the energetic optimisation technical solutions interact with each

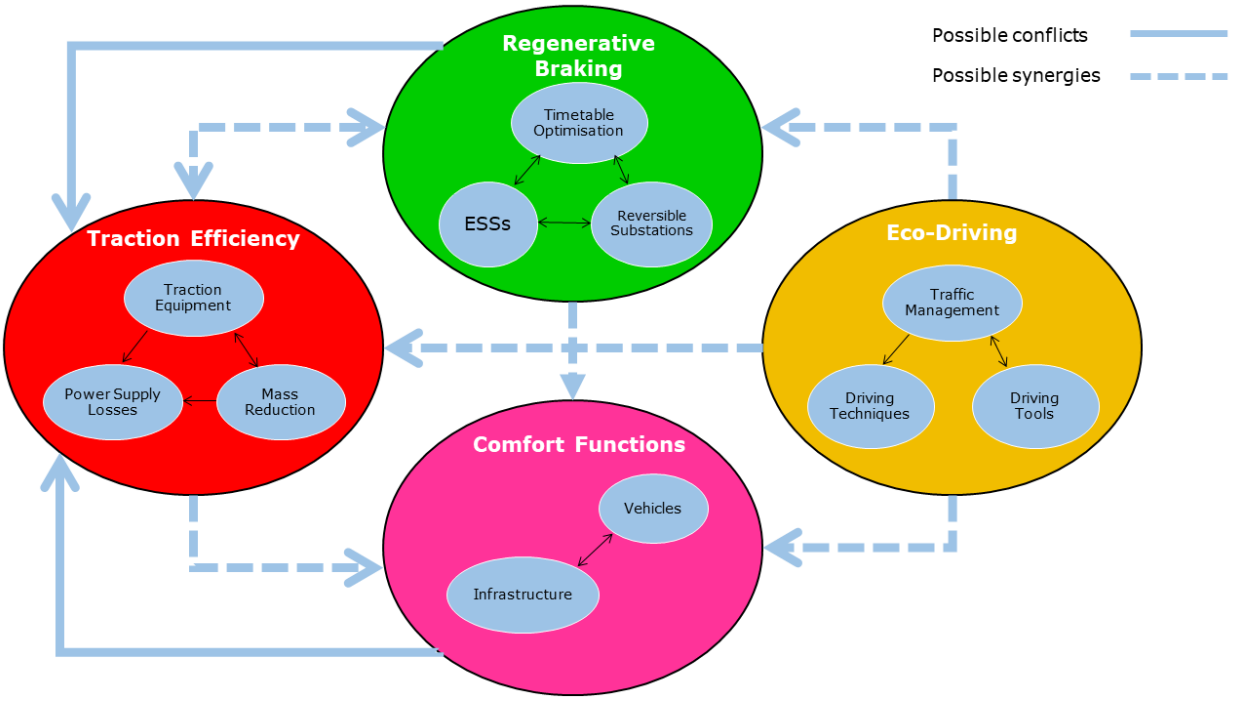

Figure 1.9: Interactions between solutions for railway energetic optimisation.

other: two or more solutions together can both enhance or worsen the final efficiency of the system; hence it is important to accurately analyse each system taking into account its particular characteristics.

Through history, electric traction has prevailed as the main traction system for railway. Nowadays, more than 70% of the Italian railway lines are electrified: this number is quite significant and, in order to fully exploit the advantages of regenerative braking, it is important to understand the main characteristics of the technologies involved in railway traction, braking and energy storage and the corresponding modelling approach.

1.2.1 Traction and braking systems

Electric traction trains have used many different types of motors: until the 1980 the most used motors were Direct Current motors, while modern trains, thanks to the strong development of

power electronics, use mainly asynchronous Alternating Current motors.

An energetic analysis of railway performances can cover both the traction phase and the braking one; however, traction efficiency can be interesting from a strictly electrical point of view (i.e. considering both motors and feeding lines), while mechanical transmission systems and other mechanical sources of losses have been thoroughly investigated and could bring their contribute only with paradigmatic changes to the railway system itself (e.g. systems based on the use of vacuum or magnetically levitated trains). So it is more interesting, in order to analyse the energetic possibility of modern railway, to concentrate on the braking phase, when the mechanical energy of the vehicle is quite high and have to be dissipated. In this scenario, electric braking, if properly used, represents a method to improve railway efficiency with costs that are negligible with respect to the costs of the entire system.

1.2.1.1 Braking in electric motors

Electric motors can operate as motors in the first quadrant but they are also able to operate as generators in the fourth quadrant: this feature allows an electric vehicle to take advantage of electric motors even in the braking phases. For the sake of synthesis, in this paragraph, braking in an externally excited DC motor will be introduced.

Considering the electric scheme of the DC motor shown in Figure 1.10, it is possible to calculate the armature voltage V_a and the electromotive force E_g as follows:

$$V_a = k_\Phi I_a \omega_m + R_a I_a + L_a \frac{dI}{dt}, \tag{1.3}$$

$$E_g = k_\Phi I \omega_m, \tag{1.4}$$

where R_a and L_a are respectively the armature resistance and inductance, I_a is the armature current, ω_m is the motor angular velocity (expressed in rad/s), k_Φ motor conversion coefficient for electric and mechanical energy and, finally, I is the current and t is time. Inductive terms are equal to zero in stationary regime; hence, from Equations 1.3 and 1.4 it is possible to obtain the following

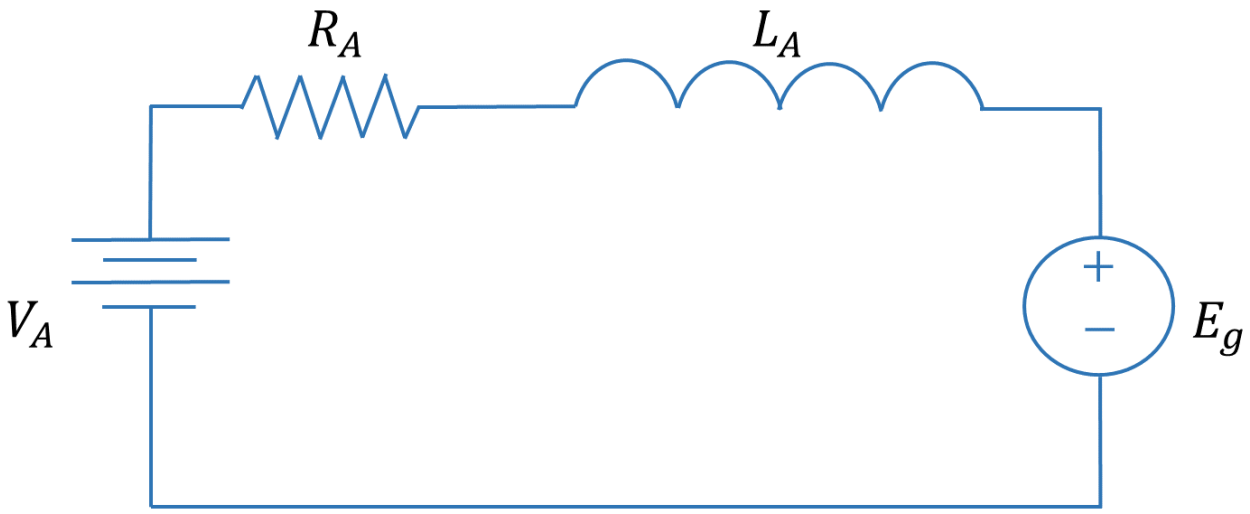

Figure 1.10: Electric scheme of a DC motor with series excitation.

expressions for the motor mechanical power P_m and for the mechanical torque T_m, provided by the motor to the load:

$$P_m = E_g I = k_\Phi \omega_m \left(\frac{V_a}{R_a + k_\Phi \omega_m} \right)^2 , \tag{1.5}$$

$$T_m = \frac{P_m}{\omega_m} = k_\Phi \left(\frac{V_a}{R_a + k_\Phi \omega_m} \right)^2 . \tag{1.6}$$

During the braking phase the Direct Current motor operates as a generator, allowing the vehicle to transform the mechanical energy, that should be dissipated in the braking event, into electrical energy, which is sent back to the armature.

The electric power produced during the braking phase must be released on a load: it is possible to store energy in a proper storage device or to send it back to the feeding line (i.e. regenerative braking) or to dissipate it on a resistive load taking advantage of the Joule effect (i.e. dissipative braking).

During the braking phase the motor power and torque change sign.

A typical DC motor needs a drive which includes the following elements:

- systems for the armature and field controls: if the excitation is separated, two different choppers are needed to control the armature and the field magnetization voltages. The most

typical drive solution is denoted as impressed voltage and includes an upstream DC BUS which feeds the converters that regulate the electrical quantities of the controlled loads;

- a braking chopper which is connected to the DC BUS and handles the power sent back to the drive during the braking phase;
- a supply system, which can operate both in DC or AC configurations. With a DC supply system the current is directly picked up from the feeding line (eventually using an intermediate chopper with a DC BUS to stabilize the voltage level); otherwise, with an AC supply system, the use of a transformer is mandatory;
- filters: the use of capacitive, inductive or *LC* filters is necessary to cut out the harmonics due to the large number of conversion stages.

The use of a step up chopper is needed during the braking phase: in fact, during the motor operation as a generator, the power is transferred from the armature to the line and the line voltage is usually higher than the voltage generated by the brake.
The regenerated current I_a can be calculated as the ratio between the motor braking torque and the electric constant k_e:

$$I_a = \frac{T_m}{k_e}; \tag{1.7}$$

it is then possible to calculate the motor voltage as follows:

$$V_a = E_g - R_a I_a, \tag{1.8}$$

where V_a represents the inlet voltage for a step up converter (e.g. a boost) which transfers the power to a different voltage level, denoted as V_{DC}.
In order to perform a complete motor control using a unique electronic device, it is then possible to use a four-quadrant chopper (see Figure 1.11).

The four-quadrant chopper is composed of a bridge of diode-switch (which can be realized using MOSFETs or thyristors) parallel connections which realize the step up-step down chopper configurations needed by the drive. In particular, it is possible to implement the following configurations (see Figure 1.11):

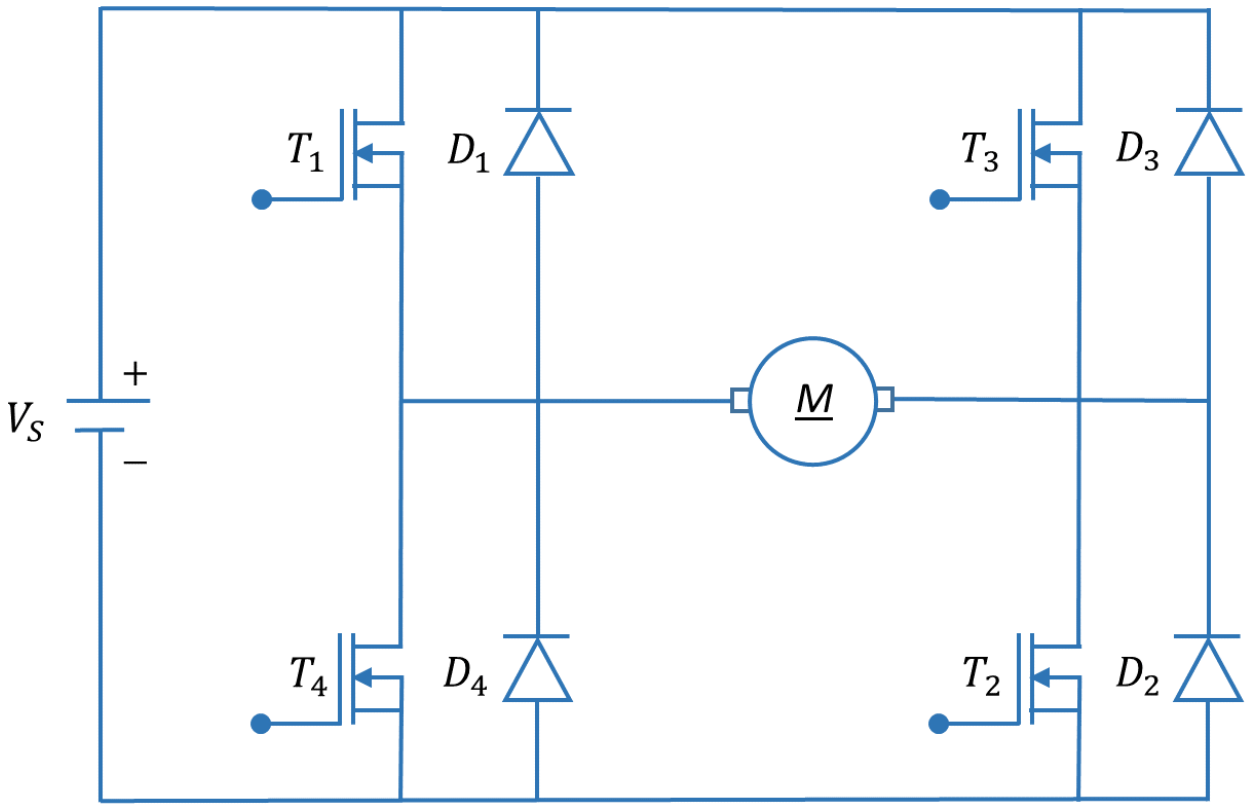

Figure 1.11: Electric scheme of a four-quadrant chopper.

- T_1 and T_2 closed, T_3 and T_4 opened: a voltage equal to V_{DC} is applied to the armature;
- T_3 and T_4 closed, T_1 and T_2 opened: an inverted voltage equal to $-V_S$ is applied to the armature;
- T_1 and T_3 closed, T_2 and T_4 opened (or viceversa): a zero voltage is applied to the armature.

1.2.1.2 Pneumatic braking

Traditionally, railway vehicles can brake using pneumatic or electric braking systems. In order to understand the advantages provided by electric braking, it is necessary to previously analyse the operation and the drawbacks of pneumatic braking.

A pneumatic brake is a braking device which uses compressed air to control and actuate the components that actually slow and stop the vehicle (e.g. discs). Pneumatic braking is usually

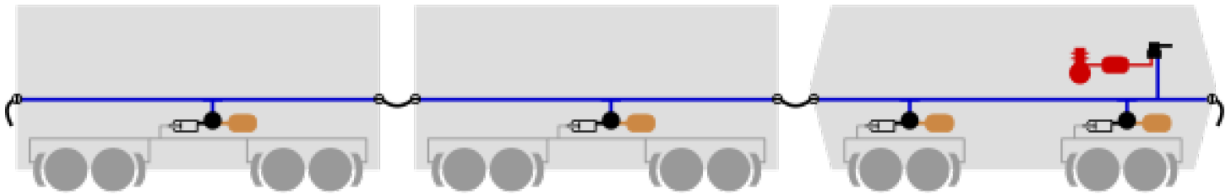

Figure 1.12: Westinghouse pneumatic braking system.

employed as the main braking system in heavy vehicles, such as trucks and freight trains.
During the braking phase, the vehicle deceleration is caused by the pressure exerted by brake shoes or pads on the wheels or on the discs mounted on the vehicle wheelsets.
Brake shoes and pads are moved through the brake cylinders, which are pushed by compressed air and actuate a leverage or directly the brake. The force exerted by the compressed air which enters the cylinders has to exceed the one exerted by a return spring. Finally, the braking action itself is due to the friction between the moving component of the wheelset (e.g. the wheel) and the braking device (e.g. the shoe).

The most used pneumatic braking system in railway is the Westinghouse continuous automatic brake (see Figure 1.12). In this system, all the wagons of the train are connected through a brake duct which contains pressurized air (the pressure is 5 *bar*, which is the brake release value). The driver actuates the brake generating through a valve a pressure drop which propagates to all the wagons through the duct and controls the air flux inside the brake cylinders. When the pressure inside the duct goes back to 5 *bar* the brake is released.
The main problem due to the use of pneumatic braking is the pads and shoes wear, which generates higher costs of maintenance and pollutant particles. For this reasons, nowadays in High-Speed applications the use of electric braking is more diffused.
By way of example, Table 1.3 shows the brake pads wear for a High-Speed train on the Milano-Napoli line: it is possible to highlight how the use of electric braking (i.e. using the pneumatic brake only if the electric one is not able to fully decelerate the train or in emergency cases) has a strong influence on pads wear and hence on maintenance costs. The data set shown in Table 1.3 is referred to a blending strategy which applies the same power to all the discs and to a mean

Table 1.3: Brake pad wear for a High-Speed train.

Brake pad	Operating scenario	Specific wear $\left[\frac{cm^3}{MJ}\right]$
Jurid 707	(a)	0.144
	(b)	0.213
	(c)	0.104
	(d)	0.136
Becorit BM47-NT	(a)	0.100
	(b)	0.143
	(c)	0.102
	(d)	0.123

deceleration equal to 0.6 m/s^2; the considered operating scenarios are the following:

- (a): service braking, 100% electric braking, feeding line 25 kV AC (v_{max}=360km/h);
- (b): service braking, 0% electric braking, feeding line 25 kV AC (v_{max}=360km/h);
- (c): service braking, 100% electric braking, feeding line 3 kV DC (v_{max}=300km/h);
- (d): service braking, 0% electric braking, feeding line 3 kV DC (v_{max}=300km/h).

For both the considered brake pads, the use of electric braking can reduce the pads specific wear up to about 30%.

1.2.1.3 Electric braking

As previously exposed, electric braking is the capability of electric motors to reduce their velocity by switching their operation from motor to generator. Electric braking can be regenerative if the energy thus generated is reused or dissipative if it is wasted.

If the braking is dissipative, the electric energy sent back to the motor driver is not fed to the line or to proper storage devices but dissipated on a proper resistance, which, in railway, is usually located on the roof of the motorized railcar. Otherwise, in case of regenerative braking, the electric energy is sent back to the feeding line (where it can be devoted to different uses) or stored on on-board or stationary energy storage devices.

The current which is supplied to the feeding line causes a rise of the available energy for other travelling vehicles on the same line span; if these vehicles do not use this energy, it can be stored on trackside energy storage devices or received by reversible energy substations which send it back to the grid.

The line receptivity can be defined as the ratio between the energy actually fed back to the line and the total potential energy which could be regenerated in the braking phase:

$$\xi = \frac{E_{ESS} + E_t}{E_b}, \tag{1.9}$$

where E_{ESS} is the energy absorbed by substations or stationary storage devices, E_t is the energy used by other accelerating vehicles and E_b is the total vehicle braking energy.

The maximum recoverable energy depends also on the line profile; however, to enhance the line receptivity, it is possible to increase the number of trains which, at the same time, accelerates and decelerates. In fact, in absence of storage devices, the only way to take advantage of regenerative braking is the optimisation of timetables.

1.2.2 Energy storage devices

The most immediate solution, even if not the only one and not always the most convenient, to take advantage of electric regenerative braking is the use of storage devices to store the electrical energy produced by the motors during braking. In the last years, the use of energy storage devices has been favored by the strong development of innovative storage technologies and power converters.

In the railway field, storage devices can be installed both on-board the vehicle or in parallel to the line electrical substations. Figure 1.13 shows different scenarios for the application of regenerative

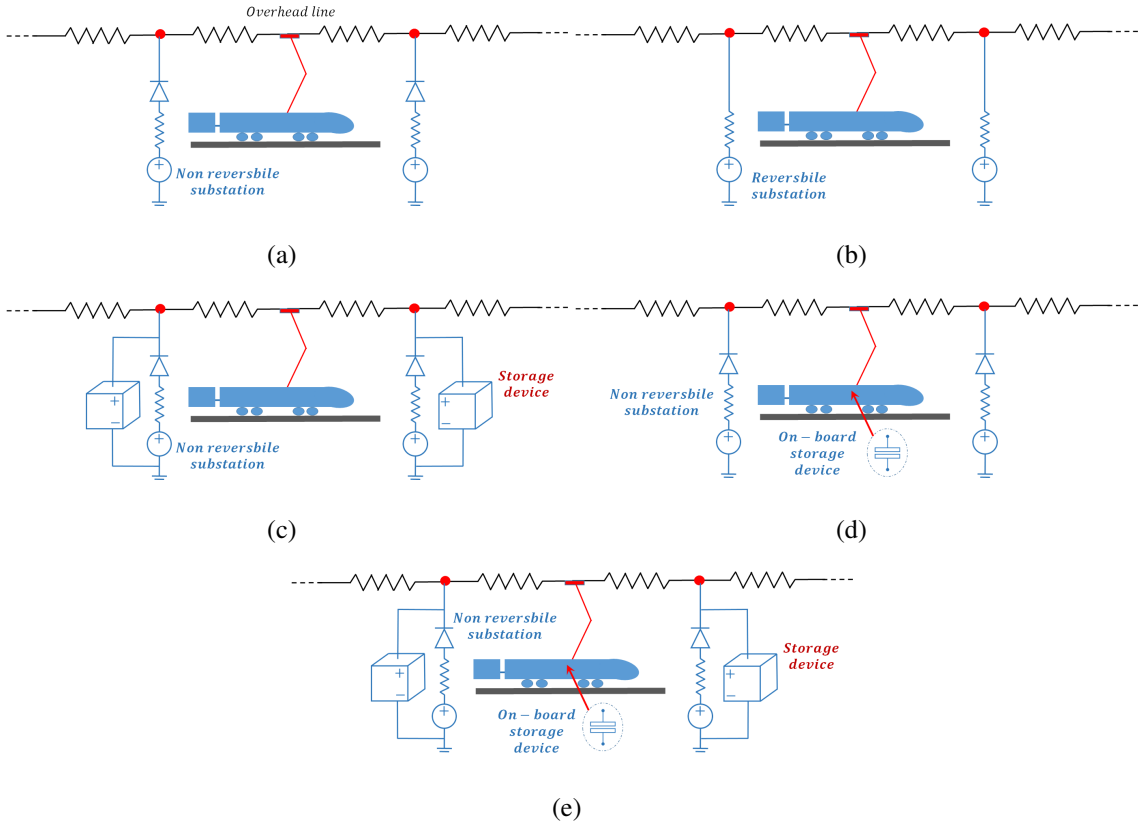

Figure 1.13: Energy storage scenarios: (a) DC non reversible substations, (b) reversible substation, (c) stationary storage devices, (d) on-board storage devices and (e) complete scenario.

braking: Figure 1.13(a) shows the basic configuration, with DC non reversible substations and without energy storage devices (i.e. only other trains can take advantage of the considered vehicle braking energy); Figure 1.13(b) shows the reversible substation scenario, in which the braking energy can be directly sent back to the grid; Figure 1.13(c) includes stationary storage devices connected in parallel to non reversible substations; Figure 1.13(d) shows the use of on-board energy storage devices and finally, Figure 1.13(e) shows a mixed scenario, where both stationary and on-board storage devices are included in the system. The systems characterised by the presence of energy storage devices include three kind of components: the storage device itself, a converter to handle the voltage difference between the line and the storage system and a controller to manage the charge and discharge processes.

The impacts expected from the use of energy storage devices are summarized in Table 1.4, which shows the "4 Cs", i.e. the 4 fundamental challenges [62] a railway system must face: satisfy the customer, improve the system capacity, reduce the system costs and reduce carbon emissions.

The two main parameters to evaluate the performances of a storage system are the specific energy and the specific power:

- the specific energy is the energy that the device is able to store for unit mass and is measured in Wh/kg; a high specific energy value is related to the possibility to store a large quantity of energy with low weights and hence to a higher autonomy;
- the specific power is proportional to the power that the device is able to provide and is measured in W/kg; a high specific power value is particularly useful in applications that require high power values with peaks that greatly overtake the mean power value.

In the railway field the most typical storage devices are batteries and supercapacitors: Table 1.5 shows a comparison between the main characteristics of these systems.

1.2.2.1 Batteries

The battery is a storage device which is able to store and provide electric energy thanks to electrochemical reversible reactions that take place between two different materials (i.e. the electrodes) in an electrolytic solution. These reactions occur within proper receptacles denoted as *cells*, which are the unitary elements that constitute a battery.

Batteries can be classified depending on the reactions inside the cells: Table 1.6 shows the comparison in terms of performances between the most used types of batteries. In particular, the most diffused battery types are the following:

- Pb-acid batteries: among rechargeable devices, they are the most technologically mature and they are widely used. When the battery is fully charged, its electrodes are constituted

Table 1.4: Energy storage devices impacts.

1.	Customer
	1.1 Reduced journey time
	1.2 Improved thermal conditions in subterranean railways
	1.3 Reduced delays due to electric power supply disturbances
2.	Capacity
	2.1 Increase in electric current-carrying capacity
	2.2 Higher vehicle acceleration rates
3.	Cost
	3.1 Reduced electricity consumption
	3.1.1 Traction electricity
	3.1.2 Power losses in the current conductor and electric insulators
	3.1.3 Substation losses
	3.1.4 HVAC energy consumption
	3.2 Reduced peak power demand
	3.3 Better utilisation of electrification assets
	3.3.1 Lower equipment power rating
	3.3.2 Reliability and life expectancy of transformer, rectifier, traction motors and current collection equipment
	3.3.3 Smaller cross section of the electric current conductor
	3.3.4 Simplified stray currents protection
	3.3.5 Increased spacing between power substations
	3.3.6 Gradual transition to discontinuous electrification
	3.4 Minimised costs of thermal conditioning of underground stations
	3.5 Minimised service delays
	3.5.1 Power supply interruptions
	3.5.2 Improved reliability of equipment
4.	Carbon - improved environmental performance
	4.1 CO_2 emissions
	4.2 Electromagnetic emissions of the current collection
	4.3 Particle emission

Table 1.5: Comparison between the main characteristics of batteries and supercapacitors.

Properties	Batteries	Supercapacitors
Operating principle	Redox reactions	Electrostatic energy
Specific energy $[Wh/kg]$	High	Low
Specific power $[W/kg]$	Low	High
Cycles/life sensitivity	Higher	Lower

Table 1.6: Characteristics of the main electrochemical storage devices used for electric traction.

Battery type	Specific energy	Specific power	Efficiency	Life (cycles)
Pb-acid	20-50 Wh/kg	25-300 W/kg	70-90 %	200-2000
Ni-Cd	30-75 Wh/kg	50-300 W/kg	60-80 %	1500-3000
Ni-MH	60-80 Wh/kg	200-250 W/kg	65-70 %	1500-3000
Li-ion	75-200 Wh/kg	100-350 W/kg	90-100 %	1000-10000
Li-Po	100-200 Wh/kg	150-300 W/kg	90-100 %	600-1500
Na-S	120-240 Wh/kg	120-230 Wh/kg	75-90 %	2000-3000
Z.E.B.R.A.	100-120 Wh/kg	150-200 W/kg	85-90 %	> 2500

of lead and lead oxide, while the electrolytic solution is a sulfuric acid solution. During the discharge phase, both the electrodes are reduced to lead sulphate and the electrolytic solution becomes water. The electrodes reactions can be expressed as follows:

- Anode:

$$Pb + SO_4^{2-} \longrightarrow PbSO4 + 2e^-$$

- Cathode:

$$PbO_2 + 4H^+ + SO_4^{2-} + 2e^- \longrightarrow PbSO_4 + 2H_2O$$

Pb-acid batteries take advantage of their low cost, coupled to a good efficiency, to a high reliability and to limited self-discharge phenomena. Nevertheless, with respect to other types

of batteries, they are characterised by a short life and low values of specific energy (even if their specific power is good); furthermore, their performances at high temperatures are poor (requiring the presence a temperature regulation system), they cannot be fully discharged and their disposal is difficult, due to the presence of lead. These batteries are typically used in low cost applications, where the low specific energy and the short life do not represent limitations. In the railway field they are only used as backup batteries for other accumulators.

- Ni batteries: the most common Ni batteries are Nickel-Cadmium (Ni-Cd) and Nickel-Metal Hydride (Ni-MH). In both cases, the positive electrode is nickel hydroxide and the electrolyte is an alkaline solution. The negative electrode is made of metallic cadmium for Ni-Cd batteries and of hydrogen, absorbed in a metal hydride, for Ni-MH batteries. The Ni-Cd battery reactions can be expressed as follows:

  - Anode:

$$Cd + 2OH^- \longrightarrow Cd(OH)_2 + 2e^-$$

  - Cathode:

$$2NiO(OH) + 2H_2O + 2e^- \longrightarrow 2Ni(OH)_2 + 2OH^-$$

  These batteries are characterised by a good reliability and need little maintenance. With respect to Pb-acid batteries, they have higher specific energy and power and a longer life; however, their cost is higher and their efficiency is lower. Furthermore, their self-discharge phenomena are not negligible. In traction applications, Ni-MH batteries are mainly used as backup devices for auxiliary systems; Ni-Cd batteries are usually avoided due to the presence of cadmium.

- Li batteries: rechargeable lithium batteries are based on lithium ions migration from one electrode to the other through the electrolyte. The battery reactions can be expressed as follows:

- Anode:

$$Li \longrightarrow Li^{+} + e^{-}$$

- Cathode:

$$MnO_2 + Li^{+} + e^{-} \longrightarrow LiMnO_2$$

The most used lithium batteries are Li-ion and Li-poly batteries. In Li-poly batteries, the electrolyte is constituted of a solid polymeric compound, while in Li-ion batteries it is constituted of a organic solution. The main advantages of lithium batteries are represented by very high specific energy and specific power, high efficiency, negligible self-discharge phenomena, reliability, long life and absence of capacitive effects. On the other hand, their cost is quite high and they need a control system to maintain their temperature, voltage and $S.O.C.$ within safe limits. These batteries are usually employed in low power applications, but their use in traction systems is quite promising.

An electrochemical storage device can be modelled according to the circuit shown in Figure 1.14 [1].

The circuit includes a voltage generator which represents the open circuit voltage (i.e. OCV); the voltage drops are represented through an internal resistance $R_{batt,1}$ and a RC parallel connection which models the charge diffusion and transfer phenomena. The contribution to voltage drops due to the RC parallel is significantly lower than that due to the resistance $R_{batt,1}$.

Figures 1.15 and 1.16 show the typical charge and discharge behaviour of Li-ion batteries [63]. These Figures are referred to real high performance Li-ion batteries: it is possible to highlight the presence of an operating range where the battery voltage is almost constant even if the $S.O.C.$ is varying. Through the use of proper devices, a battery should always be used in proximity of this part of its operating range.

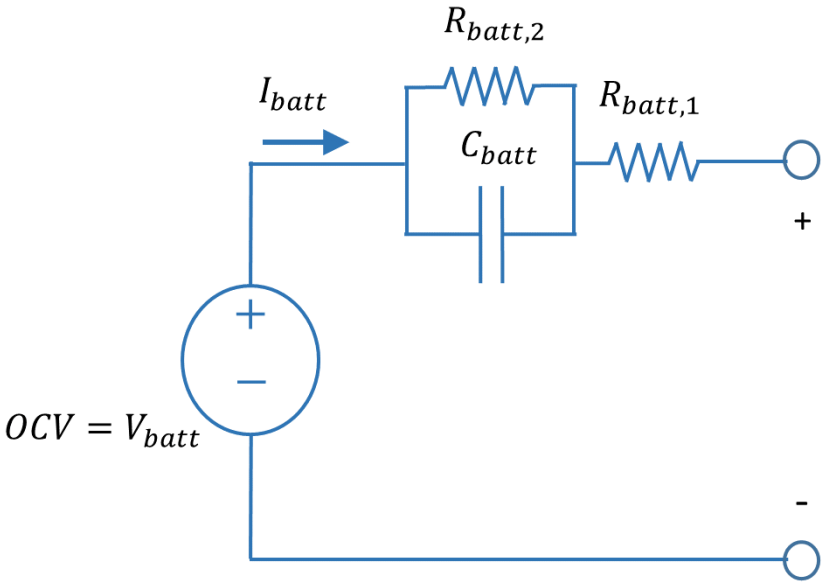

Figure 1.14: Electric scheme of a Li-ion battery.

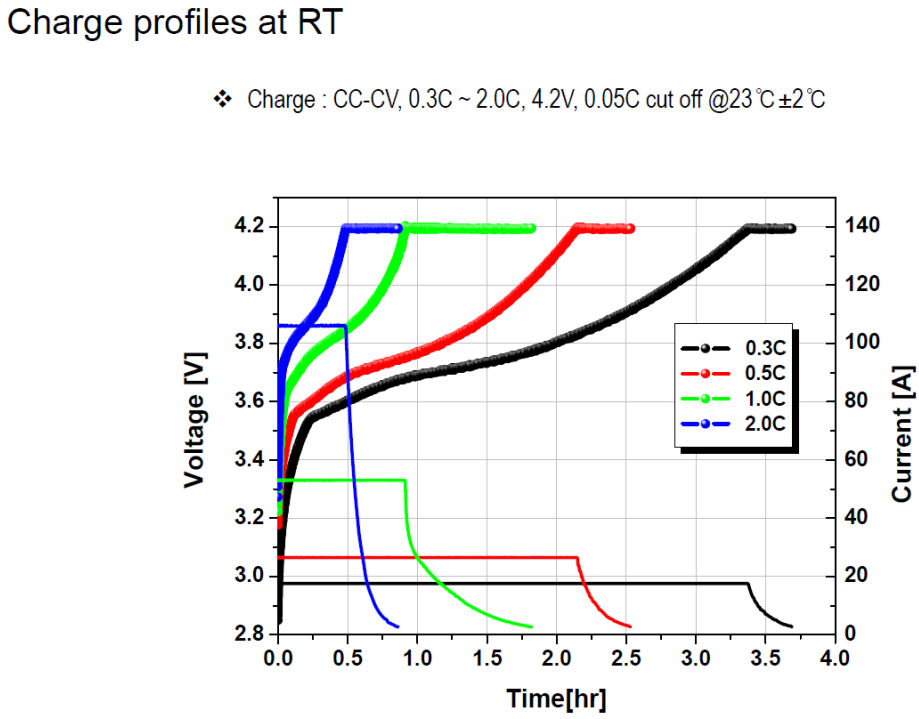

Figure 1.15: Typical battery charge behaviour [63].

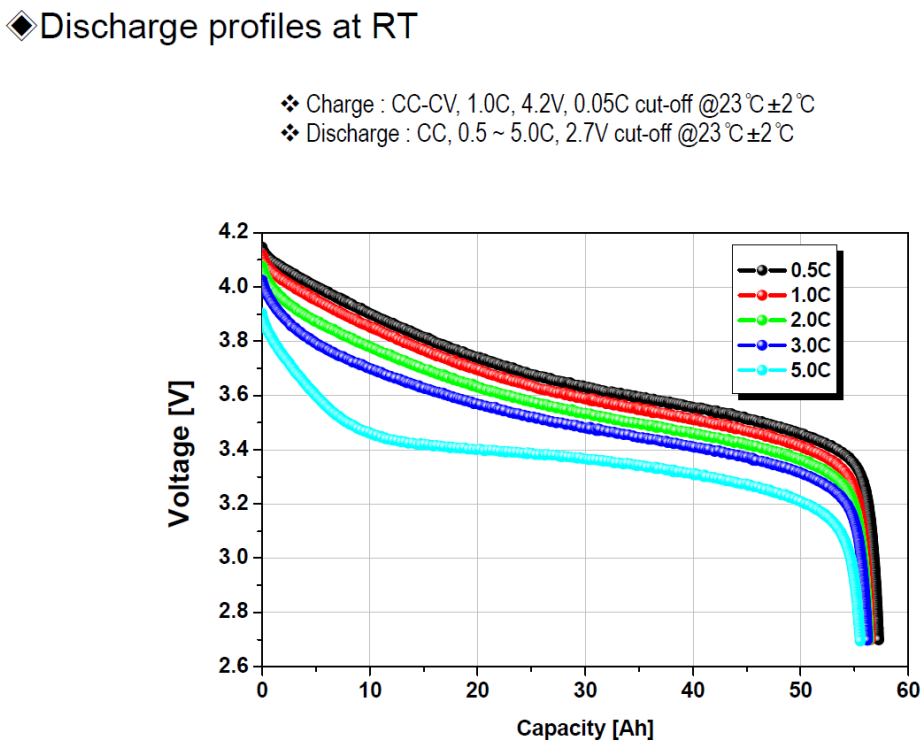

Figure 1.16: Typical battery discharge behaviour [63].

1.2.2.2 Supercapacitors

Electric double-layer capacitors (EDLC), usually denoted as *supercapacitors*, are energy storage devices which operate in the same way as conventional electrolytic capacitors: the energy is stored in an electric field through charge separation, without chemical reactions.

Supercapacitors are characterised by the presence of a large electrodes surface, by a high electrical permittivity dielectric element and by a low value of charge separation: thanks to these characteristics, the specific energy of supercapacitors is higher than that of classical capacitors.

Equation 1.10 shows how energy density u (i.e. the energy that can be stored per unit volume) is directly proportional to vacuum permittivity ϵ_0 and inversely proportional to the distance d between charges:

$$u = \frac{1}{2}\epsilon_0 \left(\frac{V}{d}\right)^2 . \tag{1.10}$$

The absence of electrodes chemical reactions allows supercapacitors to be characterised by a very low internal resistance, which corresponds to a high efficiency, usually about 95%. A typical supercapacitor can usually operate for about 10^6 charge/discharge cycles.

Furthermore, supercapacitors can manage very fast charge/discharge cycles with high currents, they can be fully discharged (while batteries usually suffer from full discharge cycles) and they can operate in a wide range of environmental conditions.

The main advantage of supercapacitors, with respect to other storage systems, is their high specific power, while the low specific energy represents their main disadvantage [64].

Another important advantage is that the state of charge of the supercapacitor, being proportional to the voltage, can be easily measured through a simple voltage measurement.

Thanks to these features, supercapacitors are a promising solution for energy storage in railway and high power applications; in particular, thanks to their fast dynamical behaviour, they are able to easily handle power peaks and to stabilize the line voltage.

EDLCs behaviour can be modelled through the circuit shown in Figure 1.17 [65]. The first branch of the circuit includes a resistance $R_{sc,1}$ and a capacitance $C_{sc,1}$ and represents the device behaviour

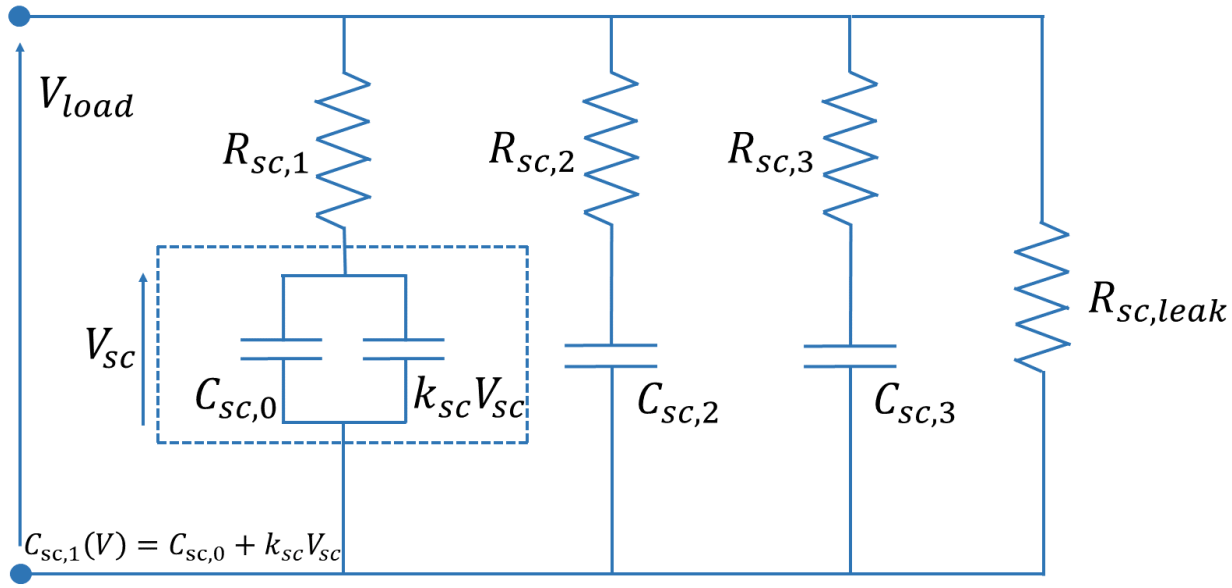

Figure 1.17: Electric scheme of a supercapacitor.

in the $10^{-3} \div 10^{-1} Hz$ frequency range; the second branch represents the device behaviour in the $10^{-6} \div 10^{-3} Hz$ range. The resistive branch connected in parallel represents the leakage resistance $R_{sc,leak}$ (usually about $2500 \div 5000 \Omega$) related to self-discharge phenomena.
The capacitance of the first branch can be expressed as follows:

$$C_{sc,1} = C_{sc,0} + k_{sc} V_{sc}, \tag{1.11}$$

where $C_{sc,0}$ is a constant capacity term, V is the capacitor voltage and k_{sc} is a constant.
Finally, the second branch represents the charge redistribution phenomenon.

1.3 Object oriented modelling languages for simulation models

Most of the previously cited research works analyse (in terms of simulation, design and optimisation) the use of energy storage systems in railway applications through simulation models developed to reproduce the following aspects:

- An accurate simulation of the railway vehicle longitudinal dynamics with a particular attention to power balances, especially during traction and braking phases.
- An electrical model of the overhead electrical line able to reproduce the effects of catenary and substations equivalent impedance, according to the line topology and to the relative positions of the loads represented by travelling trains.

In order to understand the feasibility of energy storage systems, a wide variety of different simulation scenarios should be analysed; furthermore, a high level of customization is needed to adapt models to different kind of railway vehicles, line layouts and operating conditions. Models should adopt a parametric approach to perform a large number of simulations and customized blocks must allow to be easily assembled by users with different levels of skill. Due to these reasons, the usage of high level languages is mandatory and often proposed in more recent works: Fernandez et al. developed a MATLAB®-Simulink® model of an electric power system for tramways [66], Uzunoglu et al. [67] used the MATLAB®-Simulink® environment, coupled with the SimPowerSystems tool, to analyse the behaviour of a hybrid supercapacitor system, and Hannan et al. [68] developed a MATLAB®-Simulink® control system for the management of the energy sources in electric vehicles. In particular, Pugi [69] and Conti [70] in recent works adopted a modular architecture based on MATLAB®-Simulink®, which is the current standard for the simulation of dynamical systems and the prototyping of applications involving control, diagnostic and signal processing. One of the limits of a pure MATLAB®-Simulink® architecture, such as that proposed in [69] and [70], is represented by the modelling compromises that have to be introduced to preserve code modularity and numerical efficiency. In particular, redundant integrated state are often added to the model in order to reduce algebraic loops or solve implicit

algebraic relationships, with significant losses also in terms of accuracy. More recent object oriented languages like Modelica® [30] or MATLAB®-Simscape™ allow the user to describe the response of a component in terms of balance equations, following an approach which clearly resemble the Bond-Graph one (approach also followed by Ramakrishnan et al. [71] for the analysis of the dynamical behaviour of mechatronics systems). In particular, MATLAB®-Simscape™ allows the modelling of physical systems through a lumped parameters approach, considering the constitutive equations of each element of the system: while a MATLAB®-Simulink® block receives an input and, based on the mathematical operations implemented within itself, provides an output, a MATLAB®-Simscape™ block contributes to the complete model through a set of algebraic or differential equations. The complete system of equations is then solved applying a symbolic approach. The MATLAB®-Simscape™ environment has a series of built-in physical domain, each containing a set of the elements usually employed in lumped parameters modelling. Furthermore, it is possible to develop custom domains and blocks written in the MATLAB®-Simscape™ programming language. A MATLAB®-Simscape™ model handles physical variables, considering also their units of measurement, while a MATLAB®-Simulink® model only handles numerical signals; however the two environments can be completely connected, coupling blocks developed in both ways. The main advantages of this innovative approach can be summarized as follows:

- Optimisation of the number of integrated states: the balance equations of each component are symbolically pre-processed in order to minimise the number of integrated states, avoiding the usage of redundant auxiliary states; this increases the numerical efficiency of the model and reduces the memory consumption without losses of accuracy.

- Bidirectional correspondence between the model topology and the modelled physical system: the elements of the model are implemented in terms of physical balances with respect to an assigned set of variables which depends on the specific definition of the considered physical domain (e.g. mechanical and electrical). Therefore, a single line graphical link between sub-models is automatically associated to a bidirectional exchange

of variables that reproduces the physical interactions of the modelled physical network. This feature provides important benefits in terms of modularity, simplicity and ease of use.

More details on the object oriented modelling approach followed in this research work will be given in Chapter 2.

1.4 Objectives of the thesis and architecture of the proposed model

With respect to the current state of the art, summarized in the previous paragraphs, in this work an innovative modelling approach useful to deal with the following aspects has been proposed:

- the use of regenerative electric braking within High-Speed railway systems;
- the application of energy storage systems to High-Speed railways;
- the optimisation of High-Speed railway systems in terms of energetic efficiency;

Energy recovery in High-Speed trains is a quite new field of analysis, because the advantages deriving from this application are harder to achieve with respect to light railway systems; the braking frequency and the energy involved in the manoeuvre in High-Speed railway systems are not optimal to use the same solutions found in light railway, and hence a deep analysis is needed to fully understand the possible recovery perspectives. The potential energy recovery in this sector is significant, and an accurate analysis could lead to identify how to exploit it. Furthermore, the use of the innovative MATLAB®-Simscape™ language allows to obtain accurate results with a great numerical efficiency, providing the possibility to perform a large number of simulations and investigate many different scenarios. This feature is essential to be able to perform an energetic optimisation of the system.
In order to correctly analyse the energetic prospects of the considered railway systems, before the feasibility and optimisation analyses, the proposed model has been experimentally validated considering a classical commuter train scenario and a new High-Speed Italian system.
The proposed model, whose general architecture is shown in Figure 1.18, includes two main sub-models, developed using an object oriented approach:

- a vehicle dynamical model, which simulate the train longitudinal dynamics;
- an electrical model, which includes the feeding line, the electrical substations and the storage devices.

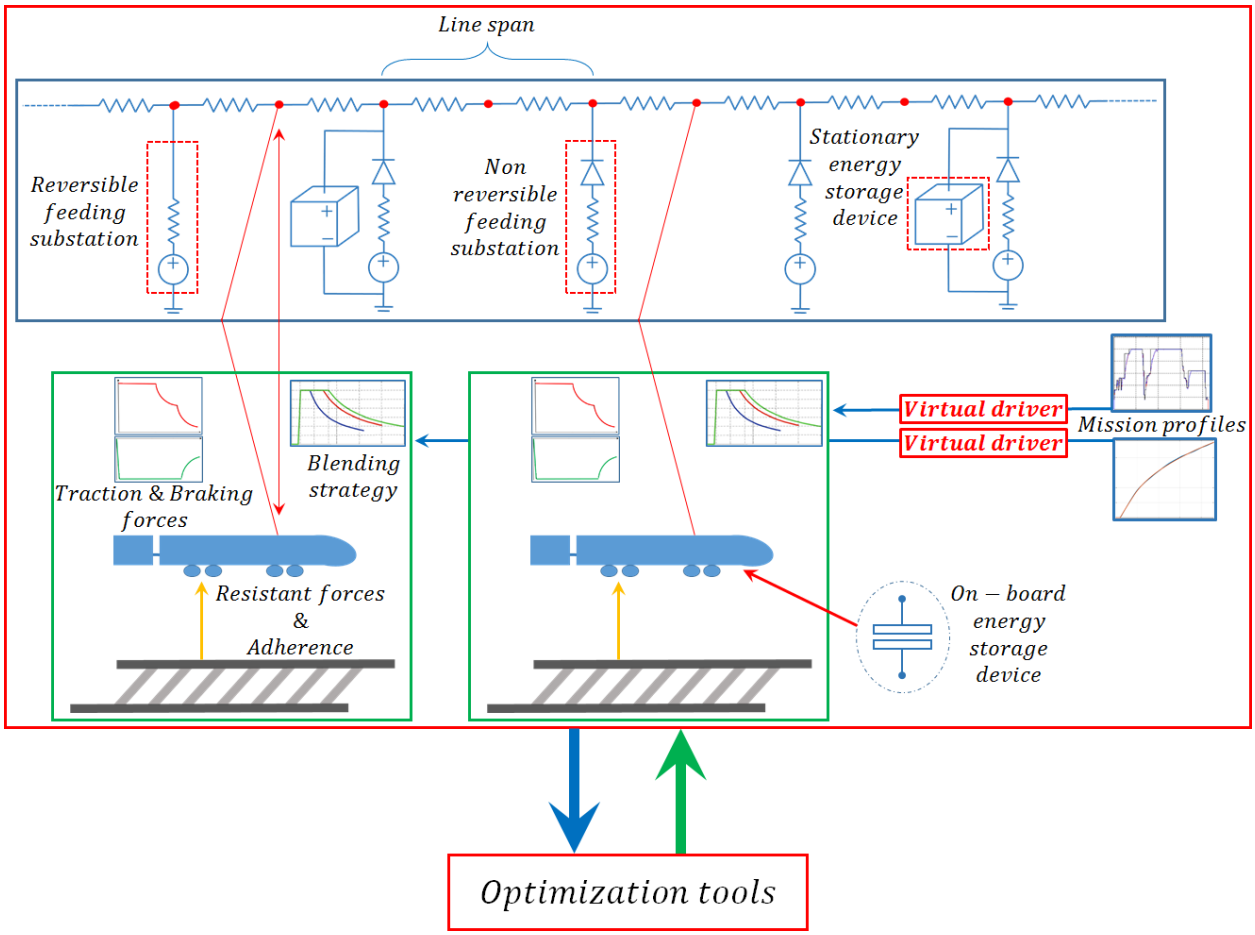

Figure 1.18: General architecture of the proposed model.

The two sub-models are simulated together in the time domain and are fully coupled with each other: the vehicle sends to the line its kinematic and energetic quantities and the line provides the electrical quantities needed by the vehicle. This couple of sub-models represent the basic unity of the proposed model: the line can be easily assembled to represent complex topologies and can include more than one travelling vehicle in both directions (see Chapter 2).

A set of simulations in the time domain, considering different scenarios and different operating parameters, allows to perform a large number of analyses in terms of feasibility for different solutions. Furthermore, in order to perform a complete optimisation of the system, the time domain model has been included in two optimisation tools (in order to compare results and computational performances): the first tool is a MATLAB® optimisation algorithm which

can easily handle the proposed MATLAB® model, while the second tool is the optimisation environment modeFRONTIER developed by ESTECO SpA, which can handle the MATLAB® model and also couple it with other simulation tools (i.e. within the TESYS Rail project, the software has been used to couple the proposed model with a model developed by Ansaldo STS and with a model developed by the University of Napoli Federico II which takes into account the behaviour of the signalling system).

The optimisation of a railway system should take into account a large set of variables: the actual energy flows and consumptions, the peculiar characteristics of the system and the potential of the proposed solutions. In fact, each technical solution should be considered from the energetic, technical and economic points of view.

Furthermore, each technical solution interacts with each other: the implementation of more than one technical solution can enhance or worsen the final results. All the different stakeholders have different objectives and interests from the system and traffic and passengers volume can vary in a completely random way (in addition to drivers behaviour, climate and other variables). Finally, each technical solution should be compared to the strong uncertainties on the systems characteristics and, above all, to the unknown future developments foreseen for the system, including both line topology and vehicles.

2

Materials and methods

Chapter 2 focuses on the exposition of the developed model, including an outline of the theory needed for a better understanding of the proposed approach, of the mathematical and software instruments needed during the research work and of the technical and experimental materials used to develop, validate and exploit the proposed modelling approach.
The proposed approach includes the following sub-systems:

- dynamical model of the vehicle;
- electrical model of the line, which includes:
  - substation models;
  - feeding line model;
  - storage devices models;
- multi-vehicle approach;
- vehicles library;
- optimisation tools;

the Chapter will thoroughly analyse these sub-systems in order to coherently analyse the obtained results (shown in Chapter 3).

The first part of the Chapter is devoted to the analysis of the core components of the model: the vehicle dynamical model and the line electrical model. The dynamical part simulates the vehicle motion, taking into account the forces which act on the train and the inputs that come from the feeding line. The electrical part simulates the behaviour of the elements of the feeding line, which answers the vehicle requests in terms of electrical quantities and imposes its limits to the vehicle motion itself.

The fundamental goal of the core part of the model is the evaluation of the vehicle power request for a certain mission profile (imposed by the user or by timetables) and, hence, of the energy that can be recovered through a proper use of regenerative braking, taking into account vehicle and line limits.

The vehicle and line models have been developed in the MATLAB® environment, using Simulink® to set the simulation environment and the Simscape™ language for its important advantages in representing the behaviour of physical systems.

The multi-vehicle approach and the vehicles library are important extensions of the core sub-models: they allow to extend the depth of the analysis and perform important comparisons. They are developed in the same modelling environment of the core tools.

Finally, this research work has taken advantage of different optimisation tools: the first one is developed in MATLAB® and the second one is the optimisation tool modeFRONTIER developed by ESTECO SpA.

In the following Sections, the main features of the elements of the proposed approach will be exposed, highlighting its novelty and the tools needed to develop it. Finally, the real operating scenarios considered as a test cases will be exposed, in order to provide a better understanding of the results obtained in this research work.

2.1 Dynamical model of the vehicle

The mechanical behaviour of the train is modelled using a simplified lumped parameters approach [72]. The model is developed using the MATLAB®-Simulink® environment coupled with a series of object oriented MATLAB®-Simscape™ blocks. Figure 2.1 shows the general architecture of the mechanical sub-model: the user can impose a position-based mission profile (alternatively, the mission profile can be calculated within the model considering the vehicle timetable) and, through the comparison with the current velocity of the vehicle, a virtual driver regulates the traction or braking requests. These forces are dynamically applied and properly saturated considering adherence limits. The calculation of the train motion takes into account both traction and braking forces and various resistant loads. Traction and braking forces and the vehicle velocity are then used to calculate the requested or provided power, taking into account a blending strategy chosen by the user and the electrical and mechanical efficiency of the system. This model provides, to

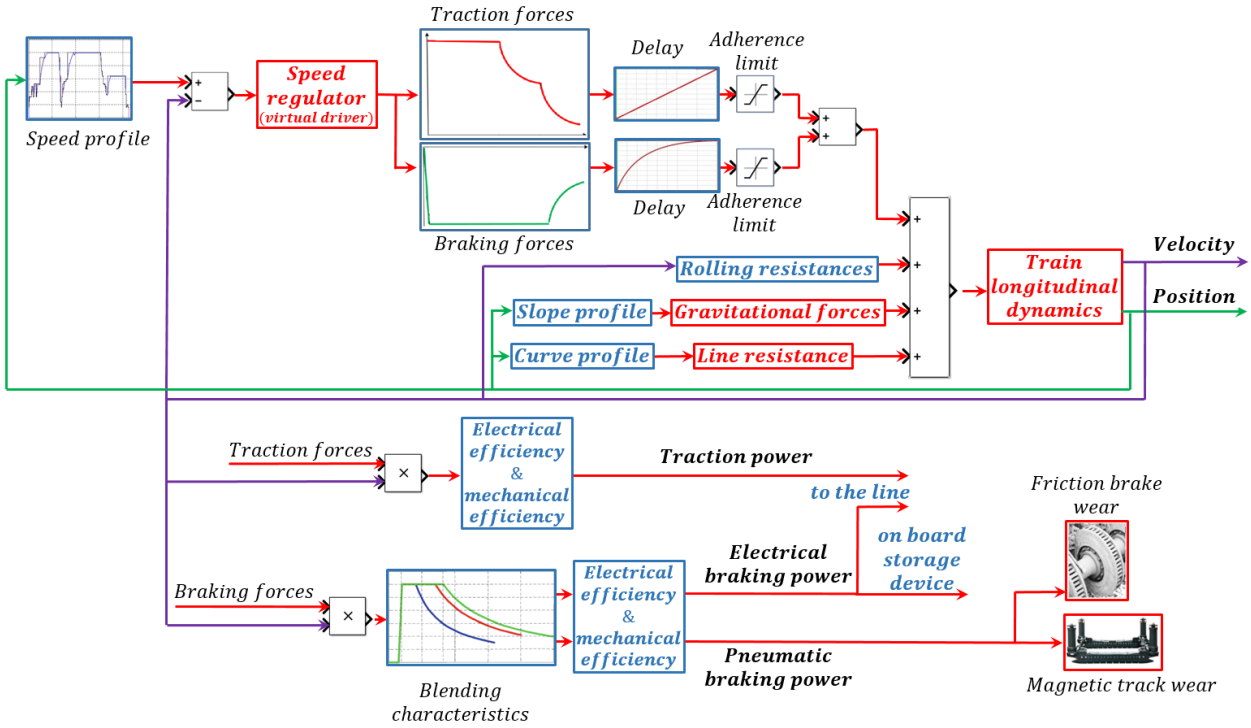

Figure 2.1: Architecture of the vehicle dynamical model.

the electrical part, the train position and the electrical traction and braking power; the pneumatic braking power can be used to estimate the wear of the braking system.
The main outputs of the mechanical model are the vehicle power request (which takes into account mechanical and electrical efficiencies), its position and velocity and the braking electric power, which is sent back to the line.

2.1.1 Vehicle longitudinal dynamics

The longitudinal dynamics of the vehicle can be analysed according to the following equation of motion:

$$m_i \ddot{x} = T - mg \sin \alpha - m\left(a\dot{x}^2 + b\dot{x} + c + d\,(r)\right) - mgi_c, \tag{2.1}$$

where m_i is the inertial mass of the vehicle, m is the vehicle mass, x is the position of the train within the line, $\alpha\,(x)$ is the slope of the line, a, b, c, $d\,(r)$ are equivalent coefficients used to calculate motion resistances as a function of speed (a, b), internal frictions of the train (c) and additional resistances ($d\,(r)$) due to curves with radius $r\,(x)$, i_c represents the resistances due to line curves and T represents the total longitudinal forces applied by traction or braking systems.
The longitudinal forces term T represents the sum of the longitudinal efforts exchanged between motorized wheelsets and rail; these forces are related to friction effects between these rolling elements. Due to the high normal loads (i.e. about 21 t per axle), the contact surfaces must be made of metal; furthermore, the longitudinal forces are limited by the available adherence.
The forces due to the altimetric profile of the track (F_p) depend on the line slope; in railway, the slope i is usually very limited (i.e. <20‰), hence $\sin \alpha$ can be substituted by the slope itself:

$$F_p = -mg \sin \alpha \approx -mgi. \tag{2.2}$$

Motion resistances F_a include the contribution of a number of different phenomena: contact losses due to wheel/rail contact, friction and internal losses of the system (e.g. bearings and transmission systems) and aerodynamic losses.

The calculation of these losses is typically based on second order polynomial interpolation formulas which depend on the vehicle velocity and mass. The values of the coefficients a, b, c and d used in the considered formula depend on the vehicle and can be obtained through the analysis of experimental data.

The resistant forces due to line curves F_c are calculated as an additional term to be added to slope losses; each curve is represented as an equivalent slope (denoted as i_c) which depends on the curve radius r and can be expressed as follows:

$$\begin{cases} i_c = \frac{650}{r-55}‰, & r > 400\,m \\ i_c = \frac{750}{r}‰, & 150\,m < r < 400\,m \\ i_c = 5‰, & r < 150\,m \end{cases} . \tag{2.3}$$

Finally, the inertial contribution to longitudinal motion F_i can be calculated through the d'Alambert approach:

$$F_i = -m_i a = -m_i \ddot{x}, \tag{2.4}$$

where the inertial mass m_i represents the vehicle equivalent inertia that contributes to longitudinal translation, including also the contribution of rotating masses (e.g. wheelsets, motors, transmission systems). For this reason, the equivalent inertia m_i is usually higher than the vehicle mass and can be evaluated by increasing the vehicle mass of about $5 \div 10\%$.

The sum between traction, braking and resistant forces provides the vehicle acceleration:

$$a = \frac{T - (F_a + F_c + F_p)}{m_i}. \tag{2.5}$$

F_c and F_p can be easily evaluated through the use of Simulink® LookUp tables, which perform the interpolation of the vehicle technical data as functions of the train position, velocity and longitudinal forces; F_a makes use of a set of coefficients which are usually directly found within the vehicle technical data.

The train acceleration can be integrated twice, thus obtaining the vehicle velocity and position: these values are then used as inputs in other parts of the model.

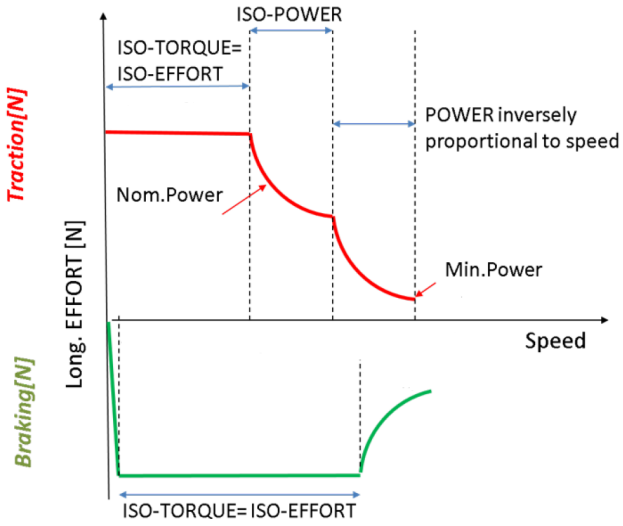

Figure 2.2: Typical traction and braking curves for an electric train.

2.1.2 Traction and braking efforts

Figure 2.2 shows typical traction and braking curves for a High-Speed train. Starting from the traction phase, the traction effort trend, as a function of the vehicle speed v, is calculated according to the following cycle:

if $v < v_{\text{nom}}$

$\quad \text{T}(v) \leftarrow \text{T}_{\text{nom}}$

else if $v >= v_{\text{nom}}$ and $v < v_{\text{max,iso}}$

$\quad \text{T}(v) \leftarrow \frac{W_{\text{nom}}}{v}$

else

$\quad \text{T}_{\text{iso}} \leftarrow \frac{W_{\text{nom}}}{v_{\text{max,iso}}}$

$\quad \text{T}(v) \leftarrow \frac{\text{T}_{\text{iso}} \cdot v_{\text{max,iso}}^2}{i^2}$

end

This cycle reproduces the ideal trend shown in Figure 2.2: this curve directly represents the vehicle behaviour but its trend is derived from the operating curve of the electric motor itself. Figure 2.3 shows the performance curves of a generic asynchronous motor. This type of electric motor operates at constant torque for the lower speed range; once reached the maximum operating power,

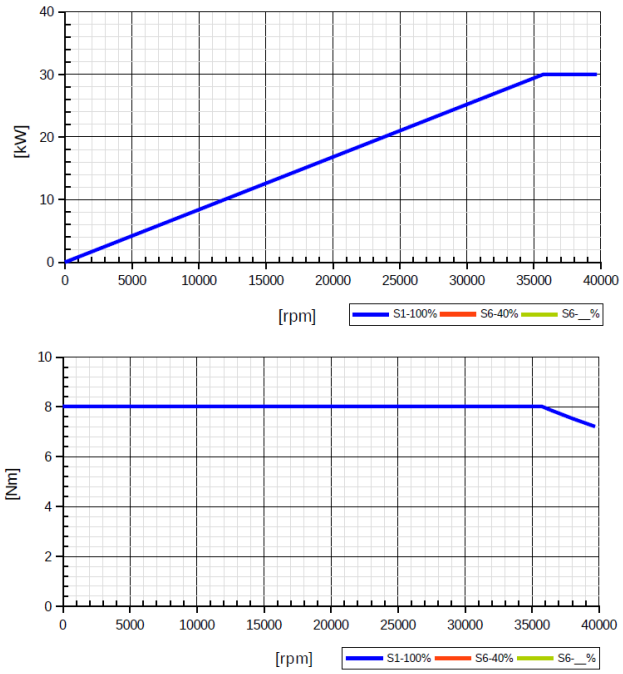

Figure 2.3: Electric motor operating curves.

the torque decreases and the motor operates in isopower regime, and, finally, the last part of the operating range is characterised by a steeper decrease of the torque value.

More in detail, referring to Figure 2.2 for the railway case, for vehicle speeds lower than the nominal speed v_{nom}, the traction effort follows the isotorque regime, according to the following Equation:

$$W = Tv, \tag{2.6}$$

i.e. the power request W is directly proportional to the vehicle speed v.

Once the vehicle has passed the nominal speed, but is still below the maximum isopower speed $v_{max,iso}$, the system operates in isopower regime, where the speed increases by decreasing the traction effort as follows:

$$T = \frac{W}{v}. \tag{2.7}$$

The third part of the operating range goes from the maximum isopower speed $v_{max,iso}$ to the vehicle maximum speed v_{max}; in this operating range the traction effort decreases strongly and can be

calculated as follows:

$$T = \frac{T_{iso} \cdot v_{max,iso}^2}{v^2}. \tag{2.8}$$

The parameters used to determine the characteristic curve of the vehicle can be calculated as follows:

- Nominal traction effort:

$$T_{nom} = m \cdot a_{max}; \tag{2.9}$$

- Maximum acceleration (a_{max}): included in the vehicle technical data;
- Nominal speed:

$$v_{nom} = \frac{W_{nom}}{T_{nom}}; \tag{2.10}$$

- Maximum isopower speed ($v_{max,iso}$): included in the vehicle technical data.

In addition to the dependency on the vehicle speed, the traction effort, which is always saturated by the available adherence, depends also on the power supply system (e.g. 3 kV DC as in the considered High-Speed test case) and on the operating conditions (e.g. dry and wet). The model can take into account these dependencies through the use of multi-dimensional LookUp tables. In fact, for a numerical implementation, the use of LookUp tables is more robust and allows to represent also train performances which are, for various reasons, not strictly adherent to the ideal curves.

Concerning braking efforts, two strategies must be taken into account: the first one is referred to braking in normal conditions while the second one is based on TSI specifications and is used to impose further limits on adherence. For both cases, the data needed for the model implementation can be taken from the vehicle technical data.

The management strategy of the different braking systems during the braking phase is usually called blending (see Leigh [73] for a review of railway braking systems and their interactions): the braking effort must be properly split between the mechanical and the electrical system and also between the regenerative and the dissipative electrical braking systems. While most of

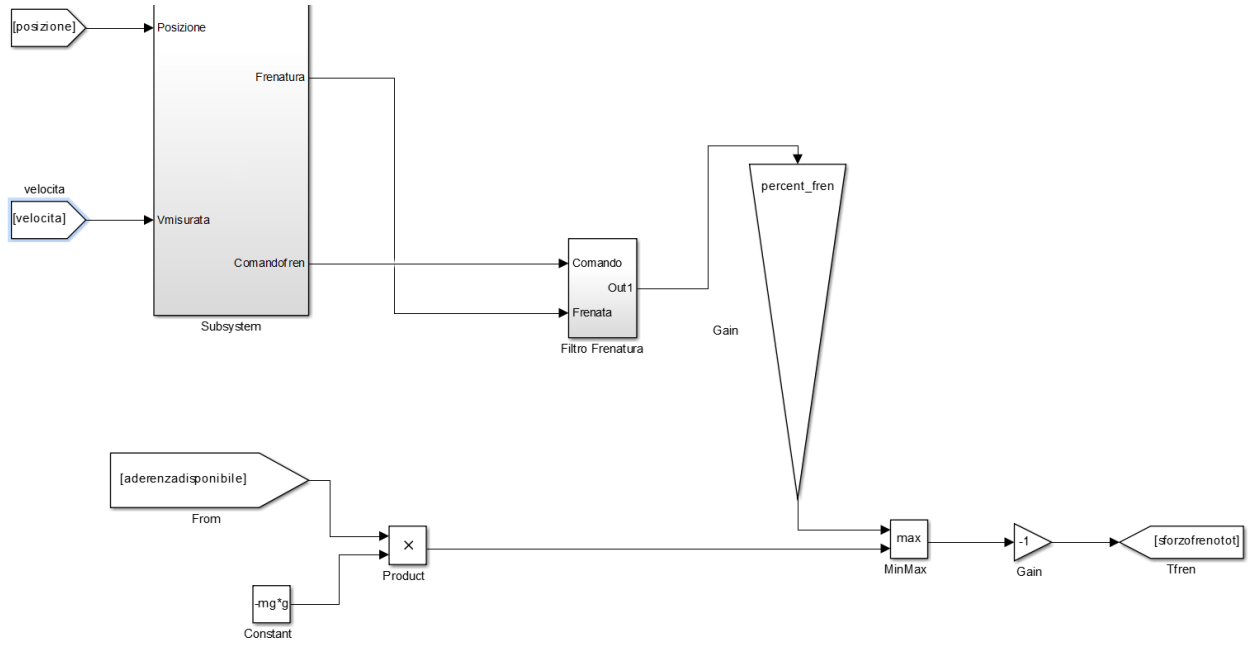

Figure 2.4: Simulink® scheme for the calculation of braking efforts.

the results shown in this thesis are referred to a 100% electric braking blending strategy (i.e. pneumatic braking is only used when the vehicle braking request exceeds the available electric braking power), the user can choose any blending strategy and analyse different technical solutions. Furthermore, the user can, through the set up of the blending strategy, choose how to recover or dissipate electric braking energy: since the feeding line can not always handle all the braking energy, the user can choose to dissipate the exceeding energy or to completely turn off regenerative braking (see Sections 2.1.7 and 2.2).

The available electric braking depends on the vehicle speed and on the maximum regenerated power that the motor drive can handle.

Figure 2.4 shows the proposed Simulink® model for the braking phase: it is interesting to highlight how, in addition to the adherence limit, the user itself is able to regulate the braking effort through the internal variable *percent_fren* (see Section 3.3 for more details). Furthermore, the braking effort, as well as the traction one, is applied through a command which is driven by the velocity error and properly filtered in order to reach the comfort characteristics prescribed by regulations (see Section 2.1.6).

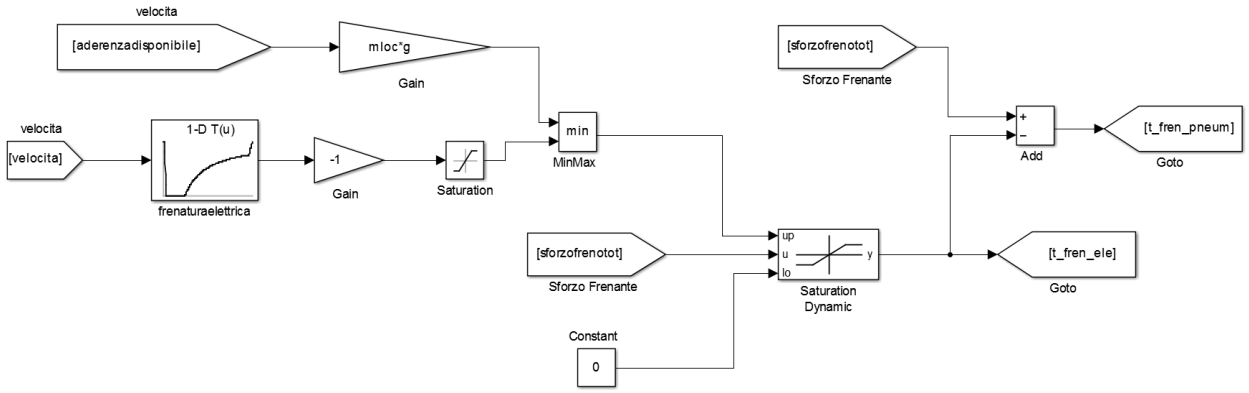

Figure 2.5: Simulink® scheme for braking blending: electrical part.

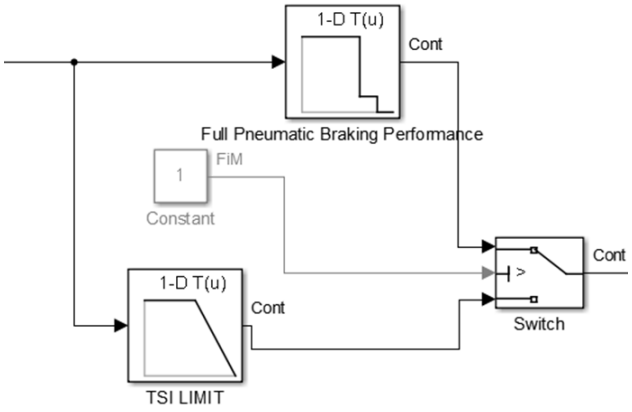

Figure 2.6: Simulink® scheme for braking blending: pneumatic braking and TSI limits.

Figures 2.5 and 2.6 show part of the implementation of the blending model: in particular, Figure 2.5 shows the management of the electric braking part, while Figure 2.6 shows the management of pneumatic braking and TSI limits.

The maximum longitudinal forces applied in the traction and braking phases are calculated according to multi-dimensional tabulated relationships which depend on the train speed and reproduce the curves reported in Figure 2.2.

2.1.3 Adherence

Traction and braking efforts are exchanged between vehicle and track at the wheel/rail interface and it is fundamental to take into account the available adherence, which depends on different parameters, such as the vehicle speed.

Within the proposed model, proper saturation elements have been introduced in order to reproduce the effect of the limited wheel-rail adhesion along the line; in particular, the traction force T_t and the braking one T_b, which can be exerted as a function of the available adherence μ, are calculated according to Equations 2.11 and 2.12:

$$T_t \leq T_{t,max} = k_m m g \mu, \tag{2.11}$$

$$T_b \geq T_{b,max} = -m g \mu. \tag{2.12}$$

The coefficient k_m is denoted as motorized weight fraction and is defined as the ratio between the vertical load on motorized axis and the total weight of the train; for the ETR 1000 the value of this coefficient is about 0.5.

Within the proposed model, the value of the wheel-rail adhesion μ is calculated both according to

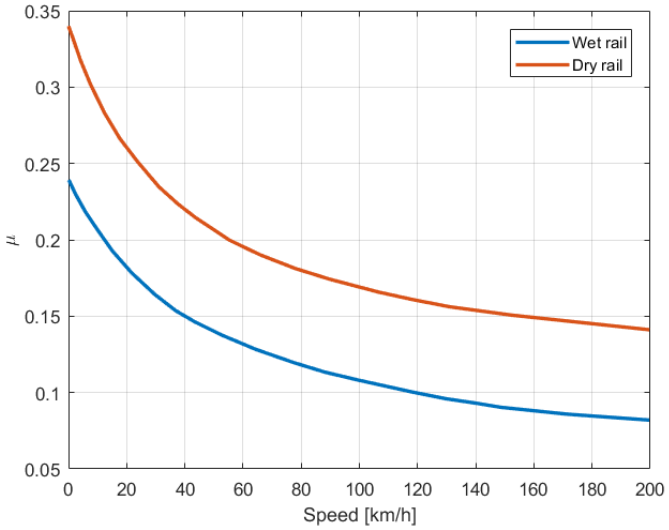

Figure 2.7: Muller correlation for adherence calculation.

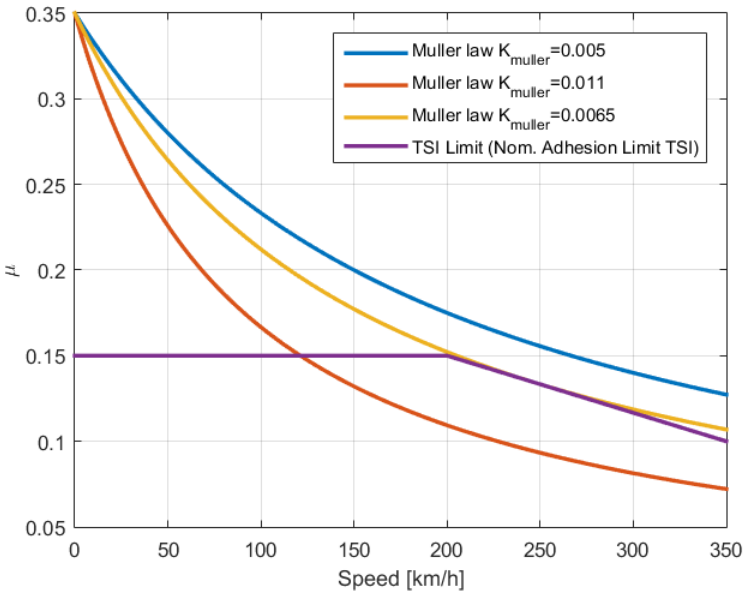

Figure 2.8: Wheel-rail adhesion as a function of the vehicle speed: comparison between the Muller model and TSI limits.

TSI limits and through the Muller correlation, taking into account the dependency of the available adherence on the vehicle speed:

$$\mu = \frac{f_0}{1 + k_{muller}\dot{x}_{kmh}}, \tag{2.13}$$

where f_0 is the static value of the friction factor, which typically varies between 0.35 and 0.4, $\dot{x}_{kmh}$ is the train speed expressed in km/h and k_{muller} is a scaling parameter which ranges between 0.005 and 0.011.

Figure 2.7 shows the Muller correlation for wet and dry operating condition, while Figure 2.8 focuses on the comparison between the Muller model and TSI adherence limits. As reported in Figure 2.8, it should be noticed that the wheel-rail adhesion predicted according to Equation 2.13 in a speed range between 200 and 350 km/h for a value of k_{muller} equal to 0.0065 is quite similar to the available adhesion prescribed by TSI regulations for the design of braking systems.

2.1.4 Virtual driver

Traction and braking manoeuvres are calculated with respect to an assigned speed profile through a PID regulator, which acts on the difference between the desired velocity and the current train velocity; this regulator has been developed in a previous version of the model [70]. The proposed control strategy (shown in Figure 2.9) is quite simple: the speed regulator is used to calculate the traction and braking forces needed to drive the train respecting the desired speed profile. The desired speed profile could be influenced by the line layout, by the timetable and by the signalling system. The virtual driver should represent the action of the human driver: hence the P.I.D. controller has been developed to act with a low dynamics and to tolerate velocity errors of about 2 m/s.

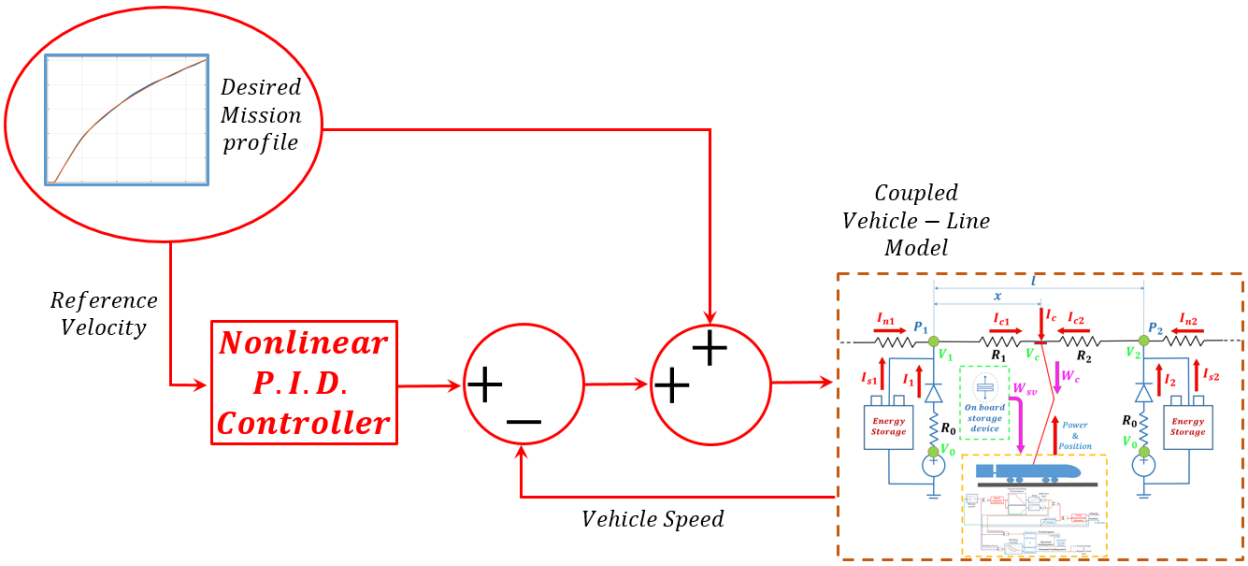

Figure 2.9: Scheme of the virtual driver implemented in the proposed model.

2.1.5 Power calculation

After the calculation of the longitudinal effort T, it is possible to determine the mechanical power W_m, delivered to the vehicle by the traction system, as follows:

$$W_m = T\dot{x}. \tag{2.14}$$

By adding this term to the power needed by on-board auxiliary systems (e.g. lights, air conditioning and plugs), it is possible to calculate the power that the vehicles requires from the line in correspondence of the pantograph.

During the braking phase, both the traction system, the conventional pneumatic brake and the motion resistances cooperate to dissipate the kinetic energy of the train; thus, a part of the mechanical power W_m (denoted as W_{mb}) is dissipated by the pneumatic brake, another part (denoted as W_{mr}) is dissipated by motion resistances, and the remaining part (denoted as W_e) is converted in electrical power by the traction system itself.

The converted power W_e can be dissipated on on-board resistors (dissipative braking, $W_{e,diss}$) or transferred to be stored or reused (regenerative braking, $W_{e,reg}$); these two terms can be calculated as follows:

$$W_{e,reg} = \eta_e W_e, \tag{2.15}$$

$$W_{e,diss} = W_e - W_{e,reg}, \tag{2.16}$$

where η_e is the electrical efficiency of the on-board traction system.

As previously exposed, most of the results exposed in this work are referred to a blending criterion that in normal operating conditions maximises W_e against W_{mb} (according to the maximum performance curves of the considered test cases, see Sections 2.6 and 2.7), but the model allows the use of any blending criteria.

It is possible to define a conversion efficiency η_{tot} (which depends on the vehicle speed and longitudinal effort) as follows:

$$\eta_{tot}(T, \dot{x}) = \eta_e \eta_m = \begin{cases} \eta_{tot} = \frac{W_m}{W_e} & if\ W_m \geq 0 \\ \eta_{tot} = \frac{W_e}{W_m} & if\ W_m < 0 \end{cases}. \tag{2.17}$$

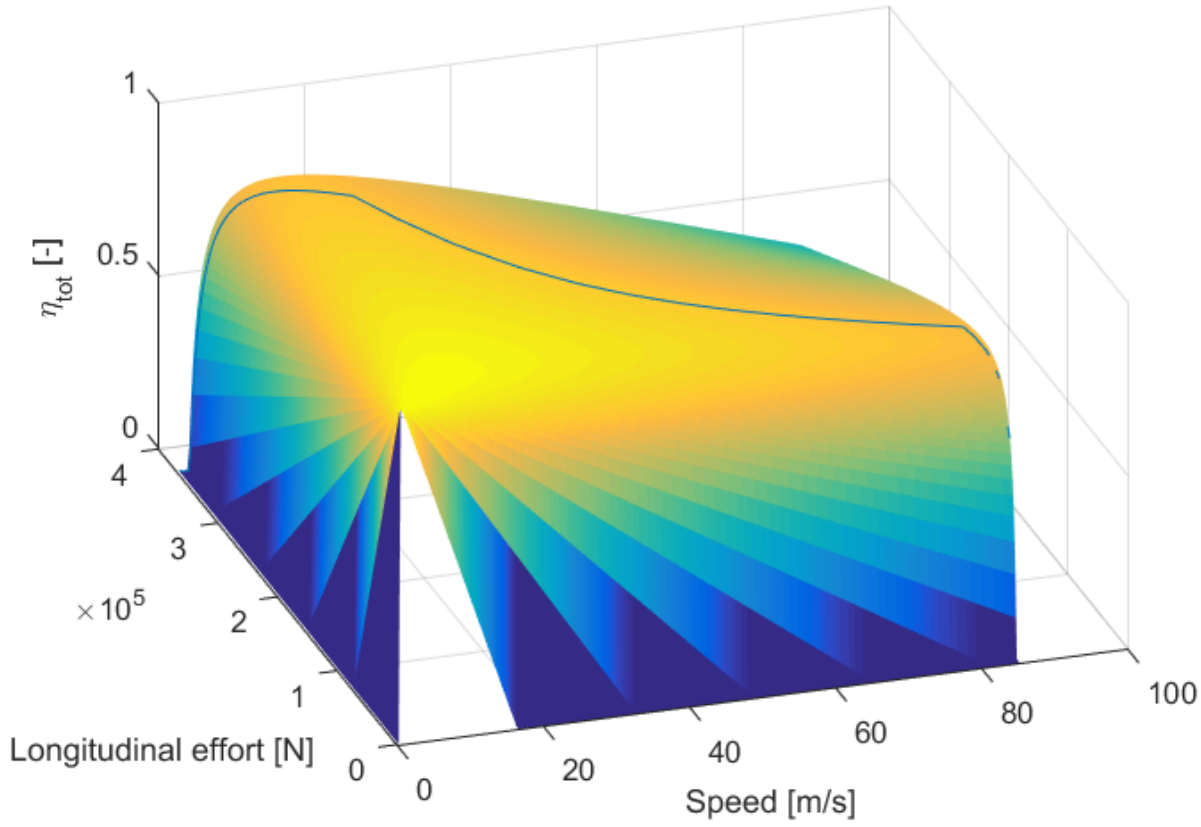

Figure 2.10: Vehicle total efficiency as a function of speed and traction and braking effort.

Equation 2.17 expresses the proportionality between the mechanical power W_m and the corresponding electrical power W_e, which can be absorbed (traction phase) or regenerated (braking phase) by the traction system; η_{tot} can also be expressed as the product of the mechanical efficiency of mechanical transmission system η_m and the electrical efficiency η_e of on-board traction equipment. The efficiency η_{tot} is typically a function of both train speed and delivered traction effort: Figure 2.10 shows the typical trend of the vehicle total efficiency.

In case of regenerative braking, the recovered power W_e can be divided in two terms: a first part, denoted as W_c, is transferred to the line and a second one, indicated by W_{sv}, is stored on a possible on-board accumulator (described in Section 2.2.3). In order to simulate the power consumption of additional on-board auxiliary systems, a further contribution, W_{aux}, must be introduced. The

complete power balance between those contributions, due to the different on-board sub-systems, is reported in Figure 2.11 and can be expressed as follows:

$$W_e = W_{aux} + W_{sv} + W_c. \tag{2.18}$$

It is important to underline that, to properly calculate the power W_c collected by the train, it is fundamental to take into account the line slope α and additional resistance $d(r)$ due to curves (which are defined as tabulated functions of the position x of the train) for each line section, since the line resistance can provide a significant portion of power losses.

The power W_c calculated through Equation 2.18 is used as an input to the line and hence to the stationary energy storage devices present within the line.

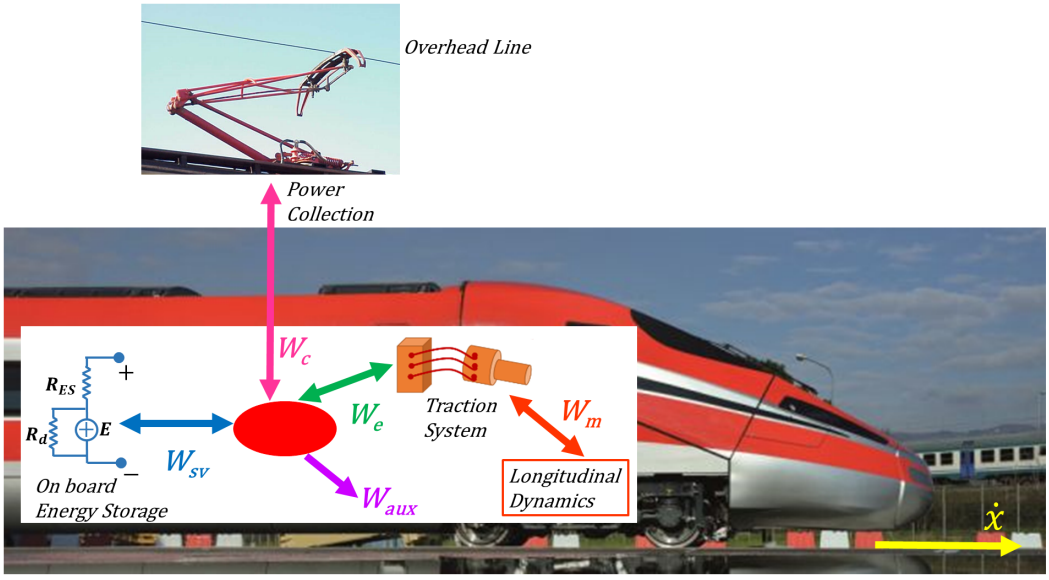

Figure 2.11: Power fluxes involved in the vehicle dynamics, considering the interactions with the electrical line.

2.1.6 Considerations on passengers comfort

Both traction and braking forces are applied with a smoothed dynamics obtained with a first order filter that reproduces the typical limitations introduced on both systems to improve the longitudinal comfort of the passengers and protect the train from excessive mechanical solicitations. The corresponding numerical implementation in terms of gradient/slew rate of both traction and braking forces is described in Table 2.1.

The application of traction and braking efforts is regulated by the RFI "Regolamento per la Circolazione dei Treni" [74].

The first order filters used in the proposed model to smooth the longitudinal efforts application are based on the Butterworth method.

$B^{(k)}(s)$ is a $k-th$ order Butterworth polynomial, whose dependent variable is denoted as s; its transfer function H can be expressed as:

$$H(s) = \frac{B^{(n)}\left(\frac{s}{\omega_0}\right)}{B^{(m)}\left(\frac{s}{\omega_0}\right)}, \tag{2.19}$$

where ω_0 is the filter cut-off frequency. The filter can be implemented if $m > n$; the filter response can be expressed as follows:

$$Att = 20log\sqrt{1 + \epsilon^2(\frac{\omega}{\omega_P})^{2n}}, \tag{2.20}$$

where ϵ is the maximum pass band gain, n is the filter order and ω_P is the filter pass band frequency.

Table 2.1: Dynamical response of High-Speed trains braking and traction systems.

Braking application	$\approx$4 s to apply the full braking effort from the brake release condition
Braking release	$\approx$12 s to completely release the brake from the full braking condition
Traction application	$\approx$7 s to apply the full traction effort from a null traction condition
Traction release	Traction is immediately deactivated without any appreciable delay

2.1.7 Voltage limiter

In this research work, a parametric tool to reproduce the behaviour of the train in case of a limited load capacity availability on the line has been introduced in the vehicle sub-model. This element allows the response of the system to be accurately represented, even when a limited load availability must be handled by the on-board traction system. This correction allows to split the energy recovered from traction motor during an electric braking in two contributions:

- Energy dissipated on on-board resistors controlled by the so called braking chopper;
- Regenerated power transferred to the line and constrained by the line overvoltage caused by a limited load availability.

This functionality allows the approximation of the system real behaviour as that of a system with two nested voltage loops realized according to the scheme of Figure 2.12. W_e represents the

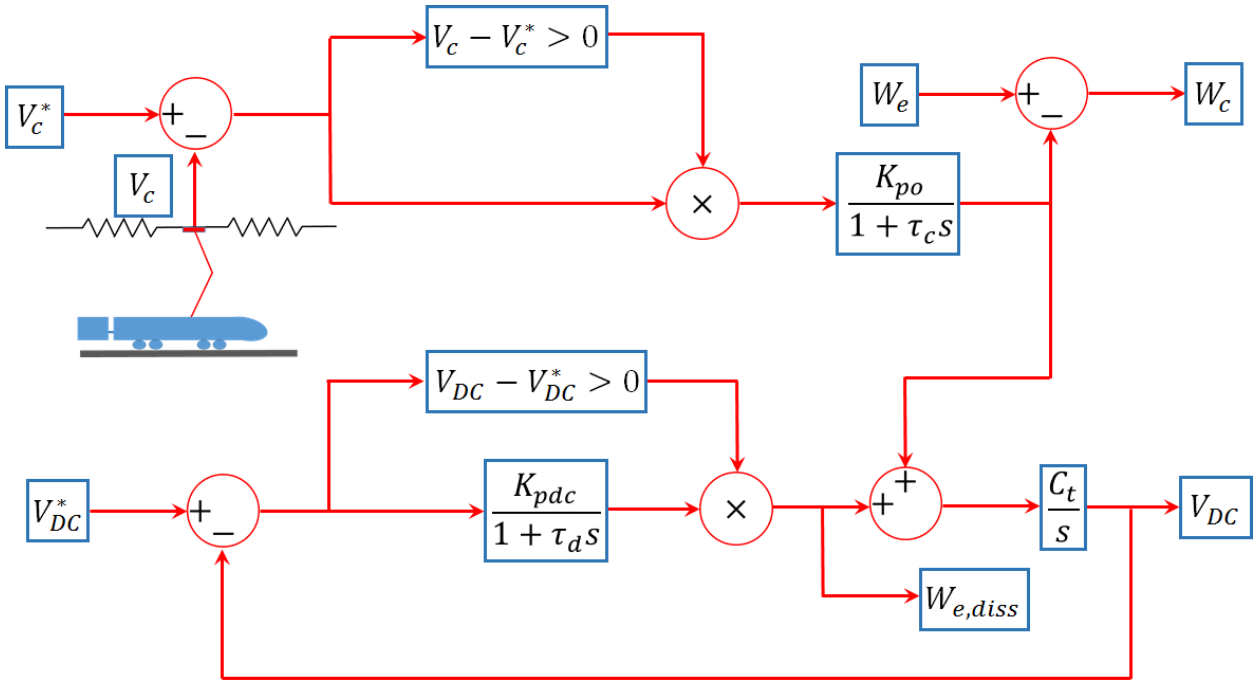

Figure 2.12: Modular scheme representing the simplified model adopted to calculate W_d and W_e and to simulate the response of the traction system when line overvoltage conditions occur.

electrical power recovered by the traction system taking into account mechanical losses on the transmission system and more generally the efficiency of the traction system: if the line is not able to receive the whole recovered power W_e, the measured voltage at the pantograph will exceed the maximum allowable limit V_c^*.

A simple proportional controller, characterised by the gain K_{po} (whose dynamics is approximated by a first order system with a time constant equal to τ_c), regulates the power which is then really transferred to the line W_c. The remaining power is transferred to the DC Bus: since the DC Bus is usually stabilized with filtering capacities, the increase of the voltage V_{DC} is roughly proportional to the integral of transferred power (i.e. transferred power is proportional to transferred current) through a proportionality constant C_t. Furthermore, an increase of the DC Bus voltage, over an assigned value V_{DC}^*, causes the intervention of a proportional control loop which dissipates a power (denoted with $W_{e,diss}$) which, in steady state conditions, is almost equal to the difference between W_e and W_c.

2.2 Electrical model of the line

The electrical model of the railway line has been developed using the object oriented Simscape™ language. As shown in Figure 2.13, this sub-model includes the catenary, the electrical substations, and stationary or on-board storage devices.

The line receives, from the vehicle model, the train position and power (both requested and provided) and provides to the vehicle itself the quantities that it needs to operate and the line operational limits (e.g. the voltage peak limit).

The line topology, at a microscopic scale (i.e. train scale), depends on the vehicles position, making

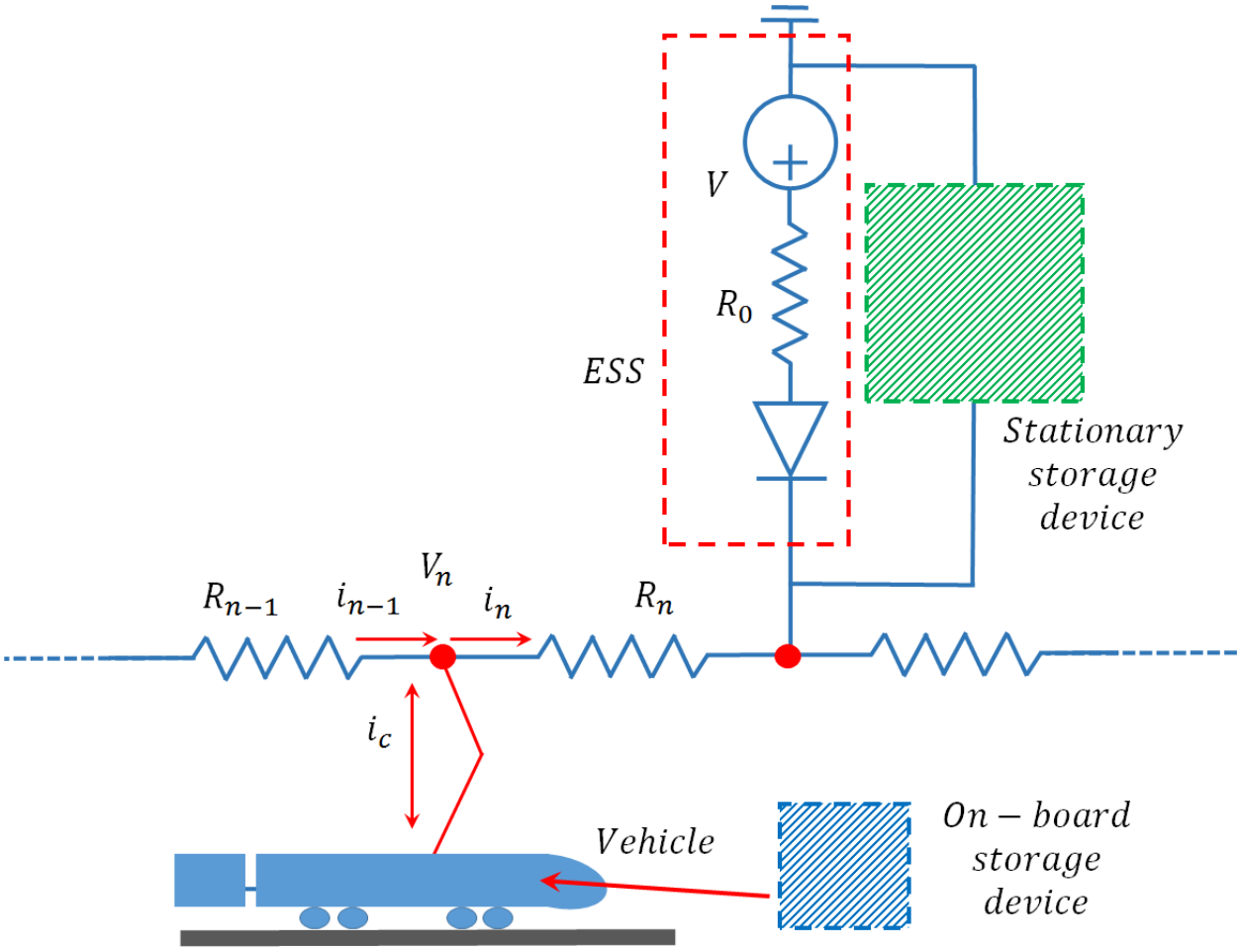

Figure 2.13: General architecture of the line electrical model.

the analysed system a time-variant one. Complex topology lines can be easily assembled and it is possible to take into account the presence of more than one travelling train within the same line span.

The main outputs of the electrical model are the electrical and energetic quantities that represent the line and storage devices behaviour.

2.2.1 Fundamental elements

In order to provide a better understanding of the proposed modelling approach, in this Section the fundamental elements used for the electrical modelling of the line will be exposed. These elements have been modelled developing proper Simscape™ blocks that implements the characteristic equations of each element. More details on the Simscape™ language are given in Section 2.5.1.

The resistor model (shown in Figure 2.14) is a simple algebraic block which implements the constitutive equation of a linear resistance:

$$V = RI, \tag{2.21}$$

where V is the resistance voltage drop, I is the current and R the constant resistance. R represents a user defined input for the element and the current is assumed to be positive if it flows from the positive pole to the negative one of the resistor. The power absorbed (i.e. dissipated) by the element is always positive. This block is useful to represent the internal losses of the line components. It is useful to highlight how the block has two connections, allowing the user to assembly the desired circuit.

Figure 2.14: Resistive element.

Figure 2.15: Variable resistance.

Figure 2.16: Capacitive element.

In order to take into account the variable impedances of the catenary, which depend on the train position, and hence the line losses, which are significant to understand the feasibility and the best location of energy storage devices, a variable impedance resistor, shown in Figure 2.15, has been used.

The value of the impedance is no more a user defined input but is dynamically provided to the element as a function of the train position within the considered line span; the block has a further connection, which is used to pass to the element the impedance value.

The capacitor model (with two connections, shown in Figure 2.16) implements the constitutive ordinary differential equation of a capacitive element:

$$I = C\frac{dV}{dt}, \tag{2.22}$$

where C is the element capacitance. It is possible to take into account parasitic effects by adding to the element proper resistive elements: this can be easily done by assembling the desired circuit, however, in a more elegant and computationally robust way, this can be accomplished modifying the element constitutive equation (see Section 2.5.1 for more details on the modelling approach). This element is fundamental for the modelling of energy storage devices.

Figure 2.17 shows the inductor model, which implements the constitutive ordinary differential

Figure 2.17: Inductive element.

equation of an inductive element:

$$V = L\frac{dI}{dt}, \tag{2.23}$$

where L is the element inductance. As previously exposed for the capacitive elements, it is possible to include parasitic effects through the addition of proper resistive elements. This element is quite useful for the modelling of most line components, especially energy storage devices and power converters.

The voltage source element (see Figure 2.18) implements the constitutive equation of an ideal voltage source which maintains a sinusoidal voltage difference between its poles regardless of the current which flows through it:

$$V = V_0 \sin(2\pi f t + \phi), \tag{2.24}$$

where V_0 is the voltage amplitude, f is the frequency and ϕ is the phase. This periodic voltage source is the core of an AC electrical substation; modifying the constitutive equation to $V = V_0$, it is possible to use this element to represent a DC voltage source.

Finally, Figure 2.19 shows the diode element, which implements the constitutive equation of a

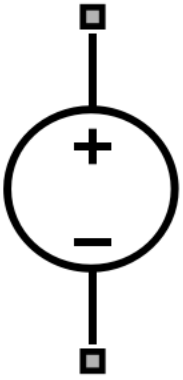

Figure 2.18: Voltage source element.

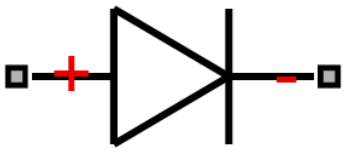

Figure 2.19: Diode element.

non-linear diode: if the voltage difference through the element is higher than a certain threshold (provided as an input to the model), the diode operates as a low impedance resistor, while, if the voltage difference is lower, the diode operates as a low conductance resistor. Above the threshold the diode is represented as follows:

$$V = V_f(1 - R_{on}G_{off}), \tag{2.25}$$

where the $R_{on}G_{off}$ term provides a zero diode current if the voltage difference is equal to zero.

2.2.2 Feeding line and electrical substation model

The energy needed by the vehicle for traction is provided by a feeding line fed by electrical substations, which are connected to the electric grid through proper transformers.
The substations can operate in different configurations:

- DC systems: typically characterised by a 3 kV substation voltage. In tramways or metro systems the voltage can be lower (e.g. 750 V);
- AC systems with industrial frequency: these systems operate at 25 kV-50 Hz, and are used in most of modern lines, especially in High-Speed systems;
- AC systems with railway frequency: these systems operate at 15 kV-16 and 2/3 Hz, and are diffused in central Europe, especially for German High-Speed systems, where they represent the standard solution.

The train power supply can be unilateral or bilateral, respectively if the line span where the train travels is fed by one or two substations; unilateral power supply is more typical in tramways, while, in a typical railway line, bilateral power supply is preferred due to the higher power levels.
The current required by the vehicle in the traction phase, or provided to the line during the regenerative braking phase, can be calculated from the vehicle power, taking into account the mechanical and electrical efficiencies of the system components:

$$W_t = \frac{W_{wheels}}{(\eta_{gearbox}\eta_{motor}\eta_{motordrive})}, \tag{2.26}$$

$$W_b = W_{wheels}\eta_{gearbox}\eta_{motor}\eta_{motordrive}, \tag{2.27}$$

where W_{wheels} is the power measured in correspondence of the wheel/rail contact, $\eta_{gearbox}$ is the mechanical efficiency of the transmission systems, η_{motor} is the efficiency of the electric motor itself and $\eta_{motordrive}$ is the electrical efficiency of the motor drive which feeds and control the motor (e.g. the inverter).
Figure 2.20 shows a more detailed scheme of the architecture of the electrical line model, developed using both standard and custom Simscape™ elements; the Figure is referred to the vehicle traction phase.

The line considered as a High-Speed test case is a 3kV DC catenary which is bilaterally fed by two electrical substations (ESSs). For the considered application (i.e. a High-Speed line), the mean distance between adjacent ESSs is about 15 km, hence the presence of two trains in the same line section should be considered uncommon, taking into account that the signalling system for a vehicle speed of about 200-250 km/h imposes a minimal distance of 5400 m from the nearest protected point. Furthermore, in order to fully exploit its maximum speed (up to 360 km/h for the considered High-Speed test case), the safety distance between the train and a protected point should be at least twice or even three times the minimal value because the braking distances are roughly proportional to the squared value of the vehicle speed.

The power W_c, collected by the train in correspondence of the pantograph and hence calculated by the vehicle sub-model described in the previous Section, is provided as an input to the electrical

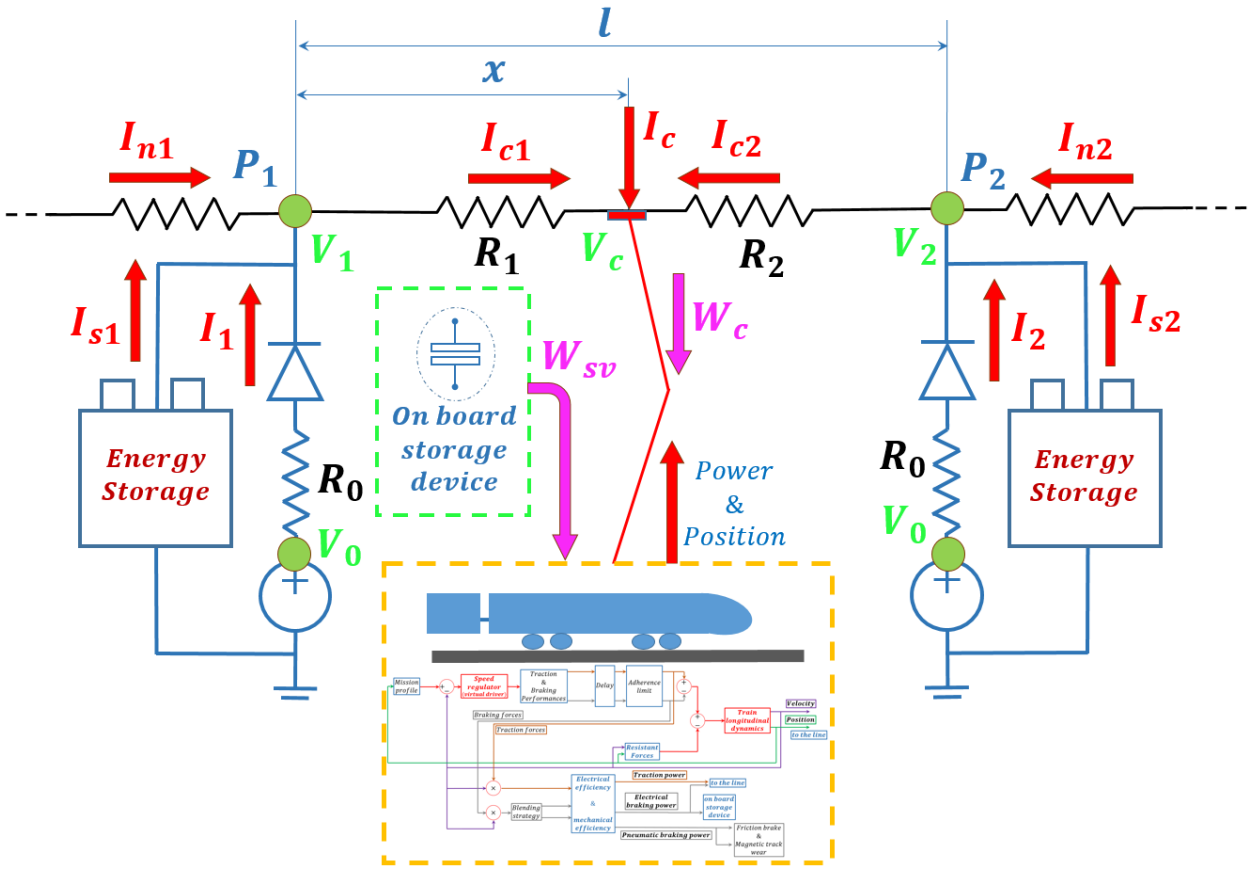

Figure 2.20: Architecture of the electrical line model, including stationary and on-board energy storage devices (traction phase).

model of the line. Figure 2.20 shows the architecture of the feeding line in a generic instant of the train traction phase, while Figure 2.21 shows the model couplings during regenerative braking: the power provided by the train can be received by stationary or on-board energy storage devices.
In order to couple the mechanical and the electrical parts, it has been necessary to introduce a delay in the variable exchange between the vehicle dynamics and the feeding line. However, since the goal of the proposed model is the analysis of the train energy consumption, it is not necessary to examine the high frequency components and the various harmonics present within the line. Hence, the presence of a time delay (needed for the model coupling), has no influence on the analysis and does not destabilize the system, because the time scale considered in the simulations is much higher than the considered delay: the integration time step used for the simulation is variable (see

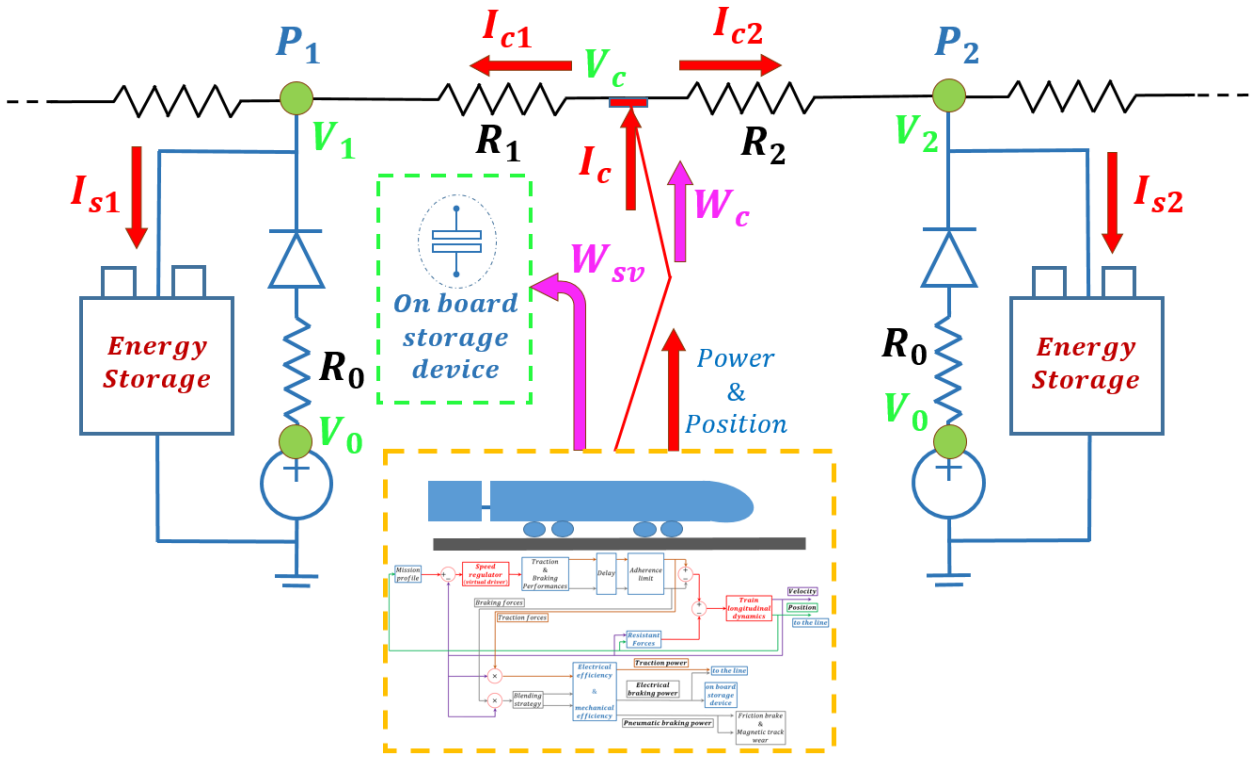

Figure 2.21: Architecture of the electrical line model, including stationary and on-board energy storage devices (regenerative braking phase).

Section 2.5.2) but its minimum value is about 5 seconds.

The vehicle virtually divides each line section in two parts, whose impedance values depend on the train position; the equivalent resistances R_1 and R_2 of those catenary sections are calculated as functions of the train position x with respect to the distance l between adjacent substations, according to Equations 2.28 and 2.29:

$$R_1 = \rho \cdot x, \tag{2.28}$$

$$R_2 = \rho \cdot (l - x)\,, \tag{2.29}$$

where R_1 and R_2 are respectively the impedance values of the line span sections before and after the train position, l is the line span length (the position of the second substation of the span is denoted as P_2) and ρ is the value of the line distributed impedance.

Due to this configuration, the voltage drop in correspondence of the vehicle pantograph is directly proportional to the train distance from the substation (i.e. the catenary impedance is higher). Hence, in order to provide the correct voltage value to the vehicle, the no-load voltage V_0 of a substation is usually up to 30% higher than the nominal value.

The pantograph collected current I_c is composed of the two contributions I_{c1} and I_{c2}, respectively from the initial and final substation of the considered line span (the contribution from other substations is negligible). Through the voltage divider representation, it is possible to calculate these contributions as follows:

$$I_{c1} = \frac{I_c \cdot (l - x)}{l}, \tag{2.30}$$

$$I_{c2} = \frac{I_c \cdot x}{l}. \tag{2.31}$$

Hence, the line voltage drop can be determined as follows:

$$\Delta V = \frac{I_c \cdot \rho \cdot x \cdot (l - x)}{l}. \tag{2.32}$$

From equation 2.32, it is possible to highlight how line losses vary with a parabolic trend; furthermore, the highest voltage drop is found at midspan between two adjacent substations and assumes the following value:

$$\Delta V_{max} = \frac{I_c \cdot \rho \cdot l}{4}. \tag{2.33}$$

It is significant to notice how, in a bilateral supply operating condition, the maximum losses are 25% of the maximum losses in an unilateral supply scenario with the same span length.

A DC line in a stationary regime has no inductive or capacitive effects within the catenary, while an AC line includes also these effects (i.e. the line circuit is assembled including capacitive and inductive elements). Figure 2.22 shows the proposed Simscape™ implementation of the DC catenary: it is interesting to highlight the presence of proper blocks (denoted as *S PS*) that allow the conversion of Simscape™ physical signal to classical Simulink® signals and viceversa (see Section 2.5.1 for more details).

A 3 kV DC electric substation, shown in Figure 2.23, is composed of three main sectors:

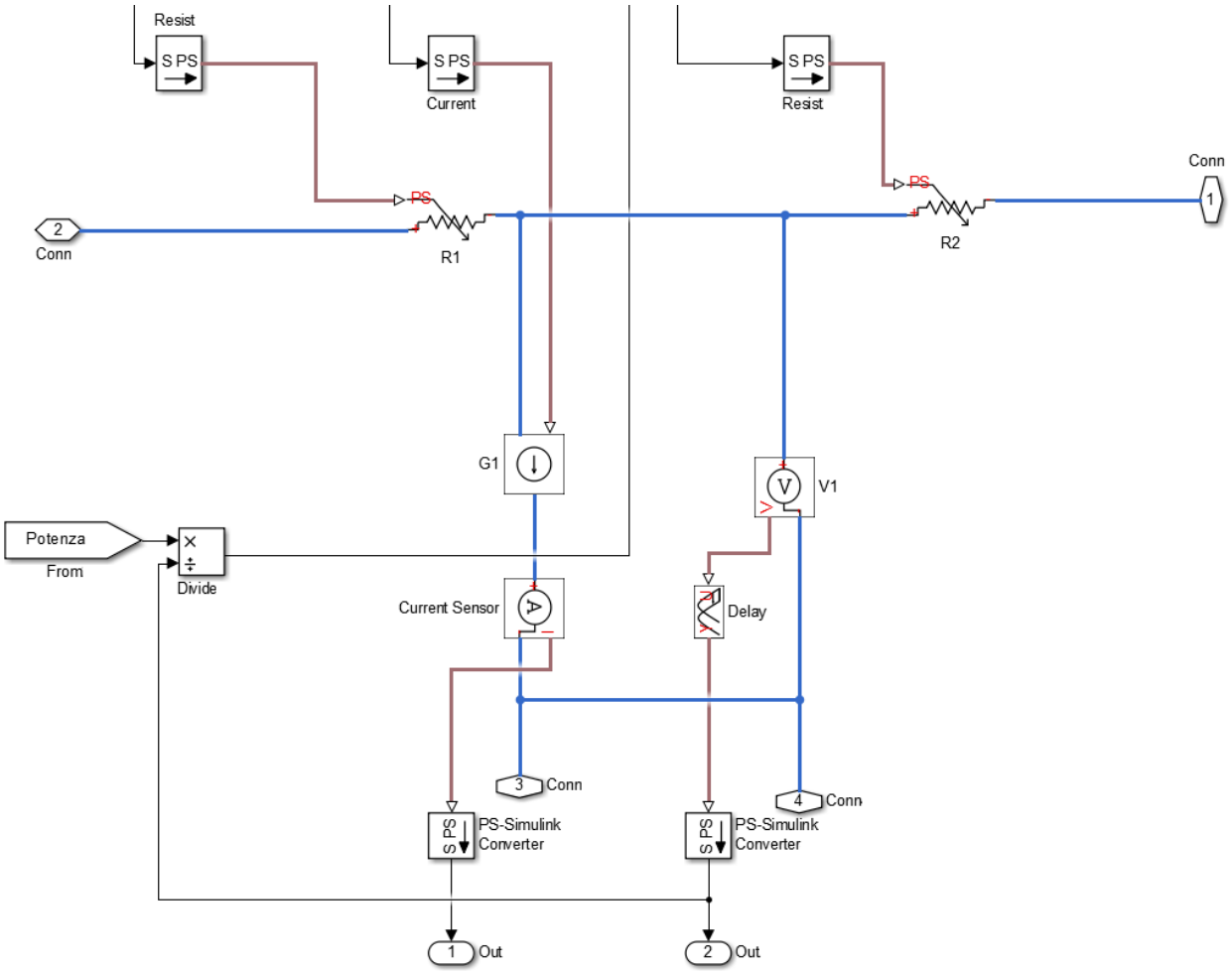

Figure 2.22: Simscape™ scheme for the feeding line.

- high voltage AC sector, outside the substation;
- 3 *kV* DC sector, inside the substation;
- 3 *kV* DC sector, outside the substation.

In the first sector the high voltage (HV) current from the grid is converted, through a proper transformer, to medium voltage (MV). This sector includes the HV-MV transformers, the infrastructure for the overhead line (e.g. poles, pylons, insulators, clamps and connection devices), the conductives and the bars, used for the derivations of the transformer group, the HV sectioner, the sectioner and switches controller, the current transformers and the voltage reducers, used for

measurements and protections.

In the second sector, the AC current is converted to DC current; a silicon rectifier group is used for the conversion. The rectifier group includes diodes, *RC* protection groups and an alarm and control system. Through a 3 *kV* DC bar, the rectifier group is connected to a capacitors cell which is used to filter high frequency harmonics.

Finally, in the third sector, the shunting and line feeding operations are carried out; the substation is here directly connected to the line and to its protection devices.

More in detail, considering the electric scheme shown in Figure 2.23, the substation circuit includes the following components:

1. primary HV three-phase line;
2. tripolar line switch;
3. HV three-phase bars;
4. tripolar group switch;
5. tripolar sectioner;
6. three-phase transformer;
7. silicon rectifier;
8. positive DC bar;
9. negative DC bar;
10. extra-fast switch;
11. DC sectioner;
12. filter;
13. contact line supply.

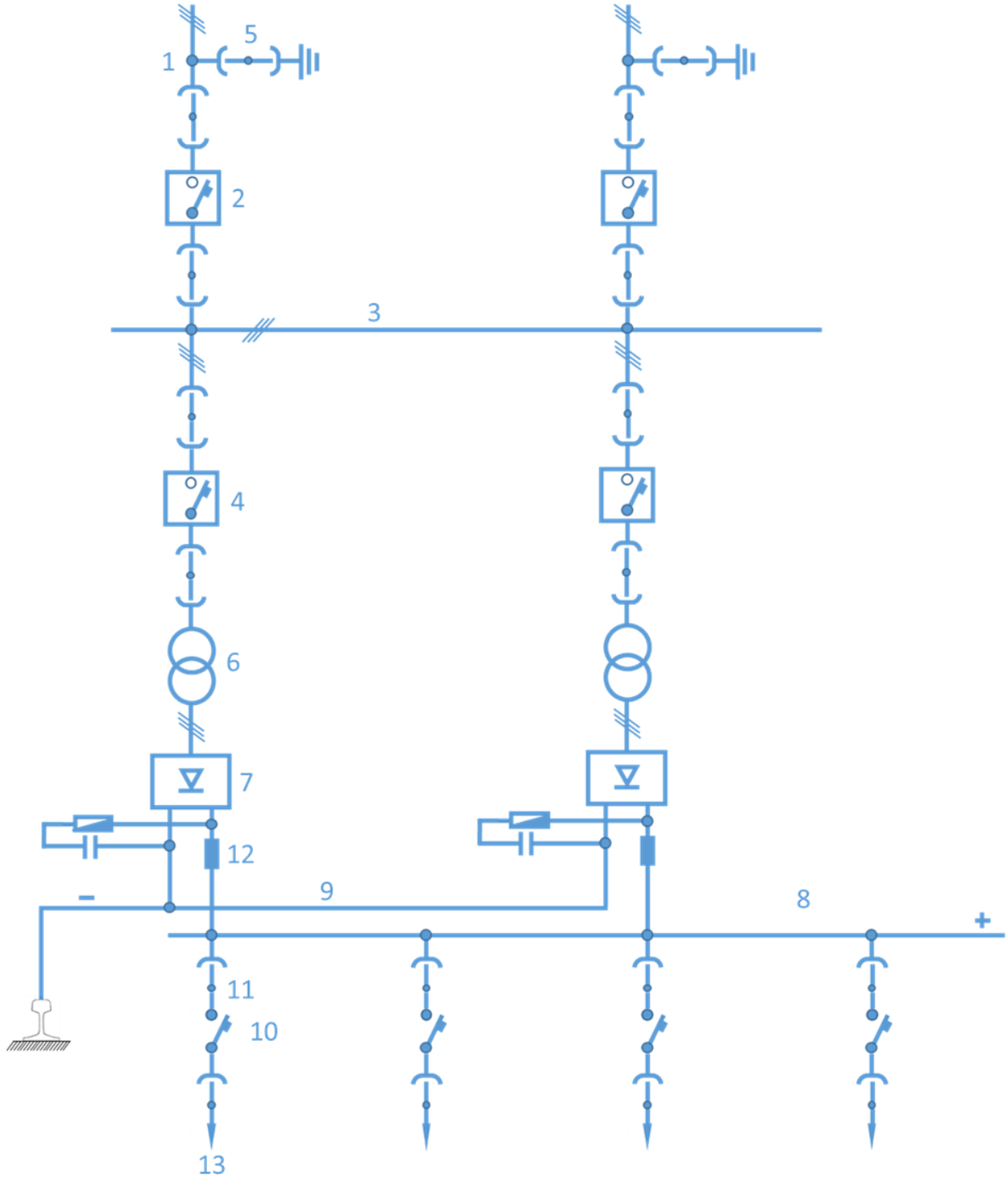

Figure 2.23: Electric scheme of a 3 kV DC electric substation.

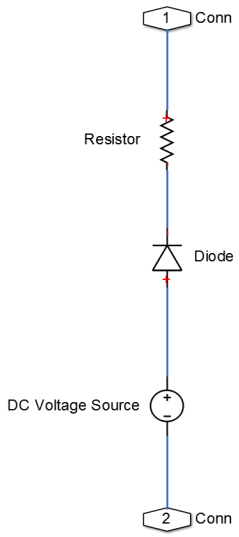

Figure 2.24: Simscape™ scheme for the electrical substation.

The fundamental task of electrical substations is the reduction of grid voltage to a level that suits railway applications. Electrical substations are based on the use of diodes: two three-phase bridges, fed by different wires of the transformers, are often employed. In this configuration, the AC grid current is converted in DC current to fed the train.

In the proposed model, the substation has not been represented taking into account all the previously exposed details but in a simplified way. As shown in Figure 2.24, which represents the proposed Simscape™ implementation of the DC substation, this kind of substation can be modelled as an ideal voltage generator with an equivalent impedance (to simulate its internal losses) and a diode (to simulate the first quadrant limitation of the system) connected in series; ESSs are often analysed with similar models in literature works (see the books written by Perticaroli [75] and Zaninelli [76] on railway electrification systems). In this configuration the substation is able to provide only traction power, while a possible recovered braking power could only be used by another train within the line (furthermore, this DC substation can be easily modified to represent an AC substation). This scenario is consistent with the considered High-Speed test case (see Section 2.6); however the model is able to represent also the four-quadrant behaviour of the line. A simple solution is based on the use of energy storage devices: the fourth quadrant operation is handled directly by those devices, which can receive the braking energy and provide part of this power

when the same vehicle or another one needs traction power. Furthermore, the fourth quadrant operation can be also modelled by using fully reversible substations (see Section 2.2.2.1), able both to provide and receive energy; this solution has been considered also by Cornic [77], who analysed the possibility to perform energy recovery through a reversible substation.

Considering the configuration shown in Figure 2.20, the line node, where the substation is connected, is represented as follows:

$$\begin{cases} V_0 - (I_{c2} - I_{c1})R_0 = V_c \\ V_2 = V_c - R_2 I_{c2} \end{cases} . \tag{2.34}$$

When the line voltage is higher than the substation voltage (i.e. $V_c > V_0$), the diode switches off and the substation is excluded from the circuit; Equation 2.34 becomes:

$$\begin{cases} I_{c2} = I_{c1} \\ V_2 = V_c - R_2 I_{c2} \end{cases} . \tag{2.35}$$

Complex topology lines with more than a single section, like the one shown in Figure 2.25, can be easily assembled because it is possible to connect to line nodes additional loads or section lines

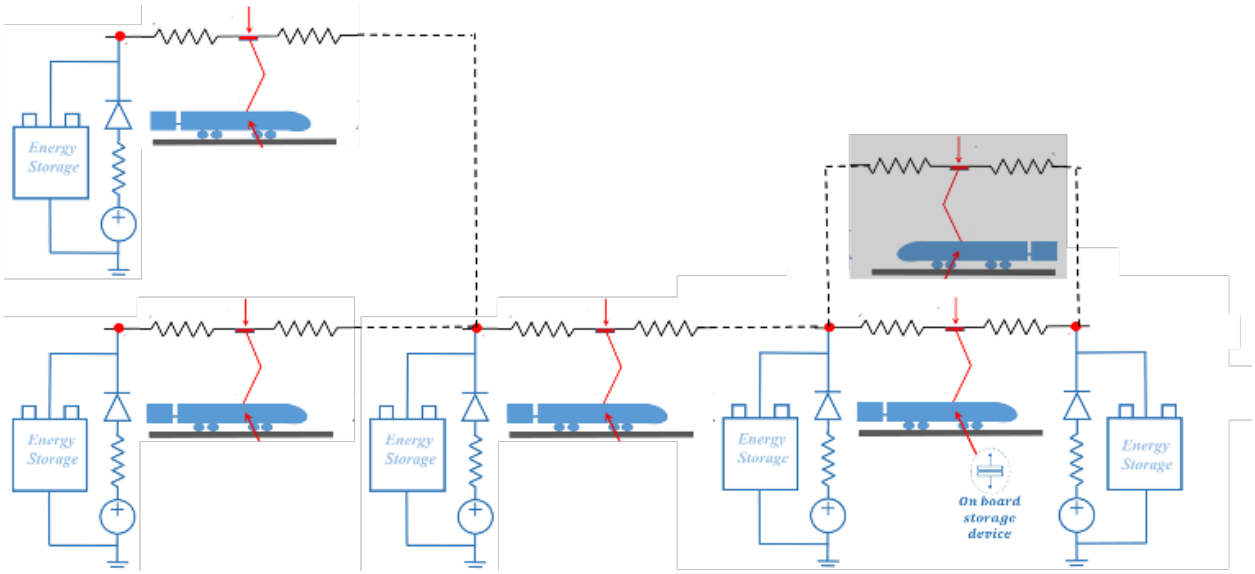

Figure 2.25: Example of complex line topology: the presence of intersections and multiple vehicles increases the complexity of the system but also the possibilities in terms of energy optimisation.

(corresponding to the external currents I_{n1} and I_{n2} shown in Figure 2.20).

By solving the electrical network, it is possible to calculate the train collected current I_c and all the other currents involved in the operation of the line sub-components.

It is interesting to highlight how the proposed model, whose main results have been obtained by assembling the whole line, can also be used in a simplified way, which does not represent a loss of generality but provides great advantages in terms of computational times. In fact, the model can be simulated using only a single assembled line span (including substations and storage devices, see Figure 2.26): the train is able to travel the whole line by crossing periodically the assembled line span. This can be easily done by changing dynamically the initial conditions of the storage devices while the line itself needs no additional modifications, since each line span already handles the train position as a relative distance from the first electrical substation.

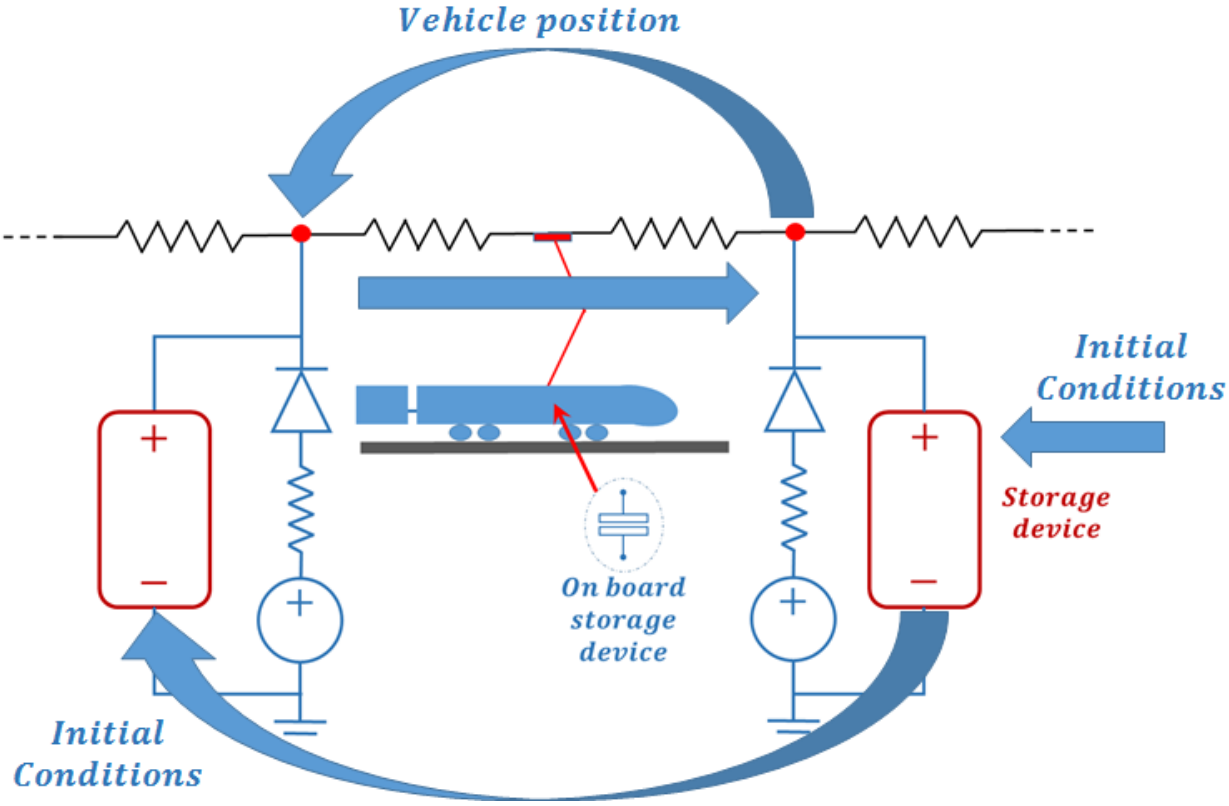

Figure 2.26: Single line span modelling approach.

2.2.2.1 Reversible and real substation models

In order to analyse a real operating scenario, two further substation models have been developed. The first one is a simple reversible substation model, obtained by eliminating the diode from the substation equivalent circuit (see Figure 2.27).

This substation model allows to represent the real case of a substation which receives the train braking energy and sends it back to the grid (the management of this energy flux after the substation is beyond the scope of this work); furthermore, this simplified model is useful to perform feasibility analyses in the first phases of the design process of a system, since it allows to understand the vehicle-line coupled behaviour without the need of a large number of parameters to operate.

A further modified substation model concerns the real substation: while the previously exposed model is able to provide infinite power to the vehicle (or to the vehicles), a real substation cannot exceed a certain power limit. After this limit (which is imposed by the grid characteristics and by the substation design itself), the vehicle power request is no more satisfied since the current provided by the substation is saturated.

The real substation model has been developed by modifying the ideal voltage source constitutive equation through the introduction of a power limit (which is a user defined input based on the considered substation technical data). The constitutive equation has been included in a cycle based on the train traction power W_t measurement and on its comparison with the substation

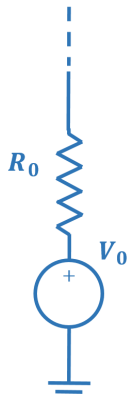

Figure 2.27: Scheme of the fully reversible substation.

maximum power $W_{ESS,max}$ (for the sake of clarity, the cycle which follows is referred to one travelling train in a bilateral power supply condition, but the approach has been developed in order to take into account a more general scenario in terms of number of vehicles and power supply system):

if $W_t \leq 2 \cdot W_{ESS,max}$

$V_{ESS} = V_0$

else

$V_{ESS} = W_{ESS,max}/I_{ESS}$

end

It is important to underline that the previously shown algorithm is not the current Simscape™ implementation of the real substation but a simplified version useful to expose the modification made to the model and its physical significance; the real substation source code is reported, by way of example, in Section 2.5.1, together with the block and domain source codes.

2.2.3 Energy storage devices

In railway applications, the most common energy storage devices are batteries and supercapacitors: in this research work, a basic modelling approach suitable for both the systems has been chosen

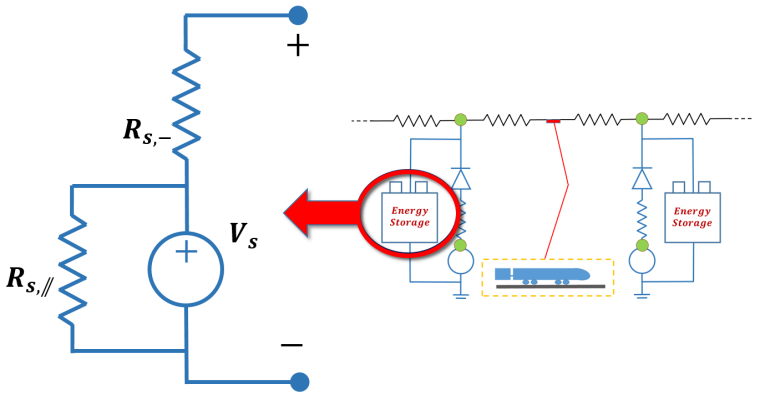

Figure 2.28: Scheme of the generic energy storage device model.

as a starting point. The proposed energy storage device model (shown in Figure 2.28) is a load connected in parallel to the ESSs and includes an ideal voltage generator, characterised by a V_s voltage, a resistance $R_{s,//}$, connected in parallel with the voltage source to simulate the device transient discharge, and finally a resistance $R_{s,-}$, connected in series.

This quite simple modelling approach allows to correctly simulate the behaviour of batteries and supercapacitors while requiring only a limited set of parameters to work. Furthermore, this energy storage device, thanks to the characteristics of the object oriented language used for the development of the model, can be easily connected or disconnected to ESSs, providing the possibility to simulate a large number of operating scenarios and to perform a first feasibility analysis of the distribution of the devices themselves, with respect to the energetic efficiency of the system. Finally, this simple model can be used also to represent an on-board storage device (mostly useful in tramway and light railway or to cut down voltage peaks during regenerative braking). This modelling approach has then been extended to the approximated modelling of complex energy storage systems in which the accumulator is coupled to the line through a two quadrant converter like the one reported in Figure 2.29.

2.2.3.1 Batteries

In order to be able to investigate more deeply the specific physical behaviour of the storage devices, a more complex battery model has been developed.

A battery, as well as a supercapacitor, is composed of a number n_{cell} of cells, each characterised by a nominal voltage V_{cell}; the battery voltage can be calculated as follows:

$$V_{0,batt} = n_{cell} \cdot V_{cell}. \tag{2.36}$$

One of the most important parameters, for the analysis of the behaviour of a battery, is the measure of the energy stored in the battery, i.e. its State of Charge, usually denoted as $S.O.C.$. In particular, the $S.O.C.$ is defined as the ratio between the stored energy E_{batt} and the maximum energy that the

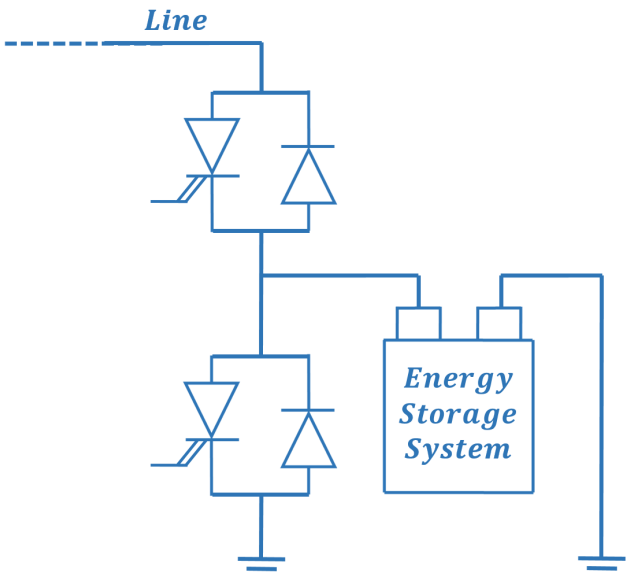

Figure 2.29: Scheme of an energy storage device connected to the line through a two quadrant converter.

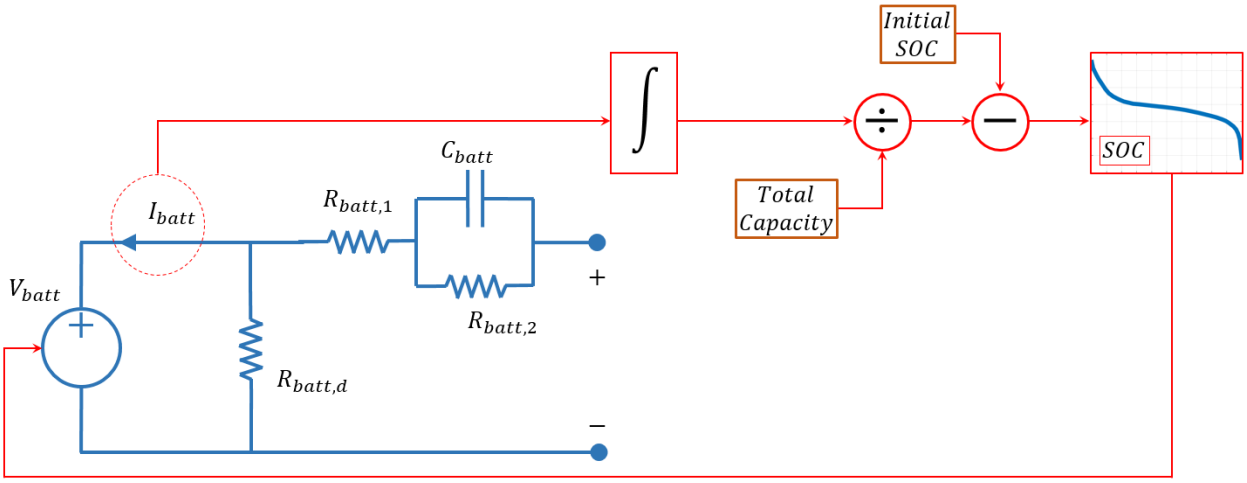

Figure 2.30: Architecture of the battery model, including the S.O.C. calculation.

battery can store $E_{batt,max}$:

$$S.O.C. = \frac{E_{batt}}{E_{batt,max}}. \tag{2.37}$$

The architecture of the battery model is shown in Figure 2.30: in this specific model, the resistance $R_{s,-}$ is substituted by the series of a resistance $R_{batt,1}$ and a parallel between a further resistance $R_{batt,2}$ and a capacitor C_{batt}. These further elements allows to better analyse the internal losses and

the transient behaviour of the device (while the resistance $R_{batt,d}$ takes into account self-discharge phenomena). The voltage of the ideal voltage generator is calculated through the estimation of the battery $S.O.C.$: the value V_{batt} of the no-load voltage of the storage system is a tabulated function of the energy storage device current I_{batt} and of the state of charge of the device. The $S.O.C.$, being a function of the storage device current I_{batt}, can be calculated as follows:

$$S.O.C. = \int \frac{\eta_{batt}\left(I_{batt}, S.O.C.\right) I_{batt}}{E_{max}} dt, \tag{2.38}$$

where η_{batt} is the efficiency of the device, i.e. a tabulated function of both I_{batt} and $S.O.C.$, and E_{max} is the maximum stored energy. Different kind of accumulators can be easily represented and their internal losses can be analysed in terms of impedances or efficiency η_{batt}.

For the analyses shown in this thesis, the investigation of the behaviour of Li-ion batteries, which could better suit to the needs of railway systems, has been carried out. The battery size has been determined starting from a reference Li-ion cell with a nominal voltage equal to 3.7 V and a nominal capacity of 53 Ah. In order to reach the line voltage (i.e. for the considered High-Speed test case), the entire battery includes stacks of 1000 cells connected in series (considering an intermediate value of the $S.O.C.$); 4 stacks are then connected in parallel to obtain the desired capacity. In particular, the capacity of the entire battery, in order to assure a long life to the

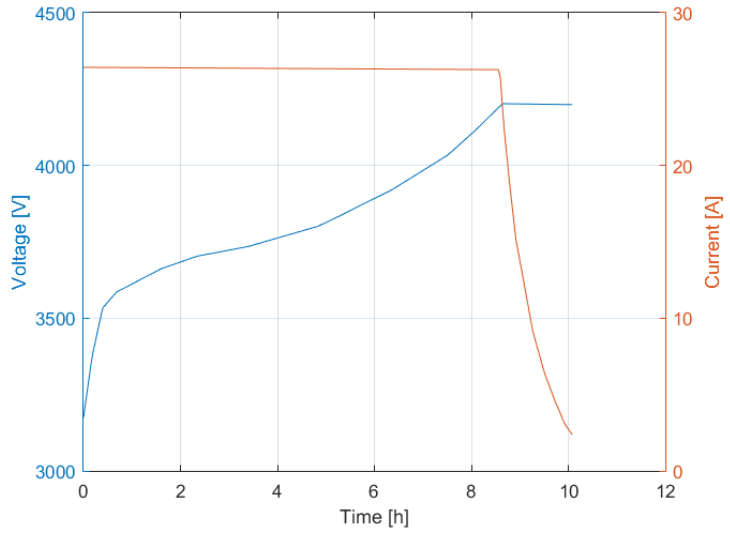

Figure 2.31: Battery charge behaviour.

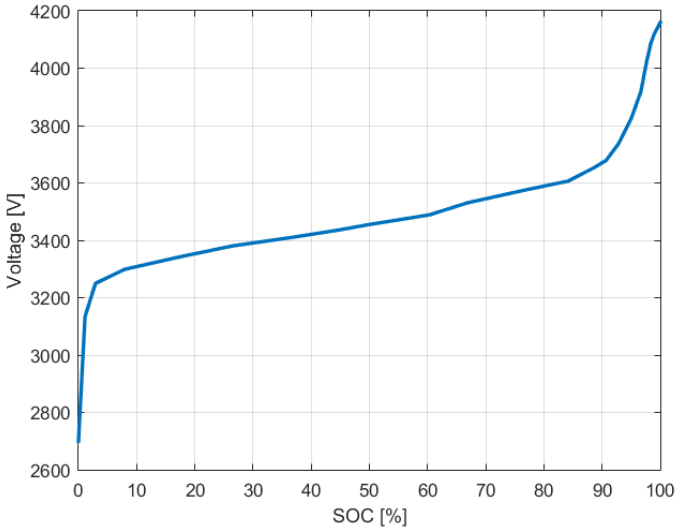

Figure 2.32: Battery discharge behaviour.

device, has been determined considering the maximum recovered braking energy (or the maximum provided traction energy) of the considered High-Speed train to be about 5-10% of the full battery capacity. Such a storage device is obviously oversized from the energy point of view; however, a greater amplitude of the charge/discharge cycle would strongly affect its operating life. Hence, this sizing represents an optimal compromise to fully exploit the operating life of the device and to take advantage of the investment.

Figure 2.31 and Figure 2.32 show respectively the charge and discharge behaviour of a battery with the previously exposed characteristics. The discharge behaviour, shown in Figure 2.32, highlights the voltage variation as a function of the $S.O.C.$: the trend is quite steep, however, considering the small percentage of energy represented by a braking manoeuvre with respect to the entire battery capacity, the voltage variations about the nominal value can be considered acceptable. In this operating range the current is constant during the charge phase. These results have been obtained simulating the behaviour of the proposed battery connected with a load (i.e. a current generator in the charge phase and a resistance in the discharge phase).

In order to obtain realistic results concerning the battery behaviour within the line, a good approach to connect this battery model to the proposed coupled model is to use an initial $S.O.C.$

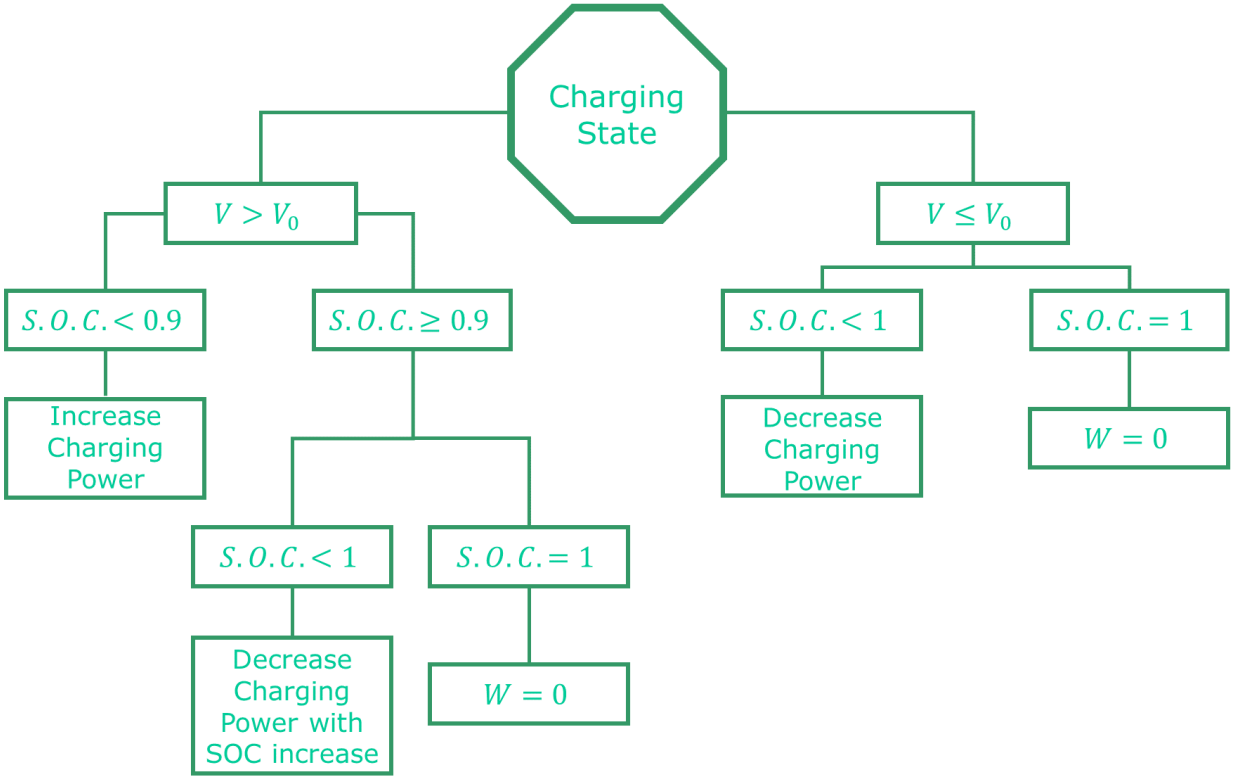

Figure 2.33: Scheme of the battery behaviour during charge process.

equal to about 50%, to work within the nominal range of the battery even with the maximum possible depth of discharge due to the passage of an accelerating train.

Figures 2.33 and 2.34 show how the proposed battery model behaves respectively during charge and discharge phase: during the charge phase, the controller (see Section 2.2.3.3) tries to keep the device voltage, denoted as V at a higher value with respect to the ESS voltage V_0, in order to receive energy only from braking vehicles and not from the substation, while during the discharge phase it is important that the line voltage does not exceed a certain limit V^*. In particular, during the charging phase, energy transfer is only possible if $V > V_0$ (or if $V \leq V_0$ the $S.O.C. < 1$): the controller intervenes in this phase increasing the charging power if the $S.O.C.$ is greater than 0.9 or decreasing it otherwise. On the other hand, during the discharge phase, discharge is only possible if $V \leq V^*$ (or if $V > V^*$ the $S.O.C. > 0.25$): in this case the controller increases the discharge power flux for high $S.O.C.$ values and decreases it otherwise.

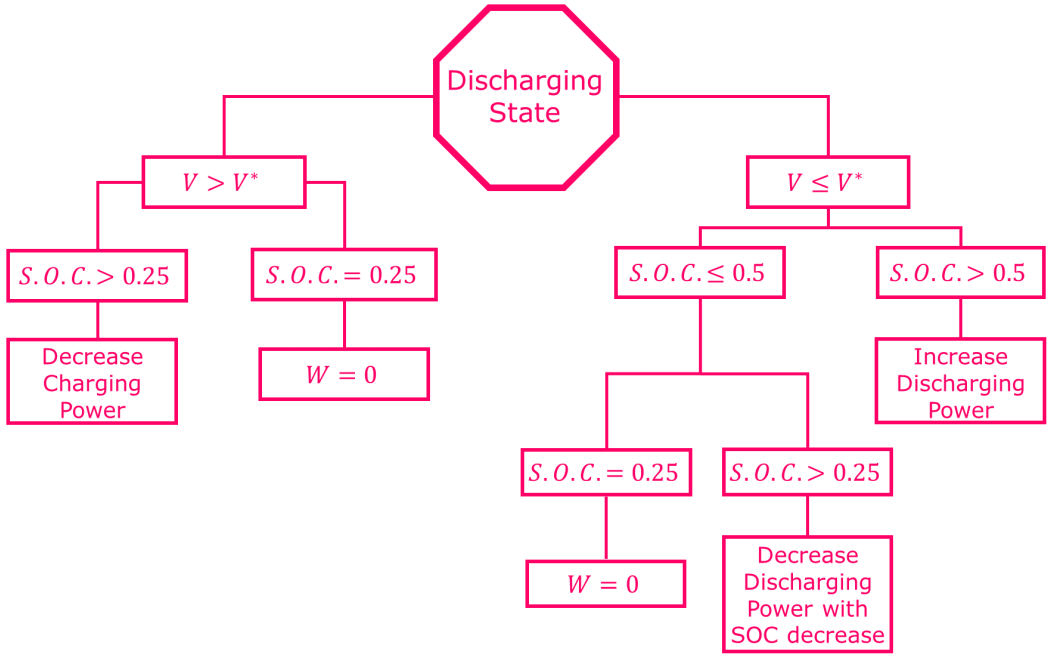

Figure 2.34: Scheme of the battery behaviour during discharge process.

Figure 2.35 shows how the battery efficiency calculation has been implemented within the proposed model: the calculation is based on a LookUp table and the model distinguishes between the charge and the discharge phase. In particular, the sign of voltage difference $V - V^*$ allows the evaluation of the battery operating phase (i.e. charge or discharge); the charge current is then multiplied by the battery efficiency, while the discharge current is divided by the battery efficiency. The battery efficiency is evaluated as a function of $S.O.C.$ through the previously cited LookUp table: the generic trend of the battery efficiency as a function of the device $S.O.C.$ is shown in Figure 2.36 and it is possible to highlight how the battery operates better for intermediate $S.O.C.$ values.

Currently the State Of Health ($S.O.H.$) of the battery is not taken into account; each battery is considered fresh. This is due to the large number of data needed to correctly model battery aging. Furthermore, the life expected from the batteries sized as previously exposed is about ten years; hence, for the analysis of the possible savings due to train regenerative braking, it is not fundamental to consider this aspect. However, in order to analyse the use within a railway system

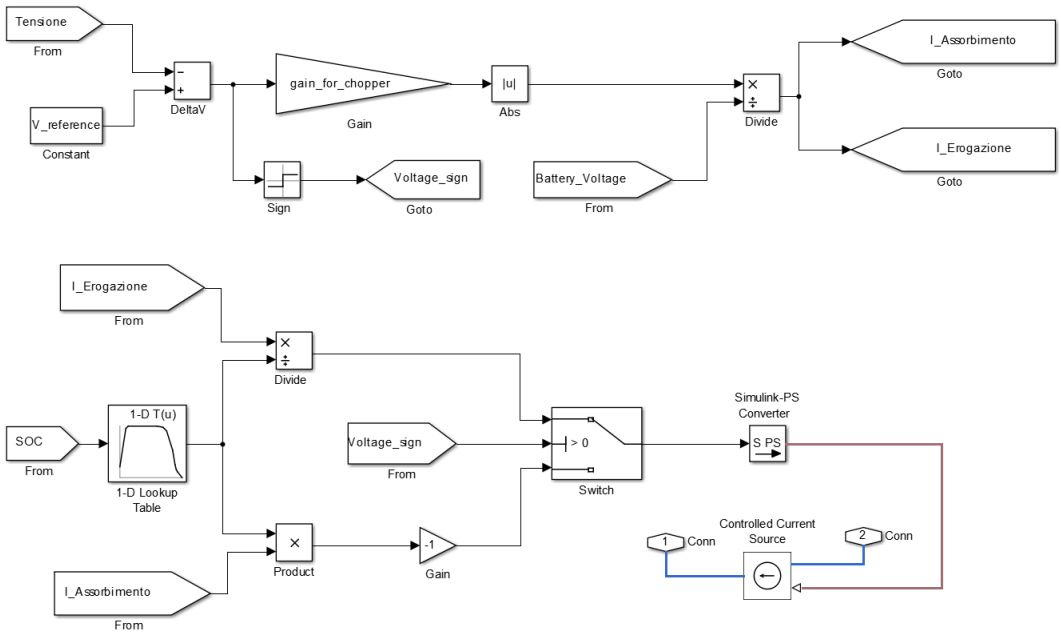

Figure 2.35: Simscape™ scheme of the battery efficiency estimation.

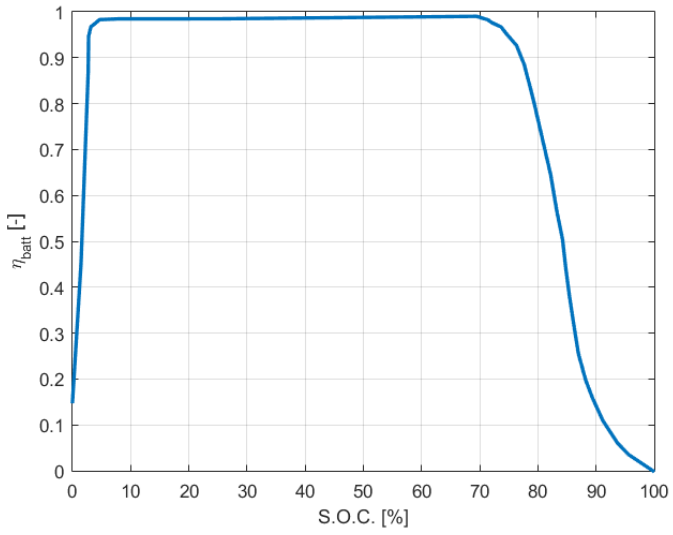

Figure 2.36: Battery efficiency as a function of $S.O.C.$.

of second-hand batteries (e.g. recovered from electric cars), in a future release of the model the estimation of the $S.O.H.$ will be implemented.

Finally, the battery model Simscape™ implementation is shown in Figure 2.37, including the

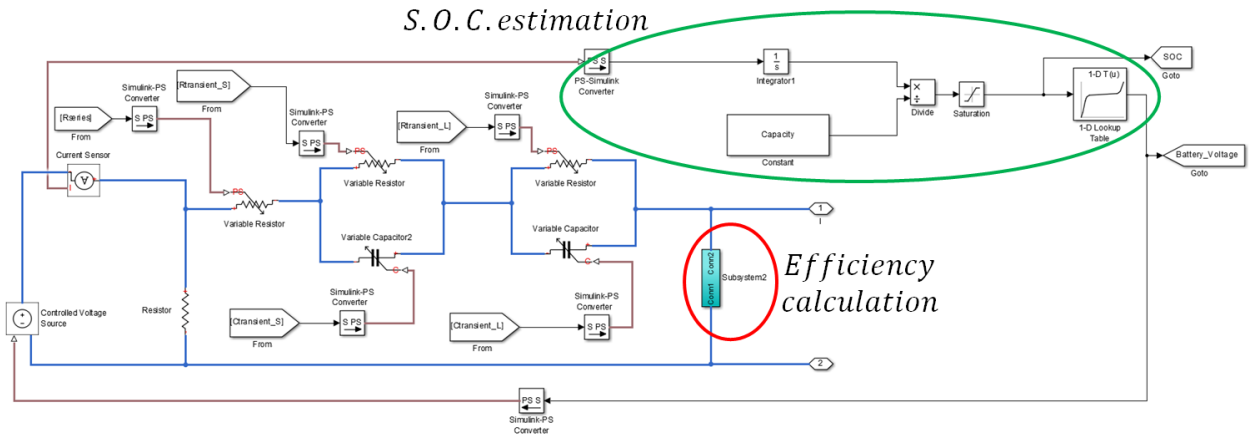

Figure 2.37: Simscape™ scheme of the proposed battery model.

$S.O.C.$ estimation and the efficiency calculation: in particular, the $S.O.C.$ is estimated in the upper branch of the system, while the efficiency calculation, according to the scheme shown in Figure 2.35, is included in the light blue subsystem connected in parallel to the battery poles.

2.2.3.2 Supercapacitors

As previously exposed, supercapacitors have been developed and optimised in order to obtain high performances in terms of specific energy and compete with traditional batteries.

A supercapacitor includes two electrodes separated by a dielectric and immersed in an electrolytic solution: an electrodes voltage difference generates an electric field which promotes the charge separation in the supercapacitor double layer.

The most simple supercapacitor model, whose architecture is shown in Figure 2.38, includes 3 circuital elements:

- a capacitor C_{sc}, which provides the desired capacity;
- a leakage resistance $R_{sc,leak}$ connected in parallel to the capacitor, which allows to take into account self-discharge phenomena;

- a resistance $R_{sc,-}$ connected in series to the capacitor, which represents resistive losses during charge/discharge cycles.

In this research work, the simplified model has been implemented in Simscape™ as a starting point; however, a more detailed model (based on the architecture shown in Figure 1.17) has then been developed and used for the analyses of the whole system.

The fundamental equation of the element can be expressed as follows:

$$V_{sc} = \frac{Q_{sc}}{C_{sc}}, \tag{2.39}$$

where V_{sc} is the supercapacitor voltage and Q_{sc} is the capacitor charge, which can be calculated as a function of the supercapacitor current I_{sc} as follows:

$$Q_{sc} = \int I_{sc} dt. \tag{2.40}$$

In order to size a supercapacitor, two main parameters represent the starting point of the process: the substation voltage (if the device have to be connected in parallel to it) and the foreseen energy fluxes. The energy E_{sc}, which can be stored by the supecapacitor, can be expressed as follows::

$$E_{sc} = \frac{1}{2} C_{sc} V_{sc}^2. \tag{2.41}$$

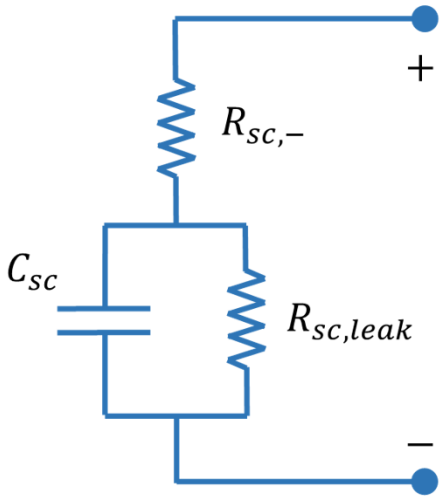

Figure 2.38: Architecture of the simplified supercapacitor model.

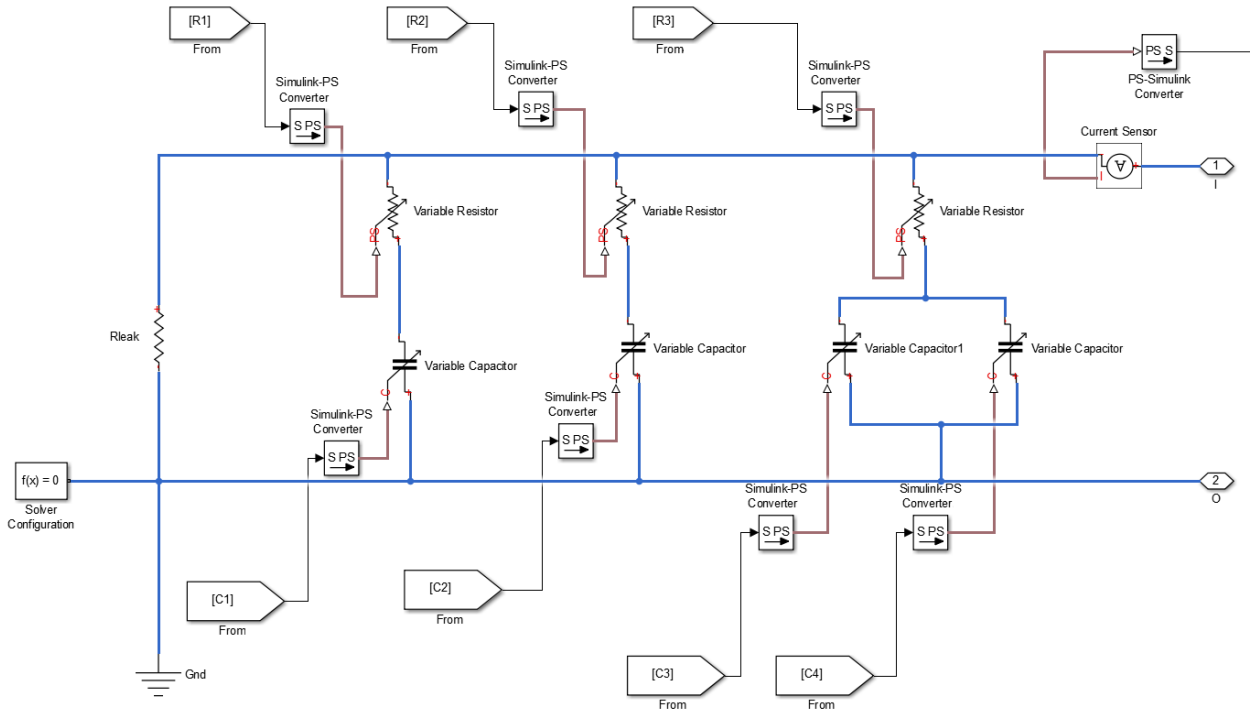

Figure 2.39: Simscape™ scheme of the proposed supercapacitor model.

From Equation 2.41 it is possible to calculate the capacity needed by the storage device:

$$C_{sc} = \frac{2E_{sc}}{V_{sc}^2}. \tag{2.42}$$

Each supercapacitor cell is characterised by a nominal voltage value, which is usually quite low: in railway systems, to reach an acceptable voltage value, a large number of cells must be connected in series. However, through series connection, the system capacitance $C_{sc,tot}$ diminishes and a further parallel connection of the series stacks is necessary to reach the desired device capacity:

- series connection of n cells:

$$C_{sc,tot} = \frac{\prod_{i=1}^{n} C_{sc,i}}{\sum_{i=1}^{n} C_{sc,i}}, \tag{2.43}$$

- parallel connection of n cells:

$$C_{sc,tot} = \sum_{i=1}^{n} C_{sc,i}, \tag{2.44}$$

where $C_{sc,i}$ is the capacitance of the i-th cell. For this reason, the series connected cells must then be connected in parallel to reach the desired capacity: this causes a significant increase of the device weight.

For a stationary supercapacitor, the storage device weight does not represent a problem, while for an on-board device it is a critical factor (the device weight reduces the possible payload); however, supercapacitos are suitable for operating scenarios where a high specific power is required.

The supercapacitor $S.O.C.$ can be calculated as follows:

$$S.O.C = \left(\frac{Q_{sc,init} - \int_0^t I_{sc} d\tau}{Q_{sc,t}} \right) \cdot 100, \tag{2.45}$$

where $Q_{sc,init}$ is the supercapacitor initial charge.

The proposed modelling approach is characterised by the following simplifying hypotheses:

- thermal effects on the electrolyte have been neglected;
- decay of materials has been neglected;
- charge redistribution is the same regardless of the voltage value;
- the supercapacitor provides DC current.

Figure 2.39 shows the Simscape™ implementation of the proposed detailed supercapacitor model: it is possible to highlight the presence of time dependent (and hence $S.O.C.$ dependent) internal impedances, represented through variable resistance blocks.

2.2.3.3 DC/DC converters

DC/DC converters are useful to fully exploit the presence of energy storage devices in all their operating range; this is especially true for supercapacitors (which have a large range of operating voltage) but they also have a fundamental role in the use of batteries. Due to their typical voltage-$S.O.C.$ trend (see Figures 1.15 and 1.16), the stationary devices (connected in parallel with

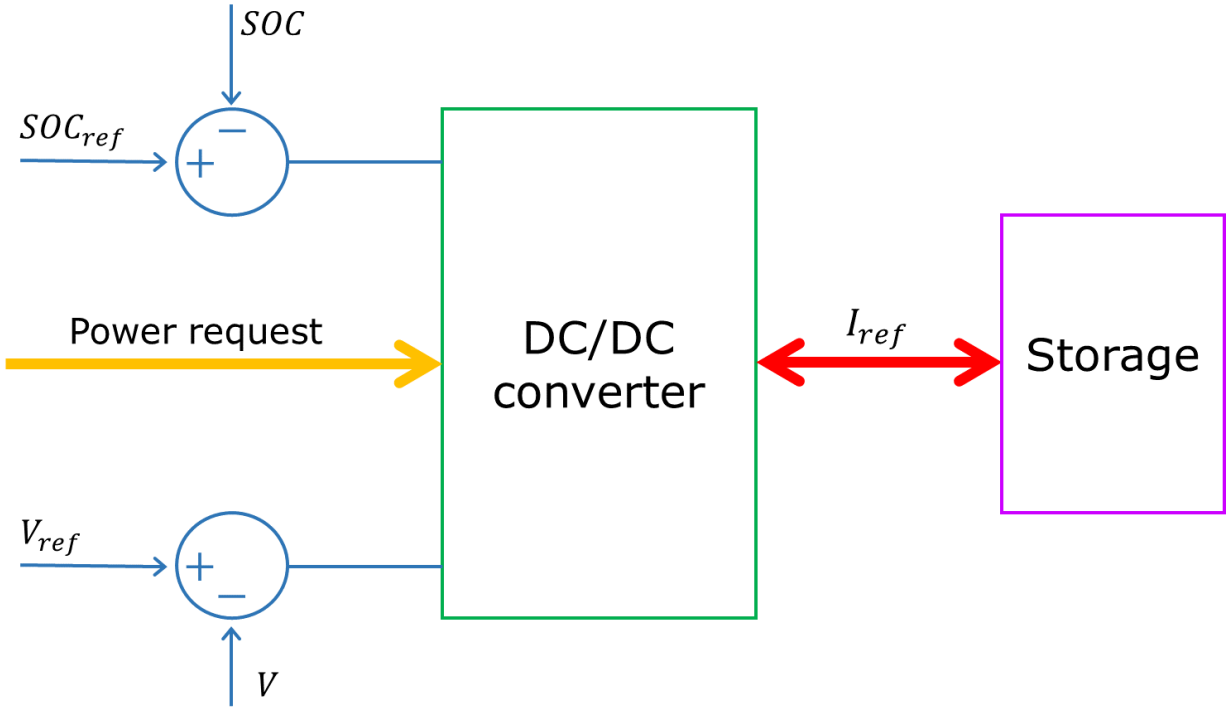

Figure 2.40: General scheme of the DC/DC converter operation.

electrical substations), without a voltage converter, would never be at voltage equilibrium with the substation and continuously perform micro charge/discharge cycles, and the on-board device would never correctly work as storage devices. The use of a DC/DC converter allows to decouple the storage device voltage from those of substation and line and to fully take advantage of their presence.

Furthermore, the converter can help to monitor and control the devices $S.O.C.$ and to protect them from excessive voltage stresses during the charge cycles. The function performed by the DC/DC converter is shown in Figure 2.40.

A simple DC/DC converter can be modelled through algebraic equations which modify the outlet current with respect to the inlet voltage (i.e. the substation voltage or the pantograph voltage), maintaining a decoupled device voltage level. In particular, the current provided to the storage device is calculated from the power flux, taking into account equivalent losses as functions of the current and including the possibility to control the device $S.O.C.$.

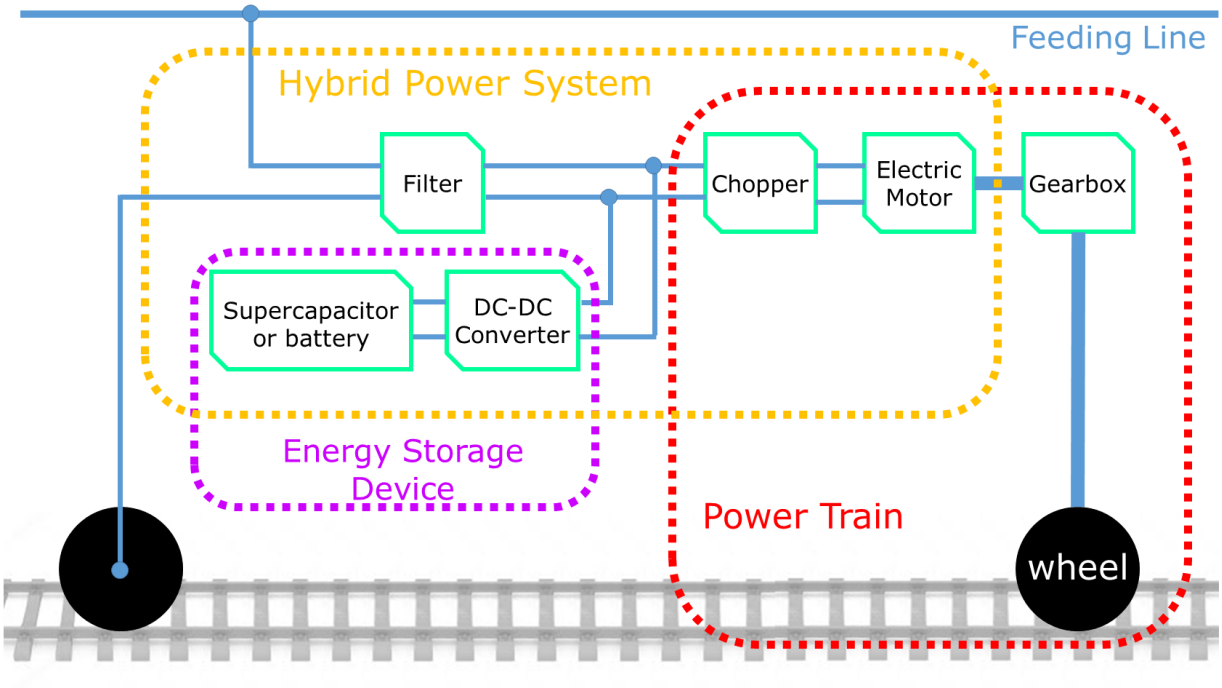

Figure 2.41: Scheme of a vehicle equipped with an on-board energy storage device and a DC/DC converter.

Figure 2.41 shows the architecture of an on-board storage device-DC/DC converter within a railway vehicle and allows to better highlight the interactions between the feeding line, the electric motor and the storage device: such a system represents a hybrid power system.

2.3 Multi-vehicle line and vehicles library

The core model, exposed in the previous Sections, has been originally developed in order to include more than one travelling vehicle within the whole line (in the fully assembled model) but only a single train within each line span, because, considering a mean substations distance of about 15 *km*, which is typical for High-Speed lines, it is not probable, if not even prohibited, to have more than one High-Speed train in the same line span; the motivations mainly lie on the regulation on safe braking distances.

However, to fully analyse the perspectives of regenerative braking, it is interesting to consider the presence of more than one travelling vehicle in the same line span and also the presence of vehicles in the opposite travelling direction. The latter point is easy to implement since it only requires the assembly of a second catenary system in each line span: the position of each vehicle is treated as a relative position with respect to the line span initial substation, so each subsystem uses its own reference system and the subsystems used for the catenary are equal for both the travelling

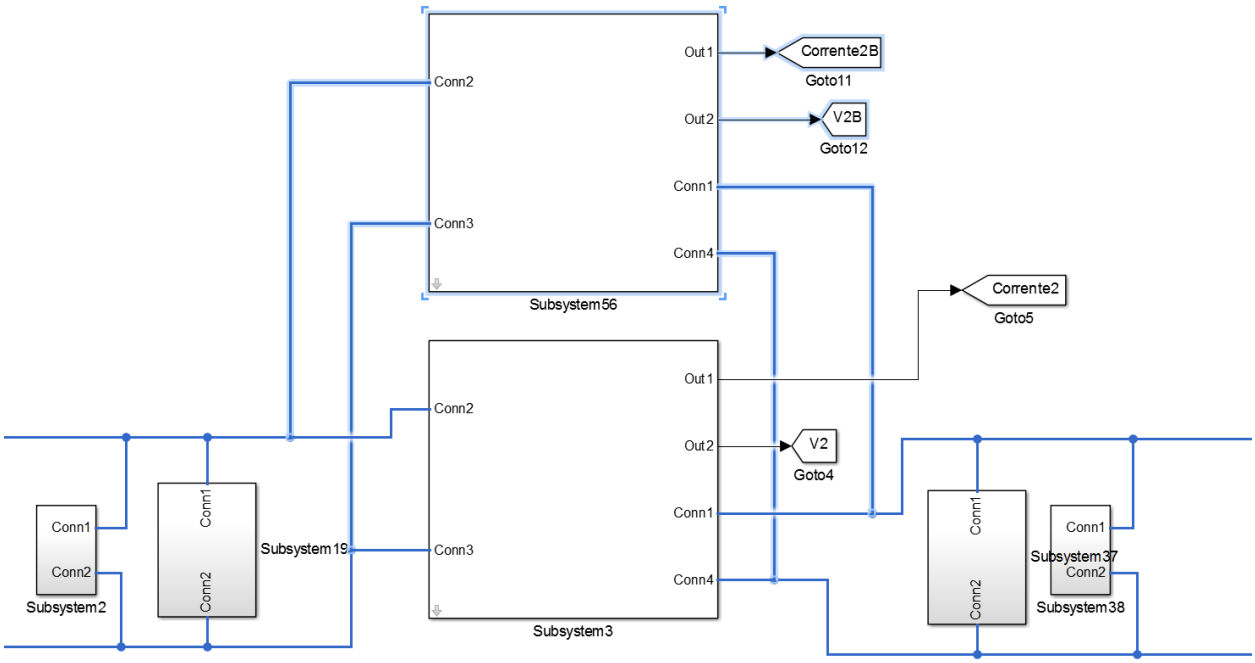

Figure 2.42: Simscape™ scheme for the multi-vehicle feeding line: trains in opposite directions.

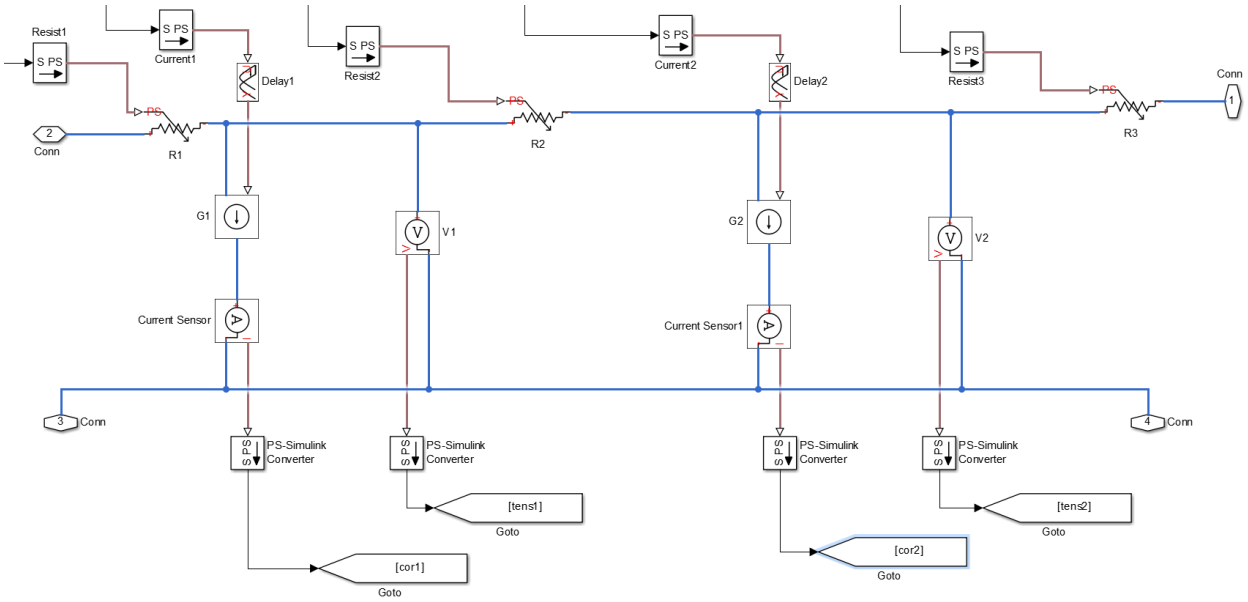

Figure 2.43: Simscape™ scheme for the multi-vehicle feeding line: trains in the same directions.

directions. This configuration is shown in Figure 2.42 and it is really useful, even in High-Speed systems, to perform an optimisation analysis based on timetables, enlarging the possibility for braking energy to be used by other vehicles in the traction phase.

The presence of more than one vehicle within a single line span is more complex (see Figure 2.43). The model has been modified by including two external MATLAB® functions and dividing the catenary in a greater number of variable impedance sectors (taking into account safety regulations, signalling, and substations power limitations, the presence of up to 5 trains in the same line span has been considered).

With this approach, the line topology is dynamically modified during the simulation and each line span can contain a variable number of vehicles; obviously, this approach will be useful mainly for commuter railway systems (or for light railway), while for High-Speed systems the previous fully assembled bidirectional model would still be preferable.

In order to enhance the value of the proposed approach, additional trains and vehicles have been added to the coupled vehicle-line model as a model library, useful to increase the scope and the ease of use of the proposed tool; some of the vehicles considered for the development of the library are shown in Figure 2.44.

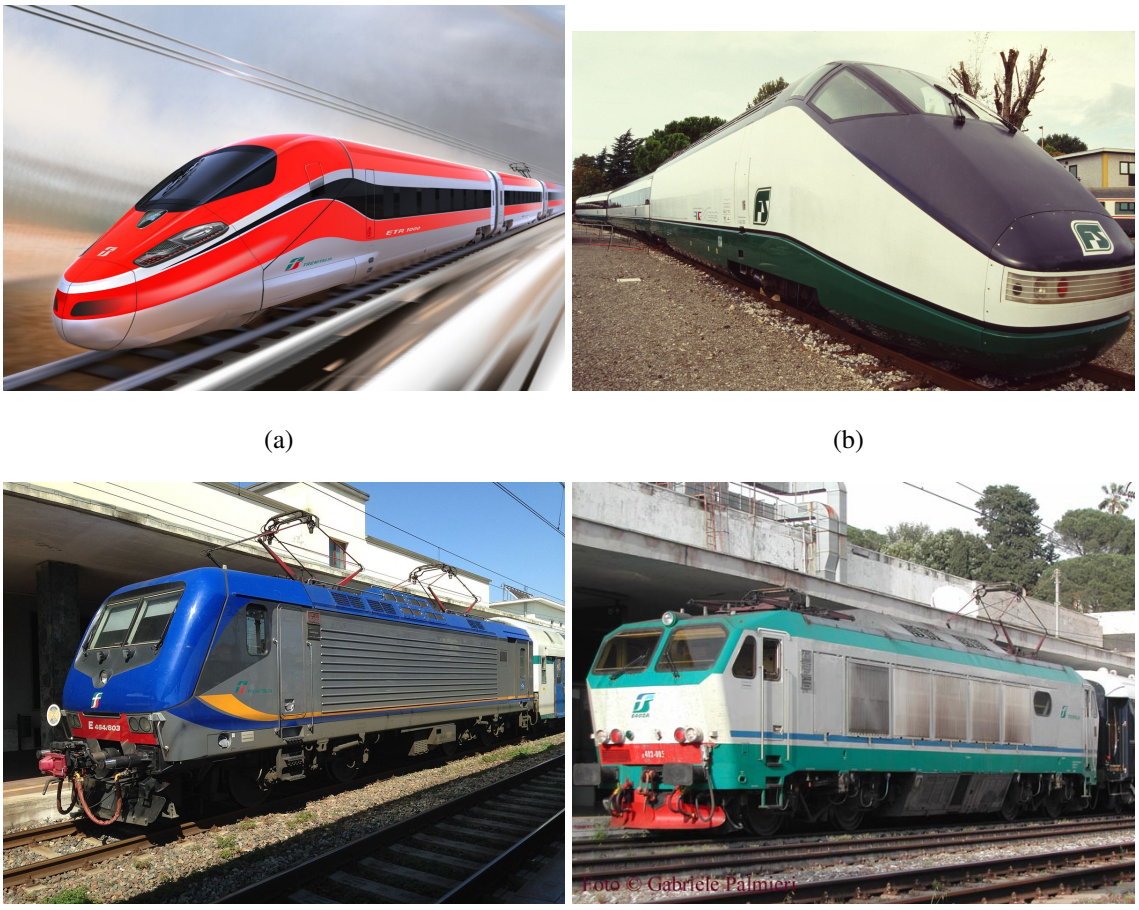

Figure 2.44: Some of the most diffused Trenitalia passenger trains: (a) ETR 1000, (b) ETR 500, (c) E 464 and (d) E 402.

The library has been developed as a typical Simulink® library, shown in Figure 2.45: the user can use the block of the chosen vehicle within the vehicle dynamical sub-model. Each block includes the characteristics of the vehicle required for its representation, e.g. mass and traction and braking performances.

The delivered traction and electric braking efforts of some trains, included in the library, are shown in Figure 2.46: Figure 2.46 shows the performances of the High-Speed train ETR 500 and of two locomotives typically adopted by Trenitalia (i.e. the E 402 and the E 464). The performances shown in Figure 2.46 for the ETR 500 are referred to a single E 404 locomotive (since the ETR

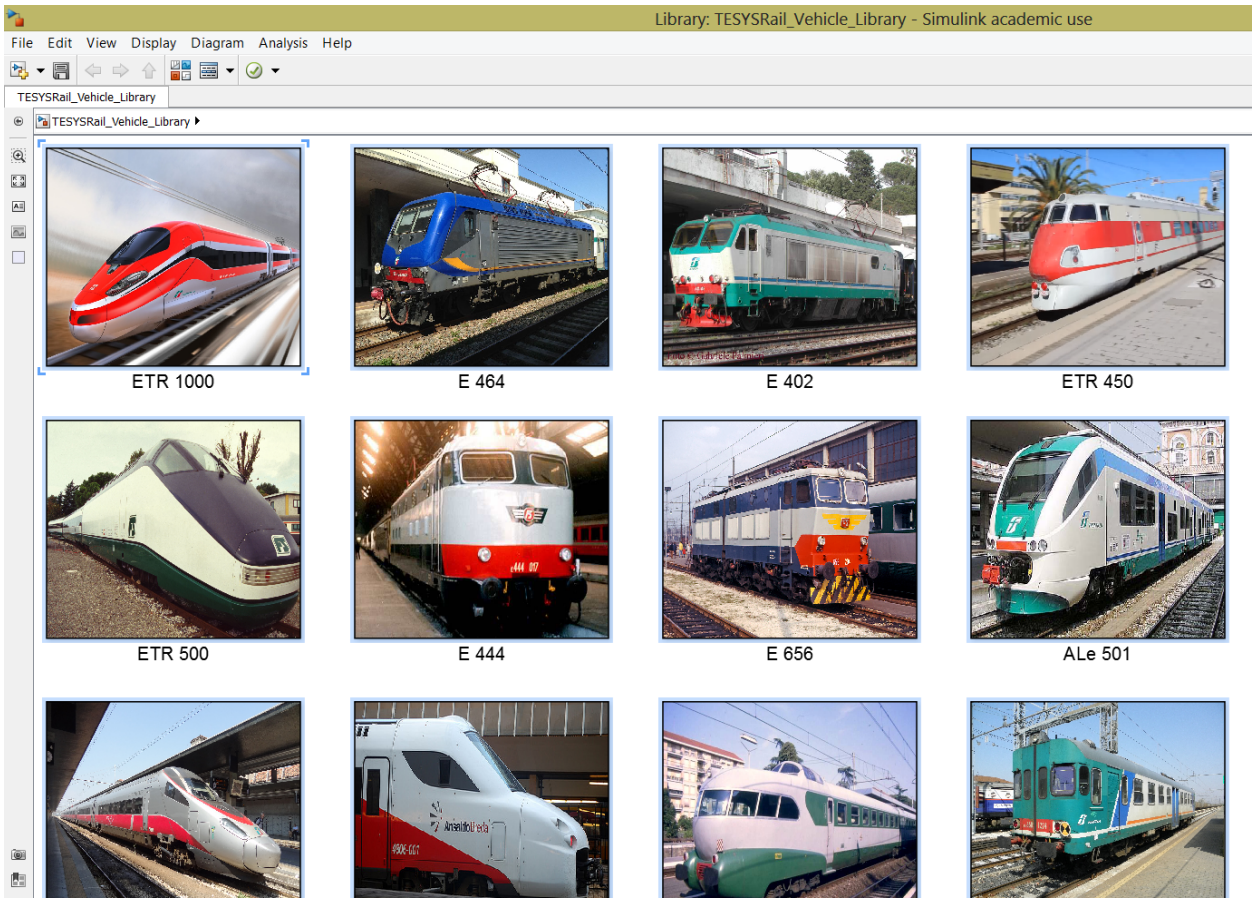

Figure 2.45: Simulink® vehicles library.

500 is not a real distributed traction train); hence, it has to be taken into account that the train composition includes two E 404 locomotives.

For conventional trains, in which the locomotives are associated to a known number of coaches, the modelling of traction and braking performances should pass through the specific data of the coaches (see the vehicle list reported in Table 2.2). In particular, data available for braking performances of coaches are expressed in terms of braking mass percentage according UIC regulations ([78], [79], [80], [81], [82], [83], [84]).

UIC code 544-1 prescribes a set of assessment curves, shown in Figure 2.47, for trains braking, which are expressed in terms of braking distance and braked weight percentage as follows:

$$s = \frac{C}{\lambda + D}, \tag{2.46}$$

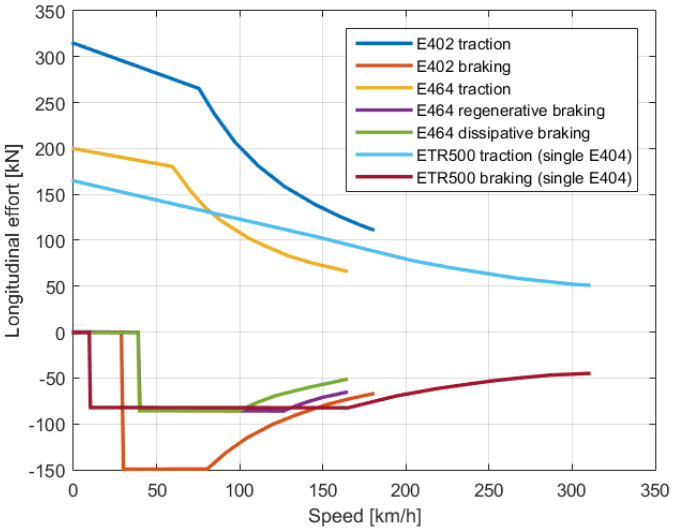

Figure 2.46: Electrical traction and braking performances of different locomotives and trains adopted by Trenitalia.

$$\lambda = \frac{C}{s} - D, \tag{2.47}$$

where λ is the braked weight percentage, s is the braking distance for rapid brake application expressed in m and C and D are constants (see Table 2.3).

The range of validity for Equations 2.46 and 2.47 is shown in Figure 2.47. For the use in the proposed model, these procedures have been converted in equivalent longitudinal efforts applied on the train composition. In particular, the braking distance s can be expressed as a function of the initial speed v of the vehicle: [85]

$$s = \frac{C'' v^2}{\lambda + D}, \tag{2.48}$$

where C'' is a coefficient which can be interpolated for different initial velocities. From the braking distance it is then possible to calculate the vehicle deceleration a_b:

$$a_b = \frac{\left(\frac{v}{3.6}\right)^2}{2\left(s - t_{b,eq}\frac{v}{3.6}\right)}, \tag{2.49}$$

where $t_{b,eq}$ is the braking equivalent time. This parameter is calculated considering the minimum time corresponding to the vehicle nominal length. From the deceleration it is easy to obtain the

Table 2.2: Main braking characteristics of some of the most diffused Trenitalia passenger trains.

Coach model	Mass C.N. [t]	Declared braking mass [t]	Braking mass with μ = 0.35 [t]	Official braking mass percentage	Braking distance with the nominal braking performance [m]
UIC-X 1^a & 2^a CL. - Cuccette 2^a CL.	52	71	74	137	538
UIC-X 1^a & 2^a CL. - Cuccette UIC-X 2^a CL. - SAN.	47	63	66	134	546
UIC-X 1^a & 2^a CL. sleeping	54	73	74	135	542
UIC-X 1^a & 2^a CL.	47	65	68	138	532
UIC-X 1^a & 2^a CL. - CU UIC-X 2^a CL.	53	72	75	136	540
UIC-Z1 1^a CL.	50	71	71	142	519
UIC-X 2^a CL.	47	65	68	138	532
UIC-X 2^a CL.	50	72	75	144	513
UIC-Z1 2^a CL.	51	69	69	135	542
UIC-X 2^a CL. semipilot	51	72	75	141	522
UIC-X - Stage coach	40	59	62	148	502
Stage coach Z1	41	62	63	151	491
VIC. Low floor - semipilot	48	63	66	131	557
VIC. Low floor - trailer	48	63	66	131	557
EUROFIMA 2^a CL.	46	65	65	141	522
M.D. (ext. doors)	43	59	60	137	535
M.D. (cent. doors)	43	59	60	137	535
Sleeping cars: MU & T2S	56	84	88	150	495
Sleeping cars: MU 92	62	92	94	148	500
Two stage wagons	54	67	69	124	585
Two stage wagons - 1	59	73	76	124	586
Two stage wagons - 2	61	76	79	125	582
VIVALTO	67	91	94	136	540

vehicle longitudinal effort.

Through these data, it is possible to take into account both electric and pneumatic braking and

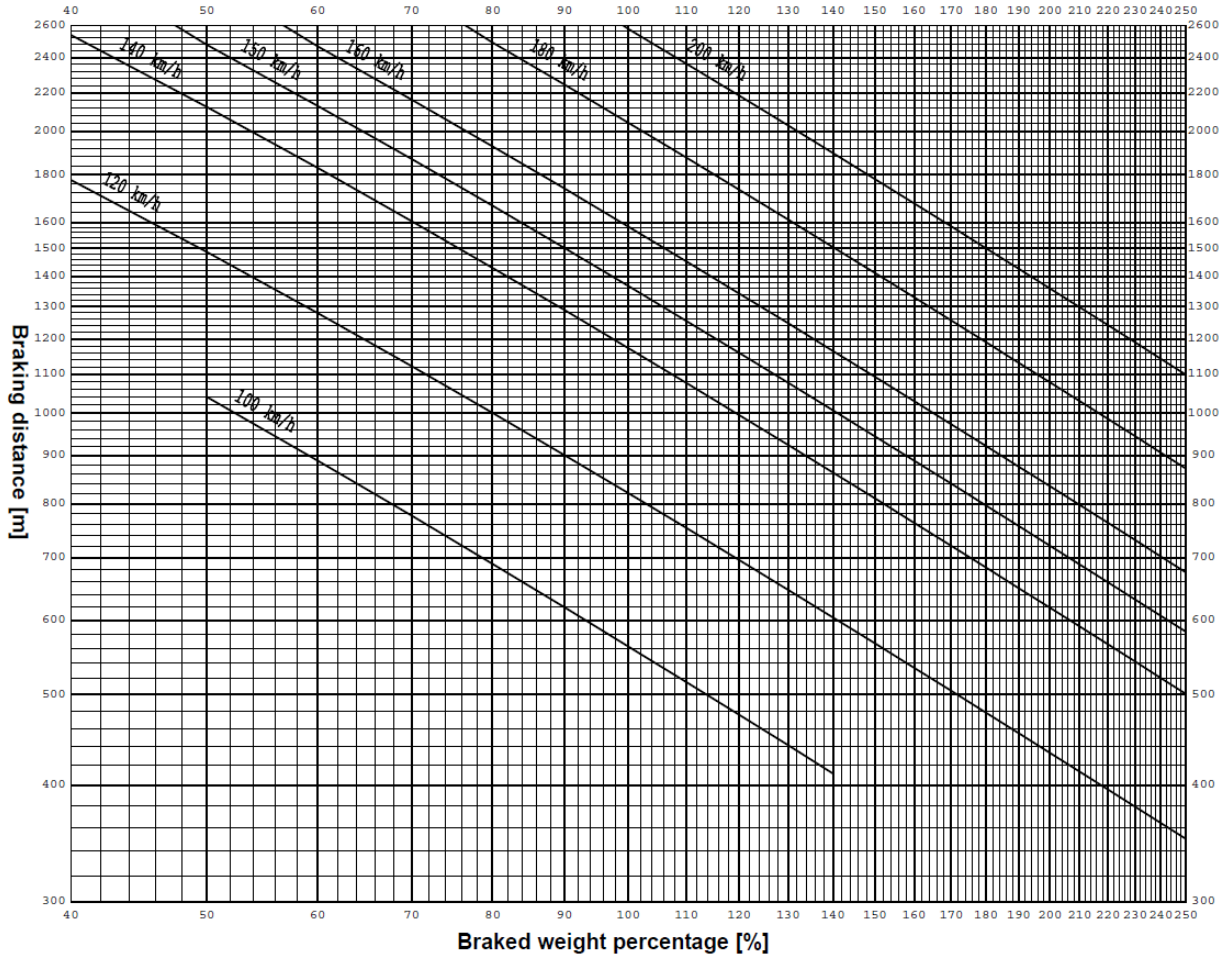

Figure 2.47: UIC method for braking effort calculation [78].

to analyse a wide range of blending strategies. The analyses performed in this thesis have taken advantage from previous literature works concerning the modelling of on-board railway systems with a particular attention to traction [86], conventional braking [87], [88] and magnetic track braking systems [89]. Furthermore, some important information, for the model generalization of this kind of subsystem, were found in the works of Quaglietta [90] and Baccari [91].

The increase in the number of modelled locomotives and coaches strongly contributes to the flexibility of the simulation tool: thanks to its modularity and to the vehicles library, the proposed model can be used to analyse not only High-Speed systems but also conventional and light railway systems.

Table 2.3: Constants for the calculation of braking performances according to UIC 544-1 [78].

v $[km/h]$	C	D
100	61300	8.9
120	91633	11.6
140	130995	11.6
150	152640	11.6
160	176714	11.6
180	228219	11.6
200	287620	11.6

2.4 Optimisation strategy and tools

In order to fully exploit the proposed modelling approach, the coupled model has been used to perform a set of optimisation analyses, considering as objective the minimisation of energy consumption and the maximisation of recovered braking energy.

To perform these analyses the model has been coupled to two different optimisation tools: the first one in MATLAB® and the second one in modeFRONTIER (see Sections 2.5.3 and 2.5.4).

The first analysis is a fundamental part of the TESYS Rail project and has been carried out in collaboration with EnginSoft, Ansaldo STS and the University of Napoli Federico II. This analysis, useful to obtain a reference scenario, does not take into account braking energy recovery and energy storage: it is a single vehicle analysis based on timetable and mission profile. In this scenario, the objective is the minimisation of energy consumption through the modification of the vehicle mission profile (i.e. the desired speed). The vehicle mission profile is fundamentally regulated by the line speed limits (which are dependent on the train position) and by the timetable (i.e. by the presence of intermediate station stops through the line). Usually, the train driver tries to reach the speed limit, to take advantage of coasting (i.e. an operating phase in which no traction or braking efforts are applied to the vehicle) when the speed limit has been reached and then to brake within the safety limits according to signalling and to speed limits, tolerating relatively small

speed errors with respect to the limits. However, in this situation,the train usually have significant time margins with respect to its timetable. Hence, it could be useful to take advantage of these margins applying more coasting phases and using the line slope profile to obtain a certain control of the vehicle speed.

Using the "human train driver" simulation as a reference for traction energy consumption, in the proposed optimisation analysis the vehicle traction and braking efforts application is modified to tolerate greater speed errors and apply more coasting phases within the available time margins on timetable. This eco-driving approach only allows relatively small energy savings, in particular in presence of other travelling vehicles on the line: in fact, the presence of other trains has a strong impact on timetables margins. However, it has an important advantage: it can be applied in real systems with almost no additional costs. Furthermore, in this research work, it provides a useful reference value for other energy saving solutions.

The second analysis is based on the use of energy storage devices, starting from a single vehicle scenario and then extending the analysis to a multi-vehicle system. The main objective is the minimisation of traction energy; however the analysis is maybe more significant, from a feasibility and costs point of view, considering the maximisation of recovered energy as objective. In fact, such an analysis could produce more general results and indicate a set of technical solutions which depends less on the specific characteristics of the simulated train and line. In this analysis, the model is simulated modifying the type of storage devices (i.e. supercapacitors and batteries), their application (i.e. stationary or on-board) and their distribution along the line. The sizing of the storage devices is performed before the optimisation analysis: the energy produced during a full braking phase of the considered train should represent about 5-10% of the total energy which the device could store, in order to guarantee a long operating life to the device.

The last analysis includes both energy storage devices, multi-vehicles and eco-driving: this analysis is useful to understand and optimise existent systems or systems which are in a late phase of the design process, since a great quantity of data is needed for the set up of the model itself. It is important to underline the large number of design variables (e.g. storage devices power and energy, management strategies, number and location of devices) that need to be considered and the

equally large number of criteria which could be followed, including qualitative goals difficult to be numerically expressed.

2.5 Softwares and mathematical tools

This research work has mainly taken advantage from MATLAB® and its dynamical simulation tools Simulink® and Simscape™. Simulink® is the classical software for the analysis of dynamical systems: it transposes the characteristics of the MATLAB® language in a dynamical environment, which is more suitable for the modelling of complex physical systems with many interactions. Simscape™ is a physics-based modelling tool, which can be used stand-alone or integrated in Simulink® itself, thus enlarging the capabilities of both the environments. MATLAB® has been used also for the optimisation analyses, in which the Simulink®-Simscape™ models have been handled directly through the MATLAB® language.
Furthermore, the optimisation analyses have been also carried out using the modeFRONTIER optimisation software, developed by ESTECO SpA.

2.5.1 Simscape™ object oriented language

Simulink® represents the standard tool for the analysis of dynamical systems [92], [93], [94]; however, in this research work, a large part of the core model has been developed using the innovative physics-based Simscape™ language.
Simscape™ is a newly developed Simulink® extension which allows to create custom simulation blocks (in addition to the libraries of standard blocks already included in MATLAB®) using an object oriented modelling language. This language permits to directly write the element constitutive equations (balance equations) and avoid their explicit resolution (i.e. Simulink® approach). Those balance equations are usually implemented following a modular approach, which suits well the representation and simulation of complex multi-physics dynamical systems [95]. This approach, denoted as Bond-Graph approach [96], has also been adopted by other high level modelling languages, such as Modelica® [30], [97], [98].
The Simscape™ language represents an extension of the MATLAB® language and can be completely integrated in MATLAB® and Simulink® models.
The equations, which characterise the blocks of a model, are handled by a symbolic solver

during the simulation initialization: the symbolic solution of this equations system provides great numerical advantages for the simulation phase. Furthermore, the developer does not need to directly consider the numerical implementation of the equations during the model development: this is why Simscape™ is denoted as physics-based.

Another important advantage is represented by the complete absence of algebraic loops, which, in complex systems, represent a significant limit of a pure Simulink® approach, where these problems can be avoided only through numerical delays or through the creation of additional auxiliary variables. Finally, the strong modularity of the approach allows to analyse complex scenarios with little effort.

Simscape™ blocks require, in order to fully exploit the language flexibility, the creation of some physical and numerical elements, which then simplify the creation of the elements code. The first step is the creation of the desired physical domain, where the characteristic variables of the elements are defined. Indeed, this is denoted as *domain* and, by way of example, can be defined as follows:

```
domain electrical
parameters
    Temperature = { 300.15 , 'K' }; % Circuit temperature
    GMIN = { 1e-12 , '1/Ohm' }; % Minimum conductance
end
variables
    v = { 0 , 'V' }; % Voltage
end
variables(Balancing = true)
    i = { 0 , 'A' }; % Current
end
end
```

This algorithm defines the electrical domain of the standard electrical Simscape™ library. Some of the standard blocks of this library have been directly used, while other custom blocks have been

developed starting from the standard electrical domain itself. The parameters are constant values which are needed by some of the library blocks, while the variables are, in this case, voltage and current. Voltage is defined, according to the Bond-Graph approach, as an A-variable, i.e. an *across* variable: this notation is related to the physical significance of the variable, which acts across the element and is measured across the element. Current is defined as a T-variable, i.e. a *through* variable, since it flows through the element. The Simscape™ language takes advantage of these definitions, denoting current as a *balancing*, or *branch* variable. It is interesting to highlight how all the quantities defined within a Simscape™ block are characterised by their units of measurements and that a Simscape™ model handles *physical signals*; the coupling with Simulink® blocks must be made through proper converter blocks (see the blocks shown in Figure 2.22).

The second step (or the third, for physical domains where it is also necessary to define physical properties or materials, like in the thermo-fluid domain) is the creation of the element blocks: this step defines the structure of the systems of equations characterising each element. To expose this step, the four-port custom block source code, developed to create the real substation element, is reported:

```
component(Hidden=true) four_port
nodes
    p1 = foundation.electrical.electrical; % +:top
    n1 = foundation.electrical.electrical; % -:bottom
    p2 = foundation.electrical.electrical; % +:top
    n2 = foundation.electrical.electrical; % -:bottom
end
variables
    i1 = { 0, 'A' }; % Input current
    v1 = { 0, 'V' }; % Input voltage
    i2 = { 0, 'A' }; % Output current
    v2 = { 0, 'V' }; % Output voltage
end
```

```
branches
    i1 : p1.i -> n1.i;
    i2 : p2.i -> n2.i;
end
equations
    v1 == p1.v - n1.v;
    v2 == p2.v - n2.v;
end
end
```

This code defines a generic block with four ports for physical signals and each port is connected to the desired physical domain: here, all the ports point to the electrical domain and, hence, each physical connection carries both the domain variables, voltage and current. The block also includes a generic system of equations, including both through and across variables. This system of equations will then be characterised and defined in the element code (i.e. different element can share the same block code). The following algorithm represents the implementation of the real, finite power electrical substation:

```
component power_limited_voltage_source
parameters
    Pot_max = { 10 ^7, 'W ' }; % Maximum substation power
end
nodes
    p1 = foundation.electrical.electrical; % +:top
    n1 = foundation.electrical.electrical; % -:bottom
    p2 = foundation.electrical.electrical; % +:top
    n2 = foundation.electrical.electrical; % -:bottom
end
variables(Access=private)
```

```
        v1 = { 0, 'V' }; % Input voltage
        i2 = { 0, 'A' }; % Output current
    end
    variables
        i1 = { 0, 'A' }; % Input current
        v2 = { 0, 'V' }; % Output voltage
    end
    branches
        i1 : p1.i -> n1.i;
        i2 : p2.i -> n2.i;
    end
    equations
        v1 == p1.v - n1.v;
        v2 == p2.v - n2.v;
        v2 == if gt(i1*v1, {Pot_max,'W'}), {3700,'V'} else {Pot_max/i1,'V'} end;
        v1 == 0;
    end
    end
```

2.5.2 ODE23t

The differential equations solver used during the simulations of the proposed model is denoted as ODE23t (i.e. Ordinary Differential Equations trapezoidal solver with variable order from 2 to 3), which is a solver suitable for stiff problems. In particular, this method takes advantage of the trapezoidal integration rule through the use of a free interpolant. ODE 23t is useful and preferable with respect to other solvers in presence of moderately stiff problems, especially if the user requires a solution free of numerical damping; furthermore, this solver can also solve differential algebraic equations systems (i.e. DAEs) [99].

Classical ODEs solver are suitable to solve differential equations systems expressed as follows:

$$\mathbf{M}(t)\,\mathbf{y}' = \mathbf{f}(t,\mathbf{y})\,. \tag{2.50}$$

The mass matrix **M** can be singular: in this situation the equations system is a DAEs one. Simulink® and Simscape™ usually have to deal with DAEs systems, which can be formulated as follows:

$$\begin{cases} \mathbf{u}' = \mathbf{f}_1(t,\mathbf{u},\mathbf{v}) \\ 0 = \mathbf{f}_2(t,\mathbf{u},\mathbf{v}) \end{cases}. \tag{2.51}$$

A DAEs system usually corresponds within the model to "algebraic loops", (i.e. a set of blocks connected in a close loop, with inputs that depend on the outputs). Due to its stability characteristics for this kind of problems, ODE23t is usually employed in presence of electrical circuits: it shows the same convergence rate for differential and algebraic variables [100].

2.5.3 MATLAB® optimisation tool

For the optimisation analysis, a very simple MATLAB® algorithm to perform a DOE (see Section 2.5.4 for more details) analysis, and automatically manage the results, has been developed: the DOE allows to perform the desired set of simulations without the need of manual intervention. By way of example, the algorithm used for the feasibility analyses is formulated as follows:

```
percent_fren_vec=0.1:0.01:1;
posiz_fren_vec=0:0.1:1;
distance_ESS=ESS(:);
tens_capt=[];
for jjj=1:length(posiz_fren_vec)
    veloc_desiderata_pos=[0 1000 distance_ESS+distance_ESS*posiz_fren_vec(jjj)
distance_ESS+distance_ESS*posiz_fren_vec(jjj)+0.1];
    for iii=1:length(percent_fren_vec)
```

```
            percent_fren=percent_fren_vec(iii);
            sim('vehicle_line_model');
            tens_capt(iii,jjj)=[max(tensione_captata(:))];
        end
    end
```

Furthermore, for more complex interactions, the MATLAB® Optimization Tool itself has been used.

2.5.4 modeFRONTIER

modeFRONTIER is a software developed by ESTECO SpA for optimisation analyses [101]. This software includes many different optimisation tools and has been used within the partners collaboration of the TESYS Rail project (i.e. EnginSoft, the dealer of the software, was one of the project partner).

modeFRONTIER is able to directly couple a large number of different simulation softwares; furthermore, it can couple almost everything through its batch mode. The most simple optimisation analysis the software can perform, is a DOE (i.e. Design of Experiments): the model (or the models) is handled in the main command window of the software and, through the management of input and output variables, it can be coupled to other parts or directly included within the DOE. The DOE is currently the most useful analysis for the purpose of this research work; however, many other complex algorithms can be used, especially concerning multi-objective optimisation.

The DOE is an efficient method to explore the design space and allows to understand how the system variables influence the results. The first step, in this analysis, is the choice of the design space limits and of the number of design configurations to be analysed. In this way, it is possible to automatically perform a large number of desired simulations and understand the best configurations.

modeFRONTIER is able to choose which configurations to analyse (if the user chooses to analyse

only a limited number of configurations), taking advantage of different optimisation algorithms. However, to fully exploit the possibilities of the software, it is possible to set up a real multi-objective optimisation analysis, in which each objective has the same weight and the user is free to evaluate the results according to the actual importance of each parameter. modeFRONTIER can implement, among many others, the following optimisation algorithms:

- Pareto approach;
- genetic algorithms;
- Monte Carlo approach (useful to take into account uncertainty and random factors);
- gradient-based algorithms.

One of the fundamental advantages offered by modeFRONTIER is the possibility to couple models developed using different commercial or in-house softwares: aside from the analyses included in this thesis, it has been used to couple the proposed model with a railway signalling model developed by the University of Napoli Federico II and with a model developed by Ansaldo STS.

2.6 Considered test case: ETR 1000 on the Firenze-Roma line

In this research work, for the validation of the proposed model from a High-Speed point of view, and for the feasibility and optimisation analyses, a High-Speed train with the characteristics of the ETR 1000 has been considered; this vehicle is the last High-Speed train developed for Trenitalia by Bombardier and AnsaldoBreda (AnsaldoBreda Group has now been purchased by Hitachi). The main technical features of the considered train are listed in Table 2.4: the vehicle has a distributed traction system, shown in Figure 2.48, whose traction and braking performances are shown in Figure 2.49 (real operating scenario).

Currently the ETR 1000 is in the first phases of its operating life, so the data described in this paper, which are mainly referred to the preliminary presentations of the train (see the technical specifications of the train [102] and the paper by Gherardi and Vannelli [103], who analysed interoperability issues between European High-Speed trains) could be subjected to slight modifications due to the final calibration and optimisation of on-board systems. The most interesting reference is represented by the proceedings of a CIFI (acronym for Collegio degli Ingegneri Ferroviari Italiani) Symposium [104], a conference where the participation of many train suppliers makes possible a deeper insight on train functionalities and performances.

The ETR 1000 is designed to operate under different electrification standards: thus, it is able to respect interoperability standards among the most important railway networks of western Europe. In particular, in this research work, the operation of the ETR 1000 within the 3kV DC Firenze-Roma line (usually denoted as *Direttissima*), which is the oldest and perhaps most important High-Speed line of the Italian network, has been considered. Figure 2.50 and Table 2.4 show the main

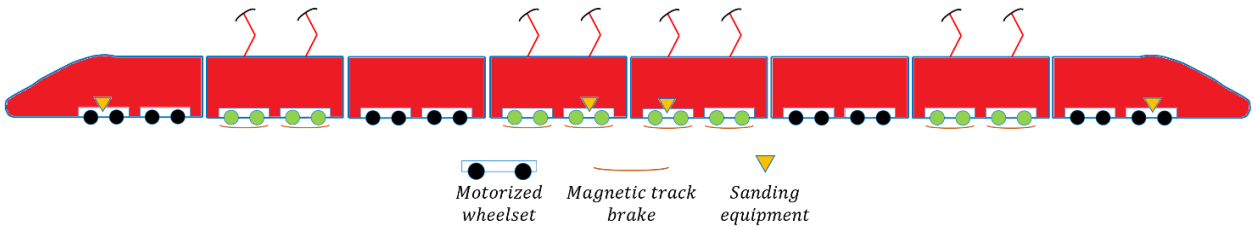

Figure 2.48: Distributed traction and braking systems of the ETR 1000 High-Speed train.

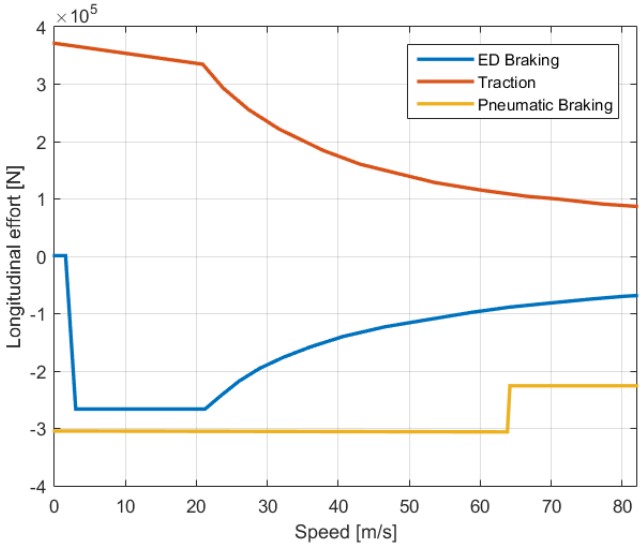

Figure 2.49: Traction and braking performances of ETR 1000 High-Speed train (referred to a 3 kV DC line).

Figure 2.50: Catenary of the Firenze-Roma *Direttissima* High-Speed line.

electrical features of the considered line.

The ETR 1000 is not equipped with on-board storage systems, but its traction system can be used in a regenerative braking configuration; however, the energy recovery is currently limited by the availability of a load along the electrical line. In fact, the electrical substations currently installed along the *Direttissima* line are designed to operate only in the first quadrant: they are not fully reversible substations and there are no stationary energy storage devices within the line.

Furthermore, in order to protect the line from potentially harmful overvoltage, the train switch from regenerative to dissipative braking if the line overvoltage exceeds a value of about 3900 V.
In this work, the feasibility and the potential advantages of the application of energy storage technologies to High-Speed trains have been investigated, to understand how to fully exploit the regenerative braking capabilities of those trains. The considered High-Speed test case has been used both for the experimental validation of the proposed modelling approach and for the energy recovery feasibility and optimisation analyses.

Table 2.4: Main characteristics of the ETR 1000 High-Speed train and of the Direttissima High-Speed line.

Total Seats	470
Car Body Construction	Aluminum Alloy
Train Mass	500 t
Train Length	202 m
Axle Load	17 t
Gauge	Standard 1435 mm
Rotating Inertia Respect to Train Mass	4 %
Wheel Diameter	920 mm
UIC Classification	Bo'Bo'+2'2'+Bo'Bo'+2'2' +2'2'+Bo'Bo'+2'2'+Bo'Bo'
Motorized Weight Fraction	0.5 [-]
Traction System	Water-cooled IGBT Converters and Asynchronous AC Traction Motors
Supported Electrification Standards	25 kV 50 Hz, 15 kV 16.7 Hz, 3 kV DC, 1.5 kV DC
Nominal Power	9.8 MW
Max Tractive Effort (standstill)	370 kN
Max Speed (design)	400 km/h
Max Speed (commercial)	360 km/h
Acceleration / Dec. Performances	0.7 ms-2 (acceleration phase) / 1.2 ms-2 (deceleration phase)
Braking System	Electro-Pneumatic, Electric Braking (both regenerative or dissipative), Magnetic Track Brake
Brake Pad Consumption	0.1-0.2 cm^3/MJ (depending on installed brake pad and demanded brake power)
Line Impedance (ρ)	About 0.05 Ω/km
ESS No Load Voltage	3700 V
ESS EQ. Impedance	About 0.09 Ω
Mean Distance between ESSs	14.7 km
Min Distance between ESSs	12 km
Max Distance between ESSs	16.8 km

2.7 Considered test case: E 464 on the Firenze-Pisa-Livorno line

Furthermore, both for the validation and for the feasibility and optimisation analyses, the E 464 locomotive with a set of 4 Vivalto coaches has been considered. The main technical features of the considered train are listed in Table 2.5; the vehicle has an electric traction and braking system in the two locomotives, while the coaches are equipped with the traditional pneumatic braking system (see Figure 2.51, which shows the architecture of the E 464 train); traction and braking performances of the E 464 locomotives are shown in Figure 2.46 (real operating scenario).

This vehicle has been chosen within the TESYS Rail project as the test case for the global

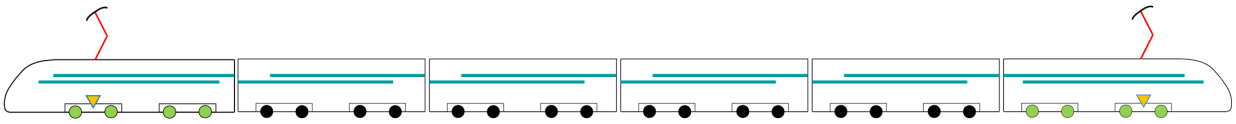

Figure 2.51: Scheme of the E 464 commuter train.

model developed by the partnership. In particular, a partner has planned an experimental campaign in collaboration with RFI with the purpose of measuring the performances of the E 464. This experimental campaign will provide the data for the validation phase of the TESYS Rail project. In particular, in this research work, the experimental campaign considers the operation of the E 464 within the 3kV DC Firenze-Pisa-Livorno line. Figure 2.52 shows the topology of the part of the line considered for the analyses and Table 2.5 show the main electrical features of the considered line.

The E 464 traction system can be used in a regenerative braking configuration; however, neither the considered line nor the vehicle include storage devices.

Table 2.5: Main characteristics of the E 464 commuter train and of the Fi-Pi-Li line.

Train Mass	324 t
Train Length	150 m
Number of coaches	6
Gauge	Standard 1435 mm
Max Power in traction	3.5 MW
Max Power in braking	2.35 MW
Motorized Wheel Diameter	1100 mm
UIC Locomotive Classification	Bo'Bo'
Motorized Weight Fraction	0.22 [−]
Traction System	FIA 5267 motors
Supported Electrification Standards	3 kV DC, 1.5 kV DC
Max Traction Effort (standstill)	200 kN
Max Traction Effort (at max speed)	67.5 kN
Max Braking Effort	85 kN
Max Speed	160 km/h
Braking System	Electro-Pneumatic, Electric Braking (both regenerative or dissipative)
Line Impedance (ρ)	About 0.04 Ω/km
ESS No Load Voltage	3600 V
ESS EQ. Impedance	About 0.1 Ω
Mean Power ESSs	5.4 MW
Mean Distance between ESSs	20 km

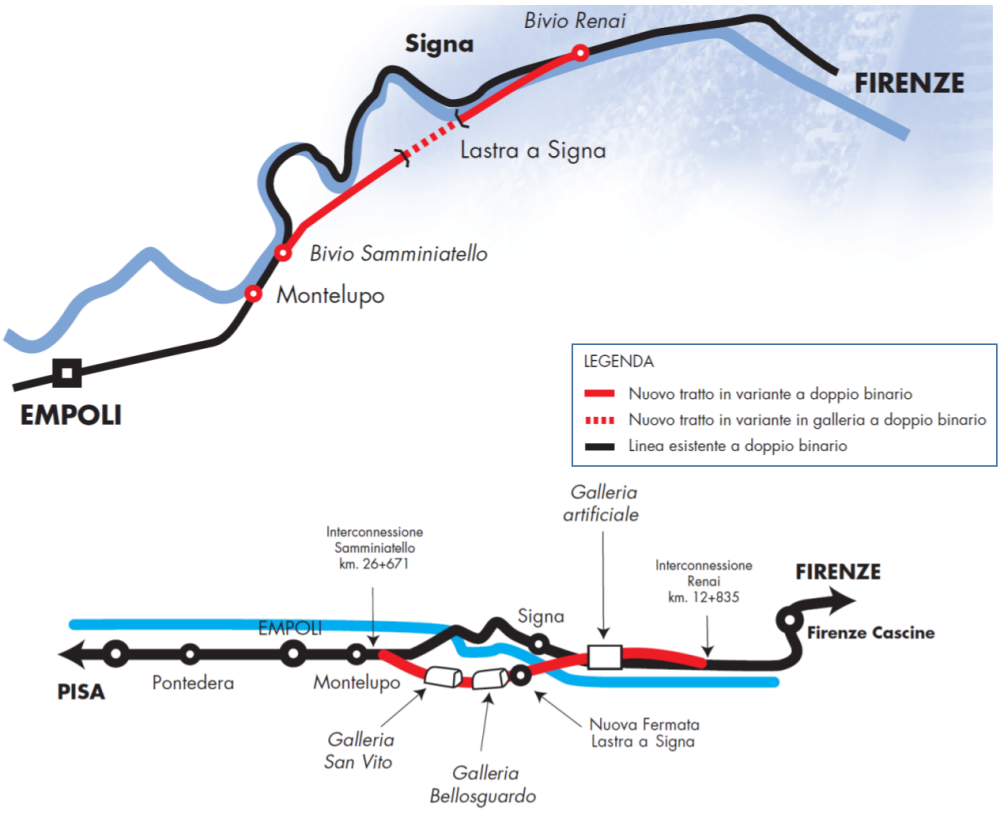

Figure 2.52: Scheme of a part of the Firenze-Pisa-Livorno line [105].

3

Results and Discussion

Chapter 3 focuses on the exposition and analysis of the results provided by the proposed model, during the research activity.

The first part of the Chapter is devoted to a general analysis of the physical behaviour of the system, showing how the model response is coherent with the physical reality.

The second part is devoted to the tuning and calibration of the model considering a set of experimental data measured on board the ETR 1000 within the *Direttissima* High-Speed line.

After the calibration phase, the model has been experimentally validated considering experimental measurements carried out for the ETR 1000 (within the *Direttissima* High-Speed line) and for the E 464 (within the Fi-Pi-Li line).

The model has then been used to perform a large scale feasibility analysis of the perspectives of regenerative braking within High-Speed systems. The feasibility analysis is followed by the proposal of a storage devices sizing approach and by an optimisation analysis of the considered High-Speed system.

3.1 General results

ETR 1000 is a relatively new project and, currently, it represents one of the most relevant investment performed by the Italian railways. During the drawing up of this research work, the train was performing its first activities on Italian High-Speed lines. The data sets, available for the preliminary validation of the proposed model, are referred to specific manoeuvres performed during the train homologation phase: during the preliminary homologation process, the train has been subjected also to experimental tests concerning high frequency measurements of collected currents and voltages (the frequency ranges from 20 kHz to 200 kHz). These tests were not performed to evaluate the train efficiency: their goal is, in fact, the evaluation of the harmonic contents of collected currents and voltages. This analysis is useful to understand various problems related to train power collection and concerning power drives, on-board filters and the quality of pantograph current collection. In order to make those data usable for this research work, they have been filtered and down-sampled to obtain smooth profiles, useful for the validation of the proposed model but with almost no industrial interest, since the information about high frequency behaviour is completely lost (a maximum sampling frequency of 10 Hz has been considered).

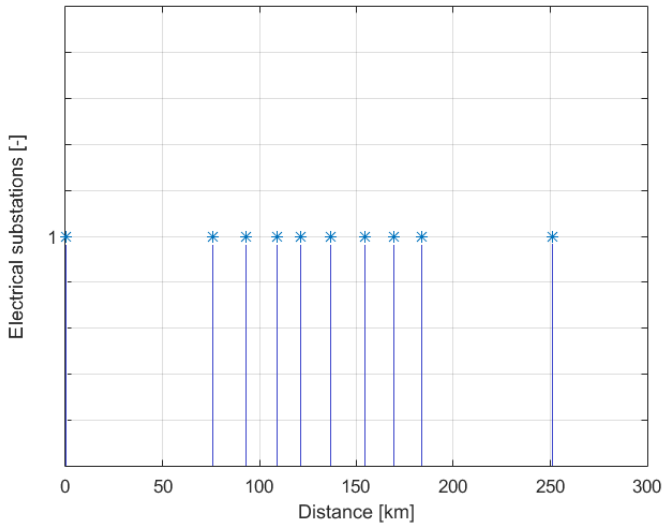

Figure 3.1: Electrical substations positions along the *Direttissima* High-Speed line.

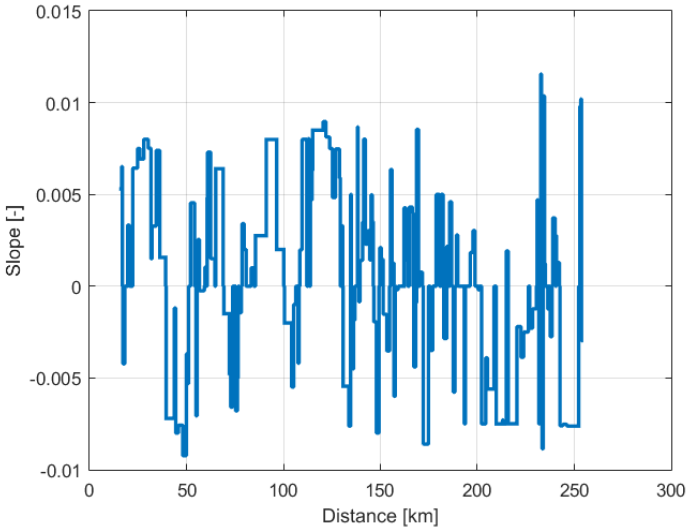

Figure 3.2: Slope of the *Direttissima* High-Speed line.

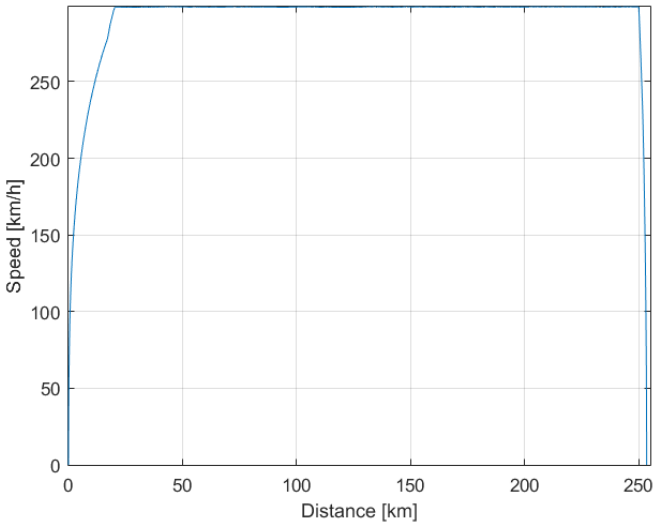

Figure 3.3: Preliminary numerical test: speed profile.

The first aim of this research work is to prove the accuracy of the results provided by the proposed model and its ability to reproduce a real High-Speed operating scenario through the comparison with experimental data.

Figures 3.1 and 3.2 show a set of the parameters, used within the model, to represent the considered

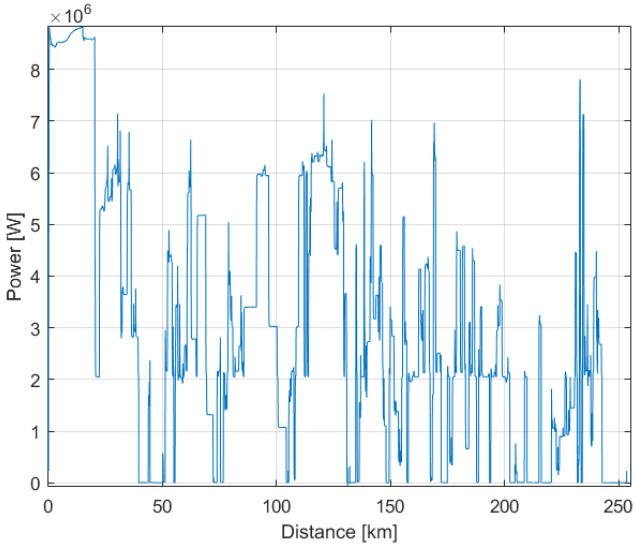

Figure 3.4: Preliminary numerical test: vehicle power consumption.

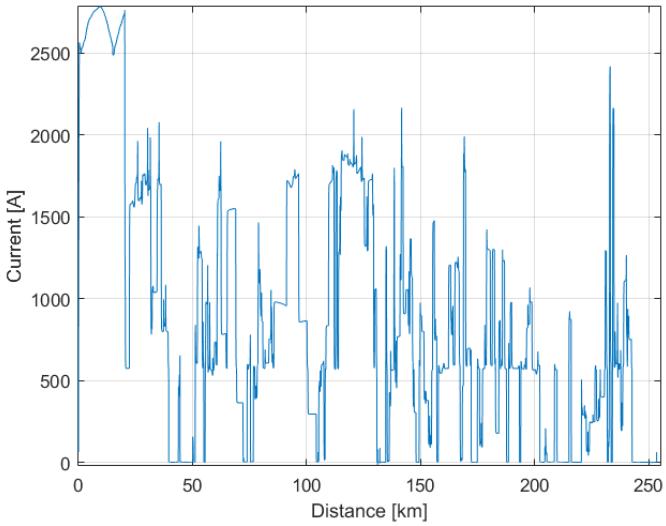

Figure 3.5: Preliminary numerical test: pantograph current.

line: Figure 3.1 shows the position of the electrical substations within the *Direttissima* line, while Figure 3.2 shows its slope.

As a starting analysis, the model, set up to represent the ETR 1000 within the *Direttissima* line, has been used to prove its coherence with the physical behaviour of the system, without taking

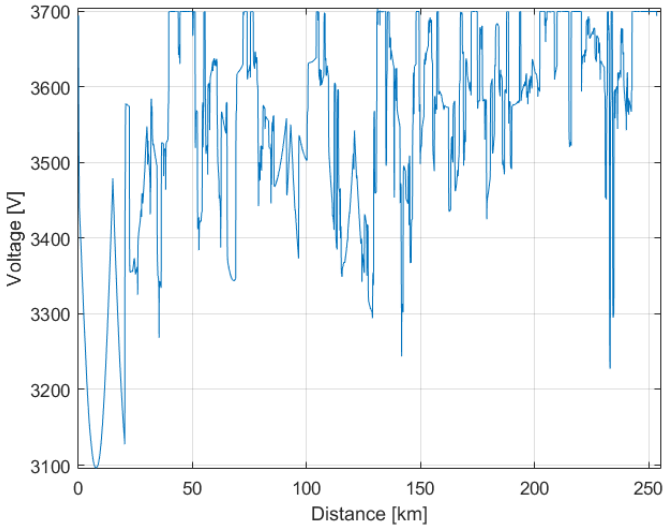

Figure 3.6: Preliminary numerical test: pantograph voltage.

into account actual infrastructure and vehicle limits (e.g. speed limits). The mission profile chosen for this analysis includes a first acceleration from standstill to 300 km/h (starting from Firenze), a constant speed phase and a final full braking in correspondence of Roma station.

Figure 3.3 shows the velocity profile calculated with the proposed model: it follows well the chosen mission profile and is in good agreement with the behaviour expected from the vehicle: in fact, it is possible to highlight how the traction and braking phases directly correspond to the traction and braking curves of the vehicle. The results, shown in Figure 3.4, Figure 3.5 and Figure 3.6, correspond to that velocity profile: it is possible to highlight how the highest power consumption corresponds to the initial acceleration phase to the maximum speed (Figure 3.4), analogously to the highest absorbed current (Figure 3.5) and to the biggest voltage drop (Figure 3.6). The other peaks and drops correspond to electrical substations and smaller accelerations due to the line characteristics; during the braking phases, the voltage does not rise over the substation value because those results are referred to the first simulation scenario, the one without energy recovery and with the fully reversible substation (see Figure 1.13(b) and Figure 2.27).

3.2 Comparisons with experimental data

Section 3.2 focuses on the comparison between some sets of experimental data and the results obtained with the proposed model. The experimental measurements have been used both to calibrate and validate the developed model; in particular, a first set of measures concerning the ETR 1000 High-Speed train has been devoted to the model tuning, two further sets of data referred to the same train have been used for the validation, and, finally, two sets of measurements referred to the E 464 commuter train have been used to complete the validation phase including also a classical regional system.

All the data sets are referred to four of the main quantities related to the energetic performances of a railway system: a kinematic variable (i.e. the vehicle velocity) and three electrical quantities, i.e. power, current and voltage.

3.2.1 Experimental calibration

In this Section, for the experimental calibration of the proposed coupled vehicle-line model, a set of experimental data concerning a specific traction manoeuvre of the ETR 1000 on the High-Speed line Roma-Firenze, from standstill to a speed equal to 250 km/h, has been used.

The manoeuvre is performed applying the maximum traction effort, corresponding to the curves shown in Figure 2.49. Figure 3.7 shows the comparison between the measured vehicle speed profile and that obtained with proposed model: it is possible to verify that the main parameters considered in the model concerning traction performances, inertia and motion resistances were substantially correct. In particular, the numerical and experimental speed profiles above 110 km/h are almost identical (with negligible errors both in terms of speed and acceleration); below 110 km/h, there are some differences between the two profiles; in particular, the real train exhibits higher performances. This error has to be carefully evaluated considering real adhesion conditions and axles skidding phenomena. Axle skidding phenomenon is strictly connected to the adherence of the track: during the traction phase it is identified as skidding, while during the braking phase

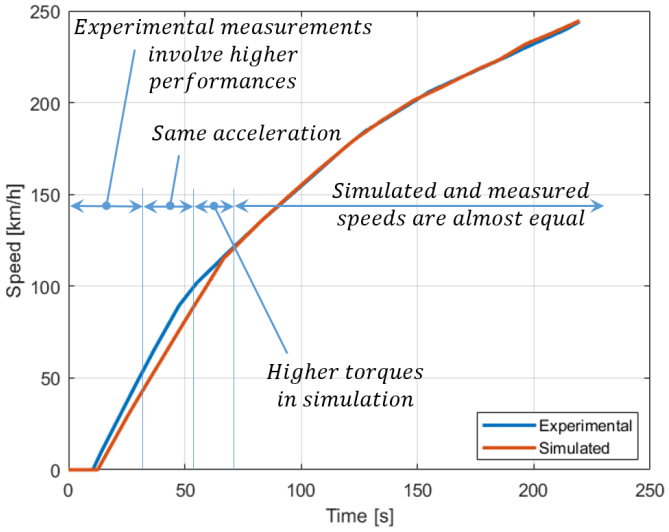

Figure 3.7: ETR 1000 experimental calibration: comparison between a real traction manoeuvre on the Firenze-Roma High-Speed line and the corresponding numerical results obtained with the proposed model.

it is denoted as sliding. In both cases the phenomenon is due to a difference between the wheelset velocity and the speed of the vehicle itself (e.g. the wheel locking during braking) and it leads to a vehicle skidding. Axle skidding can be dangerous in terms of safety; furthermore, it is important to avoid it in order to prevent excessive wheel and track wear. Train traction performances used in the proposed model are perhaps a bit lower than the real ones since they are referred to a continuous guaranteed performance; at the same time, it should be noticed that maximum performances near to standstill conditions involve the availability of an adhesion which is higher than 0.15, which is the limit usually adopted for the design of braking systems according to TSI standards. TSI limits are cautious because they are referred to the braking sub-system, which is quite safe relevant. However, considering the Muller adhesion model, shown in Figure 2.8, it has to be observed that with a vehicle speed above 85 km/h the maximum expected adherence limit is lower than 0.25. Consequently, in the speed range between 80 and 120 km/h there is a high statistical occurrence of skidding. As a matter of fact, during the experimental tests, some skidding occurred in this speed range, confirming that the maximum performances of the system are a bit higher than those

Table 3.1: Model uncertain parameters that should be further identified and refined.

Uncertain parameter	Reason/comments
Train efficiency η_{tot}	This parameter is affected by heavy uncertainties concerning both the mechanical efficiency η_m of the transmission system and the electrical one η_e. In addition, the heavy uncertainties on motion resistances can be partially compensated adjusting η_{tot}
Pos. of power connections along the line l	The positions of power stations are well known but the positions of the electrical connections along the line are affected by errors of about 50 m
ESSs voltage and impedance V_0, R_0	These parameters have to be further investigated
Equivalent resistivity of the line ρ	This parameter has to be further investigated

assumed within the proposed model but they cannot be fully reached in the most common operating conditions without causing the intervention of anti-skidding systems. The implementation of an anti-skidding sub-model in the proposed model could allow to better represent the train behaviour observed experimentally during the complete traction phase.

The aim of this first comparison is to validate the proposed model in a real operating scenario, to verify its reliability before using it to analyse the feasibility of energy recovery systems within the system.

In particular, this Section focuses on the calibration of the set of parameters described in Table 3.1, which were affected by larger uncertainties.

However, it is important to notice that the uncertainties on these quantities (i.e. vehicle efficiency, positions of power connections, ESSs voltage and impedance, line equivalent resistivity) have almost no influence on the controller used to drive the vehicle. This is due to the need to represent the behaviour of the human driver: the velocity errors are higher and the dynamics of the intervention are slower than those of an automatic driver. Hence, in terms of controller

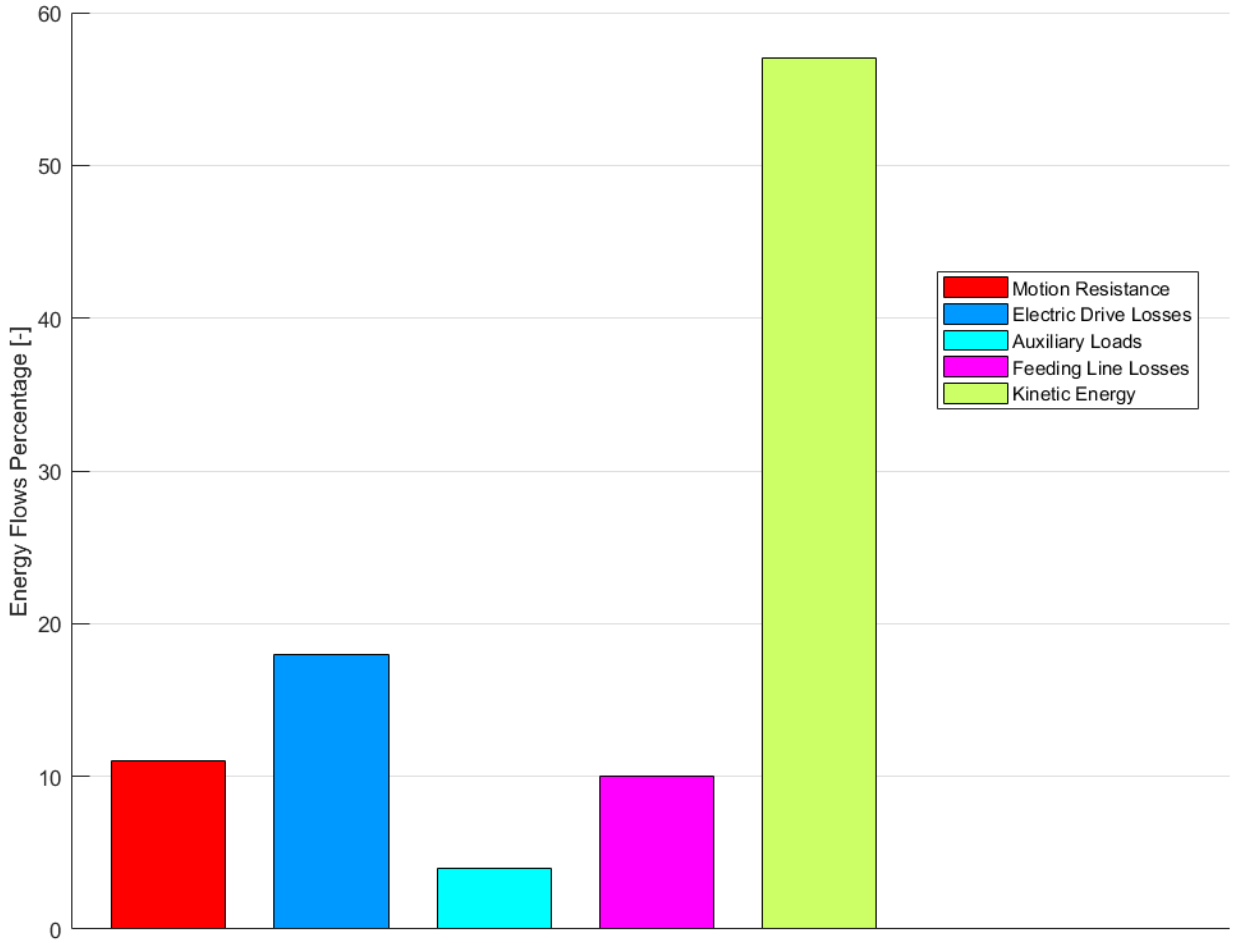

Figure 3.8: ETR 1000 energy flows during the traction phase.

effectiveness, the uncertainty on the model parameters are almost completely compensated by the approximation of the controller itself.

Figure 3.8 shows the energy flows for the considered High-Speed train during the traction phase: it is possible to highlight how more than 40% of the traction energy is dissipated by the different losses sources present within the system.

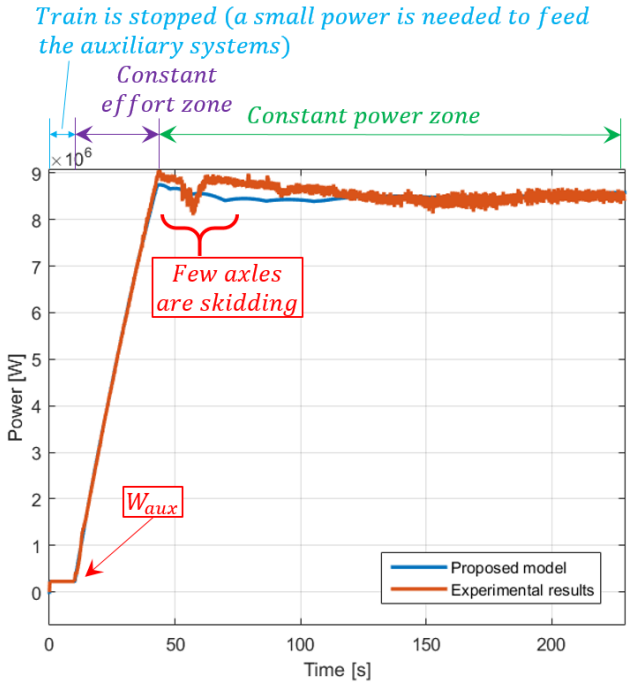

Figure 3.9: ETR 1000 experimental calibration: comparison between the experimental power consumption W_c during the traction phase and the corresponding numerical values obtained with the proposed model.

3.2.1.1 Calibration of the efficiency η_{tot}

The comparison between the experimental and numerical power consumption can be analysed in Figure 3.9. The test begins with a phase in which the train is stopped and its motors are not working. In this phase, which corresponds to the first 10 seconds of the experimental record, it is possible to measure the small power flux that must be collected from the line to feed all the auxiliary systems of the train. It is not a very accurate measurement; however, a constant power W_{aux} equal to about 230 kW seems to be a realistic approximation, because it corresponds to a mean consumption of about 29 kW for each wagon. This power flux is needed for the operation of air conditioning, lights, and every on-board sub-system such as compressors for pneumatic brakes and battery chargers.

Furthermore, by comparing the collected power W_c provided by the proposed model with that

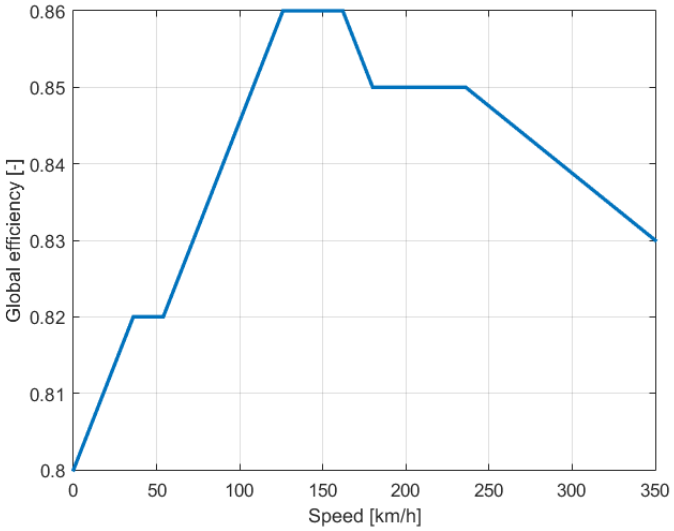

Figure 3.10: ETR 1000 calibration of the global efficiency η_{tot} (100% of the traction effort).

experimentally measured, it is possible to perform a calibration of the train global efficiency η_{tot}; the results of this preliminary calibration are reported in Figure 3.10 and Table 3.2. Within the proposed model, η_{tot} is taken into account after the dynamical analysis of the vehicle, in correspondence of the power consumption calculation: this value of W_c takes into account both the chosen blending strategy and the system global efficiency. Considering the good agreement with the experimental measurements (e.g. in terms of velocity profile, see Figure 3.7) of the results produced by the dynamical part of the model and the absence of blending (i.e. the considered manoeuvre only includes a traction phase), all the possible errors in terms of power consumption can be attributed to the erroneous value of the global efficiency. Then, the comparison between experimental and numerical W_c allows to tune the value of η_{tot}. Due to lack of more detailed experimental measurements, η_{tot} has been calibrated taking only into account the vehicle speed and neglecting the dependency on the traction effort. However, it should be noticed that the mechanical efficiency of the transmission systems typically increases, as the transmitted power increases while the efficiency of power electronics components is typically higher for partial loads. Consequently, the mutual compensations of these phenomena should produce a reduced fluctuation of the global efficiency around its most common value, which is about 0.84.

Table 3.2: Preliminary calculation of the global efficiency η_{tot} with 100% of the traction effort applied.

Speed range	Global efficiency η_{tot} at 100% of the traction effort
0–36 km/h	From 0.8 to 0.82
36-54 km/h	0.82
54-126 km/h	From 0.82 to 0.86
126-162 km/h	0.86
162-180 km/h	From 0.86 to 0.85
180-236 km/h	0.85
236-350 km/h	From 0.85 to 0.83

Finally, it is possible to highlight that the efficiency value equal to 0.82, calculated in the speed range between 40 and 120 km/h, is a bit low due to the axle skidding phenomenon: in fact it produces rapid transients and hysteretic load cycles which penalize the global efficiency of the system.

3.2.1.2 Calibration of substation parameters

After a preliminary evaluation of the traction system efficiency, it is possible to refine some parameters related to the electrical line. This analysis concerns the identification of the position, the no-load voltage and the equivalent impedance of the power stations within the line, starting from the measurements of the voltage V_c in correspondence of the pantograph, which are reported in Figure 3.11.

In particular, it is possible to calculate and verify the value of the substations no-load voltage V_0 by considering the measured voltage in correspondence of the standstill condition: in this case, the collected power is small and causes negligible losses; hence, the measured voltage in correspondence of the pantograph can be assumed to be equal to V_0.

Furthermore, the position of the power connection can be refined (within the data uncertainty of

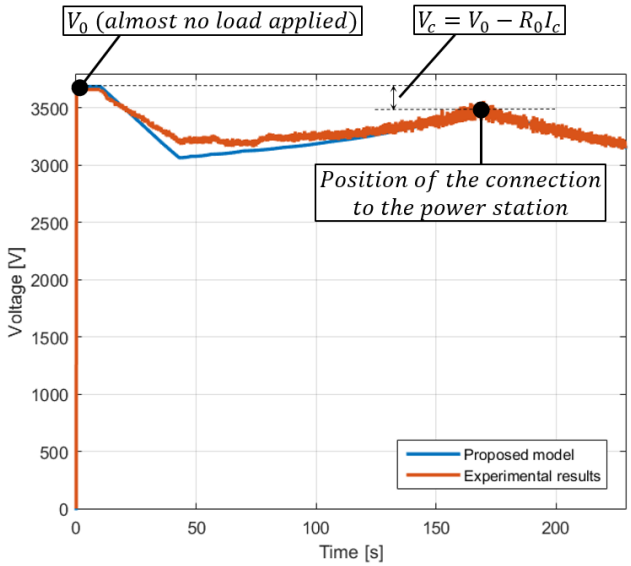

Figure 3.11: ETR 1000 experimental calibration: comparison between the line voltage V_c experimentally measured at the pantograph during the traction phase and the corresponding numerical values obtained with the proposed model.

about 50 m) considering that the passage under a power connection in a constant power operating condition (see Figure 3.9) produces a peak in the pantograph measured voltage V_c (shown in Figure 3.11). In this case, almost all the power, needed by the train, is collected locally. Consequently, the line circuit behaviour can be analysed through Equation 3.1 and the linearized equivalent impedance of the electrical substation R_0 can be estimated as follows:

$$V_c = V_0 - R_0 I_c \Rightarrow R_0 = \frac{V_0 - V_c}{I_c}. \tag{3.1}$$

3.2.1.3 Calibration of line impedance

Figure 3.11 and Figure 3.12 show, respectively, the comparisons between the measured and numerical pantograph voltage V_c and collected current I_c. Comparing numerical and experimental results, it is possible to adjust the value of the line equivalent resistivity ρ compensating the tolerances and the approximations on data (typically no more than 5-10%).

It is possible to highlight how the matching between simulated results and experimental

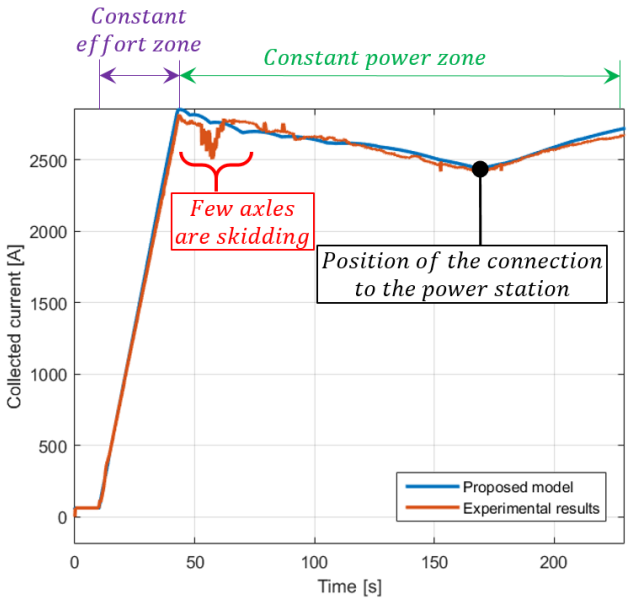

Figure 3.12: ETR 1000 experimental calibration: comparison between the collected current I_c experimentally measured at the pantograph during the traction phase and the corresponding numerical values obtained with the proposed model.

measurements is quite good even considering the tolerances on several parameters; higher errors can only be found in the zone where the train speed is lower, due to the presence of axle skidding in the experimental measurements.

3.2.2 Experimental validation

After the calibration of the model through the use of the first set of experimental data, further sets of experimental measurements have been used for the experimental validation of the tuned model. Section 3.2.2.1 shows the experimental validation of the proposed model through the comparison of the numerical results with two sets of measurements referred to the considered High-Speed test case, while Section 3.2.2.2 shows the experimental validation considering two data sets referred to the E 464 commuter train within the Firenze-Pisa-Livorno line.

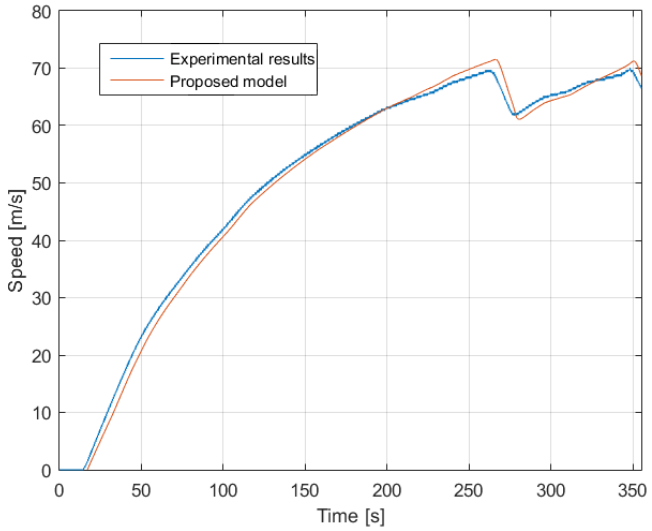

Figure 3.13: ETR 1000 experimental validation, first mixed manoeuvre: comparison between numerical and measured speed profiles.

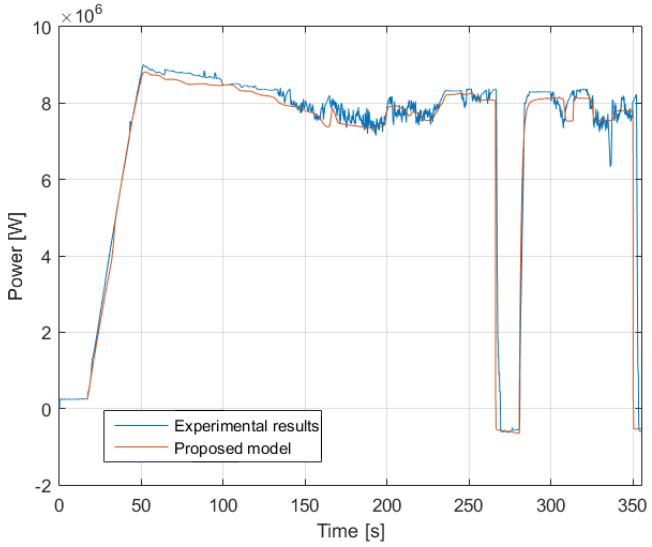

Figure 3.14: ETR 1000 experimental validation, first mixed manoeuvre: comparison between numerical and measured power consumptions.

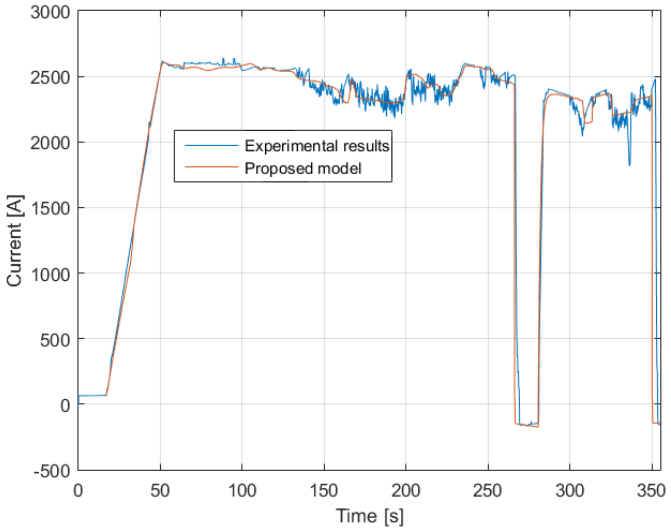

Figure 3.15: ETR 1000 experimental validation, first mixed manoeuvre: comparison between numerical and measured pantograph currents.

3.2.2.1 ETR 1000 experimental validation

The first of the two further sets of data concerning the ETR 1000 is referred to a mixed manoeuvre: the train accelerates up to 70 m/s, performs a brief braking to 60 m/s, then accelerates again up to 70 m/s. Figure 3.13 shows the comparison between experimental data and numerical results in terms of mission profile: it is possible to highlight how the agreement between them is very good. Furthermore, Figure 3.14 shows the comparison in terms of power consumption, Figure 3.15 is referred to pantograph currents and Figure 3.16 shows the pantograph voltage. In all these Figures it is possible to highlight the good agreement between numerical and experimental data.

The second of these sets of data is referred to another mixed manoeuvre: the train accelerates up to 60 m/s, and then performs a full braking. Figure 3.17 shows the comparison between experimental data and numerical results in terms of mission profile, Figure 3.18 shows the power consumptions comparison and Figure 3.19 and Figure 3.20 are respectively referred to pantograph currents and voltage. The results provided by the proposed model are characterised by a good accuracy, showing a good agreement with experimental measurements.

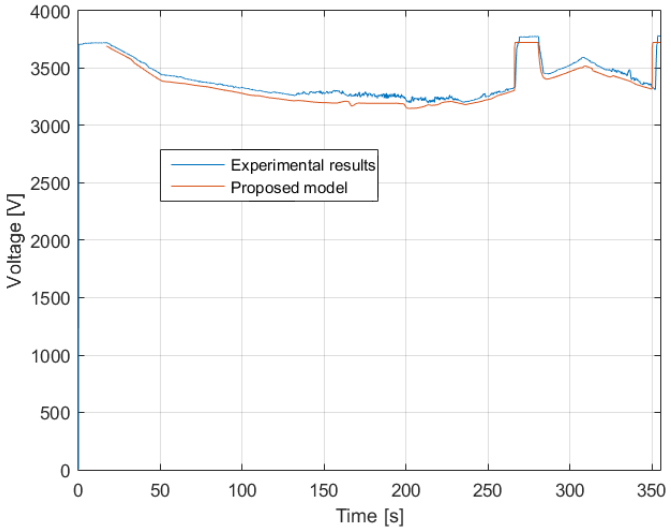

Figure 3.16: ETR 1000 experimental validation, first mixed manoeuvre: comparison between numerical and measured pantograph voltages.

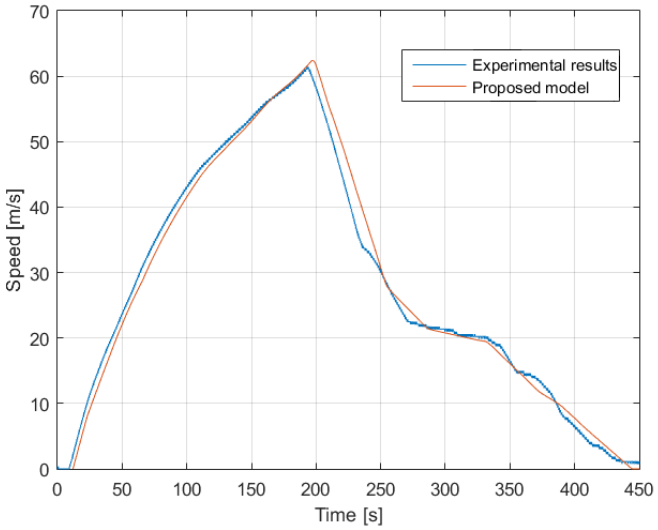

Figure 3.17: ETR 1000 experimental validation, second mixed manoeuvre: comparison between numerical and measured speed profiles.

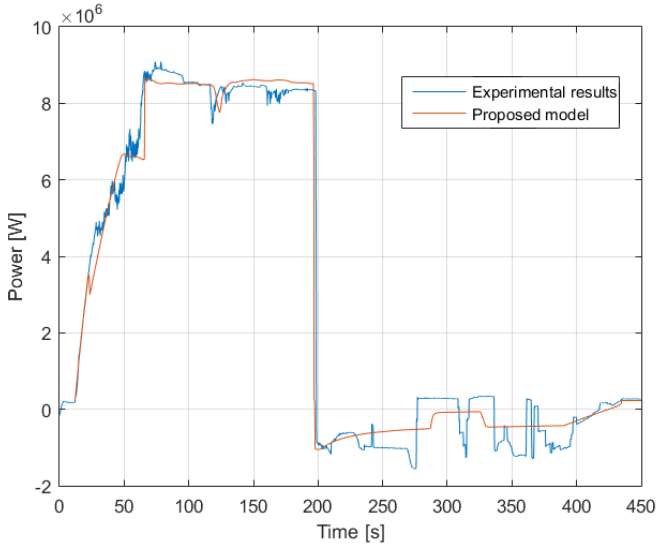

Figure 3.18: ETR 1000 experimental validation, second mixed manoeuvre: comparison between numerical and measured power consumptions.

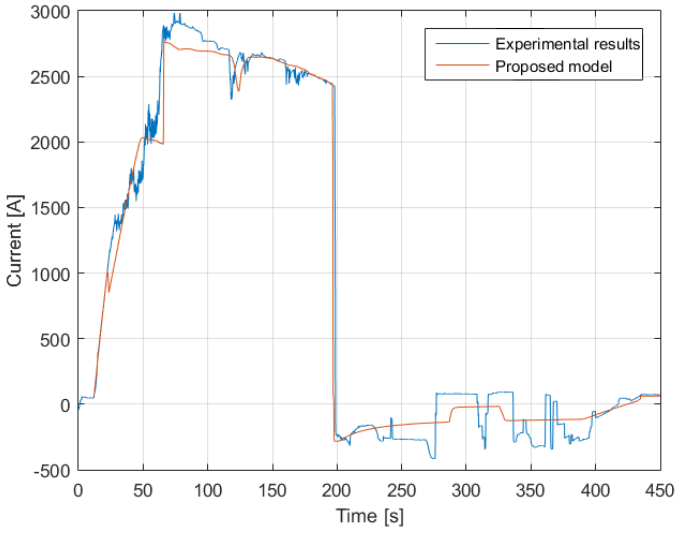

Figure 3.19: ETR 1000 experimental validation, second mixed manoeuvre: comparison between numerical and measured pantograph currents.

3.2.2.2 E 464 experimental validation

The first data set concerning the E 464 is referred to a mixed manoeuvre: the train accelerates up to 45 m/s, performs a first brief braking to 42 m/s, another brief braking to 37 m/s, accelerates again

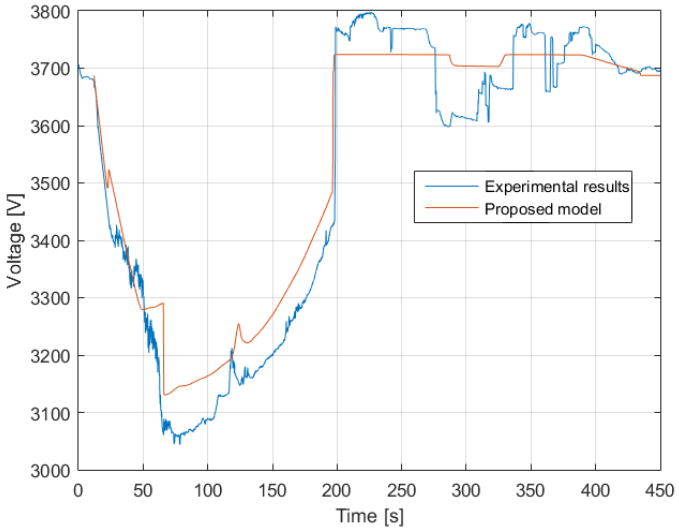

Figure 3.20: ETR 1000 experimental validation, second mixed manoeuvre: comparison between numerical and measured pantograph voltages.

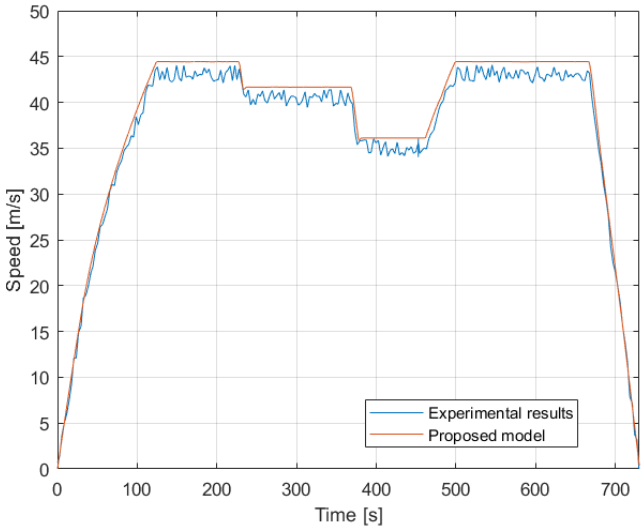

Figure 3.21: E 464 experimental validation, first mixed manoeuvre: comparison between numerical and measured speed profiles.

up to 45 m/s and, finally, performs a full braking. Figure 3.21 shows the comparison between experimental data and numerical results in terms of mission profile: it is possible to highlight

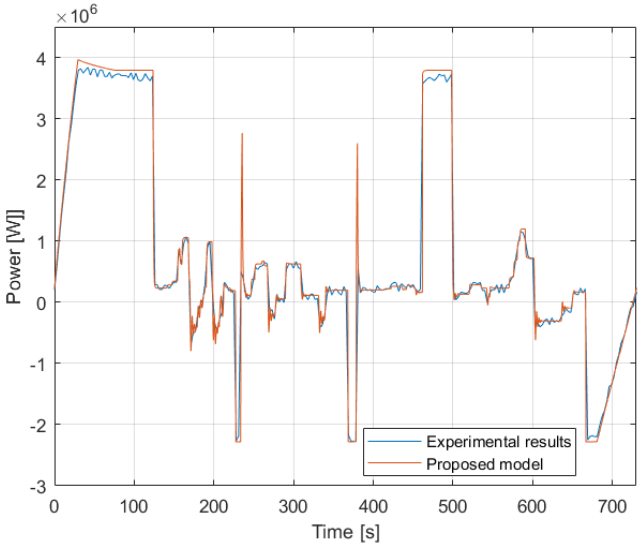

Figure 3.22: E 464 experimental validation, first mixed manoeuvre: comparison between numerical and measured power consumptions.

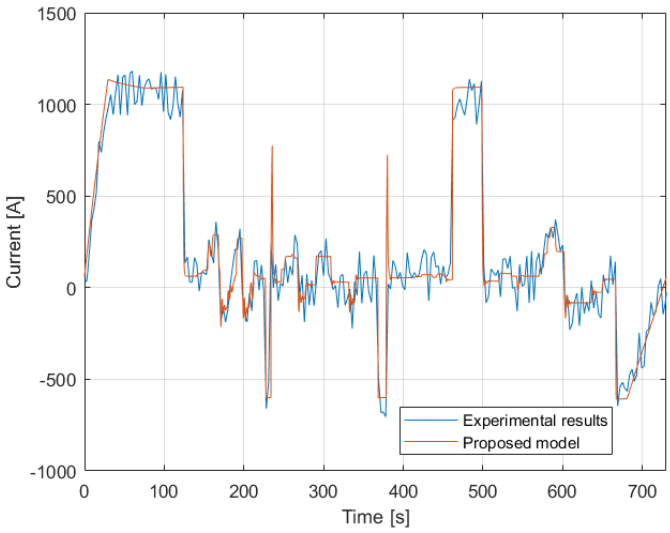

Figure 3.23: E 464 experimental validation, first mixed manoeuvre: comparison between numerical and measured pantograph currents.

how the agreement between them is very good and how the main source of error is the difference between the real human driver and the model virtual driver. Figure 3.22 shows the comparison

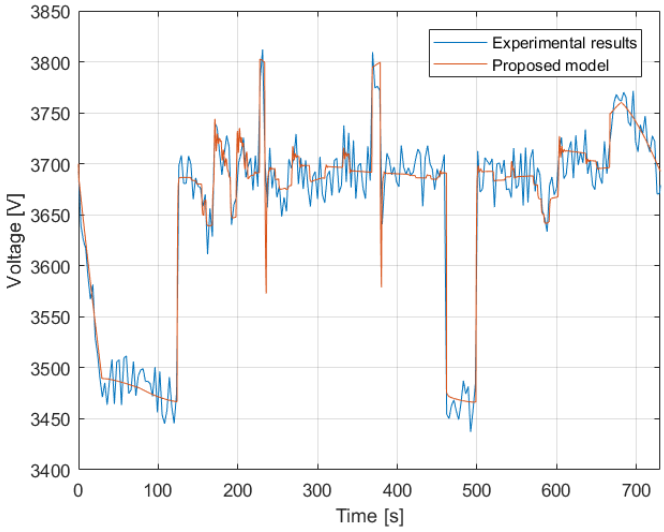

Figure 3.24: E 464 experimental validation, first mixed manoeuvre: comparison between numerical and measured pantograph voltages.

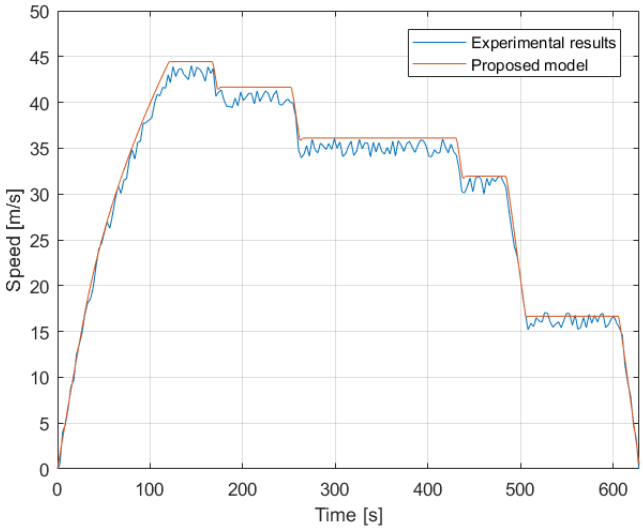

Figure 3.25: E 464 experimental validation, second mixed manoeuvre: comparison between numerical and measured speed profiles.

in terms of power consumption, Figure 3.23 is referred to pantograph currents and Figure 3.24 shows the pantograph voltage. In all these Figures, it is possible to underline the good agreement

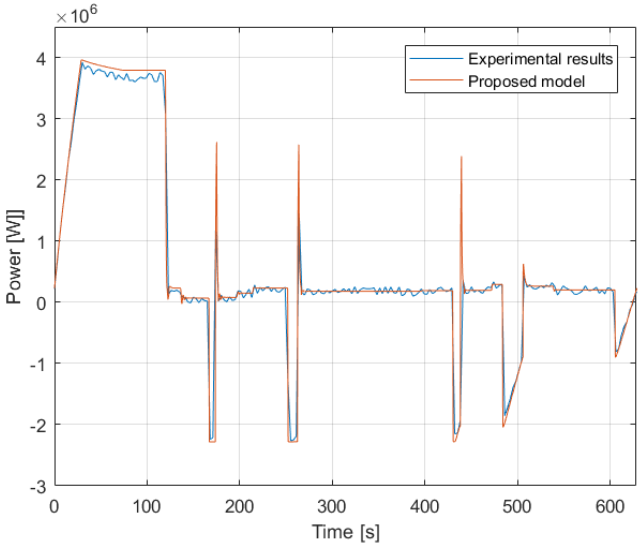

Figure 3.26: E 464 experimental validation, second mixed manoeuvre: comparison between numerical and measured power consumptions.

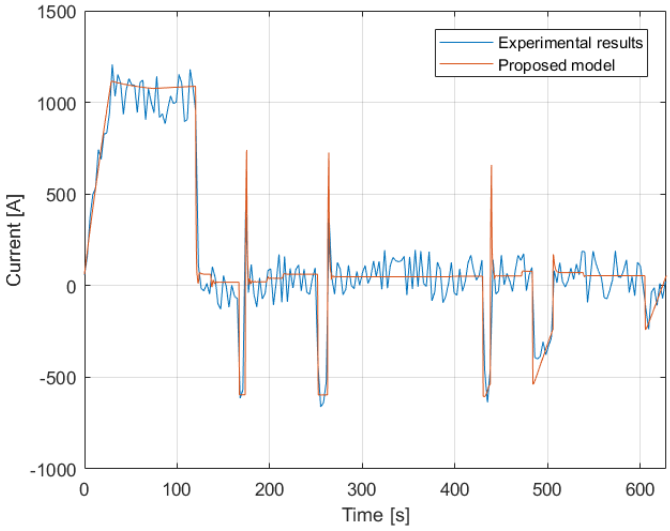

Figure 3.27: E 464 experimental validation, second mixed manoeuvre: comparison between numerical and measured pantograph currents.

between the results provided by the proposed model and the experimental measurements. The high frequency behaviour of the electrical quantities has been filtered, but a small component of

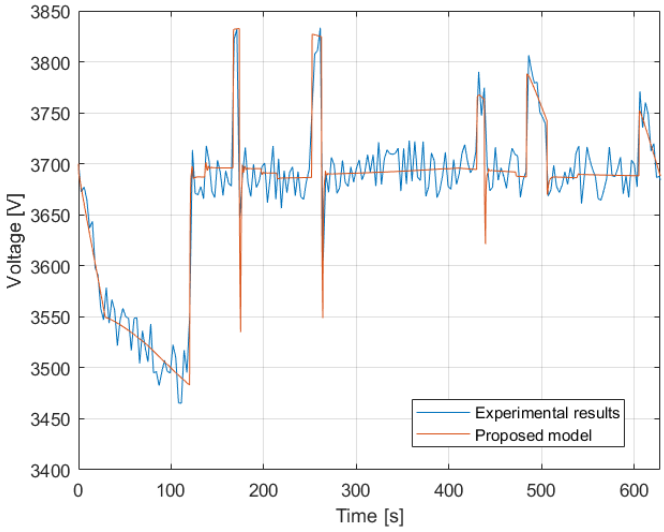

Figure 3.28: E 464 experimental validation, second mixed manoeuvre: comparison between numerical and measured pantograph voltages.

it is still present in the shown data: this component does not represent a source of error for the proposed model, since it goes beyond the scope of this research work. The second data set, used for the validation of the E 464 model, is referred to another mixed manoeuvre: the train accelerates up to 45 m/s, and then performs a series of partial braking phases, from 45 to 42 m/s, from 42 to 37 m/s, from 37 to 32 m/s, from 32 to 17 m/s and finally from 17 to 0 m/s,. Figure 3.25 shows the comparison between experimental data and numerical results in terms of mission profile: as already noted, for Figure 3.21 the agreement is good, with the only errors due to the difference between the human and the virtual drivers. Figure 3.26, Figure 3.27 and Figure 3.28 show the comparisons in terms of power consumption, pantograph currents and pantograph voltage. In all these Figures, it is possible to highlight the good accuracy of the results provided by the proposed model and their agreement with the experimental results.

3.3 Feasibility analysis within a High-Speed system

After the model experimental validation, in order to investigate the feasibility of energy storage systems within the considered High-Speed railway application, a set of parametric simulations has been performed. The proposed model has been used to analyse a series of different operating scenarios, all of them considering the same line (i.e. the *Direttissima* Firenze-Roma line). The velocity profile, considered for this feasibility analysis, is shown in Figure 3.29 and includes a first acceleration (applying the maximum traction effort) from standstill to 70 m/s, a constant speed phase and a final braking (considering, as a blending strategy, the maximisation of the electrical converted power). In this operating scenario, the peak power involved in the braking phase is about 4-5 MW.

Since the results obtained through the simulation of the proposed model could be influenced by the particular behaviour or features of the considered energy storage device, for the feasibility analysis it has been preferred to refer the numerical results to an ideal configuration in which the storage device has a near to infinite capacity ($E = constant$) and its no-load voltage is equal to V_0 (i.e. no unbalance with respect to ESSs). As a further simplifying hypothesis, it has been assumed that the

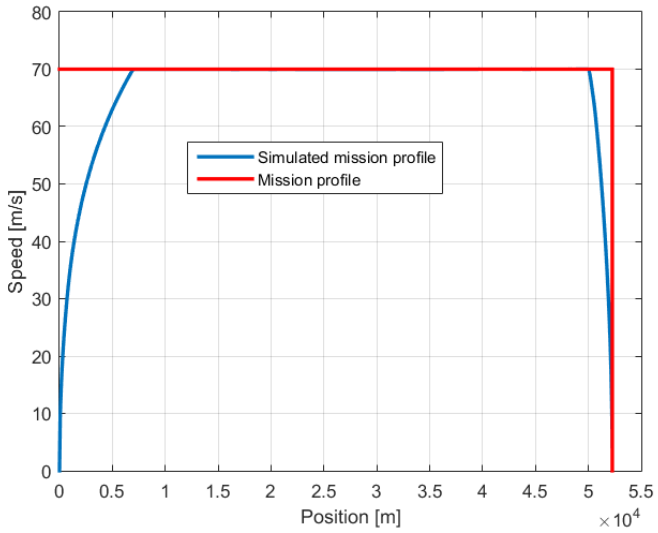

Figure 3.29: Mission profile chosen for the feasibility analysis.

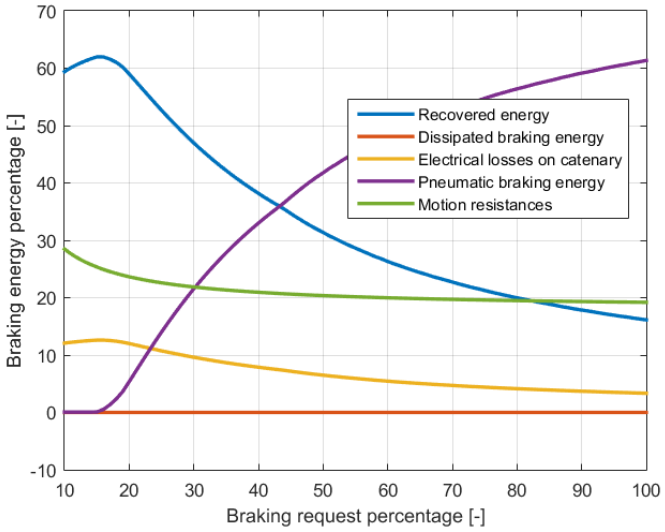

Figure 3.30: Energy percentages involved in the train braking phase (measured at the pantograph) as a function of the braking effort percentage, without voltage limitations.

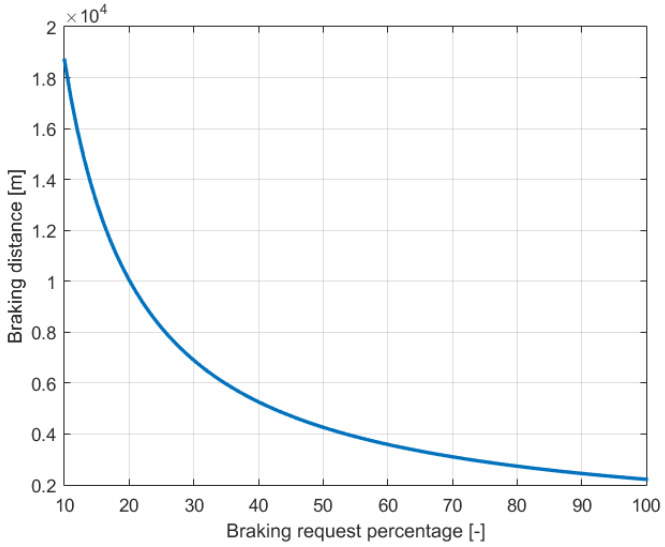

Figure 3.31: Braking distance as a function of the braking effort percentage, without voltage limitations.

equivalent impedances of both the ESSs and the coupled energy storage devices are equal to R_{eq}. Under these hypotheses, the coupled ESS-energy storage device system is equivalent to the fully

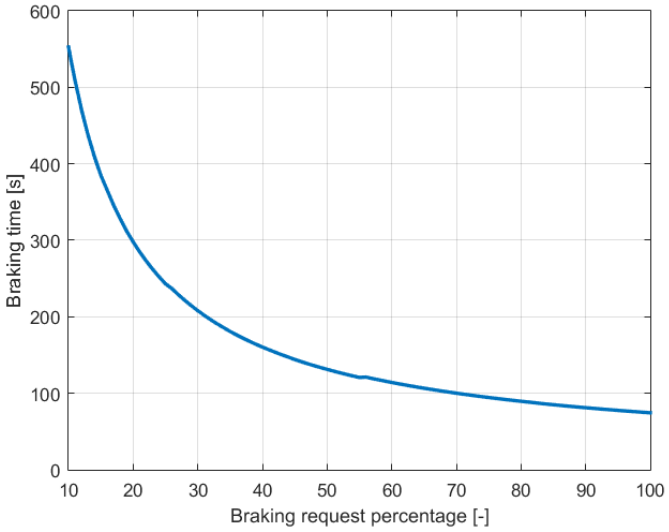

Figure 3.32: Braking time as a function of the braking effort percentage, without voltage limitations.

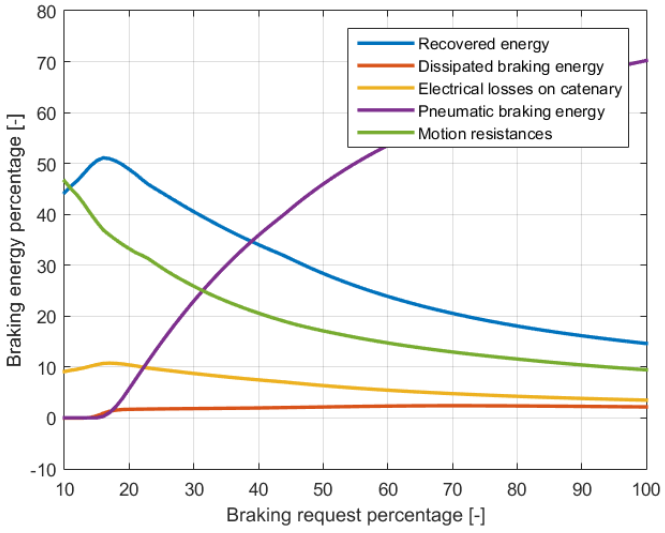

Figure 3.33: Energy percentages involved in the train braking phase (measured at the pantograph) as a function of the braking effort percentage, voltage peak limited to 3900 V.

reversible substation shown in Figure 2.27, considering a modified value of the internal resistance $R_0 = R_{eq}$.

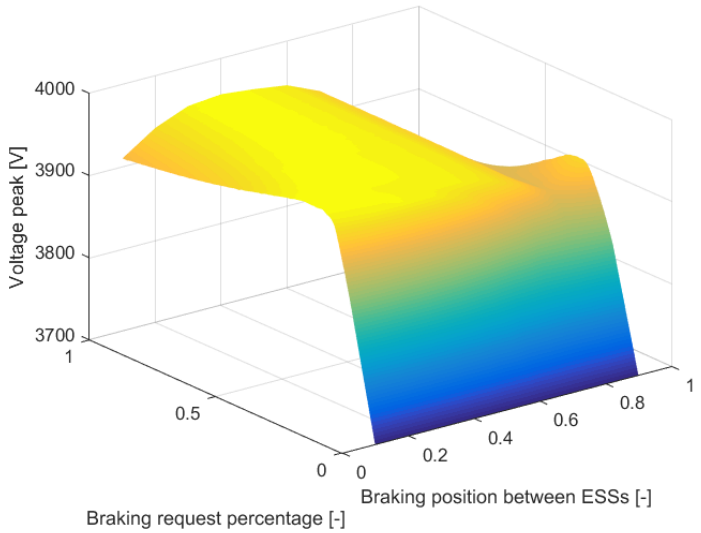

Figure 3.34: Line voltage peak during the braking phase as a function of the braking effort percentage and of the braking position between two adjacent electrical substations, without voltage limitations.

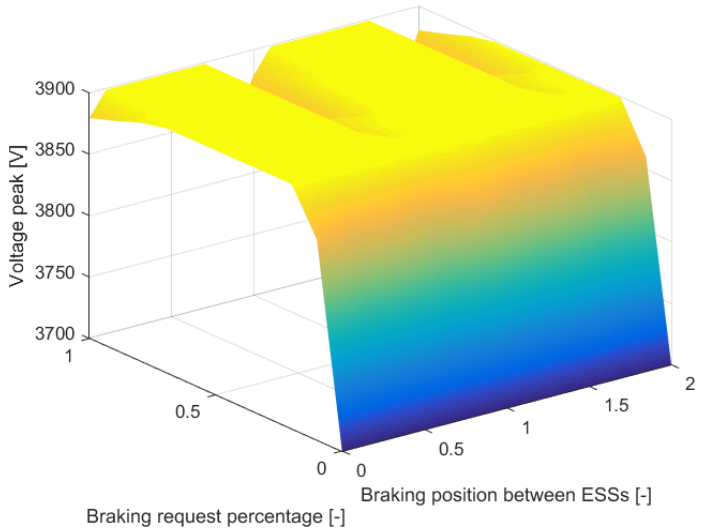

Figure 3.35: Line voltage peak during the braking phase as a function of the braking effort percentage and of the braking position between two adjacent electrical substations, voltage peak limited to 3900 V.

This approach has been adopted in order to easily evaluate the performance of the system regardless of the constraints dependent on the storage technology. Figure 3.30, Figure 3.31, Figure 3.32 and Figure 3.33 show most of the main quantities considered in this analysis; the results shown in those Figures are all referred to scenarios where the braking manoeuvre starts at midspan between two adjacent ESSs, while the influence of the braking position is reported in Figures 3.34 and 3.35.
Figure 3.30 shows the energy fluxes involved in the train braking phase as functions of the braking request, which can be defined as follows:

$$Braking\ request = \frac{T_{b,des}}{T_{b,nom}}, \tag{3.2}$$

where $T_{b,nom}$ is the available braking effort, calculated according to the train performance characteristics (see Figure 2.49) and $T_{b,des}$ is the actual value of the applied braking effort. By varying the braking request, it is possible to vary the percentage of recovered energy since a higher braking request could saturate the braking effort and hence the braking energy. The recovered energy shows a maximum in correspondence of a 15% braking request; however, this low value of the braking request involves that the braking distance and the braking time (respectively reported in Figure 3.31 and Figure 3.32) are quite high, beyond the acceptable limits usually considered in High-Speed applications. A good operating condition could be represented by the 50% braking request, where about 30% of the braking energy can be recovered but the braking time and distance are acceptable. The braking energy dissipated on the on-board resistors is constantly 0% since no voltage limiter is included in this first analysis.
Figure 3.33 shows the results obtained in terms of energy fluxes using a voltage limiter (considering a limit value equal to 3900 V) during the braking phases. Figure 3.33 is essentially equal to Figure 3.30, since the voltage peak values obtained in absence of the voltage limiter were not significantly higher than the considered limit. However, it is possible to highlight how a small percentage of energy is dissipated on on-board resistors. Figure 3.34 shows the voltage peak due to regenerative braking, as a function of the braking request and of the position between two adjacent electrical substations where the train begins the braking manoeuvre. According to Figure 2.20, the braking

position between ESSs can be defined as follows:

$$Braking\ position = \frac{x}{l}. \tag{3.3}$$

It is possible to highlight how the voltage peak, after a strong initial increase, is almost constant (or even decreasing) after the 20% braking request. On the contrary, the position where the braking phase begins has a significant influence on the voltage peak: in fact, it is possible to underline how a braking manoeuvre which begins near a substation leads to lower voltage peaks on the line. This analysis could then be refined considering the device that cuts off regenerative braking (i.e. activates dissipative braking) if the voltage exceeds the 3900 V limit value; however, even this first analysis provides realistic results, since the voltage peaks are not significantly higher with respect to the 3900 V limit.

Figure 3.35 shows the results obtained in terms of voltage peaks, using a voltage limiter (considering a limit value equal to 3900 V) during the braking phases. Figure 3.35 allows highlighting the small difference between the two scenarios: in fact the voltage peaks are saturated to the limit value for most of the braking position values. The voltage peaks, analogously to those obtained in absence of voltage limiter, are below the limit only in proximity of the ESSs, where a storage device can be able to completely handle the energy peak provided in correspondence of the braking phase. It is important to underline how the overvoltage can be handled in two different ways in presence of real storage devices: completely deactivating regenerative braking in case of overvoltage or controlling, in a more accurate way, the braking phase in order to dissipate only the exceeding energy and to continue to recover a smaller percentage of energy.

3.4 Vehicles library

The proposed vehicles library represents a significant contribution in terms of model value and flexibility. In fact, the possibility to easily represent the behaviour of different vehicles could allow, in the future developments of this research work, to extend the proposed optimisation approach to a large number of different scenarios and to investigate more complex interactions. The results exposed in this Section show the comparison between the behaviour of a set of vehicles and the ETR 1000, in order to highlight the possibilities provided by the library.

Figure 3.36, Figure 3.37, Figure 3.38 and Figure 3.39 show the comparison between the performances of the trains considered in Figure 2.46 and the ETR 1000. Figure 3.36 shows the considered mission profile: it includes a first acceleration from standstill to the maximum vehicle speed, a constant speed phase and a final full braking. The comparison has been carried out considering the Firenze-Roma line.

The power consumption and the collected current (see respectively Figure 3.37 and Figure 3.38) of the two High-Speed trains (i.e. ETR 1000 and ETR 500) are significantly higher with respect

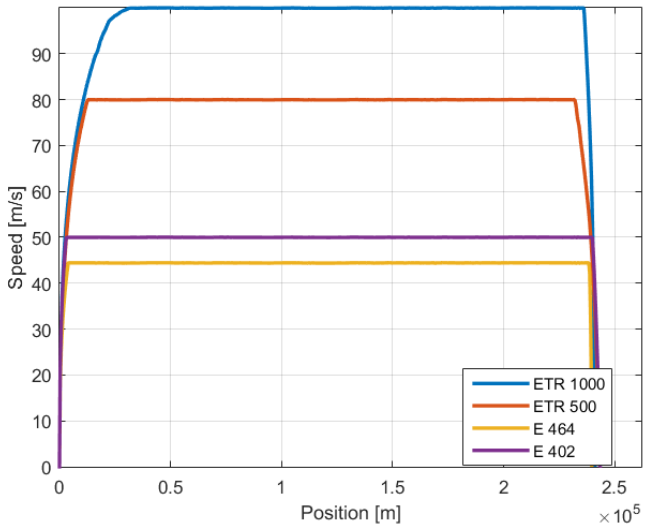

Figure 3.36: Comparison between the simulated vehicle speed of different Trenitalia trains along the *Direttissima* line (Roma-Firenze).

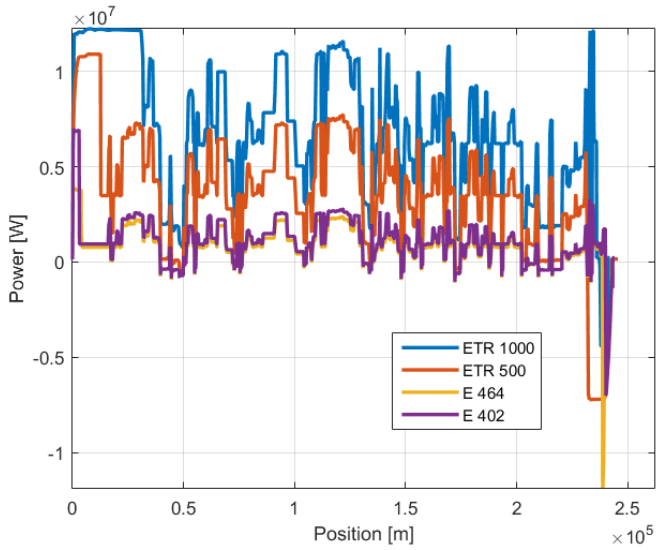

Figure 3.37: Comparison between the simulated power consumption of different Trenitalia trains along the *Direttissima* line (Roma-Firenze).

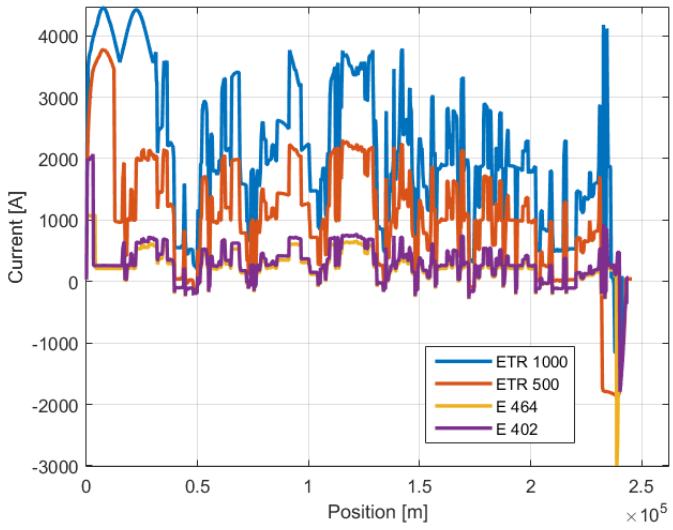

Figure 3.38: Comparison between the simulated collected current of different Trenitalia trains along the *Direttissima* line (Roma-Firenze).

to the two local trains. Furthermore, their voltage drops (see Figure 3.39), in correspondence of the accelerations (both the first full traction phase and the others within the line, due to the line

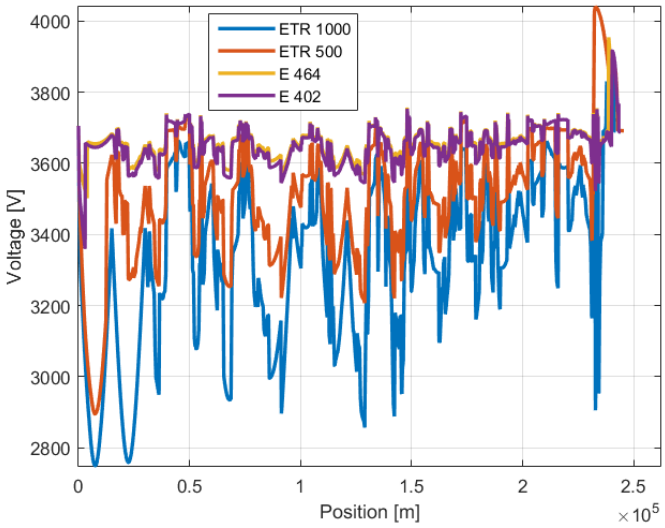

Figure 3.39: Comparison between the simulated pantograph voltage of different Trenitalia trains along the *Direttissima* line (Roma-Firenze).

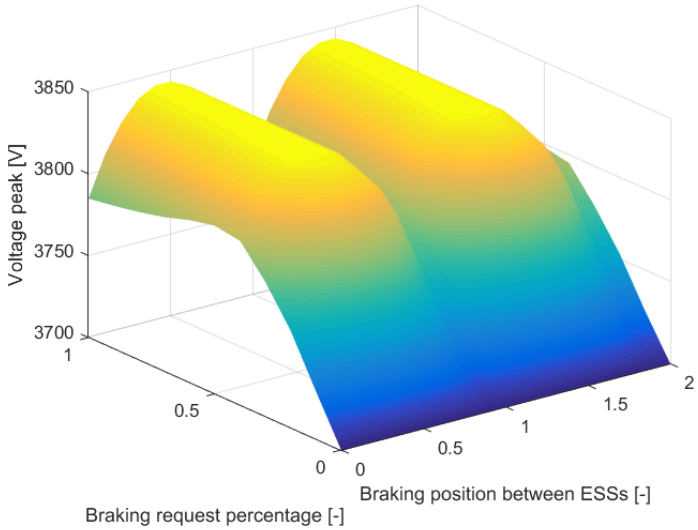

Figure 3.40: Line voltage peak during the braking phase for the E 464 commuter train, voltage peak limited to 3900 V.

topology) are bigger. Despite their better traction performances, the two High-Speed trains reach their maximum speed farther than the others: this is due to the much higher speed levels. In fact

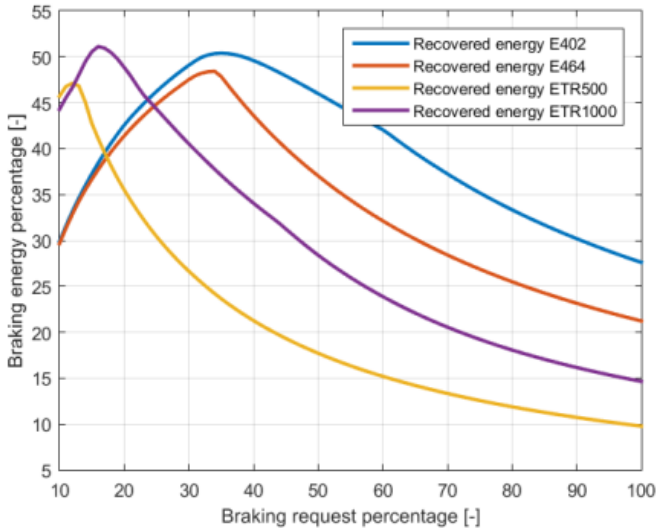

Figure 3.41: Energy percentages involved in the train braking phase for some of the vehicle included in the developed vehicles library.

the full acceleration time is not significantly different among the whole group.

Figure 3.40 shows, by way of example, the feasibility analysis concerning the braking voltage peaks for the E 464 commuter train: it is possible to highlight how, due to the lower speed and hence kinetic energy, the voltage peak for this commuter vehicle is always below the line limit (i.e. 3900 V). Due to these reason, the use of regenerative braking is quite promising for commuter trains, where the braking frequency is higher than in High-Speed systems. However, even though this could seem a reasonable result, not only High-Speed trains but also commuter trains suffer a significant lack of regenerative braking applications.

Figure 3.41 shows the comparison between the recovered energy which could be obtained with the previously considered vehicles: it is interesting to highlight how, despite the line voltage limitations, the percentage of recovered energy for High-Speed trains is significant even with respect to slower commuter trains that do not suffer from the voltage limitations.

3.5 Storage system sizing

After the feasibility analysis, this research work has focused on the correct sizing of stationary and on-board storage devices which could better fit the needings of a High-Speed system, following the same approach already shown in previous works [106], [107], [108]. Thanks to the collaboration with the University of Pisa, also the software Modelica® has been used to carry out the research work. The sizing of energy storage devices also allows to understand the economic impact of such investments.
The following storage system scenarios have been considered:

1. Stationary systems, interfaced with the feeding line through DC/DC converters:

   1.1. Supercapacitors systems;

   1.2. High power lithium batteries systems.

   The sizing has been performed considering the High-Speed test case, i.e. the ETR 1000 High-Speed train within the stations of Firenze and Roma. Since the line has only these two stops, it is useful to locate the storage device in correspondence of the electrical substations of the two railway nodes. Furthermore, the storage devices have been sized considering only the energy flows coming from the DC High-Speed lines and neglecting the contribution due to DC low speed lines and AC High-Speed lines. This is due, aside from the possibility to perform a significant analysis without the need of an extremely large set of data, to two main reasons: DC low speed lines are characterised by energy flows which are much smaller than those of DC High-Speed lines and AC High-Speed lines can fed their recovered energy directly to the feeding grid taking advantage of reversible substations.

2. On-board systems, interfaced through DC/DC converters:

   2.1. Supercapacitors systems;

   2.2. High power lithium batteries systems.

For on-board storage devices, the sizing process has been carried out taking into account the energy produced by the considered vehicle itself; furthermore, it is important to take into account the available volume and the storage device weight, which produces an increment of the total vehicle weight and a possible reduction of the payload.

All the considered systems include a DC/DC converter. This further component obviously provides an increment in terms of volume, weight and complexity of the entire system. However, it is possible to obtain several advantages by interposing a voltage converter between the storage device and the feeding line:

- enhancement of energy recovery: without the interposition of a converter (i.e. floating device), the braking energy flow is primarily driven by the presence of a voltage difference between the line and the storage device and this gradually reduces the flow of energy to the storage system. The introduction of a DC/DC converter maintains a fixed reference voltage level (e.g. the electrical substation voltage), in order to keep the substations from charging the storage system;
- more flexibility for the storage device sizing: the device voltage is no more directly constrained to line voltage and the only limit to be taken into account is the safety current value. Furthermore, the device $S.O.C.$ can be directly controlled; these features allow to significantly increase the device life.

A comparison between storage devices behaviour within a tramway system in presence and in absence of voltage converter can be found in [109] and [110], while an analysis of floating storage devices within a High-Speed system is shown in in [106].

3.5.1 Stationary high power lithium battery systems

This Section focuses on the stationary battery system, considering the use of lithium batteries. Table 3.3 shows the fundamental features of the battery system, composed of NMC high power

Table 3.3: Main characteristics of the battery pack, stationary configuration.

Battery pack (NMC cells based)	
Nominal cell voltage	3.7 V
Nominal cell capacity	400 Ah
Battery pack nominal energy	1406 kWh
Battery pack mass	10032 kg
Battery pack volume	5046 L
Recovered energy	222 kWh
SOC variation	15%

cells. The increment of recovered energy, allowed by the presence of a DC/DC converter, provides different results from those exposed in [106]; the sizing takes into account the maximum charging current declared by the manufacturer, since the allowed current directly influences the nominal storable energy.

The line equivalent impedance and the allowed current generate a voltage drop within the line, which could make regenerative braking uneffective: in fact, recovered current decreases due to line voltage limit. By defining the mean distance between train and storage device, it is possible to estimate the best device distance (which is different if the overvoltage causes the complete turning off of regenerative braking or if a more complex blending strategy is adopted); the estimation is based on the difference between the voltage limit and the storage device nominal voltage and on the allowed current:

$$I_s < \frac{V_{max} - V_s}{R_{dist}}, \tag{3.4}$$

where I_s is maximum allowed storage device current, V_{max} is the line voltage limit, V_s is the storage device nominal voltage and R_{dist} is the impedance of the catenary part, included between the braking vehicle and the stationary storage device. If a large part of energy is transferred to the storage device, due to the favorable voltage difference, a smaller part will be transferred to other accelerating vehicles; this situation must be accurately taken into account, since the transfer to

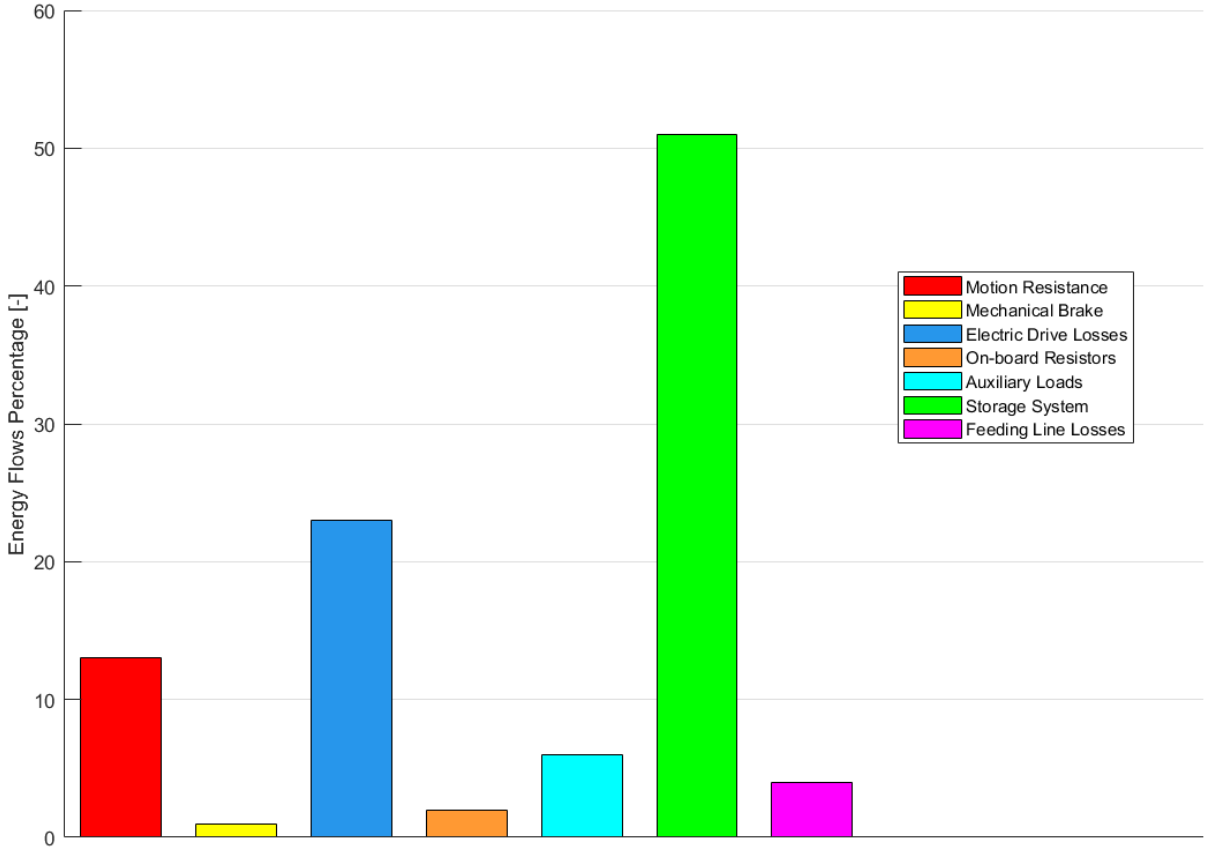

Figure 3.42: Energy flows during braking, stationary storage system.

other vehicle is usually more efficient.

Furthermore, within the sizing process, it is important to select a number of constitutive cells that allows the battery, even in absence of a DC/DC converter, to operate with an intermediate $S.O.C.$ value (i.e. in the operating range where the voltage is almost constant). Another important aspect is the discharge velocity of the device: a quick discharge phase allows the device to be always ready for new recharge cycles.

The mass and volume of the system have been evaluated from the cells characteristics, taking also into account a further 20% increment due to the balance of plant (i.e. B.O.P.).

Finally, a fundamental aspect to be considered is the device life: considering a mean value of 25 trains which pass from the substation and a system life of 15 years, the system has to bear about

105 full charge/discharge cycles. Taking into account literature [111], [112] and manufacturer data, the depth of discharge of each micro-cycle due to a train passage should not exceed about 15% of the battery $S.O.C.$.

Figure 3.42 shows the energy flows during the ETR 1000 braking manoeuvre, when the railway system is equipped with stationary storage devices with the previously shown characteristics; the results are obviously different from those previously exposed in the feasibility analysis, since in that analysis an ideal storage device has been considered.

The train kinetic and potential energies are partly dissipated by mechanical contributions (i.e 13% by motion resistance and 1% by mechanical braking), while the remaining part is handled by the electric system: 6% of the energy is consumed by auxiliary systems and 23% is dissipated by the electric drive. The losses on the catenary sum to 4% of the total energy amount, while the on-board resistors contribute with a 2%. Finally, 51% of the total energy is stored on the stationary energy storage device. These results are different from those exposed in [106], where the DC/DC converter was absent. This proves the importance of a voltage converter to reduce the on-board resistors contribution and enhance the energy recovery. However, it is also important to underline how the DC/DC converter introduces further internal losses which have to be considered during the system sizing, since they could affect the recovered energy, reducing it up to 5%.

The analysis is referred to rush hour, but it could be extended to low load and holiday hours in order to better understand the behaviour of the system. During rush hours, the $S.O.C.$ of the considered system varies of about 4%.

3.5.2 Stationary supercapacitor system

Usually, in correspondence of a train station, the braking time of a High-Speed train is higher than 100 s and the amount of energy that needs to be stored is significant: in this scenario, a stationary supercapacitor seems less competitive than in tramways applications, where the storage device needs to handle peak power flows just for a few seconds [110] (see [88] for a comparison between the behaviour of supercapacitors and batteries).

Table 3.4: Main characteristics of the supercapacitor stack, stationary configuration.

Supercapacitor stack	
Nominal cell voltage	2.7 V
Nominal cell capacitance	3000 F
SC stack nominal energy	223 kWh
SC stack mass	52200 kg
SC stack volume	41760 L
Recovered energy	222 kWh
SOC variation	99 %

Table 3.4 shows the characteristics of the proposed supercapacitor sizing.
As for the previous case, the sizing takes into account the characteristics of commercial products and the B.O.P.. It is possible to highlight, with an equivalent level of recovered energy, a significant increase in the system mass and volume with respect to the battery system. In this case, like in the previous one, the current limit has been considered (i.e. 2000 A for the considered SC cell), while the depth of discharge is not limited (i.e. $S.O.C.$ can vary up to almost 100%), since a supercapacitor could operate for hundreds of thousands of full charge/discharge cycles.

3.5.3 On-board high power lithium battery systems

The fundamental drawback of stationary systems is the unavoidable presence of line losses through the catenary. The use of on-board storage devices contributes to the recovery of braking energy without line losses and also to avoid the problem of line voltage limit: this is particularly important in presence of high power peaks, which can easily lead to energy dissipation instead of recovery. Another important aspect is that an on-board storage device, being free of the line overvoltage problem, is not influenced by the blending strategy. Furthermore, each storage device needs to handle only the load of its vehicle [110], with significant advantages in terms of sizing: the need to

Table 3.5: Main characteristics of the battery pack, on-board configuration.

Battery pack (NMC cells based)	
Nominal cell voltage	3.7 V
Nominal cell capacity	400 Ah
Battery pack nominal energy	1006 kWh
Battery pack mass	5984 kg
Battery pack volume	3612 L
Recovered energy	164 kWh
SOC variation	15%

manage only a single vehicle allows the device to be free of extra current peaks due to the presence of other braking vehicle.

For a single vehicle the on-board solution allows more energy recovery than the stationary device solution, but the whole system should be taken into account to perform a significant analysis.

The on-board solution requires higher initial investments, since each train needs its own device; a further disadvantage is represented by the device mass and volume themselves, which also contribute to an increment in energy consumption. A partial solution for the encumbrance problem can be achieved by replacing the on-board resistors with the storage device; this is possible since UIC 544-1 (2013) and TSI (2014) prescribe the complete management of safety emergency stops to mechanical brakes: the braking is so ensured even in case of the storage device failure.

The sizing has been performed considering the volume and mass of current on-board resistors: for the ETR 1000, i.e. the considered High-Speed test case, the dissipative units occupy about 3620 L and weighs about 3200 kg, according to manufacturer data [113].

Table 3.5 shows the characteristics of a battery system with an equivalent volume. The system weight is about 2.8 t higher than the resistors one (i.e. about 0.5% of the train mass): this increment is lower than the limit imposed by EN 14363 regulation [104], which prescribes to modify the homologation procedure for mass increments higher than 10% of the total train mass. Figure

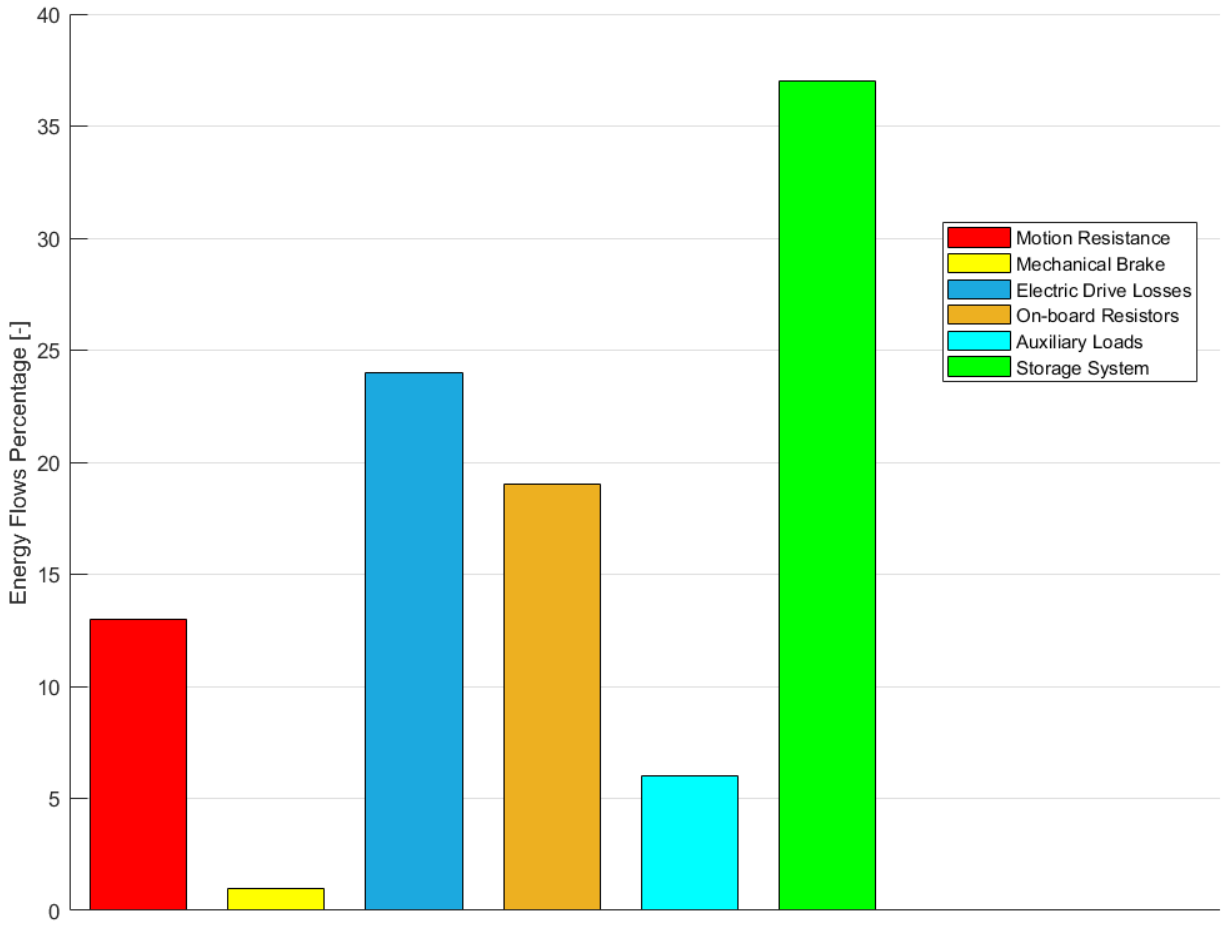

Figure 3.43: Energy flows during braking, on-board storage system.

3.43 shows the energy flows during the ETR 1000 braking manoeuvre when the railway system is equipped with on-board storage devices with the previously exposed characteristics; the results are quite different from those referred to the stationary storage device system shown in Figure 3.42. In particular, the motion resistance contribution is higher due to the presence of the on-board device (i.e. weight increase), catenary losses are completely absent, while the contribution of on-board resistors is higher (i.e. 19%): this is due to the fact that the on-board storage device could not be able to store the full amount of braking energy, having been sized according to volume limitations. In fact, only 37% of the train total energy is stored in the on-board device.

3.5.4 On-board supercapacitors systems

The on-board supercapacitor system has been sized according to mass and volume constraints and its characteristics are shown in Table 3.6. With the same encumbrance of the on-board battery system, the on-board supercapacitor is able to store only a limited amount of energy, even if the mass increment is only 0.2% of the total vehicle mass, well within EN 14363 limits [104]. To reach a significant amount of the storable energy, the volume of the supercapacitor should be greatly increased, with important drawbacks in terms of payload reduction and weight increase.

Table 3.6: Main characteristics of the supercapacitor stack, on-board configuration.

Supercapacitor stack	
Nominal cell voltage	2.7 V
Nominal cell capacitance	3000 F
SC stack nominal energy	19.4 kWh
SC stack mass	4521 kg
SC stack volume	3617 L
Recovered energy	19.2 kWh
SOC variation	99%

3.6 Cost-benefit analysis

The cost-benefit analysis is referred to the storage systems whose sizings have been exposed in Section 3.5. Two main parameters have been taken into account:

- The initial investment needed for the installation of storage systems, power converter and B.O.P.. High power NMC cells batteries need an initial investment of about 600 €/kWh, including cells, BMS and packaging. Supercapacitors require, including the assembly costs for the entire system, an investment of about 0.02 €/F. For both the systems, the same investment has been considered both for stationary and on-board systems. A further investment of 60 k€ is required for the DC/DC converter [114]. Those investments are higher than those required in tramways applications [30]: in fact both the power and the voltage are significantly higher in High-Speed applications (i.e. respectively >2 MW and >3 kV);

- The annual energy savings. This parameter can be estimated considering the braking energy recovered and stored within the storage devices. With stationary storage devices, other vehicles can use the stored energy and require a lower amount of energy from the electrical substations. It is important to take into account the charge/discharge cycle efficiency (i.e. a reference value of 0.9 has been considered). The annual amount of saved energy can be estimated considering a reference value of 25 $trains/day$, for 350 $days/year$. The estimation for on-board devices is completely analogous, with the only difference that each storage device feeds only the train in which it is installed. The reference price for electrical energy has been considered equal to about 100 €/MWh.

The most important outputs of the analysis are the investments payback time (i.e. P.B.T.) and net present value (i.e. N.P.V.); the expected life of the system is 15 years and the maintenance costs have also been taken into account.

The results of the analysis are reported in Table 3.7: not only the systems sizings previously exposed have been considered, but also other sizes with a 30% reduced storable energy, in order

Table 3.7: Cost-benefit analysis.

Location	Cell typology	Nominal energy [kWh]	Storage system cost [$k€$]	Energy saving [$k€/y$]	Payback time [y]	N.P.V. [$k€$]
Stationary	Li-bat	1406	904	175	5.9	998
Stationary	Li-bat	1055	693	133	5.9	755
On-board	Li-bat	1006	664	126	6	714
On-board	Li-bat	755	513	100	5.8	578
Stationary	SC	223	5280	175	-	-3209
Stationary	SC	168	3976	133	-	-2406
On-board	SC	19	512	15	-	-329
On-board	SC	15	399	11	-	-262

to understand how the device sizing can impact on the value of the investment. It is possible to highlight how a stationary battery system (in the configuration exposed in Section 3.5.1, with a storable energy of 1406 kWh) provides a P.B.T. of about 6 years and a N.P.V. of about 998 $k€$. A smaller storage system (i.e. 1055 kWh) can provide the same P.B.T. but a reduced N.P.V..

The payback time is still 6 years for on-board battery configurations, but their net present value is significantly reduced: the configuration shown in Table 3.5 has a N.P.V. of 714 $k€$, while the smaller system (755 kWh) of 578 $k€$. This is due to the reduced available volume on-board the train. However, the installation on-board the train presents much more uncertainties with respect to stationary systems.

Supercapacitors competitiveness is strongly limited by the initial investment and by the reduced value of storable energy. Table 3.7 shows how, with the same annual energy saving, supercapacitor systems require an investment of about 5.3 $M€$ (more than five times higher than that of the large stationary battery system). P.B.T. is longer than the system life and the N.P.V. after 15 years is negative.

On-board supercapacitors show even worst performances: not only P.B.T. is too long and N.P.V. is negative, but also the storable energy is negligible (up to 19 kWh).

Extending the previous considerations, some further observations can be made. First of all, the previously exposed analysis focuses on the use of one stationary storage device within a system: while a single storage device shows a quite good P.B.T., the use of more than one device should be accurately evaluated. This is true also for on-board devices: they show almost no advantages with respect to stationary solutions; in particular, if too much vehicles are equipped with on-board storage systems, the investment would probably end in a complete failure.

Finally, supercapacitors seem not competitive in a High-Speed system, but an interesting possibility could be the coupled use of batteries and supercapacitors: in fact, supercapacitors are able to better handle power peaks at the beginning of the braking and traction phases, while batteries are able to handle the remaining part of energy during the other phases of the trip. This hybrid solution could provide important benefits in terms of performances and operating life.

3.7 Considerations on the optimisation of the system

In this Section, some of the results, obtained in the model optimisation phase, are reported. As previously exposed in Section 2.4, different aspects have been investigated and two different tools have been used. The results shown in this Section have been obtained with both the considered tools and they are reported considering only the numerical results of the process.

The first part of the optimisation process concerns the implementation of eco-driving techniques, i.e. enlarging coasting phases whenever is possible, coherently with timetable margins.

Since this research work is included within the scope of the TESYS Rail project, the eco-driving part of the optimisation process has been performed in collaboration with the project partners, considering the E 464 commuter train, for which an experimental campaign concerning eco-driving techniques was foreseen by one of the project partners.

Figure 3.44 shows the first manoeuvre considered for the analysis, which is referred to the first mixed mission profile used for the validation of the E 464 model (see Figure 3.21). The line speed limits regulate the vehicle mission profile, but the time margins on the timetable allows the vehicle to take advantage of significant additional coasting phases: in particular, the difference between

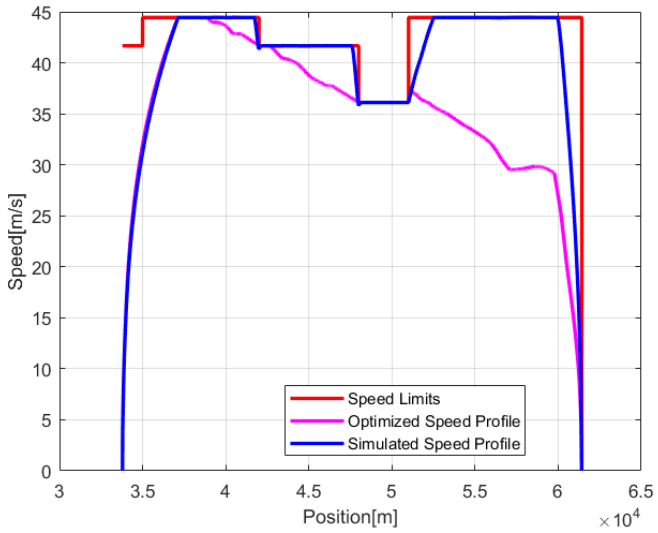

Figure 3.44: Eco-driving optimisation for the E 464, first manoeuvre.

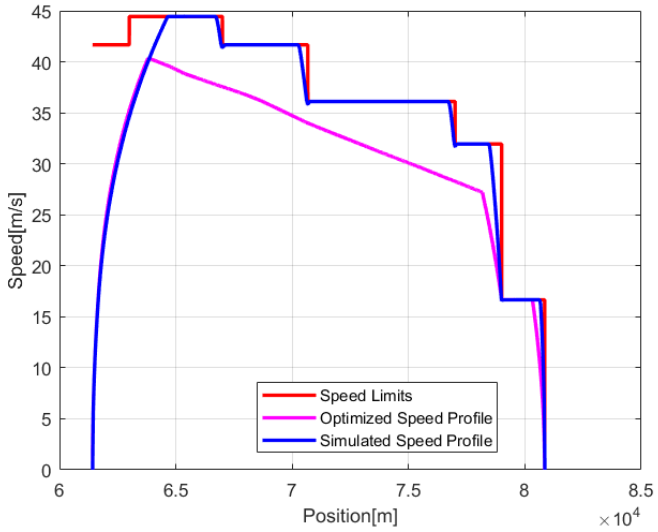

Figure 3.45: Eco-driving optimisation for the E 464, second manoeuvre.

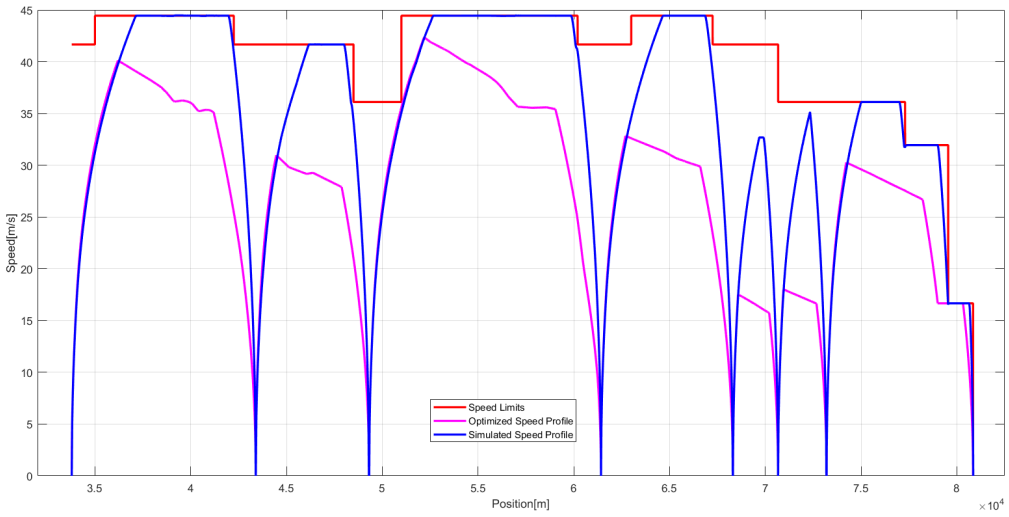

Figure 3.46: Eco-driving optimisation for the E 464, complete mission.

the nominal and the eco-driving speed profiles is quite important after the second traction phase. Figure 3.45 shows the eco-driving results for the manoeuvre previously used for the second part of the E 464 model validation (see Figure 3.25), while Figure 3.46 shows the eco-driving results for a longer part of the line, also including intermediate stops.

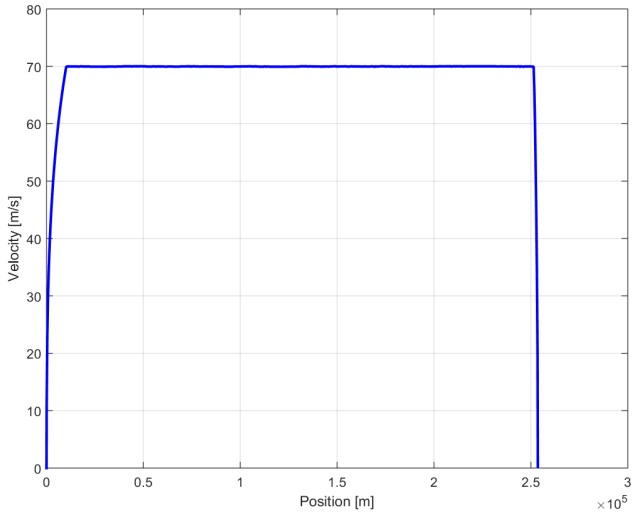

Figure 3.47: ETR 1000 nominal mission profile considered for the optimisation process.

It is possible to highlight how, in presence of intermediate stops, the use of coasting is very significant: the brief distances between the train stops allow to avoid full traction phases (and hence save significant percentages of traction energy) and also full braking phases (thus avoiding line overvoltages and reducing the solicitations on all the train braking systems).

Summarizing the eco-driving results, it is possible to observe that with a 5% time margin it is possible to save up to 20% of traction energy. To maximise energy savings, it is useful to implement D.A.S. (i.e. Driver Advisory Systems) and A.T.O. (i.e. Automatic Train Operation) systems, for a real time control of the mission profile, and A.T.R. (i.e. Automatic Train Regulation) systems, to guarantee proper time margins also in presence of other vehicles within the line.

Furthermore, it is interesting to highlight how eco-driving techniques, in addition to energy savings, are able to provide significant advantages in terms of passengers comfort, due to an increase in driving smoothness, and in terms of reduced wheel/rail wear, since smaller traction and braking efforts are applied to the system.

While the first part of the optimisation process mainly represents a first benchmark for more advanced solution, the second and the third part of the process are deeply interconnected and, hence, their results are shown without a separation. Furthermore, the following results are no more

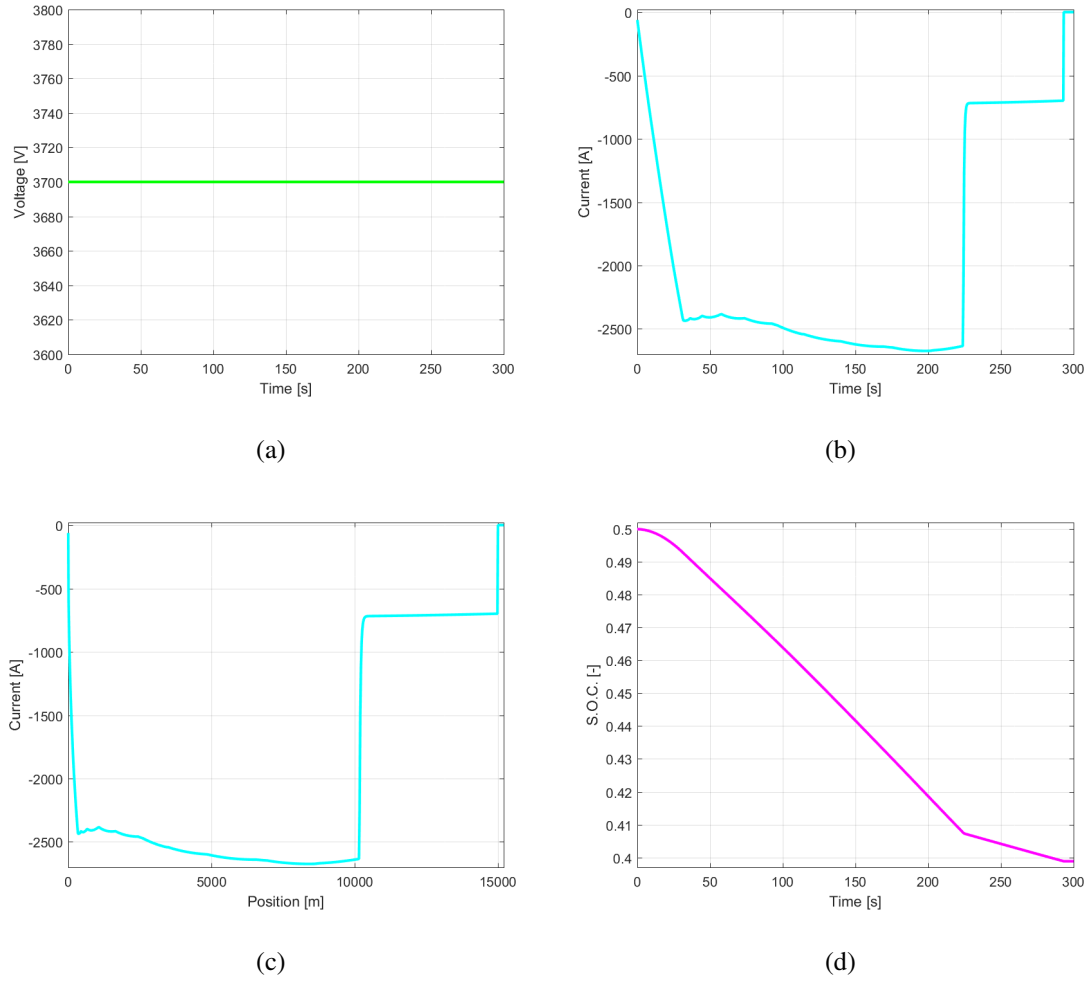

Figure 3.48: Stationary battery located in the departure station: (a) voltage, (b) current as a function of time, (c) current as a function of position and (d) $S.O.C.$.

referred to the E 464 commuter train, but concern the High-Speed system represented by the ETR 1000 within the *Direttissima* line: they thus represent the main objective of this research work.

The second part and the third part of the optimisation process take into account the use of stationary and on-board storage devices within the ETR 1000-*Direttissima* High-Speed system. The first step, needed to understand how the presence of an energy storage device influences the entire system, is the analysis of the device behaviour. Considering the typical mission profile followed by the ETR 1000 (i.e. acceleration after the first station up to 70 m/s, constant speed

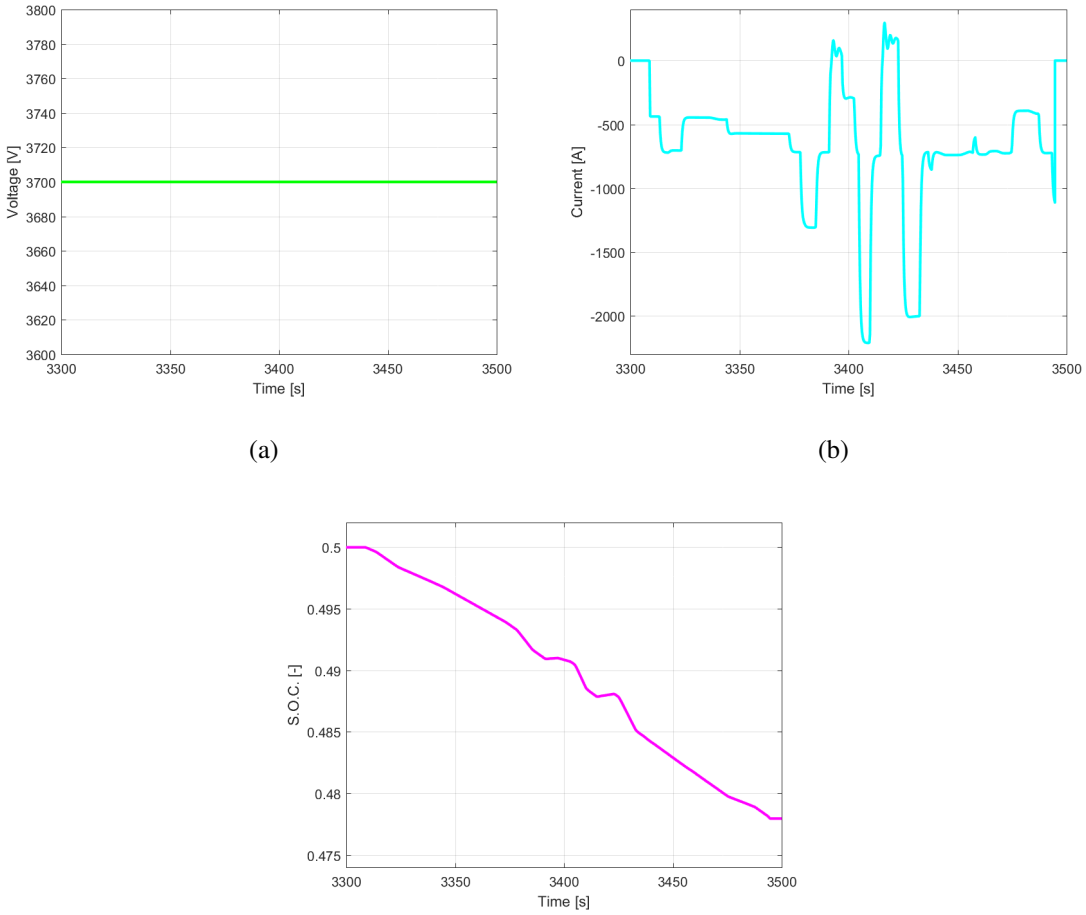

(a) (b)

(c)

Figure 3.49: Stationary battery located at *km* 226: (a) voltage, (b) current and (c) $S.O.C.$.

phase and final braking in correspondence of the final station, see Figure 3.47), Figures 3.48 to 3.55 show, as a benchmark for the following simulations and results, the voltage, current and $S.O.C.$ of the stationary and on-board storage devices whose characteristics have been exposed in Section 3.5.

Figure 3.48(a), Figure 3.48(b), Figure 3.48(c) and Figure 3.48(d) show, respectively, the voltage, current as a function of time and vehicle position and $S.O.C.$ of a stationary battery, located in the departure station of the considered line. Thanks to the presence of the DC/DC converter, the voltage (shown in Figure 3.48(a)) remains constant, while the battery current (shown in Figure

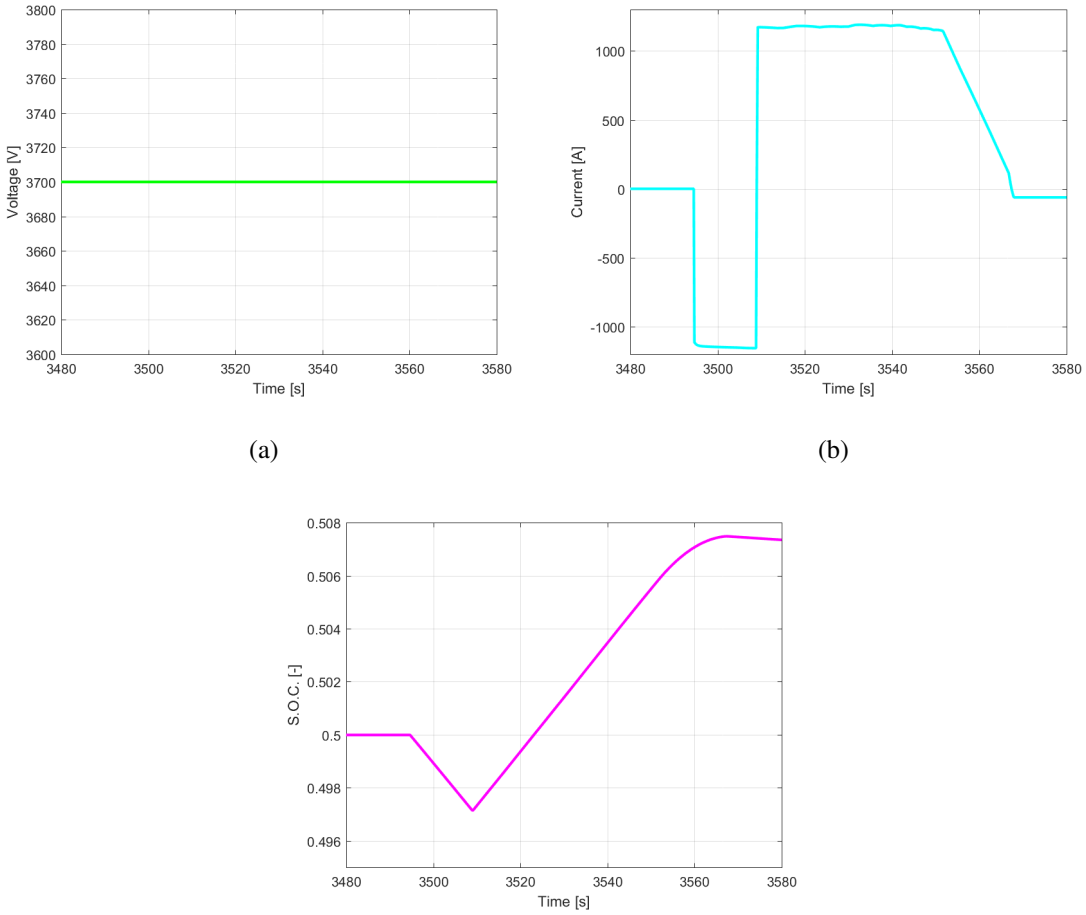

(a) (b)

(c)

Figure 3.50: Stationary battery located in the arrival station: (a) voltage, (b) current and (c) $S.O.C.$.

3.48(b)) follows the vehicle pantograph current trend: the current is negative because the train is accelerating and the battery is providing current to the vehicle. Figure 3.48(c) allows to highlight how the influence of the battery finishes after the second substation of the line span (i.e. after *km* 15). Finally, Figure 3.48(d) shows how the train full traction phase requires more than 10% of the battery capacity. Figure 3.49(a), Figure 3.49(b) and Figure 3.49(c) show respectively the voltage, current and $S.O.C.$ of a stationary battery located at *km* 226 of the considered line. The results of an intermediate storage device allows to evaluate its influence: the voltage (shown in Figure 3.49(a)) is still constant, thanks to the presence of the DC/DC converter, and the current (which is shown

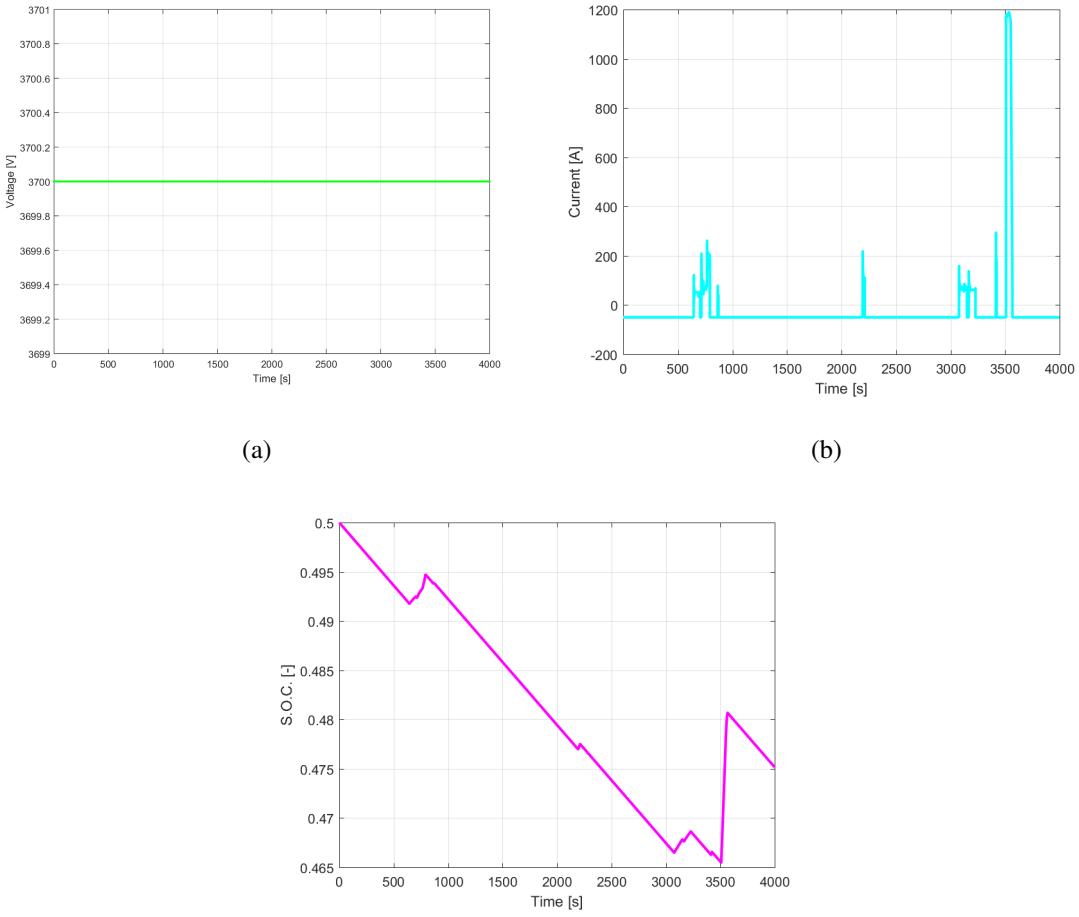

(a) (b)

(c)

Figure 3.51: On-board battery: (a) voltage, (b) current and (c) $S.O.C.$.

in Figure 3.49(b) and follows the vehicle pantograph current), needed to maintain the constant speed mission profile, is mainly negative but some partial braking phases contributes to the battery recharge. In fact, even if the $S.O.C.$ (shown in Figure 3.49(c)) loses only about 2.5%, the partial brakings can be detected in its trend; the small $S.O.C.$ variation is due to the fact that the vehicle is not performing full accelerations but is only maintaining its constant speed. Finally, closing the analysis of the stationary batteries performances, Figure 3.50(a), Figure 3.50(b) and Figure 3.50(c) show, respectively, the voltage, current and $S.O.C.$ of a stationary battery located in the arrival station of the considered line.

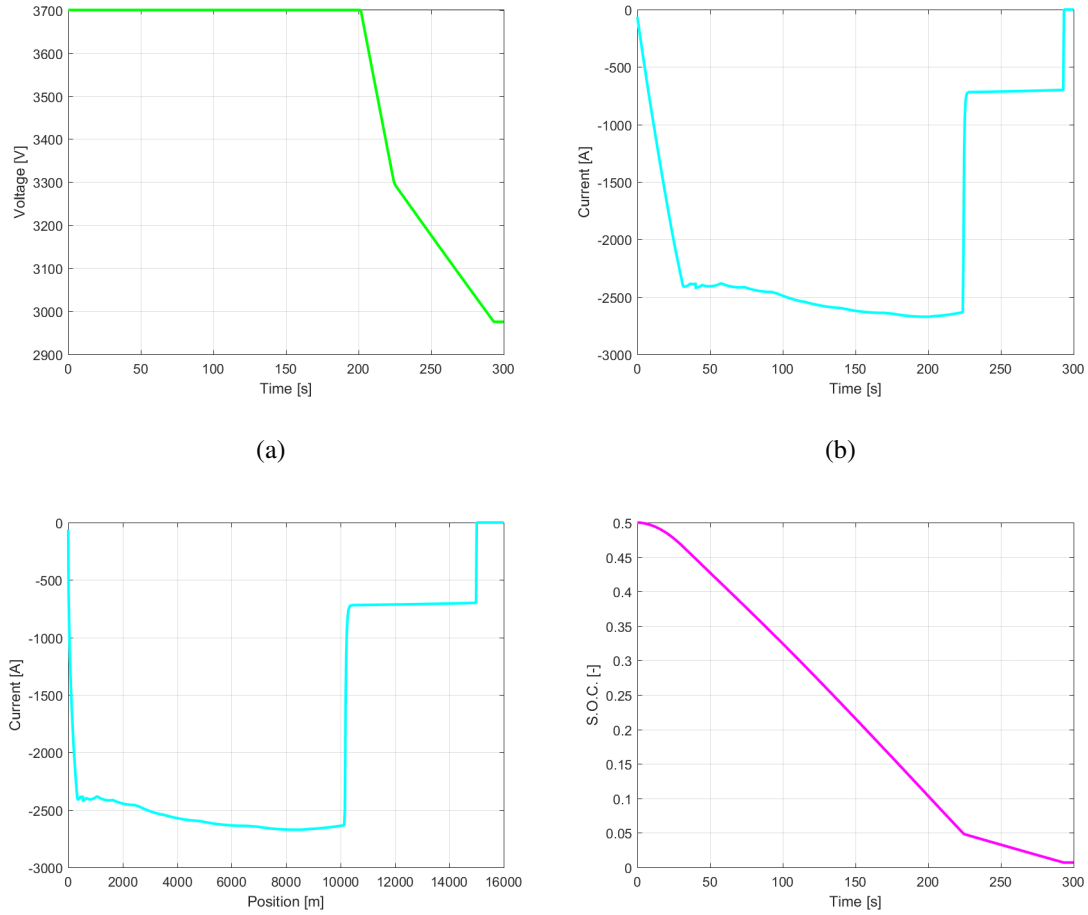

Figure 3.52: Stationary supercapacitor located in the departure station: (a) voltage, (b) current as a function of time, (c) current as a function of position and (d) $S.O.C.$.

Figure 3.50(a) shows how the voltage is still constant, while Figure 3.50(b) shows how in the first part of the line span the train is still absorbing current from the battery to preserve its speed profile and how in the final part of the line span, the final full braking phase provides a significant quantity of energy to the battery. The $S.O.C.$ (see Figure 3.50(c)), initially diminishes, but the final braking phase causes a significant increase.

The performance of the on-board battery are slightly different; Figures 3.51(a), 3.51(b) and 3.51(c) show respectively the voltage, current and $S.O.C.$ of the on-board battery. Figure 3.51(a) shows

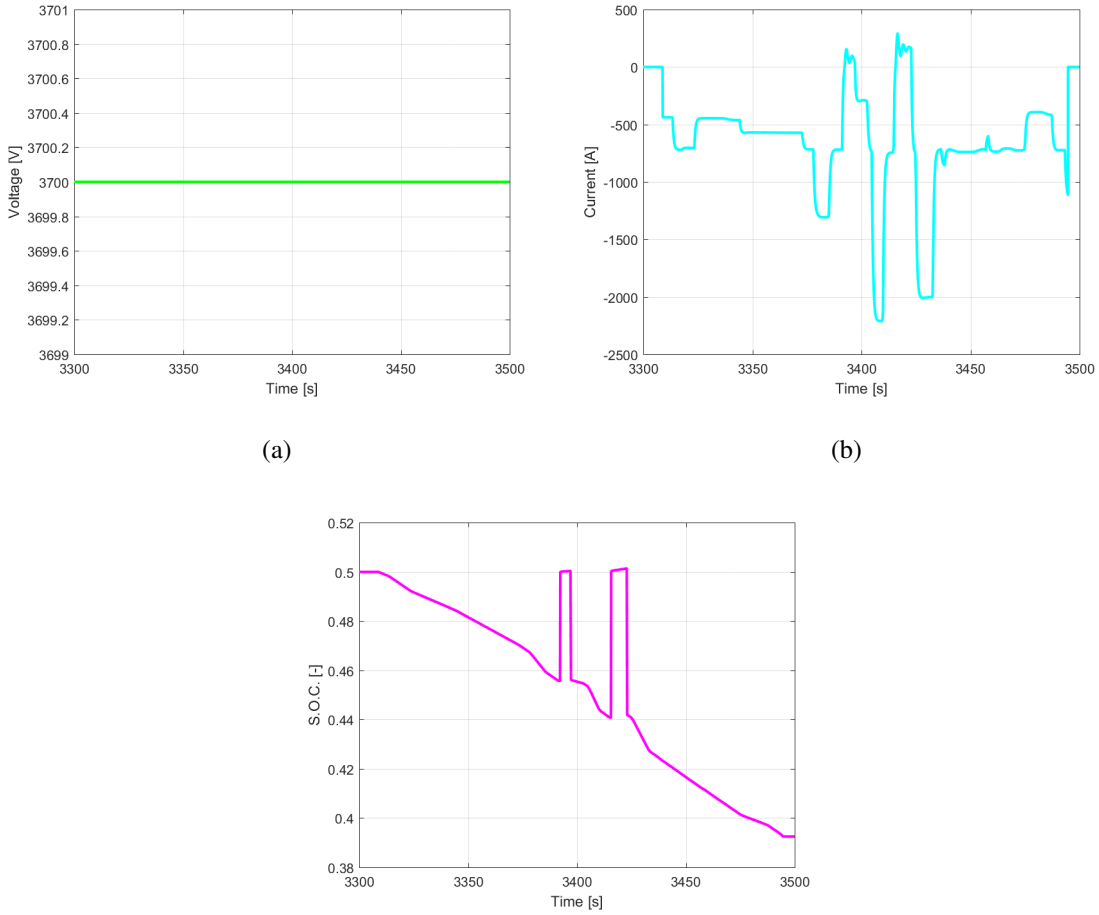

(a) (b)

(c)

Figure 3.53: Stationary supercapacitor located at *km* 226: (a) voltage, (b) current and (c) $S.O.C.$.

the battery voltage, still kept constant by the DC/DC converter: this is particularly important, since the on-board battery is subjected to heavier load variations with respect to the stationary ones. The current (shown in Figure 3.51(b)) is limited in the absorption phase, since an on-board device could not be able to handle a full traction phase of a High-Speed train but it can be easily used as a support for auxiliary system; instead, the charge current is not limited. The $S.O.C.$ variation (see in Figure 3.51(c)), is due to the auxiliary loads absorption and to the energy provided by partial and full braking phases; its operation is more variable than those of stationary devices.

Stationary and on-board supercapacitors are characterised by significantly different behaviours,

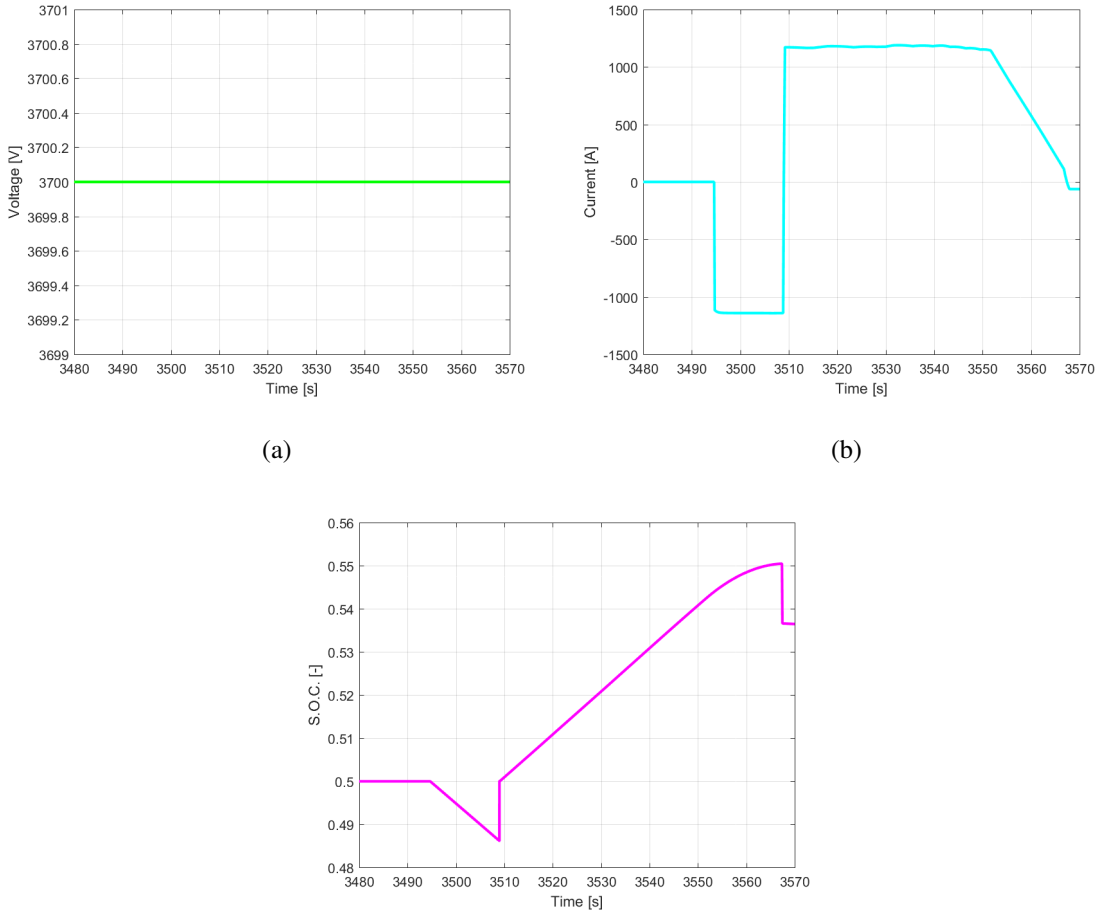

(a) (b)

(c)

Figure 3.54: Stationary supercapacitor located in the arrival station: (a) voltage, (b) current and (c) $S.O.C.$.

since their capacity (due to the different dynamic performance) is different and, above all, their dynamic response is faster and their life is less influenced by full charge/discharge cycles. Figures 3.52(a), 3.52(b), 3.52(c) and 3.52(d) show respectively the voltage, current and $S.O.C.$ of a stationary supercapacitor located in the departure station of the considered line. Figure 3.52(a) shows the supercapacitor voltage, which is no more constant while the vehicle crosses the line span, because the $S.O.C.$ variation is much more important than in batteries. The current, both as a function of time and position (see Figure 3.52(b) and Figure 3.52(c)) is completely analogous

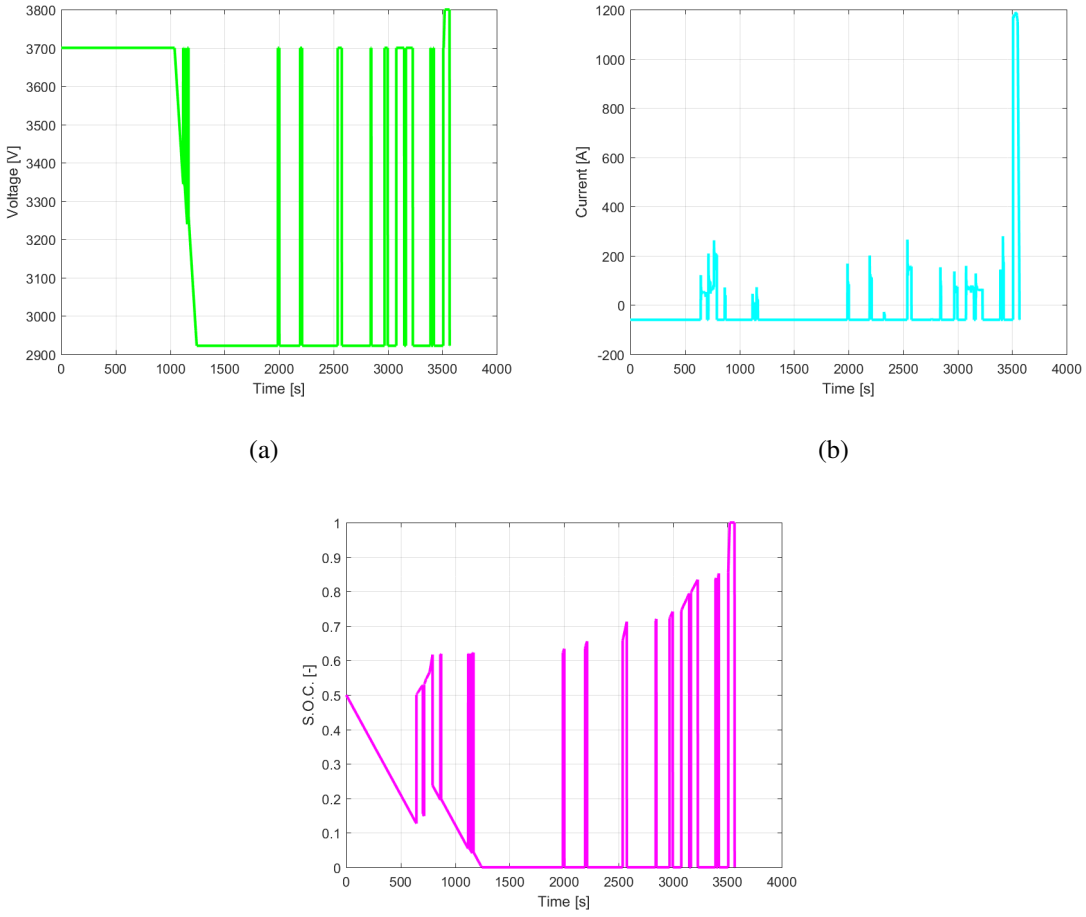

(a) (b)

(c)

Figure 3.55: On-board supercapacitor: (a) voltage, (b) current and (c) $S.O.C.$.

to those shown for the corresponding stationary battery (i.e. vehicle full traction phase) but the $S.O.C.$ represents the main difference: Figure 3.52(d) shows how the operating flexibility of the supercapacitor allows the device to spend almost 50% of its capacity for the vehicle full traction phase.

Figure 3.53(a), Figure 3.53(b) and Figure3.53(c) show, respectively, the voltage, current and $S.O.C.$ of a stationary supercapacitor located at km 226 of the considered line. Analogously to the battery, the supercapacitor voltage (see Figure 3.53(a)) remains constant, and the current (see

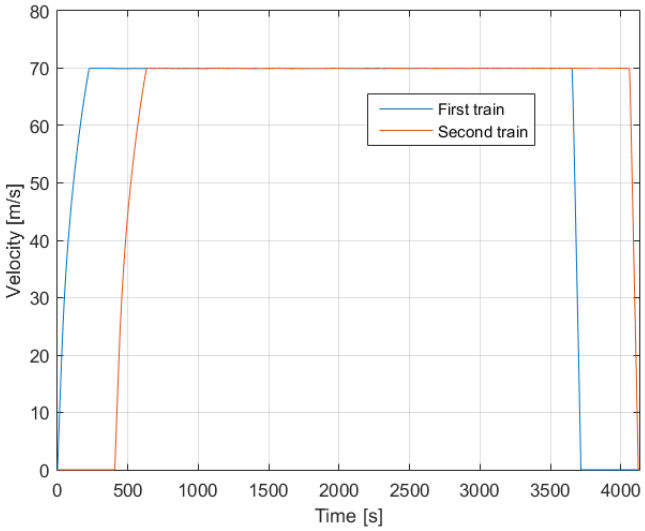

Figure 3.56: Two travelling vehicles in the same direction: velocity profiles.

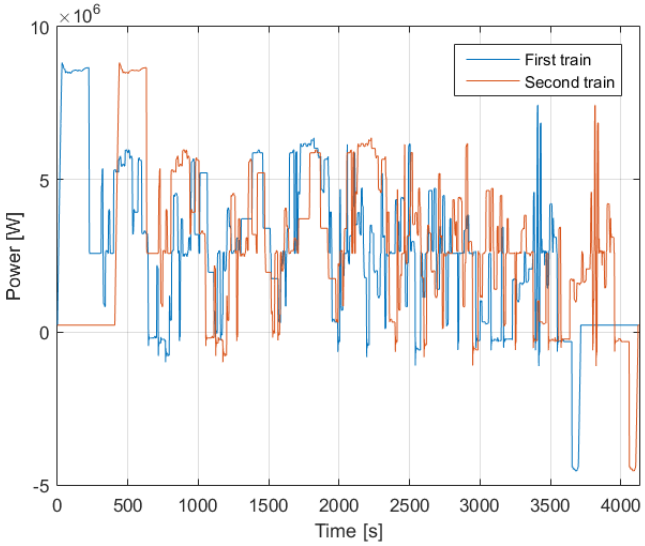

Figure 3.57: Two travelling vehicles in the same direction: power consumptions.

Figure 3.53(b)) is limited in the absorption phase to feed only the auxiliary systems during constant speed operation. The $S.O.C.$ however, is more influenced by partial braking phases: Figure 3.53(c) shows how a partial braking provides about 5% of the supercapacitor capacity.

Finally, Figure 3.54(a), Figure 3.54(b) and Figure 3.54(c) show respectively the voltage, current

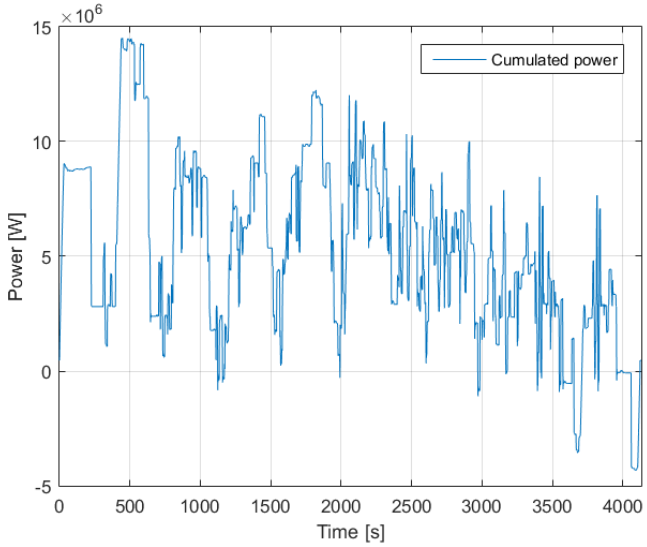

Figure 3.58: Two travelling vehicles in the same direction: total power consumption.

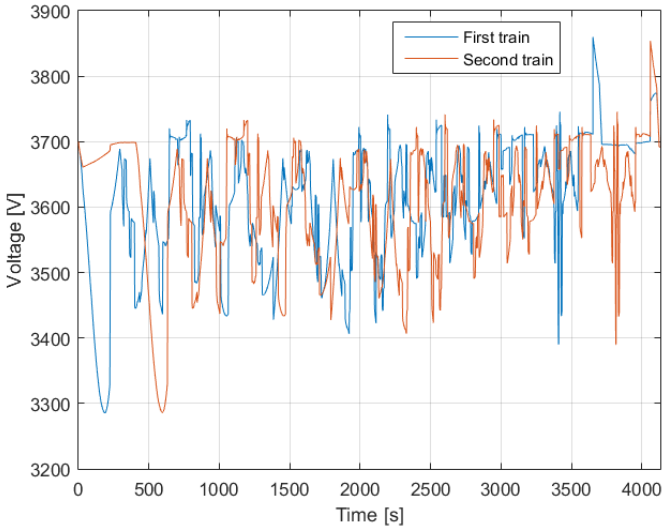

Figure 3.59: Two travelling vehicles in the same direction: voltage pantograph profiles.

and $S.O.C.$ of a stationary supercapacitor located in the arrival station of the considered line. Even in this case, the voltage and current (see Figure 3.54(a) and Figure 3.54(b)) are analogous to those of the corresponding stationary battery. The $S.O.C.$ (shown in Figure 3.54(c)), is more influenced by the final full braking with respect to the corresponding battery, even if the advantage is less

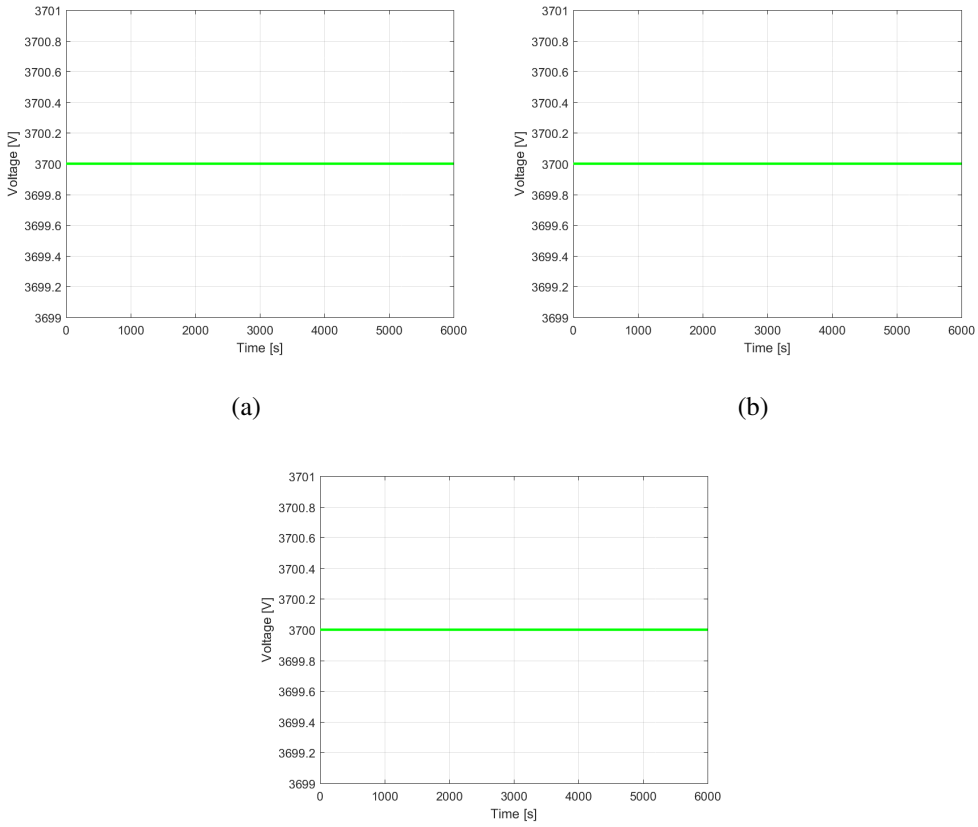

(a) (b)

(c)

Figure 3.60: Two travelling vehicles in the same direction: stationary storage devices voltage, (a) Firenze, (b) *km* 126 and (c) Roma.

significant than that obtained for partial brakings.

The behaviour of the on-board supercapacitor is even more distant from that of the on-board battery. Figures 3.55(a), 3.55(b) and 3.55(c) show respectively the voltage, current and $S.O.C.$ of the on-board supercapacitor. The voltage (shown in Figure 3.55(a)) oscillates significantly, following the $S.O.C.$ variations, while the current, shown in Figure 3.55(b) and limited, for the consumption phase, to the auxiliary systems power, is analogous to that seen for the battery. The most significant difference is due to the $S.O.C.$: Figure 3.55(c) shows how the device continuosly performs full charge/discharge cycles.

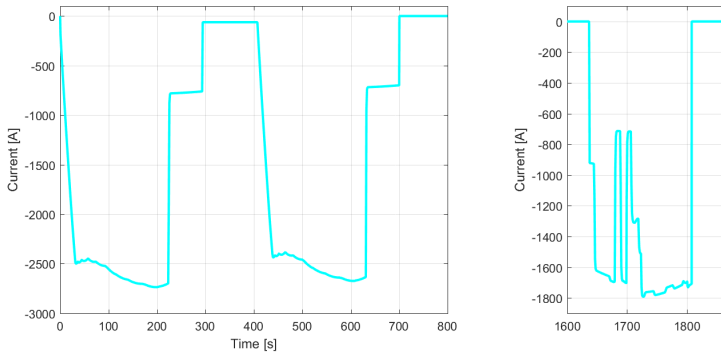

(a)

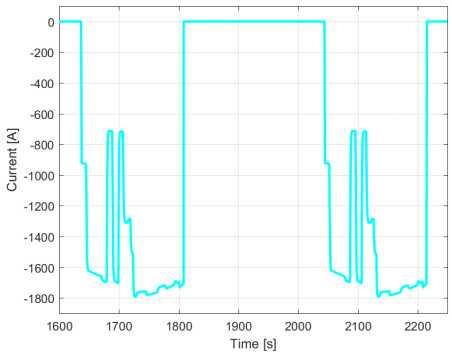

(b)

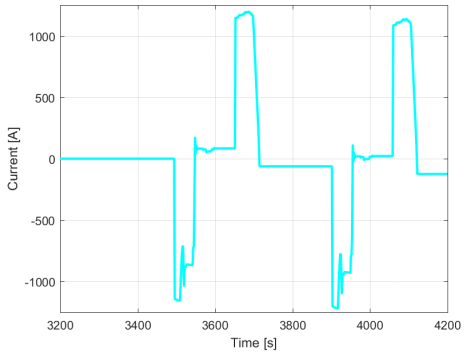

(c)

Figure 3.61: Two travelling vehicles in the same direction: stationary storage devices current, (a) Firenze, (b) *km* 126 and (c) Roma.

The results shown in Figures 3.48 to 3.55, which expose the behaviour of stationary and on-board supercapacitors, are coherent with the expected physical behaviour of those system. However, it is clear that an experimental validation of these sub-models will be necessary within the future developments of the proposed research work: only after an accurate experimental validation, a numerical model can be fully declared able to correctly represent the physical system.
Nevertheless, since the main contribution of the proposed approach, constituted by the coupled vehicle line model, has been extensively validated, and the storage devices sub-models exhibit substantially coherent results, the considerations exposed in this Section can be considered quite appropriate indications towards an optimised High-Speed railway system.

Among the large set of simulated scenarios, the following results are referred to the two basic scenarios: two vehicles that travel in the same direction and two vehicles that travel in opposite directions within the *Direttissima* line. This choice is due to two main reasons: the first one is that these two configurations represent the basic behaviour of multi-vehicle systems and the second one is that more complex scenarios are not so immediate to be represented in a comprehensible graphical way.

Figures 3.56 to 3.62 show the results referred to an operating scenario in which two High-Speed trains travel within the *Direttissima* line, with the same mission profiles but with different departure times.

Figure 3.56 shows the mission profile of the two vehicles: the most significant difference is the delay between the departure of the trains. The vehicles follow the line speed limits and their distance is regulated by the signalling system.

Figure 3.57 shows the vehicles power consumptions: sometimes the braking and traction phases of the vehicles are simultaneous while sometimes they are not coordinated. This is a first important aspect which must be taken into account to harmonise the use of energy storage devices with optimised timetables. Figure 3.58 shows the cumulated power consumption of the vehicles, which is fundamental to understand the requirements for the line.

The power consumption is strictly related to the pantograph voltage of the vehicles, shown in Figure 3.59: the line voltage limit must be taken into account in order to maximise energy recovery and avoid dissipation. Figure 3.60 shows the voltage of the storage devices included within the simulated scenario: Figure 3.60(a), Figure 3.60(b) and Figure 3.60(c) show the voltage of the devices respectively located in correspondence of the departure station, at *km* 226 and in correspondence of the arrival station. Analogously to the results previously shown for the analysis of the storage devices, the voltage is constant for the three considered devices, thanks to the operation of the DC/DC converters.

The current, which is handled by the stationary storage devices located within the line, is shown in Figure 3.61: the devices contributes to the power exchange between travelling vehicles and, hence, to the maximisation of energy savings. Figure 3.61(a), Figure 3.61(b) and Figure 3.61(c)

show the current flows of the devices, repectively located in the departure station, at *km* 226 and in the arrival station: in all the three cases, it is possible to highlight the passage of the two vehicles, which, being characterised by the same mission profile, absorb and provide current one after the other with the same trend. The energy provided by the first train could be used by the second one. Finally, Figure 3.62 shows the $S.O.C.$ of the considered stationary storage device: this Figure allows to verify if the performances required from the devices are acceptable considering their operating lives and technological limits. Figure 3.62(a), Figure 3.62(b) and Figure 3.62(c) respectively show the $S.O.C.$ of the departure, intermediate and arrival storage devices. It is possible to highlight how, coherently with the current fluxes shown in Figure 3.61, the two vehicle contributes in the same way, but in different moments, to the devices charge and discharge cycles. In particular, while the first two devices are equally discharged by the passage of the vehicles, the last device absorbs a significant part of the energy provided by the first vehicle and provides it back to the second vehicle.

Figures 3.63 to 3.69 show the second basic scenario considered during the optimisation process: two High-Speed trains that depart at the same time respectively from Firenze and from Roma. Figure 3.63 shows the mission profiles of the two vehicles: they go through the whole line with the same speed value (the velocity of the Roma-Firenze train is represented as negative in order to highlight its travelling direction) and they *meet* in correspondence of *km* 126. The power consumptions of the two vehicles are shown in Figure 3.64: the trend is similar but, aside from the fact that the two trains depart from different stations, the main difference are due to the line slope, which changes sign for the two vehicles (instead curves, expressed in terms of equivalent slope, provides forces with the same sign for the two vehicles).

Figure 3.65 shows the cumulated power of the two vehicles as a function of the line progressive: the power consumption of the vehicles in a certain line position are not simultaneous, but the storage devices overcome this problem and contribute to the energy exchange between them. Figure 3.66 shows, then, how the pantograph voltage for the two vehicles is completely analogous.

Concerning the stationary storage devices included within the considered system, Figure 3.67

shows their voltage levels (Figure 3.67(a), Figure 3.67(b) and Figure 3.67(c) are respectively referred to the Firenze, *km* 126 and Roma substations): thanks to the presence of the DC/DC converters, the voltage levels remain constant through all the simulation.
Figure 3.68 shows the current flows of the considered storage devices: Figure 3.68(a) represents the Firenze substation device, which operates while the departing train accelerates and while the arriving train brakes; Figure 3.68(b) shows the *km* 126 device, which is interested by the passage of both trains in the same time interval and, finally, Figure 3.68(c) shows the Roma substation device, which operates analogously to the Firenze device.
Finally, Figure 3.69 shows the $S.O.C.$ of the three devices. The Firenze device, shown in Figure 3.69(a), is significantly discharged by the departing vehicle and then receives recovered energy from the final braking phase of the arriving train. Figure 3.69(b) shows how the intermediate device is discharged by both the vehicles, which use its energy to maintain their constant speed mission profiles. The last device, located in correspondence of the Roma substation, is shown in Figure 3.69(c) and behaves in a completely analogous way with respect to the Firenze device.

Starting from these results, the first considerations can be made concerning the number of storage devices employed within the system. Figure 3.70 shows the percentage of saved traction energy within the system, as a function of the number of stationary storage devices: the percentage of energy which is saved, thanks to the presence of storage devices, initially increases, but, with more than three-five devices, the increment is negligible. The Figure allows also to highlight the difference between an optimised timetables scenario and a non optimised one: the behaviour is asymptotic in both cases, but in absence of a timetables optimisation the saved energy percentage is more limited.

An analogous behaviour characterises the use of on-board energy storage devices; while for a single vehicle the presence of an on-board storage device allows to save more traction energy than its absence, the advantages for the whole system are not so immediate to be evaluated.
Figure 3.71 shows the percentage of saved traction energy within the system as a function of the number of on-board storage devices: the percentage of energy, which is saved thanks to the presence of storage devices, initially increases but then assumes an asymptotic behaviour, which

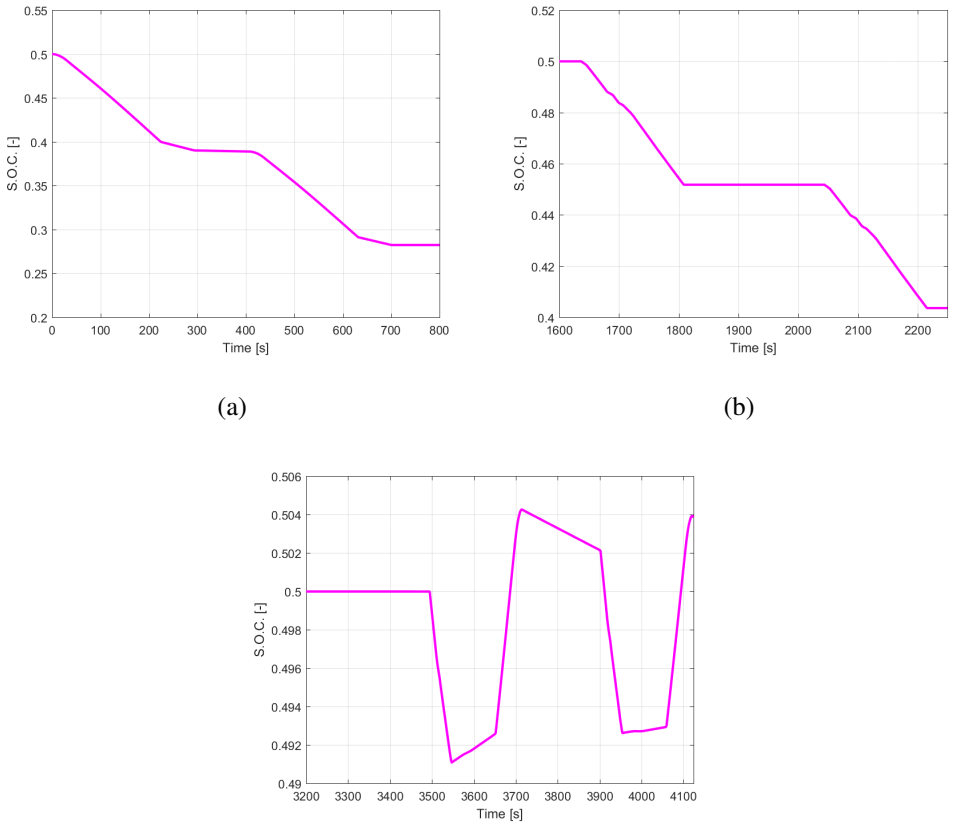

Figure 3.62: Two travelling vehicles in the same direction: stationary storage devices $S.O.C.$, (a) Firenze, (b) *km* 126 and (c) Roma.

is not so different from that previously highlighted for stationary devices. The trend leads to the deduction that the number of devices, needed to reach the limit, is higher than for stationary devices and that the limit percentage of saved energy is lower. This is due to the fact that each device handles only the energy due to its train and hence, even if a number of devices bigger than one can provide a little advantage, it is not possible for on-board devices to have a thorough impact on the whole system. However, also in presence of on-board devices, the optimisation of timetable has a significant impact.

Another important aspect is the capacity of the device: in fact, both for stationary and on-board devices and, analogously to what happens for the number of devices, the percentage of saved

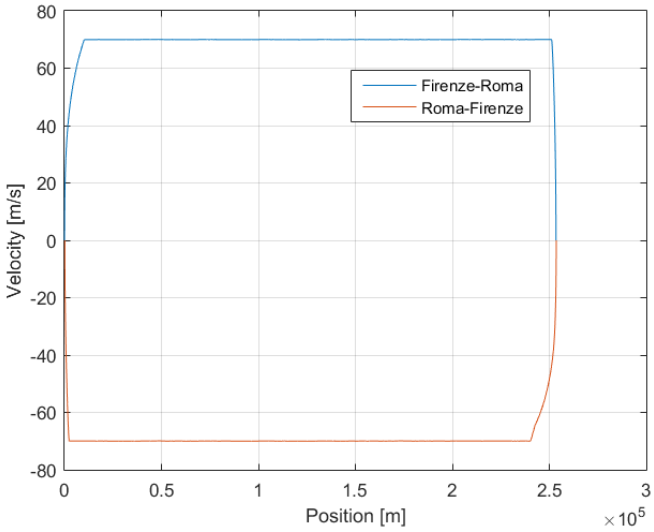

Figure 3.63: Two travelling vehicles in opposite directions: velocity profiles.

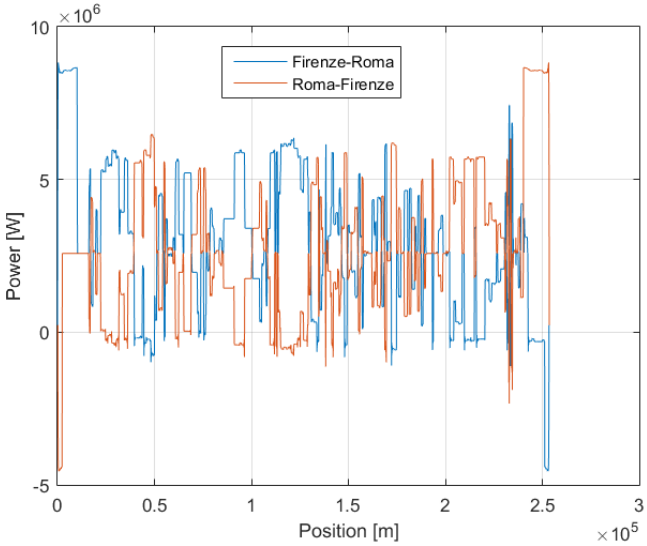

Figure 3.64: Two travelling vehicles in opposite directions: power consumptions.

energy does not increase indefinitely with the devices capacity.

Figure 3.72 shows the percentage of saved energy as a function of the device capacity in presence of stationary storage devices; the results are parametrized considering the presence of a different number of devices through the line and considering three different traffic scenarios, i.e. low,

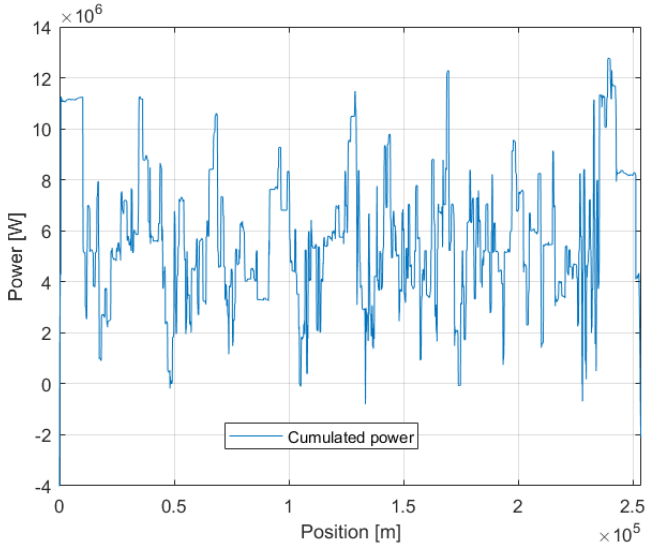

Figure 3.65: Two travelling vehicles in opposite directions: total power consumption.

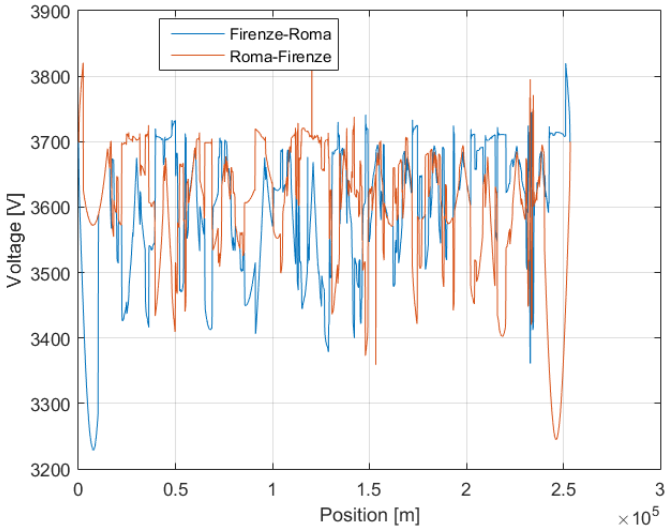

Figure 3.66: Two travelling vehicles in opposite directions: voltage pantograph profiles.

medium and high traffic. It is possible to highlight how the saved energy has an asymptotic trend: an exaggerated oversizing of the device capacity would not provide advantages, but only additional costs. Traffic has a negative effect on the saved energy, since the presence of more vehicles complicates the mission profiles optimal management.

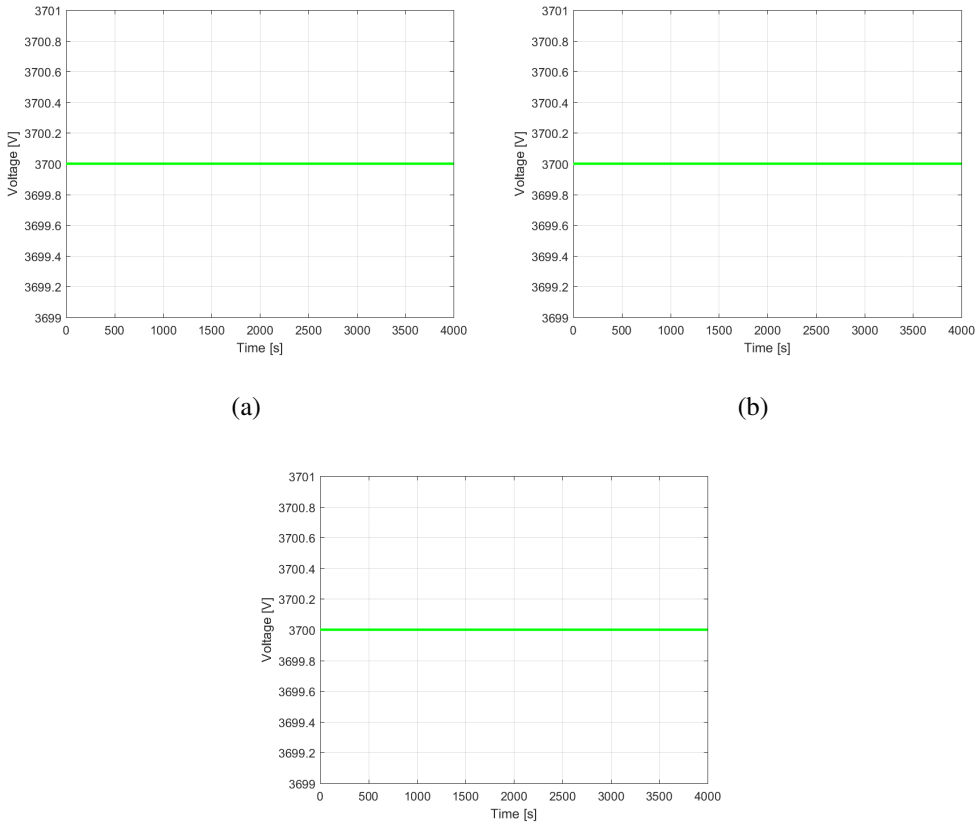

(a) (b)

(c)

Figure 3.67: Two travelling vehicles in opposite directions: stationary storage devices voltage, (a) Firenze, (b) *km* 126 and (c) Roma.

Figure 3.73 shows the results concerning the device capacity for the on-board scenario. In this scenario, only the results referred to a single device are shown: also in this case the traffic has a negative influence on the saved energy and the main results is still represented by the asymptotic behaviour of the saved energy as a function of the device capacity.

Figure 3.74 shows then the value of the different scenarios considered for the use of storage devices, i.e. stationary and on-board batteries and supercapacitors, with two different sizes. The results have been scaled considering the initial investment: it is possible to highlight how, due to the exiguous quantity of energy they are able to store, all the superacapacitor configurations are unable to recover the initial investment, resulting in significant economical losses and very small energy savings. On

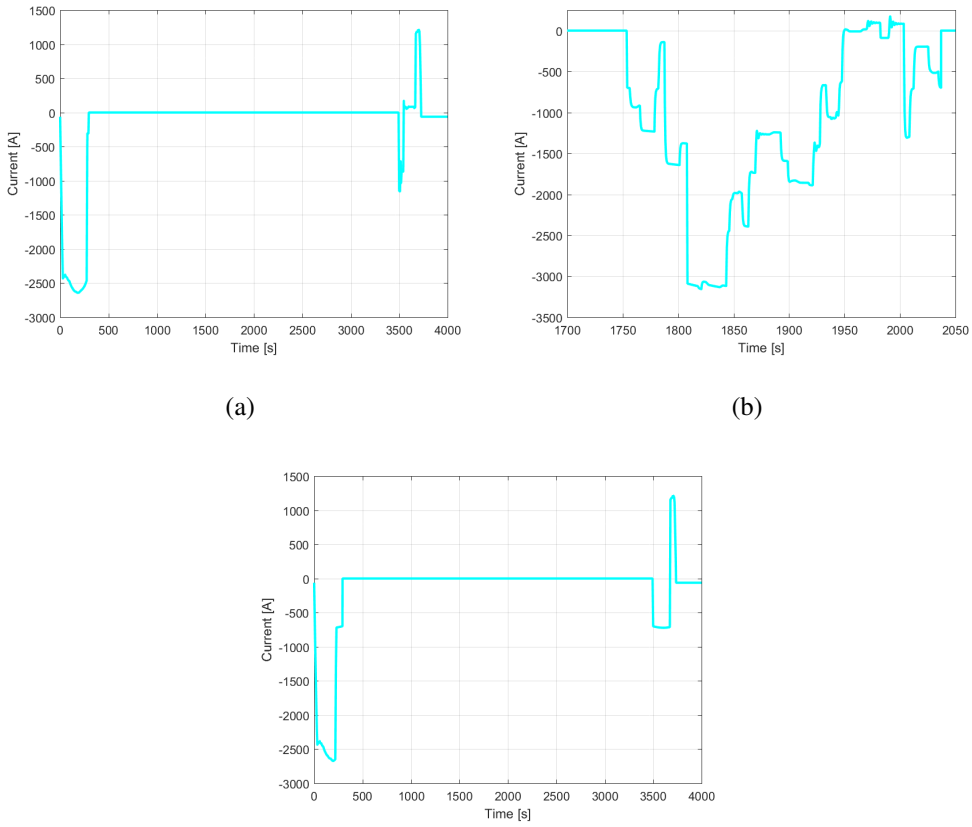

Figure 3.68: Two travelling vehicles in opposite directions: stationary storage devices current, (a) Firenze, (b) *km* 126 and (c) Roma.

the other hand, from the economic point of view, all the battery configurations perform very well, producing significant energy savings and profit margins.

Figures 3.56 to 3.69 show the results referred to two of the most representative configurations among the many different ones which have been analysed; Figure 3.75 shows a scheme of the operating scenario, which has been indicated by the final optimisation analysis as the best one for the maximisation of energy savings. In this scenario, which includes the use of on-board and stationary batteries and of optimised timetables, the system includes 5 stationary batteries and only 6 vehicles equipped with on-board batteries (all sized according to Section 3.5). Furthermore, the vehicles distances (i.e. timetables) has been optimised in order to coordinate their mission profiles

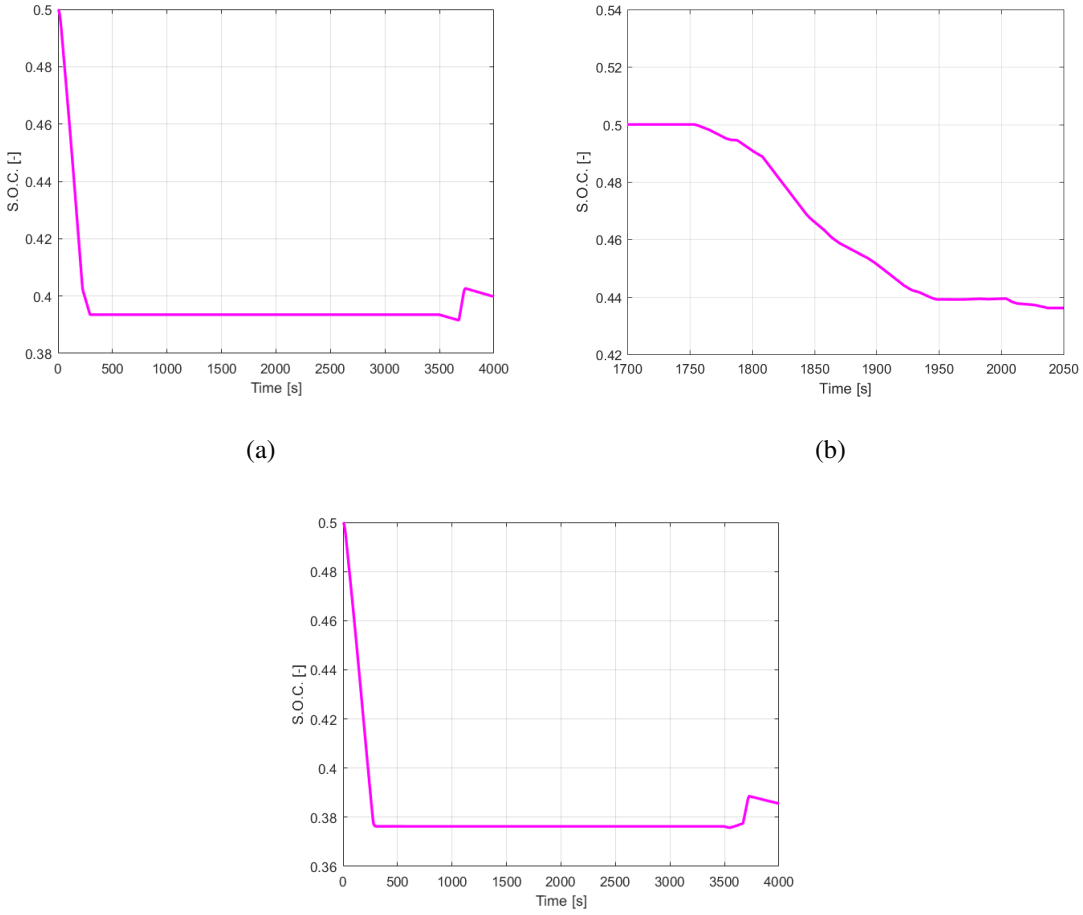

Figure 3.69: Two travelling vehicles in opposite directions: stationary storage devices $S.O.C.$, (a) Firenze, (b) *km* 126 and (c) Roma.

and maximise the energy recovery.

Summarising the results exposed in this Chapter, it is possible to make a few final remarks on the optimisation of a High-Speed railway system. First of all, energy savings, in particular considering eco-driving techniques, but also in presence of energy storage devices, are significantly influenced also by line topology: it is important to consider line potential energy for on-board storage device sizing, since it could provide important energy peaks.

Considering the results shown in this Chapter and the existing technical and literature solutions,

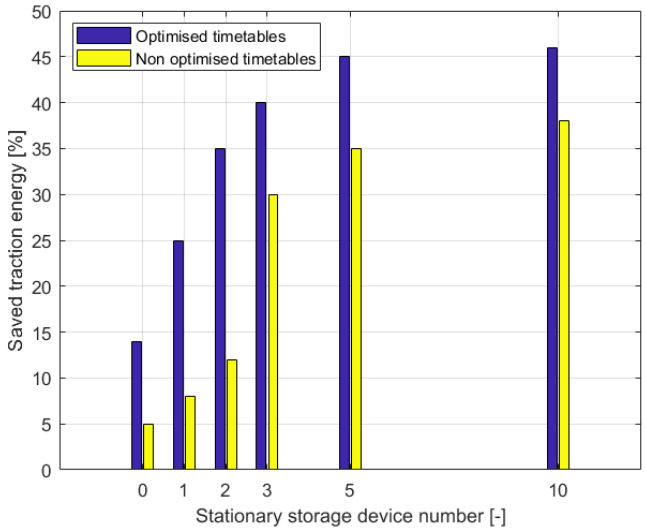

Figure 3.70: Saved energy as a function of the number of stationary storage devices.

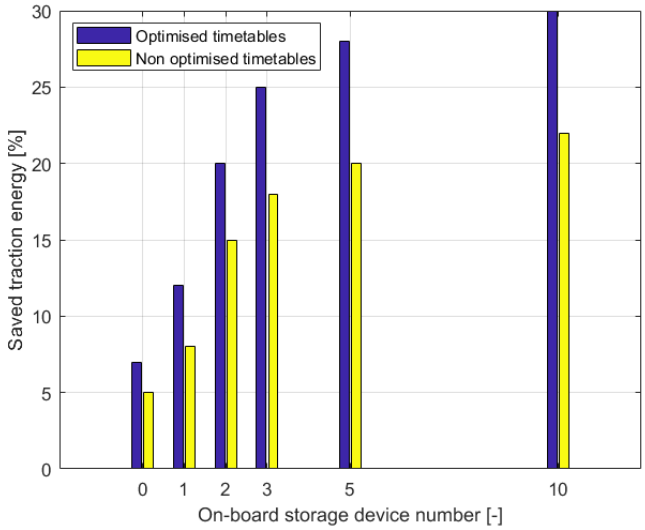

Figure 3.71: Saved energy as a function of the number of on-board storage devices.

it is also possible to distinguish between different possible scenarios. The optimisation of trains timetables can produce, even in absence of energy storage devices, energy savings up to 14%; however, a proper real time controller is needed on-board the vehicle to adapt the mission profile to unforeseen events.

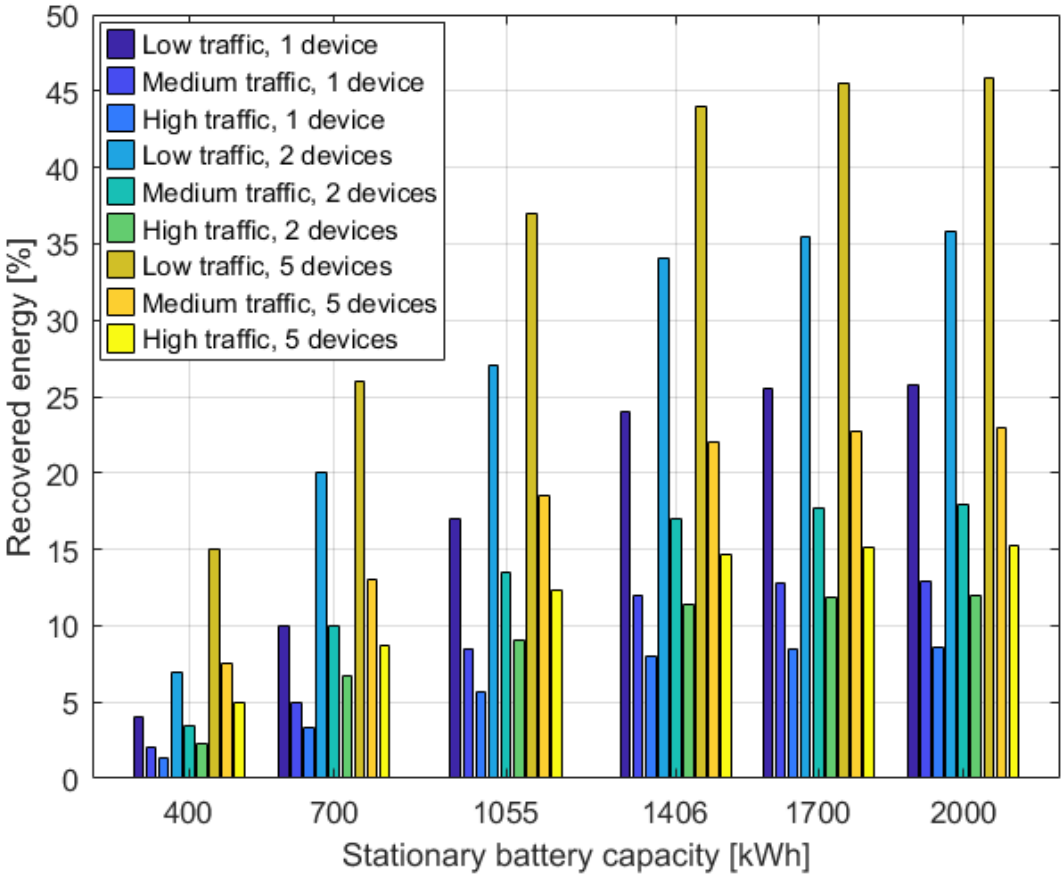

Figure 3.72: Saved energy as a function of the stationary storage devices capacity and of the traffic scenario.

The use of reversible substation is a very interesting option, since they are always receptive and, hence, they allow a full braking energy recovery. They are also characterised by small internal losses with respect to non-reversible substations; however, the line losses have to be accurately taken into account and the investment required for their installation is significantly high.
Considering the use of stationary storage devices, and aside from considerations on the P.B.T., it is important to stress how the energy savings do not increase constantly with the number of devices: up to a certain number of devices the recovered energy increases, then the trend is asymptotic and a further investment will never be justified. Furthermore, in absence of a proper blending strategy, the number of devices needed to reach the energy recovery limit is higher.

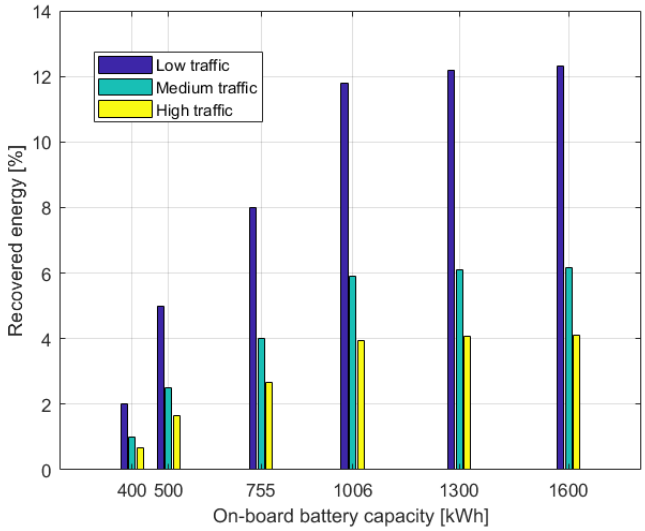

Figure 3.73: Saved energy as a function of the on-board storage device capacity and of the traffic scenario.

In this research work, the proposed model and approach have been used to try to perform the energetic optimisation of a specific High-Speed system; however, the indications obtained from these results represent maybe the most important output of the work.

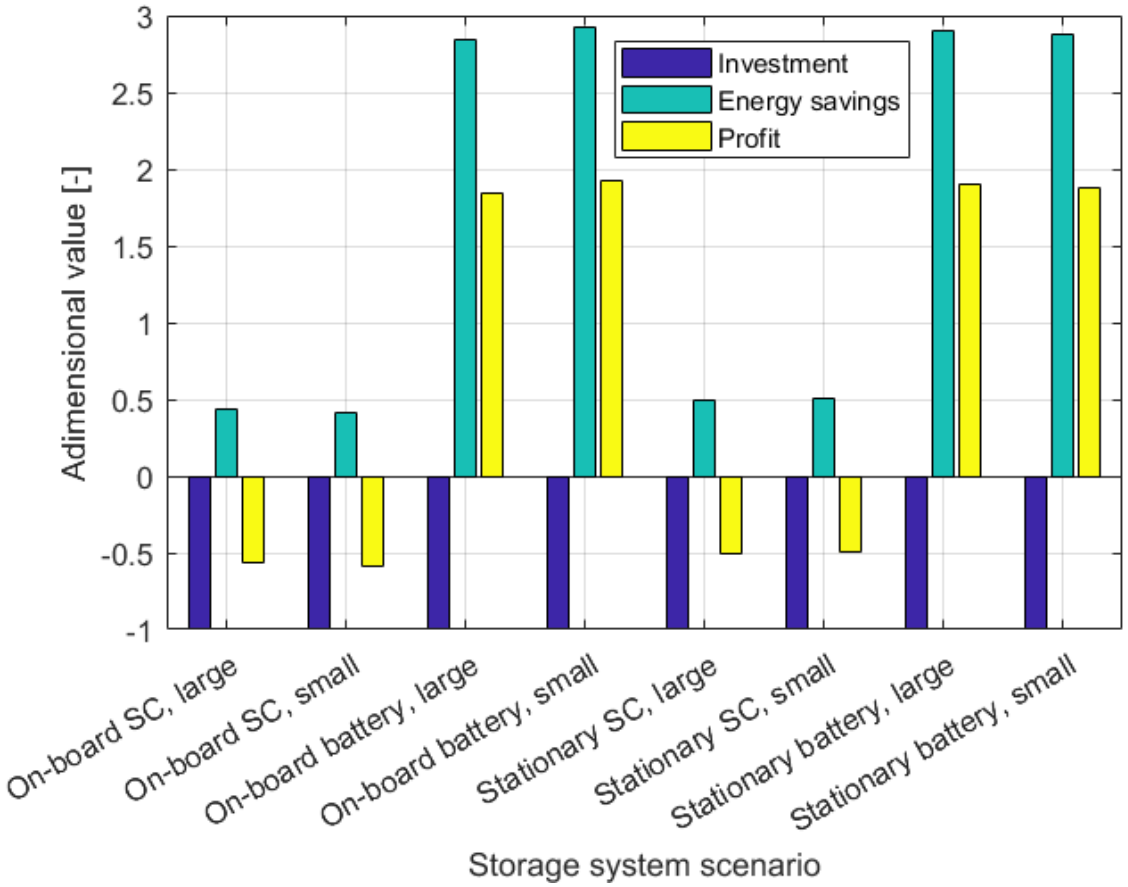

Figure 3.74: Value of the use of storage systems.

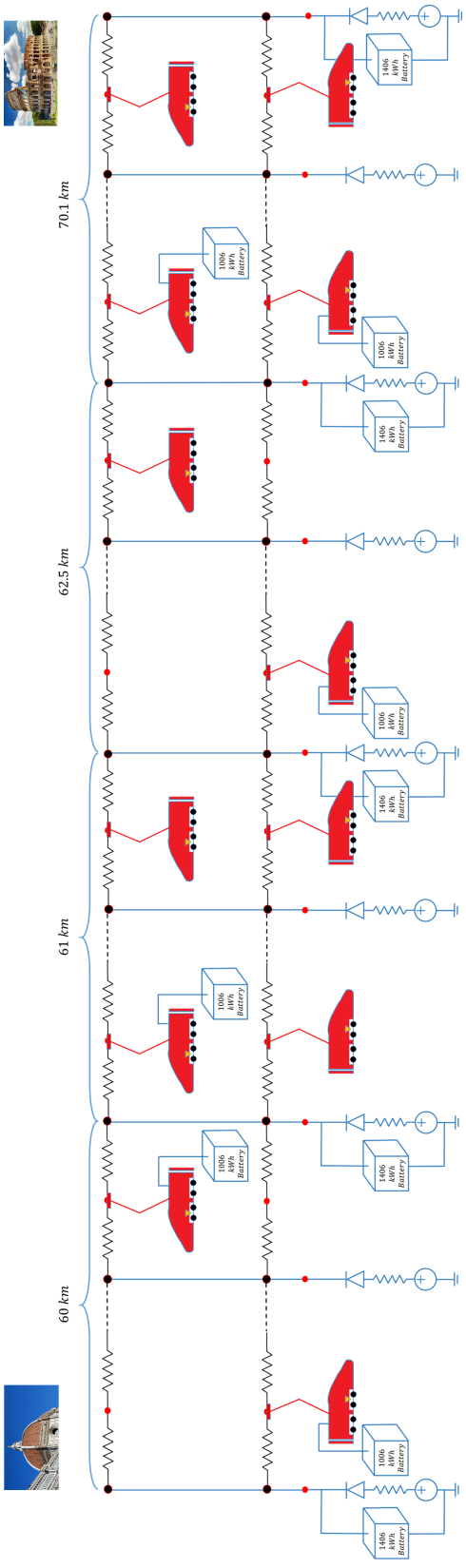

Figure 3.75: Optimised scenario.

3.8 Computational performances

Finally, as reported in Table 3.8, together with characteristics of the computer used for the simulations, the proposed model proved to be highly efficient from the computational point of view: the simulation of the manoeuvres used for the validation requires less than 1 s of computational time, while a simulation of the complete *Direttissima* line (250 km) requires 5 s.

Table 3.8: Machine features and computational times.

CPU	Intel CORE i7
Clock frequency	230 GHz
RAM memory	8 Gb
Operative system	Windows 10 - 64 bit
$\frac{machine\ time\ [s]}{time\ to\ be\ simulated\ [s]}$	$4 \cdot 10^{-4}$

4

Conclusions and future developments

The ever increasing attention to the environment and to pollution problems, connected with transportation, is pushing towards the achievement of higher energetic efficiency in all the transport

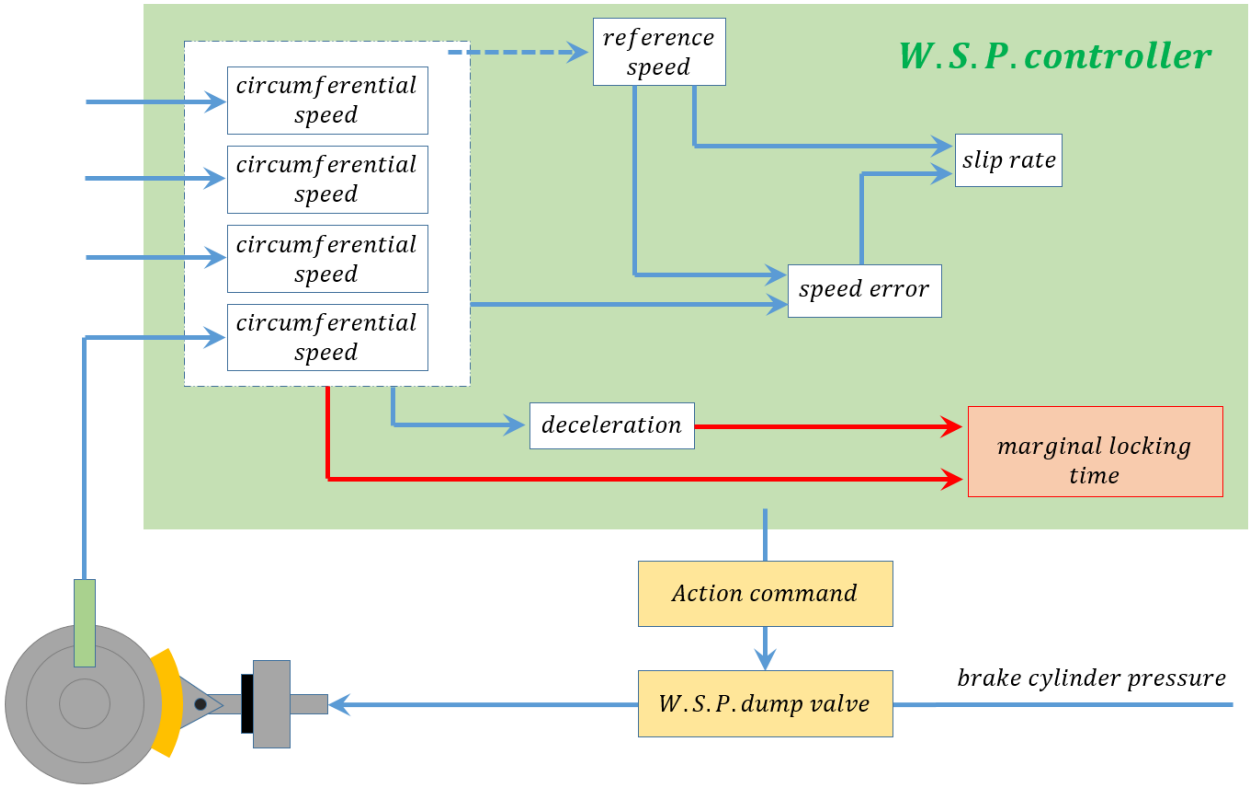

Figure 4.1: Architecture of a W.S.P. device.

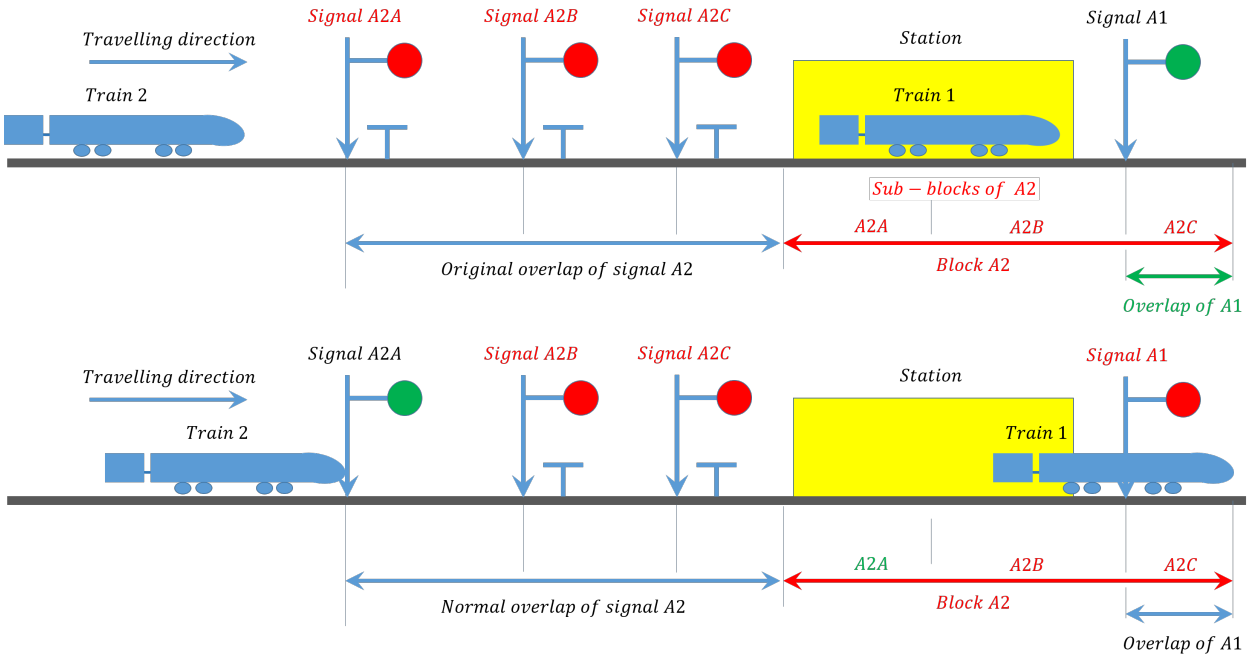

Figure 4.2: Scheme of a signalling system.

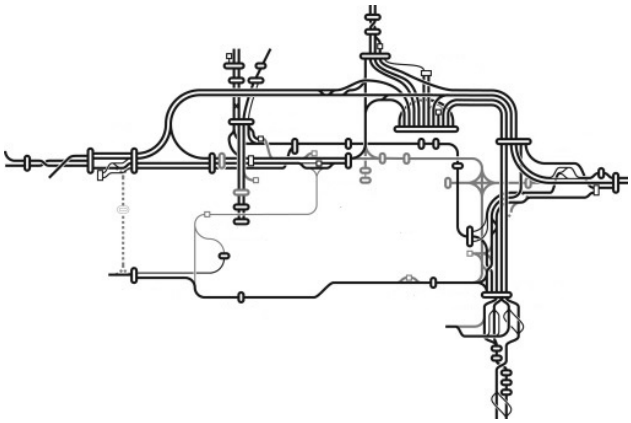

Figure 4.3: Scheme of a complex railway node.

sectors. Railway is currently in a favorable position, but in order to preserve its competitiveness, it is fundamental to further optimise the energetic efficiency in the entire railway sector. One of the possible way to reach this goal is the use of energy recovery systems, in order to regenerate the kinetic energy of the vehicle that otherwise is dissipated during the braking phases.

Regenerative braking and energy recovery systems have been widely analysed considering their

application in the light railway field; however, the possibility to apply energy recovery in High-Speed trains is a quite new research field. High-Speed railway has different needs with respect to light railway; hence, it is necessary to understand which practical solutions could fit the energetic characteristics of the considered application.

In this research work, for the analysis of the interactions between the vehicle longitudinal dynamics and the electrical line, an innovative model, which can be used to analyse the effects due to the introduction in the system of stationary or on-board energy storage devices, has been developed. The model has been calibrated and validated considering proper sets of experimental data referred to manoeuvres of a commuter train (i.e. the E 464) within the Firenze-Pisa-Livorno line and of a High-Speed train (i.e. the Italian ETR 1000) within the *Direttissima* line. The results, obtained with the proposed model, which has been developed using an innovative object oriented modelling language, proved to be really accurate; furthermore, the computational efficiency of the model is extremely high since it allows to analyse train operation in a line of about 250 *km* in a few seconds of simulation time. After the validation, the model has been used in order to analyse the feasibility of energy storage systems in a High-Speed railway application. From this analysis, it has been found that the use of stationary energy storage devices, located in correspondence of the electrical substations, could allow significant savings even in a High-Speed system, where the braking frequency is quite low: the first outcome is that, considering an acceptable braking request, it is possible to recover more than one third of the energy involved in the train braking phase. Nowadays, those results are widely acknowledged by professional operators of the sector.

After the feasibility analysis, a sizing approach for on-board and stationary energy storage devices has been proposed and a complete optimisation analysis, taking into account the use of energy storage device, the presence of more than one travelling vehicle within the line and the optimisation of timetables, has been performed.

The optimisation analysis, through a large set of analysed scenarios and results, has allowed, even before the detection of an optimal operating scenario, to understand some important guidelines for the energetic optimisation of a High-Speed railway system. The analysis has unearthed the role of the number of storage devices and of their capacity, the impact of traffic and timetable

management. Those outcomes, more general than a single optimised scenario, maybe represent the most important contributions originated from this research work.

This thesis does not represent an arrival point, but, rather, a departure point from which further research works concerning the energetic efficiency of High-Speed railway systems could start towards new and significant innovations.

The research activity will continue in order to improve both the model itself and the simulated scenarios. The first step will be represented by the implementation of W.S.P. (i.e. wheel slide protection, see Figure 4.1) and anti-skid sub-models within the proposed coupled model, in order to improve the representation of vehicle longitudinal dynamics and to be able to analyse more complex manoeuvres.

The second move will be the implementation of a more detailed signalling model (see Figure 4.2), useful to analyse with the proposed model a complex scenario like a great railway node, where a large number of vehicles constantly arrive and depart.

The optimisation of a complex node (like Milano or Roma, where a large number of High-Speed trains arrive or depart, see Figure 4.3) will indeed be the final step, coupled with a large scale validation of the approach.

Appendices

A

Published papers on railway

In this Appendix the papers concerning railway that have been published during the Ph.D. period for International Journals and Conferences are reported.

Energy Conversion and Management 129 (2016) 200–215

Contents lists available at ScienceDirect

Energy Conversion and Management

journal homepage: www.elsevier.com/locate/enconman

Energetic optimization of regenerative braking for high speed railway systems

Amedeo Frilli, Enrico Meli, Daniele Nocciolini, Luca Pugi*, Andrea Rindi

Dept. of Industrial Engineering, University of Florence, Florence, Italy

ARTICLE INFO

Article history:
Received 29 February 2016
Received in revised form 19 September 2016
Accepted 1 October 2016

Keywords:
Railway
Energy storage systems
Simulation
Object oriented languages
High speed trains

ABSTRACT

The current development trend in the railway field has led to an ever increasing interest for the energetic optimization of railway systems (especially considering the braking phases), with a strong attention to the mutual interactions between the loads represented by railway vehicles and the electrical infrastructure, including all the sub-systems related to distribution and smart energy management such as energy storage systems. In this research work, the authors developed an innovative coupled modelling approach suitable for the analysis of the energetic optimization of railway systems and based on the use of the new object oriented language Matlab-Simscape™, which presents several advantages with respect to conventional modelling tools. The proposed model has been validated considering an Italian Direct Current High-speed line and the High-speed train ETR 1000. Furthermore, the model has been used to perform an efficiency analysis, considering the use of energy storage devices. The results obtained with the developed model show that the use of energy recovery systems in high-speed railway can provide great opportunities of energy savings.

1. Introduction

1.1. Energy and railway transportation free markets and their role in a new green revolution

Global Warming and more in general the issues related to pollution are enforcing a growing interest to the increase of efficiency of transportations systems [1], which still represent in Europe and in all industrial countries about 30% of CO_2 pollution sources. This situation has been investigated by both the Europe Environment Office [2] and the Association of American Railroads [3]; furthermore, Fridell et al. [4] performed a number of experimental tests and found out that, in the railway sector, a significant part of emissions is due to mechanical braking. Railway transportation represents the most efficient technology in terms of pollution and energetic efficiency, but the continuous technological improvements accomplished by its competitors (i.e. ground and air vehicles) are reducing this gap. Furthermore, the current market growth for high-speed and freight sectors in industrialized countries with high population densities would be strongly enhanced by the improvement of the efficiency of the system.

Another important aspect, which is pushing towards a strong energy optimization of the railway system, is the liberalization process of both energy and transportation markets: this process is stimulating all the stakeholders in the railway sector (i.e. energy infrastructures and suppliers, railway infrastructures and vectors) to accurately measure and quantify energy consumptions and their costs. In particular, the combined liberalization of both energy and railway sectors should give to the infrastructure managers the opportunity to apply different costs to traveling trains according to the real measured energy efficiency. Furthermore, the possibility of acquiring energy from different suppliers would allow to optimize costs with respect to the line geographic location, to seasonal factors involving the availability of different resources and, finally, to specific requirements of railway vectors/transport manager. In this scenario, the competition between the different subjects involved in the entire railway field and the need to respect interoperability issues established by the European Railway Agency in the Technical Specifications for interoperability (TSI) [5], will further stimulate the optimization of train energy consumptions, as reported in the analysis of different methods to improve railway energy efficiency performed by Douglas et al. [6].

1.2. Regenerative braking and energy storage systems: state of the art and literature review

In modern railways, aside from the classic considerations that should be made concerning the traction systems and the electrical line, one of the greatest source of energy savings is the use of

* Corresponding author.
E-mail address: luca.pugi@unifi.it (L. Pugi).

http://dx.doi.org/10.1016/j.enconman.2016.10.011
0196-8904/

2016. Energetic optimization of regenerative braking for high speed railway systems. In ENERGY CONVERSION AND MANAGEMENT, vol. 129. A. Frilli, E. Meli, D. Nocciolini, L. Pugi, A. Rindi.

Energy Storage Systems and Regenerative Braking Optimization, Different Approaches Aiming to Improve Efficiency of Modern High-Speed Trains

Massimo Ceraolo, Giovanni Lutzemberger, Amedeo Frilli, Enrico Meli, Luca Pugi, Andrea Rindi
Stefano Bianchi, and Giuseppe Pancari,

***Abstract*—The growing attention to environmental sustainability of transport systems made necessary to investigate the possibility of energy optimization even in sectors typically characterized by an already high level of sustainability, as in particular the railway system. One of the most promising opportunity is the optimization of the braking energy recovery, which has been already considered in tramway systems, while it is traditionally overlooked for high-speed railway systems. In this research work, the authors have developed two vehicle-line simulation models able to reproduce the behavior of high-speed trains entering in a railway node, and to analyze the impact of regenerative braking, including the possibility to store it in energy storage systems, on the total electrical feeding energy demand. These two models, developed respectively in the Matlab-Simscape environment and in the open source Modelica language, have been experimentally validated considering an Italian high-speed train (the ETR 1000). After validation, the authors have performed an extensive feasibility analysis considering the use of stationary and on-board storage systems, also by taking into account capital costs of the investment and annual energy saving, to evaluate cost-effectiveness of the different proposed solutions. The analysis has effectively shown the possibility to significantly improve the efficiency of high-speed railway systems, by improving braking energy recovery through the installation of such storage systems.**

***Index Terms*—Railway, high-speed trains, energy storage, regenerative braking, energetic efficiency.**

I. Introduction

NOWADAYS large part of railway vehicles is able to combine the standard pneumatic braking to an electrical braking system, made possible by the electric traction system: in this way, the kinetic energy of the train is converted in electrical energy, which can be handled in different ways. The first and simplest way to manage that energy is to dissipate it on a set of specifically developed resistors placed on-board trains; obviously, this solution comes along with some significant consequences, as example how to properly manage the heat thus generated. A second way is to perform the energy recovery: the electrical energy can be sent back to the contact line where it can be used by other trains during their traction phases, or stored in properly sized energy storage systems located along the feeding line or on-board the trains.

However, electrical braking allows significant advantages also in terms of maintenance costs: in fact, it allows to preserve friction materials of the mechanical brake (pads and discs) from excessive wear rates. This effect is very significant in terms of environmental pollution, since mechanical brakes particles count for a significant percentage of the air pollution related to railway systems and should be reduced. Different studies on this topic are in [1], [2], [3]. Also maintenance costs should be accurately evaluated, since the wear of braking pads depends on the percentage of train kinetic energy, which is mechanically dissipated. This aspect is detailed in UIC 541 rules [4], [5], where a wear rate index defined as the ratio between the worn volume of tested friction material and the amount of dissipated energy for the testing and homologations of pneumatic braking systems is defined. Additional benefits should be obtained also in terms of protection of brake units from overheating, since electrical braking should be used also when extended braking maneuvers occur. Moreover, the access to braking units for maintenance involves additional time and costs that have to be considered.

Regarding brake blending, i.e. the strategy to optimally apply the action of mechanical and electrical braking systems, several studies are shown in literature. In particular, blending of high speed trains was the object of previous publications [6], [7], which analyzed the influence of blending strategy on braking pads wear and on the braking system performance, taking into account the variation of the pads friction coefficient due to wear and hence vehicle safety issues. In fact, from the safety point of view, UIC rules [4], [5] clearly specifies that emergency stop maneuver must be entirely ensured by mechanical braking devices, without usage of electrical braking: for this reason, an optimal management of electrical braking would not only allow energy savings but improve also the system safety.

When electrical braking is performed, two main ways to manage the generated power must be considered:

- Dissipative Braking: generated electrical energy is dissipated over an array of resistors typically controlled by a static converter.
- Regenerative Braking: generated electrical energy is available to be stored on board or redirect to the overhead

M. Ceraolo and G. Lutzemberger are with the Department of Energy, Systems, Territory and Constructions Engineering, University of Pisa, Largo Lucio Lazzarino n. 1, 56123, Pisa, Italy, e-mail: massimo.ceraolo@unipi.it, lutzemberger@dsea.unipi.it.

A. Frilli, E. Meli, L. Pugi and A. Rindi are with the Department of Industrial Engineering, University of Florence, Via di Santa Marta n. 3, 50139, Firenze, Italy, e-mail: [amedeo.frilli, enrico.meli, luca.pugi, andrea.rindi]@unifi.it.

S. Bianchi and G. Pancari are with Italcertifer, Largo F.lli Alinari n. 4, 50123 Firenze, Italy, e-mail: s.bianchi@italcertifer.it, g.pancari@italcertifer.it

Manuscript received —; revised —.

UNDER REVIEW: 2017. Energy Storage Systems and Regenerative Braking Optimization, Different Approaches Aiming to Improve Efficiency of Modern High-Speed Trains. In IEEE TRANSACTIONS ON TRANSPORTATION ELECTRIFICATION. M. Ceraolo, G. Lutzemberger, A. Frilli, E. Meli, L. Pugi, A. Rindi, S. Bianchi, G. Pancari.

First International Conference on Rail Transportation
Chengdu, China, July 10-12, 2017

Innovative Model for the Efficiency Optimization for High-Speed Trains through the Recovery of Braking Energy

Elisa BUTINI[1], Amedeo FRILLI[1], Enrico MELI[1], Daniele NOCCIOLINI[1], Simone PANCONI[1], Luca PUGI[1], Andrea RINDI[1] and Benedetta ROMANI[1]
[1]*Department of Industrial Engineering, School of Engineering, University of Florence, Florence, 50139, Italy*
**Corresponding author email: enrico.meli@unifi.it*

Abstract: Nowadays, the competitors of railway systems are going through a strong development phase, concerning the energy savings and the emissions in the environment, typically fields where railway vehicles assume a position of advantage. Due to the diffusion of distributed traction in railway vehicles, the recovery of braking energy, through appropriate technical solutions, represents an important purpose of research. In this work, the authors, as partner of the Tesys Rail project (an Italian project which involves important academic and industrial partners), have developed an innovative model, which includes a vehicle dynamical model, coupled with an electrical model of the feeding line, using the innovative object oriented Matlab-Simscape™ language. The line model is made up of the contact line, the electrical substations and stationary and on-board energy storage devices. The authors have focused their attention on the performances of high-speed trains. In particular, the proposed model has been validated through a set of experimental measurements performed on the Italian high-speed train ETR 1000 within the Firenze-Roma 3kV Direct Current line. Once proved the good accuracy of the results, the model permits to perform a feasibility analysis of the energetic perspectives of a high-speed railway system, concerning different operating scenarios and various energy storage systems configurations. Through appropriate driving strategies and energy storage configurations, the results show that it is possible to recover a significant percentage of the braking energy. Finally, the proposed model proved to be characterized by a great computational efficiency: it is possible to simulate the behaviour of the train along a 250 km distance in only 5 seconds of simulation.
Keywords: Regenerative braking; vehicle-line interactions; energetic efficiency; railway optimization.

1 Introduction

Due to pollution increase and to global warming, the development of transport systems able to allow a significant improvement of environmental sustainability, is a strong matter of concern: railway has typically assumed a position of advantage with respect to the other competitors in transport sector. This gap is going to decrease, thanks to the ever growing attention to energy saving and pollution. Therefore, the energetic optimization of railway vehicles is an important research field. The research work, proposed by the authors, placed within the Tesys Rail national project (Italian acronym for Methods and Instruments to Improve Environmental Sustainability of Railway System), introduces an innovative model, which investigates the electrical feeding line coupled with the rail vehicle.

As Fridell at al. showed through experimental tests (Fridell et al., 2011), in the railway field, a non-negligible part of emissions is due to mechanical braking systems. Moreover, considering the distributed traction increased diffusion in railway vehicles, regenerative

2017. Innovative model for the efficiency optimization of high-speed trains through the recovery of braking energy. In Proceedings of the INTERNATIONAL CONFERENCE ON RAIL TRANSPORTATION 2017, Chengdu, China. E. Butini, A. Frilli, E. Meli, D. Nocciolini, S. Panconi, L. Pugi, A. Rindi, B. Romani.

AIMETA 2017
XXIII Conference
The Italian Association of Theoretical and Applied Mechanics
Luigi Ascione, Valentino Berardi, Luciano Feo, Fernando Fraternali and Antonio Michele Tralli (eds.)
Salerno, Italy, 4–7 September 2017

IMPROVEMENT OF HIGH-SPEED TRAINS EFFICIENCY THROUGH THE USE OF REGENERATIVE BRAKING

Amedeo Frilli[1], Enrico Meli[1], Simone Panconi[1], Luca Pugi[1], Andrea Rindi[1] and Benedetta Romani[1]

[1]Department of Industrial Engineering, University of Florence, Florence, Italy
address: via di Santa Marta 3, 50139, Florence, Italy
e-mail: [amedeo.frilli; enrico.meli; simone.panconi; luca.pugi; andrea.rindi; benedetta.romani]@unifi.it

Keywords: traction and braking systems, energy storage, regenerative braking.

Abstract. *Currently, the energetic optimization represents a main aspect in transport vehicle development [1]. In railway field , the interaction between the electric infrastructure and the vehicle dynamical behaviour is investigated: the authors of this work focused their attention on the development of an innovative model, which analyses the vehicle-electric infrastructure system [2]. The model has been developed through Matlab-SimscapeTM, an object-oriented language which permits computational efficiency and modularity advantages, where a block represents the physical component or the relation which describes it. The whole model is made up of a vehicle dynamical behaviour model and a model of the electrical feeding line: in particular, the last one is composed by the contact line, the substations and on-board and stationary energy storage devices [3]. The mentioned two models are coupled through the vehicle position and the required power, which permits to calculate the voltage and the current along the line. The Italian DC High Speed line, labeled Direttissima and travelled by the ETR 1000 High Speed train, has been used to validate the authors model. The model is used to carry out accurate results and a feasibility investigation of the energetic optimization, including different operating scenarios and various energy storage systems configurations. Finally, it has been proved that the proposed model is characterised by a high computational efficiency, since it can simulate the rail vehicle behaviour through 250 km in 5 seconds of simulation.*

2017. Improvement of high speed train efficiency through the use of regenerative braking. In Proceedings of the AIMETA CONFERENCE 2017, Salerno, Italy. A. Frilli, E. Meli, D. Nocciolini, S. Panconi, L. Pugi, A. Rindi, B. Romani.

Braking energy recovery in high speed trains: an innovative model

Amedeo Frilli, Enrico Meli, Daniele Nocciolini, Simone Panconi, Luca Pugi, Andrea Rindi

Abstract Modern railway development trend is pushing towards a strong enhancement of the energy efficiency of lines and vehicles, with particular attention to braking energy recovery. In this research work the authors have developed an innovative and numerically efficient vehicle-line coupled model, using the object oriented Simscape language: the model has been validated considering a set of experimental measurements concerning the Italian High Speed train ETR 1000 and has then be used to analyze the feasibility of the application of energy storage systems in high speed application. This analysis has shown that the use of stationary energy storage devices can provide significant energy savings even in high speed applications.

1 Introduction

Nowadays transportation still represents a significant source of CO_2 emissions worldwide [8], [5]: from this point of view, railway has started from a favorable position but its competitors (i.e. planes and cars sectors) are strongly pushing towards ever higher energetic and environmental efficiencies. Hence, there is a growing interest in the possibility to enhance the energetic performances of railway vehicles. Furthermore, due to the recent liberalization process in the railway sector and to interoperability issue, the interest to accurately calculate and measure the actual trains energy consumptions is ever increasing.
One of the most important possibility to seek for better energetic efficiencies in modern railways is the recovery of braking energy [7]: this technique is particularly interesting due to the great diffusion of train with distributed traction system. Regenerative braking allows not only to reduce energy consumption but also to get significant savings in terms of reduced wear and maintenance and design costs [2],

A. Frilli, E. Meli, D. Nocciolini, S. Panconi, L. Pugi, A. Rindi
Dept. of Industrial Engineering, University of Florence, Florence, Italy, e-mail: [amedeo.frilli; enrico.meli; daniele.nocciolini; simone.panconi; luca.pugi; andrea.rindi]@unifi.it

2016. Braking energy recovery in high speed trains: an innovative model. In Proceedings of the IFTOMM ITALY 2016, Vicenza, Italy. A. Frilli, E. Meli, D. Nocciolini, S. Panconi, L. Pugi, A. Rindi.

First International Conference on Rail Transportation
Chengdu, China, July 10-12, 2017

An Efficient Wheel-Rail Conformal Contact Model for Multibody Simulation

Elisa BUTINI[1], Amedeo FRILLI[1], Lorenzo MARINI[1], Enrico MELI[1*], Simone PANCONI[1], Andrea RINDI[1] and Benedetta ROMANI[1]
[1.] *Department of Industrial Engineering, University of Florence, 50139, Italy*
**Corresponding author email: enrico.meli@unifi.it*

Abstract: To simulate the rail vehicle dynamics, an important aspect is represented by the characterization of the wheel-rail contact patches. The conformal contact case is a usual scenario in railway field, in particular in sharp curves and when rail and wheel profiles are affected by wear: the patches are large and complex, typically curved and not planar, and the hypothesis based on the contact in a single geometric points or on elliptic patches is not valid anymore. The authors have developed an innovative wheel-rail contact model for conformal contact, which can be employed in the classical railway multibody software. The model, built by the authors, calculates the contact force and it represents an improvement of the non-Hertzian Piotrowski model (Piotrowski and Kik, 2008), and, at the same, includes an improvement of the Kalkers FASTSIM algorithm (Kalker, 1990), in order to calculate the tangential forces on not-planar contact areas. The authors' activity has been carried out in collaboration with Hitachi Rail, which provides the experimental data, useful for the preliminary validation. Furthermore, an experimental campaign, based on the wheel-rail forces, are schedules.
Keywords: multibody modelling of railway vehicles, wheel-rail contact, conformal contact.

1 Introduction

The contact patch between wheel and rail represents one of the main characteristics needed for the simulation of vehicle dynamics, since it represents the application points of the contact forces. In the wheel-rail contact field, the conformal contact constitutes a usual scenario: it occurs in sharp curves, i.e. when the contact takes place between the rail gauge corner and the wheel flange, or where there are rail and wheel worn profiles. The conformal contact patches are large and complex and hence the hypothesis of contact on single geometric points or on a planar elliptic area cannot be applied. The authors' model has been developed especially for the conformal contact: the contact area identification is based on an improved GRID method (Malvezzi et al., 2008). The contact force estimation is the aim of the proposed model. The normal problem has been handle excluding the iterative calculation in accordance with Piotrowski: the non-Hertzian Piotrowski approach is extended to no-planar conformal case, introducing the natural abscissa in the wheel-rail surface discretization. Concerning the tangential problem, the proposed model includes an improved Kalker's Fastsim algorithm, which permits the estimation of the tangential forces on the not elliptical and not planar contact areas. As shown in Figure 1, the contact model is coupled with a multibody model of the vehicle, which reproduces the vehicle dynamics: as displayed, the two models exchange information each other. To preliminarily validate the authors' model, the experimental data, provided by Hitachi Rail, has been used and they have been carried out through the bogie acceleration measure of the MLA MetroBus Brescia, which is a metropolitan scenario characterized by sharp curves.

2017. An Efficient Wheel-Rail Conformal Contact Model for Multibody Simulation. In Proceedings of the INTERNATIONAL CONFERENCE ON RAIL TRANSPORTATION 2017, Chengdu, China. E. Butini, A. Frilli, L. Marini, E. Meli, S. Panconi, A. Rindi, B. Romani.

An Extended Library of Models of Railway Vehicles for Fast Simulation and Optimization of Regenerative Braking and Energy Management

Amedeo Frilli, Enrico Meli, Daniele Nocciolini, Simone Panconi, Luca Pugi, Andrea Rindi
University of Firenze
Via Santa Marta, 3 I-50139 Firenze
luca.pugi@unifi.it

***Abstract* — As a part of the Tesys Rail Project authors have developed a parametric and computationally affordable model of a railway DC line in order to analyze the complex energetic interactions arising between different travelling vehicles. In order to fully exploit the features of the proposed approach and its capability to investigate complex operating scenarios, the authors have further developed the model by including a wider variety of on-board functionalities and a more extended list of simulated vehicles. In this research work, the authors expose some improvements of a previously developed High Speed train model (based on the ETR 1000) and the development of additional models of older Italian High Speed Trains, such as the ETR 500, which are still in service on Italian High Speed lines.**

Keywords*— *regenerative braking, simulation of longitudinal railway dynamics, smart energy management, smart energy storage systems.

I. Introduction

The analysis of the interactions between railway vehicles and the feeding line is assuming a great importance for the improvement of the energy efficiency of the railway system itself. In fact, nowadays the attention towards energy savings and efficiency is ever growing. The railway sector, which is currently the most environmentally sustainable transport method but also the slowest in terms of environmental and energetic development, must push towards a deeper insight (both numerical and experimental) to its energy consumptions and to possible improvements.
A key factor in this research field is represented by the possibility to recover the train braking energy through appropriate technical solutions: the energy can be fed to the line and used by a following vehicle but the main savings would be obtained using proper energy storage systems.
As a part of the Tesys Rail Project, the authors have previously developed efficient models able to reproduce energy interactions between vehicles and surrounding infrastructures [1-3], investigating feasibility and opportunity of energy storage systems along the line. The proposed coupled model, based on the dynamical analysis of the vehicle and on the electrical study of the line, was characterized by a good compromise between accuracy and computational speed and by a strong modularity, useful to analyze different operating scenarios.

In this research work, the authors have improved the previously developed model by adding new features useful to better represent the physical behavior of the whole system. The model has been calibrated and experimentally validated through two sets of experimental data concerning the traction and braking phases of a High Speed train (i.e. the Italian ETR 1000). Finally, the model has been greatly enriched by developing an extended library of railway vehicles: through the introduction of a number of different existent trains, the possibilities to investigate the behavior of the system and to optimize it have been significantly enlarged.

II. Proposed Model

The model proposed by the authors in a previous work [2] includes both a mechanical part and an electrical one: its general architecture is shown in Figure 1.

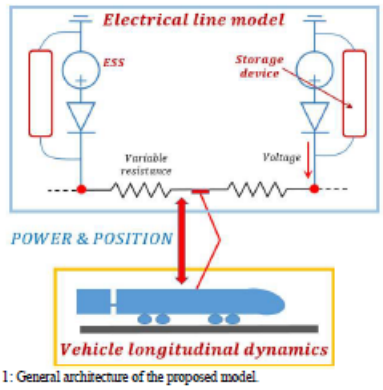

Figure 1: General architecture of the proposed model.

The approach followed to discretize the continuous line circuit into lumped elements was derived by the Bond-Graph approach [4-5], also adopted by the authors for the distributed modelling of hydraulic networks [6].

2016. An extended library of model of railway vehicles for fast simulation and optimization of regenerative braking and energy management. In Proceedings of the AEIT CONFERENCE 2016, Capri, Italy. A. Frilli, E. Meli, D. Nocciolini, S. Panconi, L. Pugi, A. Rindi.

Development and validation of a model for the optimization of regenerative braking of high speed trains

Luca Pugi, Amedeo Frilli, Daniele Nocciolini
DIEF, Department of Industrial Engineering
University of Florence
Via Santa Marta 3, 50139 Florence, Italy
Luca.Pugi@unifi.it

Enrico Meli , Andrea Rindi
MDMTEAM SRL
Via Santa Marta 3 50139 Florence,Italy
Andrea.rindi@unifi.it

***Abstract*—The interest for the energetic optimization of railway systems is constantly increasing due to recent developments concerning Technological Standards and Regulations. A particular attention is usually paid to the coupling between the dynamical behaviour of railway vehicles and the electrical infrastructure, including all the subsystems related to energy distribution and storage. In this research work, the authors propose a newly developed modelling approach for the analysis of the railway vehicle-line system, based on the use of the object-oriented language Simscape that introduces significant advantages with respect to other conventional simulation tools in terms of computational efficiency and modularity. In order to validate the modelling approach, the Italian DC High Speed line, considering a high-speed train with distributed traction power based on the new ETR1000, has been used as a benchmark. The proposed model provides accurate results with a high computational efficiency, proving to be an important tool for the analysis of railway systems. This tool has then be used to perform a preliminary energetic optimization of the considered system)**

***Keywords*—railway longitudinal dynamics; traction and braking systems; mechatronics; energy storage; regenerative braking.**

I. INTRODUCTION

Global Warming and the public attention to energetic problems worldwide are producing an increasing interest in the efficiency of transportation systems: in fact, the transportation field is still responsible for a large percentage of the CO2 emissions in Europe and in most of the industrial countries worldwide [1], [2]. In this scenario, railway is still the most efficient transport method from the energetic and environmental points of view but its competitors are continuously improving their performances and hence the challenge to improve the energetic efficiency has become very important even in this field. Furthermore, the optimization of railways energetic consumptions can bring advantages not only from the environmental point of view but also from the economic one, considering also the possibility to increase the diffusion of High Speed trains. Figure 1 shows an important factor which is strongly pushing towards the energy optimization of railways: the ever growing liberalization process of energy and transportation markets is stimulating all the involved stake holders (i.e. the energy infrastructure, the energy supplier the railway infrastructure and the railway vector) to accurately analyse, through simulations and measurements, the energy fluxes involved in the system and their cost.

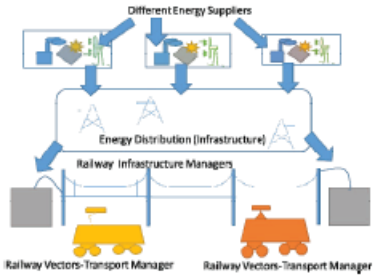

Fig. 1. Interactions between the different subjects involved in the railway system

This complex energetic-economic scenario yields the possibility to differentiate the cost of railway vehicle according to their energetic efficiency. Furthermore, the possibility to acquire energy from different suppliers will allow the optimization of costs based on a number of external factors, e.g. the geographic location of the line. The interoperability and the competitions arising from this liberalized market [3] will further stimulate the need for a strong energy optimization of the railway system, including all the aspects of this transport field, from the traction and braking systems to the entire electric line. Another interesting aspect from the energetic point of view characterizes modern railways: the diffusion of

978-1-5090-2320-2/16/$31.00 ©2016 IEEE

2016. Development and validation of a model for the optimization of regenerative braking of highspeed trains. In Proceedings of the EEEIC CONFERENCE 2016, Florence, Italy. L. Pugi, A. Frilli, E. Meli, D. Nocciolini, A. Rindi.

Regenerative braking in high speed railway applications: analysis by different simulation tools

Massimo Ceraolo, Giovanni Lutzemberger
DESTEC
University of Pisa
Pisa, Italy
lutzemberger@dsea.unipi.it

Amedeo Frilli, Luca Pugi
DIEF
University of Florence
Florence, Italy
luca.pugi@unifi.it

***Abstract*—Technical investigations continuously evaluate the possibility to recover significant amount of braking energy. The application normally involve conventional tramways, characterized by several stops in short-range routes. However, this possibility is becoming more and more attractive also when high-speed trains are considered. In fact, braking energy can be recovered during entry in the station, and delivered later to other trains engaged in starting acceleration. In this work, authors propose an approach based on simplified models performed with object-oriented tools as Modelica or Matlab-Simscape, which easily introduce several advantages in modelling and simulation techniques. The approach has been applied to the preliminary evaluation of one energy storage system installed along a DC line, considering a high-speed train with distributed traction power as the new Italian ETR 1000.**

Keywords—high-speed train; modelling; regenerative braking; simulation; storage

I. INTRODUCTION

With growing diffusion of trains with distributed traction systems, the percentage of energy that can be recovered during braking is drastically increasing.

In this way, a relevant part of the kinetic energy of the train is converted in electric power, and not dissipated over the friction surfaces of the pneumatic brakes, with an immediate advantage in terms of maintenance costs.

In particular, reduced wear and prolonged life of brake pads and discs also produce benefits in terms of pollution since the wear produce solid particles and contaminants whose impact on the surrounding environment is still the matter of monitoring and research [1][2][3].

The application of regenerative braking involves the availability of a load or a storage able to manage the energy recovered from the braking of the train. The peak power to be managed during regenerative braking is roughly proportional to train speed, mass and imposed deceleration.

On tramways and light urban railways, traveling speed and equivalent inertia of the train are smaller respect to high-speed train, but the frequency of braking phases is much higher. For this reason, power management of regenerative braking is typically easier and more convenient on tramways, metro and light urban railways respect to high-speed lines. Additionally, the length of metro and tramway lines is typically lower respect to conventional lines, making easier the implementation of customized or innovative solutions. For these reasons application of energy storage systems on metro, tramways and more generally on light rail systems have been widely investigated by different authors [4][5][6].

On the other hand, travelling speed and equivalent inertia are much higher in case of high-speed trains, thus increasing the amount of kinetic energy that can be potentially recovered. However, reduced number of braking phases and length of railway lines recommend to install this stationary storage capability only in correspondence of the entry inside station, to recover the braking energy and allowing to deliver that energy later, to the other high-speed trains during their starting acceleration.

In this work, the authors have developed two simulation tools based on object-oriented programming technique as Modelica and Matlab-Simscape, which easily introduce several advantages in comparison to conventional standard tools.

The aim was to evaluate pros and cons of these object-oriented tools on an existing case study, related to a high-speed railways application. In particular, the effects of the installation of one storage system on the feeding DC network, mainly in terms of energy saving from the electrical feeding substations (ESSs), have been analysed.

II. THE SIMULATION MODELS

Modelling and simulation of railway systems typically require a simulation tool able to simulate the network equations, the vehicle dynamic equations, i.e. the driver, and different running phases.

A wide variety of different simulation scenarios needs to be simulated, and a high customization is required to adapt models to different kind of railway vehicles, line design and operating conditions. Models should adopt parametric approach and

978-1-5090-2320-2/16/$31.00 ©2016 IEEE

2016. Regenerative braking in high speed railway applications: analysis by different simulation tools. In Proceedings of the EEEIC CONFERENCE 2016, Florence, Italy. M. Ceraolo, G. Lutzemberger, L. Pugi, A. Frilli.

Improved Sustainability of Railway Systems: The Tesys Rail Project

Amedeo Frilli[1], Enrico Meli[1], Daniele Nocciolini[1], Luca Pugi[1], Andrea Rindi[1], Massimo Ceraolo[2], and Giovanni Lutzemberger[2]

[1]*Department of Industrial Engineering, University of Florence*
[2]*Department of Energy, Systems, Territory and Construction Engineering, University of Pisa*

Abstract

While an important part of the total CO_2 emission is still caused by transport systems, the impact of railway systems is significantly lower with respect to the other ground and air concurrent systems. However, the current development trends will produce a significant improvement of the efficiency of cars and planes, thus reducing the sustainability advantages of railway systems. This research work, based on the activities of the TESYS Rail Project, deals with the optimization of railway energy consumptions in order to increase the efficiency of the system. From the simulation of railway systems, the aim of the activity is to investigate how the use of energy storage devices can really improve efficiency in different operating scenarios, and involving different train typologies. A further goal of the activity is the development of integrated design, simulation and optimization tools and the generation of a code that can be integrated in real time applications. Finally, the model proposed in this paper has been validated with a set of experimental results provided by an industrial partner.

Keywords: Railway, longitudinal dynamics, regenerative braking, contact line, electrical substations, energy storage.

1 Introduction

According to data available in literature [1], more than 30% of the total CO_2 emission of the European community is still caused by transport systems (see Figure 1). Currently the impact of railway systems in terms of ratio between equivalent emissions and transported load (usually expressed in gCO_2/pkm) is less than one third respect to the other ground and air concurrent systems. As a consequence, the sustainability of railway systems is widely recognized. However, as reported in Figure 2, it is

2016. Improved sustainability of railway systems: the Tesys Rail project. In Proceedings of the RAILWAYS CONFERENCE 2016, Cagliari, Italy. M. Ceraolo, G. Lutzemberger, A. Frilli, E. Meli, D. Nocciolini, L. Pugi, A. Rindi.

Object Oriented Simulation of Longitudinal Train Dynamics

Efficient tools to optimize sustainability and efficiency of Railway Systems

Amedeo Frilli, Enrico Meli, Daniele Nocciolini, Luca Pugi, Andrea Rindi
DIEF, Dipartimento di Ingegneria Industriale
Università di Firenze
Via Santa Marta 3, 50139 Firenze, Italia
luca.pugi@unifi.it

***Abstract* — As a partner of the Tesys Rail Project, the University of Florence has developed an innovative model of the longitudinal railway vehicle dynamics that can be easily adapted to different kind of applications and mission scenarios, ranging from tramways or freight to passenger or even high speed train. The aim of the model is the efficiency and energy optimization of railway systems. A particular attention has been paid to the modularity of the proposed approach and to the possibility of real time implementation on different application targets. The proposed modeling approach reaches a good compromise between the capability of the model to reproduce the behavior of the simulated physical systems and the simplification needed to make the model more general and suitable to represent different technological solutions. In this work, the proposed modeling approach is exposed and, in order to highlight its main features, some benchmark tests are shown.**

Keywords—railway longitudinal dynamics; traction and braking systems; mechatronics; energy storage; regenerative braking.

I. INTRODUCTION

The purpose of the Tesys Rail Project (acronym of "Methods and Instruments to improve environmental sustainability of railway systems") is to increase the sustainability of railway systems by joining the know-how of 8 major research and industrial partners such as Ansaldo STS, Thales, ATS PMI Toscana , Fondazione Politecnico di Milano, University of Florence, University of Naples. The contribution of the University of Florence, which is exposed in this work, is focused on the development of a computationally efficient model of the longitudinal dynamics of railway vehicle; this model is devoted to the optimization of the system and of its mission profiles in terms of efficiency, sustainability and reliability. In particular, the model is able to reproduce the following phenomena:

- *Longitudinal dynamics of the train*: the mechanical behavior of the system is a result of the interactions between traction and braking forces and resistances to motion (both due to the vehicle and line induced and including the limitations that arise from limited wheel-rail adhesion);
- *Power demand and energy flows*: energy consumption and recovery, efficiency, calculated currents and corresponding interactions with the surrounding infrastructure.

The model has been developed in order to obtain the following characteristics:

- *General and scalable approach*: the model is able to reproduce a variety of different scenarios ranging from light railway and tramway systems to freight and passenger trains (including high speed trains);
- *Modularity*: the model is easily adaptable to different system configurations, allowing the analysis of different energy saving techniques;
- *High level language*: the use of a high level modeling environment allows an easier maintenance and usage for industrial and research applications;
- *RT Implementation*: the model can be used to produce code for real time applications like diagnostic, monitoring or control applications;
- *Portability*: the model is easily adaptable to different target/real time environment (different RTOS or even micro-controllers).

The development of efficient numerical models for the simulation and for the optimization of railway vehicle systems is an open research field and has a great industrial interest, as stated by recent contribution available in literature [1]. Most of these works [2]-[6], deal with the application of energy recovery and storage techniques in order to improve the efficiency of the system, reduce voltage and current fluctuations over the line and more generally improve the sustainability of the whole railway system. Most of the techniques used for energy recovery are commonly applied to tramways and light railway applications. In order to extend these techniques to conventional railways it is necessary to take into account in the train longitudinal dynamics analysis the variability of technical solution that can be adopted for the construction and the control of both traction and braking systems. Such variability is heavily influenced by the type of railway application (freight, conventional passenger or high speed trains). Furthermore, this type of analysis requires an accurate modeling of the braking phase and in particular of the blending between pneumatic braking, electric braking and adhesion independent device such as magnetic track system.

2015. Object oriented simulation of longitudinal train dynamics. In Proceedings of the AEIT CONFERENCE 2015, Napoli, Italy. A. Frilli, E. Meli, D. Nocciolini, L. Pugi, A. Rindi.

B

Published papers on rotordynamics

In this Appendix, the papers concerning rotordynamics that have been published during the Ph.D. period for International Journals and Conferences are reported.

Andrea Rindi
Professor
Department of Industrial Engineering,
University of Florence,
Florence 50100, Italy
e-mail: andrea.rindi@unifi.it

Stefano Rossin
General Electric Oil & Gas,
Florence 50100, Italy
e-mail: stefano.rossin@ge.com

R. Conti
Department of Industrial Engineering,
University of Florence,
Florence 50100, Italy
e-mail: roberto.conti@unifi.it

A. Frilli
Department of Industrial Engineering,
University of Florence,
Florence 50100, Italy
e-mail: amedeo.frilli@unifi.it

E. Galardi
Department of Industrial Engineering,
University of Florence,
Florence 50100, Italy
e-mail: emanuele.galardi@unifi.it

E. Meli
Department of Industrial Engineering,
University of Florence,
Florence 50100, Italy
e-mail: enrico.meli@unifi.it

D. Nocciolini
Department of Industrial Engineering,
University of Florence,
Florence 50100, Italy
e-mail: daniele.nocciolini@unifi.it

L. Pugi
Department of Industrial Engineering,
University of Florence,
Florence 50100, Italy
e-mail: luca.pugi@unifi.it

An Efficient Quasi-Three-Dimensional Model of Tilting Pad Journal Bearing for Turbomachinery Applications

The constant increase of turbomachinery rotational speed has brought the design and the use of journal bearings to their very limits: tilting pad journal bearings (TPJBs) have been introduced for high-speed/high-load applications due to their intrinsic stability properties and can be used both in transient and steady-state operations obtaining superior performances. An accurate analysis of the TPJBs behavior is essential for a successful design and operation of the system; however, it is necessary to reach a compromise between the accuracy of the results provided by the TPJB model and its computational cost. This research paper exposes the development of an innovative and efficient quasi-3D TPJB modeling approach that allows the simultaneous analysis of the system rotordynamics and the supply plant behavior; the majority of existing models describe these aspects separately but their complex interaction must be taken into account to obtain a more accurate characterization of the system. Furthermore, the proposed model is characterized by a high numerical efficiency and modularity, allowing for complex transient simulations of the complete plant and for the representation of different kind of bearings. The TPJB model has been developed and experimentally validated in collaboration with an industrial partner which provided the technical data of the system and the results of experimental tests. [DOI: 10.1115/1.4031408]

1 Introduction

Compressors, pumps, and turbines are used in many industrial fields in a wide range of sizes and powers. In the analysis of such rotating machines, TPJBs (Fig. 1) represent a key element, because they couple all the elements of the plant (i.e., supporting structures, rotors, lubricant supply plant), deeply affecting their behavior.

TPJBs are increasingly used in turbomachinery, because they present several advantages compared to fixed geometry journal bearings. In particular, TPJBs ensure stability in high-speed applications, even with heavy external loads, both for transient and steady-state conditions, due to their possibility to follow the rotor motion and adapt to the system dynamical equilibrium. The complete rotor-bearing-plant system is very complex, due to the presence of a number of different dynamical phenomena, both mechanical and fluid dynamical; therefore, the accurate modeling of TPJBs represents a challenging issue. At the same time, the complexity of the system requires a compromise between the accuracy of the TPJB model and its numerical efficiency: in a single plant there could be a large number of bearings, so it is necessary that a bearing model returns reliable results in reasonable times.

The state-of-the-art models of the fluid dynamical behavior of the bearings (including simple representations of the supply plant) are often based on a simplified lumped parameters approach [1–4]. Analogously, rotor dynamical models of the TPJBs usually consist of lumped parameters spring-damper systems [5–8]. These models are very simple and characterized by small computational

Contributed by the Technical Committee on Vibration and Sound of ASME for publication in the JOURNAL OF VIBRATION AND ACOUSTICS. Manuscript received November 10, 2014; final manuscript received June 23, 2015; published online October 6, 2015. Assoc. Editor: Patrick S. Keogh.

2015. An efficient quasi-three-dimensional model of tilting pad journal bearing for turbomachinery applications. In ASME JOURNAL OF VIBRATION AND ACOUSTICS, vol. 137. A. Rindi, S. Rossin, R. Conti, A. Frilli, E. Galardi, E. Meli, D. Nocciolini, L. Pugi.

Andrea Rindi
Professor
Department of Industrial Engineering,
University of Florence,
Florence 50139, Italy
e-mail: andrea.rindi@unifi.it

Stefano Rossin
General Electric Oil & Gas,
Florence 50127, Italy
e-mail: stefano.rossin@ge.com

R. Conti
Department of Industrial Engineering,
University of Florence,
Florence 50139, Italy
e-mail: roberto.conti@unifi.it

A. Frilli
Department of Industrial Engineering,
University of Florence,
Florence 50139, Italy
e-mail: amedeo.frilli@unifi.it

E. Galardi
Department of Industrial Engineering,
University of Florence,
Florence 50139, Italy
e-mail: emanuele.galardi@unifi.it

E. Meli
Department of Industrial Engineering,
University of Florence,
Florence 50139, Italy
e-mail: enrico.meli@unifi.it

D. Nocciolini
Department of Industrial Engineering,
University of Florence,
Florence 50139, Italy
e-mail: daniele.nocciolini@unifi.it

L. Pugi
Department of Industrial Engineering,
University of Florence,
Florence 50139, Italy
e-mail: luca.pugi@unifi.it

Efficient Models of Three-Dimensional Tilting Pad Journal Bearings for the Study of the Interactions Between Rotor and Lubricant Supply Plant

In many industrial applications, tilting pad journal bearings (TPJBs) are increasingly used because they are very suitable both for high-speed and high external loads. Their study is fundamental in rotating machines and a compromise between accuracy and numerical efficiency is mandatory to achieve reliable results in a reasonable time. This paper mainly focuses on the development of efficient three-dimensional (3D) models of TPJBs, in order to contemporaneously describe both the rotor dynamics of the system and the lubricant supply plant in long simulations (from the initial transient phase to the steady-state condition). Usually, these two aspects are studied separately, but their interactions must be considered if an accurate description of the whole system is needed. The proposed model architecture considers all the six degrees-of-freedom (DOFs) between supporting structures and rotors and can be applied to different types of TJPB layout with different lubricant supply plants. In this research activity, the whole model has been developed and validated in collaboration with Nuovo Pignone General Electric S.p.a. which provided the required technical and experimental data. [DOI: 10.1115/1.4030509]

1 Introduction

The present paper deals with the development of an efficient numerical model for the simulation of the dynamic behavior of TPJBs (Fig. 1). TPJBs are particular fluid dynamical bearings widely used in turbomachinery: the continuous increase of turbomachines rotational speed, with the aim of improving the machines aerodynamic performances, has brought the classical fixed geometry journal bearing to the limits of their operating range. The intrinsic problems in operating at high-speed with fixed geometry bearings (e.g., the onset of instability phenomena like *oil whip* and *oil whirl* due to the coupling between the forces exerted by the bearing on the rotor in the transverse directions) have led to the introduction of the TPJBs in order to achieve satisfactory performances even in very challenging operating conditions. In a TPJB, the bearing surface delimiting the oil film is not a complete cylinder but is divided in a certain number of sectors capable, through appropriate constraints, of one or more rotations: the bearing geometry is no more fixed and is able to follow the rotor motion and to adjust to the dynamic loads applied to the system. Thanks to their dynamical characteristics, TPJBs are appropriate for high-speed applications and heavy external loads both in transient and steady-state operations (ensuring stability in both cases) [1–3]: the bearing operating range is wider with respect to fixed geometry bearings and this enables to operate the supported machine near or beyond its critical speeds.

TPJBs, due to their supporting action to a pressurized lubricant fluid (which also performs the secondary function of removing the heat generated in the rotor-bearing system), interposed between the rotor surface and the bearing pads surfaces: the lubricant is supplied by the hydraulic network used for all the auxiliary needs

Manuscript received October 1, 2014; final manuscript received April 27, 2015; published online July 17, 2015. Assoc. Editor: José L. Escalona.

2016. Efficient models of three-dimensional tilting pad journal bearings for the study of the interactions between rotor and lubricant supply plant. In ASME JOURNAL OF COMPUTATIONAL AND NONLINEAR DYNAMICS, vol. 11. A. Rindi, S. Rossin, R. Conti, A. Frilli, E. Galardi, E. Meli, D. Nocciolini, L. Pugi.

Tribology International 103 (2016) 449–464

Contents lists available at ScienceDirect

Tribology International

journal homepage: www.elsevier.com/locate/triboint

An efficient quasi-3D rotordynamic and fluid dynamic model of Tilting Pad Journal Bearing

R. Conti [a], A. Frilli [a], E. Galardi [a], E. Meli [a,*], D. Nocciolini [a], L. Pugi [a], A. Rindi [a], S. Rossin [b]

[a] MDM Lab-Department of Industrial Engineering-University of Florence, Via di Santa Marta n°3, Italy
[b] General Electric Nuovo Pignone, Via Felice Matteucci, Italy

ARTICLE INFO

Article history:
Received 19 February 2016
Received in revised form
8 July 2016
Accepted 27 July 2016
Available online 2 August 2016

Keywords:
Tilting Pad Journal Bearing
Thin film lubrication
Hydrodynamic lubrication
Mineral oils

ABSTRACT

Over the last few decades the use of Tilting Pad Journal Bearings (TPJBs) has spread due to their better performances in the most demanding operating conditions (i.e. in the presence of high loads and speeds). This research paper describes the development and experimental validation of a new quasi-3D TPJB model, able to analyze both the fluid dynamics (also including the supply plant) and rotor dynamics of the system and their complex interactions. The developed model is characterized by a high numerical efficiency, thus allowing for complex simulation tasks, and strongly modular, with the possibility to easily represent different layouts of TPJBs. The proposed model has been developed and experimentally validated in collaboration with *Nuovo Pignone General Electric S.p.a.* considering a complete plant test rig which includes rotor, bearings and lubrication circuit. Finally, an innovative heuristic law is proposed in order to predict the TPJB fluid dynamical characteristics taking into account the coupled effects neglected by classical simplified models.

1. Introduction

Nowadays Tilting Pad Journal Bearings (TPJB, Fig. 1) are widely used for the support of rotating machinery in the full range of available sizes and powers, thus representing the coupling element between the different components of a plant (i.e. lubricant supply plant, supporting structures, rotors).

Compressors, turbines and pumps benefit from the presence of TPJBs because their performances largely overtake those of fixed geometry journal bearings [1,2]. Compared to classical journal bearings, TPJBs fit better for high speed applications [3] and for heavily loaded rotors thanks to the possibility to adjust their supporting action to the rotor motion, thus ensuring optimal stability [4–6] both in transient [7,8] and steady state conditions [9]. The behavior of the rotor–bearing–plant system depends on the complex interactions between the fluid dynamical (including the effects of the lubricant supply plant) and rotor dynamical phenomena involved in the process: an accurate modelling of both the aspects is mandatory for the correct design and operation of the entire plant. On the other hand, the system complexity itself (a plant can include several different bearings) requires a TPJB model as computationally efficient as possible; therefore a compromise between the accuracy and the numerical efficiency of a TPJB model is necessary to fulfill industrial requirements.

The classical literature TPJBs models are often based on the lumped parameters approach [10–12]: from the rotor dynamical point of view TPJB are usually represented in terms of stiffness and damping matrices, whose forces are applied in the rotor node corresponding to the bearing center. While a procedure for the calculation of dynamic coefficients for journal bearings was already available [13], the first to develop a calculation method for Tilting Pad Journal Bearings was Lund [14]. Starting from that pioneering work, many researchers have investigated how to improve the lumped parameters dynamical representation of TPJBs: Tschoepe and Childs [15] and Brockwell et al. [16] experimentally validated the dynamic coefficients prediction taking into account pivot contact flexibility and different pad geometries; Wilkes and Childs [4] and Rodriguez and Childs [17] analyzed the influence of frequency and model degrees of freedom on the calculation of coefficients and on stability; Lihua et al. [18] investigated the calculation of dynamical coefficients in gas lubricated bearings and Cha et al. [19] analyzed the influence of pad compliance on the bearing dynamic characteristics. Similarly, from the hydraulic point of view the behavior of TPJBs within the lubrication auxiliary plant is typically treated as that of a lumped parameters orifice [13,20]. The numerical efficiency of these simplified models is very high and their use is widely diffused in many applications,

* Corresponding author.
E-mail addresses: roberto.conti@unifi.it (R. Conti), amedeo.frilli@unifi.it (A. Frilli), emanuele.galardi@unifi.it (E. Galardi), enrico.meli@unifi.it (E. Meli), daniele.nocciolini@unifi.it (D. Nocciolini), luca.pugi@unifi.it (L. Pugi), andrea.rindi@unifi.it (A. Rindi), stefano.rossin@ge.com (S. Rossin).

http://dx.doi.org/10.1016/j.triboint.2016.07.024
0301-679X/

2016. An efficient quasi-3d rotordynamic and fluid dynamic model of tilting pad journal bearing. In TRIBOLOGY INTERNATIONAL, vol. 103. R. Conti, A. Frilli, E. Galardi, E. Meli, D. Nocciolini, L. Pugi, A. Rindi, S. Rossin.

A. Rindi
Professor
Department of Industrial Engineering,
University of Florence,
Florence 50139, Italy
e-mail: andrea.rindi@unifi.it

L. Baldassarre
General Electric Oil & Gas,
Florence 50127, Italy
e-mail: Leonardo.Baldassare@ge.com

D. Panara
General Electric Oil & Gas,
Florence 50127, Italy
e-mail: daniele.panara@ge.com

E. Meli
Department of Industrial Engineering,
University of Florence,
Florence 50139, Italy
e-mail: enrico.meli@unifi.it

A. Ridolfi
Department of Industrial Engineering,
University of Florence,
Florence 50139, Italy
e-mail: allessandro.ridolfi@unifi.it

A. Frilli
Department of Industrial Engineering,
University of Florence,
Florence 50139, Italy
e-mail: amedeo.frilli@unifi.it

D. Nocciolini
Department of Industrial Engineering,
University of Florence,
Florence 50139, Italy
e-mail: daniele.nocciolini@unifi.it

S. Panconi
Department of Industrial Engineering,
University of Florence,
Florence 50139, Italy
e-mail: simone.panconi@unifi.it

An Efficient Iterative Approach for the Analysis of Thermal Instabilities in Rotating Machines

Most of the technological developments achieved in the turbomachinery field during the last years have been obtained through the introduction of fluid dynamic bearings, in particular tilting pad journal bearings (TPJBs). However, even those bearings can be affected by thermal instability phenomena as the Morton effect at high peripheral speeds. In this work, the authors propose a new iterative finite element method (FEM) approach for the analysis of those thermal–structural phenomena: the proposed model, based on the coupling between the rotor dynamic and the thermal behavior of the system, is able to accurately reproduce the onset of thermal instabilities. The authors developed two versions of the model, one in the frequency domain and the other in the time domain; both models are able to assure a good tradeoff between numerical efficiency and accuracy. The computational efficiency is critical when dealing with the typical long times of thermal instability. The research activity has been carried out in cooperation with General Electric Nuovo Pignone SPA, which provided both the technical and experimental data needed for the model development and validation. [DOI: 10.1115/1.4037143]

1 Introduction

In the last decades, the turbomachinery field has gone through a strong development phase to increase the efficiency and the power of the machines; from a rotordynamic point of view, important results have been achieved through the introduction of tilting pad journal bearings (TPJBs) (see Fig. 1) [1,2].

Fluid bearings are characterized by superior rotordynamic performances, being able to follow the rotor motion and adjust their dynamic response [3,4]; this characteristic allows TPJBs to overcome the classical limitations of fixed geometry journal bearings in terms of fluid dynamic instabilities (i.e., oil whirl and oil whip) [5,6]. However, even TPJBs are subjected, in certain operating conditions, to the onset of thermal instability phenomena [7–9] (e.g., the Morton effect [10–13]).

The Morton effect was first described by Keogh and Morton [14]: this unstable behavior mainly occurs when the rotor has an overhung part and is heavily loaded [15]. If the rotor vibration is mainly driven by residual unbalance, the rotor performs a fairly circular orbit synchronous with the rotation. In this situation, a rotor point is always closer to the bearing surface while the opposite point is constantly at the maximum oil-film thickness [16]. This situation can lead to the onset of thermal instability: if the viscous shear stresses present in the lubricant films are sufficiently high (i.e., if the rotor speed is sufficiently high), they produce a strong temperature gradient on the rotor journal and hence a rotor bow, which then increases the effect of the overhung unbalance [17]. The increase of the rotor synchronous vibration amplitude can grow unbounded, even leading to the system failure.

Contributed by the Technical Committee on Vibration and Sound of ASME for publication in the JOURNAL OF VIBRATION AND ACOUSTICS. Manuscript received November 2, 2016; final manuscript received June 8, 2017; published online August 17, 2017. Assoc. Editor: Patrick S. Keogh.

2017. An efficient iterative approach for the analysis of thermal instabilities in rotating machines. In ASME JOURNAL OF VIBRATION AND ACOUSTICS. A. Rindi, L. Baldassarre, D. Panara, E. Meli, A. Ridolfi, A. Frilli, D. Nocciolini, S. Panconi.

Proceedings of the ASME 2016 Turbomachinery Technical Conference & Exposition &
ASME TURBO EXPO 2016
June 13-June 17, 2016, Seoul, South Korea

GT2016-57401

DEVELOPMENT AND VALIDATION OF AN EFFICIENT TEHD MODEL OF TILTING PAD JOURNAL BEARINGS

R. Conti, A. Frilli, E. Meli, D. Nocciolini, S. Panconi, L. Pugi, A. Rindi
Department of Industrial Engineering
University of Florence
Email: [roberto.conti, amedeo.frilli, enrico.meli, daniele.nocciolini, simone.panconi, luca.pugi, andrea.rindi]@unifi.it

S. Rossin
General Electric Nuovo Pignone
Italy
Email: stefano.rossin@ge.com

ABSTRACT

The large success of Tilting Pad Journal Bearings (TPJBs) for the use in high speed/high load applications is due to their intrinsic stability properties, which allow superior rotor dynamic performances. TPJBs operation involves different physical phenomena, like the pads flexibility and the heat exchange between solids and fluids: an accurate analysis of these phenomena is fundamental in order to successfully employ TPJBs. In this paper, the authors, in cooperation with General Electric Nuovo Pignone, develop an innovative 3D TPJB modelling approach that allows an accurate analysis of the interactions between the fluid dynamic and thermal phenomena with the elastic behaviour of the solid components (ThermoElastoHydroDynamic analysis). The main objective of the proposed model is to provide accurate 3D results with low computational times. The TPJB model has been also experimentally validated, focusing on the thermal characteristics of the system and the interactions due to the TEHD behaviour of the bearing system.

NOMENCLATURE

A Area.
C Viscous damping matrix.
C_d Duct flow coefficient.
C_p Specific heat capacity at constant pressure.
$\mathbf{D}$ Elastic stiffness matrix.
$\mathbf{F}$ Force.
G Gyroscopic effect matrix.
H Circulatory matrix.
I_p Polar moment of inertia.
I_t Transversal moment of inertia.
K Bulk modulus.
K Stiffness matrix.
$\mathbf{M}$ Moment.
M Mass matrix.
Q Flow rate.
R Radius.
S Surface.
T Temperature.
Vol Volume.
W_t Rotor section torsional modulus.
d_0 Rotor section diameter.
$\mathbf{f}$ FEM generalized loads.
f Frequency.
h Oil film thickness.
h Convective heat transfer coefficient.
m Mass.
$\mathbf{n}$ Outgoing unitary vector.
p Pressure.
$\mathbf{q}$ FEM generalized displacements.
t Time.
$\mathbf{v}$ Fluid velocity.
$\mathbf{x}$ Position.
$\dot{\mathbf{x}}$ Velocity.

Greek Letters

2016. Development and validation of an efficient tehd model of titling pad journal bearings. In Proceedings of the ASME TURBOEXPO 2016, Seul, South Korea. R. Conti, A. Frilli, E. Meli, D. Nocciolini, S. Panconi, L. Pugi, A. Rindi, S. Rossin.

ECCOMAS Thematic Conference on Multibody Dynamics
June 29 - July 2, 2015, Barcelona, Catalonia, Spain

Development of efficient flexible multibody techniques for rotordynamics systems including rotors an supporting structures

S. Rossin*, A. Frilli#, E. Meli#, G. Pallini#, S. Panconi#, A. Rindi#

* General Electrics
Nuovo Pignone Oil&Gas
Via Matteucci 2, 50127, Florence, Italy
stefano.rossin@ge.com

Department of Industrial Engineering
University of Florence
Via di Santa Marta 3, 50139, Florence, Italy
amedeo.frilli@unifi.it
enrico.meli@unifi.it
giovanni.pallini@unifi.it
simone.panconi@unifi.it
andrea.rindi@unifi.it

ABSTRACT

In the study of the rotor dynamic performances of a rotating machine, it is possible to divide the plant in four main components: rotor, stator, bearings and supporting structure. The current trend for rotating machinery considers the reduction of weight an important problem. As a consequence of the complex behavior the last generation plants, characterized by low weights and flexible support structures, the separation margin between rotor critical speeds and operative conditions is quite difficult to be reached. The presence of flexible supports can generate dangerous coupling effects among the different bearings. Therefore the model of a complete rotor dynamical system must consider all the phenomena coming from the coupling of its mechanical components [1]. The aim of this work is to demonstrate the importance of taking into account the support structure since the preliminary project phases. To this end, this study investigates a problem of enhanced vibration level on a five stage MCL rotor, part of a compression system made up of a gas turbine driver with two centrifugal compressors and one gearbox. Each rotating machine was installed on a separate baseplate steel structure and the individual rotors were connected by elastic coupling. This research work has been developed cooperating with Nuovo Pignone General Electric S.p.a., that has provided the technical and experimental data required for the model validation.

Keywords: Rotating machines, Supporting structures, Bearings, Dynamical bearing interaction.

1 INTRODUCTION

A rotordynamics machinery is a very complex component composed of many elements which are linked each other. In particular this research work focus on the interaction of the following components:

1. rotor;
2. bearings;
3. support structure.

Because of the need of high efficiency, the turbomachinery development trend brings towards more and more compact systems characterized by reduced weight. Consequently, the structures must necessarily become more lighter and flexible. The introduction of system components that can not be considered absolutely rigid in the operative range, leads to the need of a deeper study of the dynamic behaviour of rotating machines to guarantee safe operating conditions. For example the support structures and the anchoring system (visible in Figure 1) for off-shore installations is isostatic because of deck flexibility. This is obtained through the use of hinge and spherical joints,

2105. Development of efficient flexible multibody techniques for rotordynamics systems including rotors and supporting structures. In Proceedings of the ECCOMAS THEMATIC CONFERENCE ON MULTIBODY DYNAMICS 2015, Barcelona, Spain. S. Rossin, E. Meli, G. Pallini, S. Panconi, A. Rindi, A. Frilli.

AIMETA 2017
XXIII Conference
The Italian Association of Theoretical and Applied Mechanics
Luigi Ascione, Valentino Berardi, Luciano Feo, Fernando Fraternali and Antonio Michele Tralli (eds.)
Salerno, Italy, 4–7 September 2017

INNOVATIVE TEHD TILTING PAD JOURNAL BEARING MODEL FOR ROTORDYNAMIC ANALYSES

E. Boccini[1], A. Frilli[1], E. Meli[1], D. Nocciolini[1], S. Panconi[1], A. Rindi[1], and B. Romani[1]

[1]Department of Industrial Engineering, University of Florence, Florence, Italy
via di Santa Marta 3, 50139, Florence, Italy
e-mail: enrico.boccini; amedeo.frilli; enrico.meli; daniele.nocciolini; simone.panconi; andrea.rindi; benedetta.romani@unifi.it

Keywords: Tilting pad journal bearings, rotordynamics, thermoelastohydrodynamic analyses, lubrication.

Abstract. *The large success of Tilting Pad Journal Bearings (TPJBs) for the use in high speed/high load applications is due to their intrinsic stability properties, which allow superior rotor dynamic performances [1]. TPJBs operation involves different physical phenomena, like the pads flexibility and the heat exchange between solids and fluids: an accurate analysis of these phenomena is fundamental in order to successfully employ TPJBs [2]. In literature, the TPJBs analysis has been made on the different aspect of the bearing system separately: some models looked at the fluid dynamic behaviour; other models investigated the rotor dynamic characteristics, using the stiffness and damping matrices to simplify the bearing action. In this paper, the authors, in cooperation with General Electric Nuovo Pignone, develop an innovative 3D TPJB modelling approach that allows an accurate analysis of the interactions between the fluid dynamic and thermal phenomena with the elastic behaviour of the solid components (ThermoElastoHydroDynamic analysis [3]). The authors have developed the proposed model in the COMSOL Multiphysics®5.2 environment, which guarantees high modularity, for an easy representation of the TPJB, and a significant numerical efficiency. The main objective of the proposed model is to provide accurate 3D results with low computational times. The TPJB model has been also experimentally validated, focusing on the thermal characteristics of the system and the interactions due to the TEHD behaviour of the bearing system and the vibration amplitudes of the rotor system, performed in various scenario, has been calculated, analysing the onset of instability phenomena, which represent an important future development for this research work.*

2017. Innovative TEHD Tilting pad journal bearing model for rotordynamic analyses. In Proceedings of the AIMETA CONFERENCE 2017, Salerno, Italy. E. Boccini, A. Frilli, E. Meli, D. Nocciolini, S. Panconi, A. Rindi, B. Romani.

Tilting Pad Journal Bearing TEHD Analysis: An Innovative Model

Amedeo Frilli, Enrico Meli, Daniele Nocciolini, Simone Panconi, Luca Pugi, Andrea Rindi, Stefano Rossin

Abstract Tilting Pad Journal Bearings (TPJBs) are widely used in the turbomachinery field due to their superior dynamical performances, but their operation involves several different physical phenomena. In this research work the authors propose an innovative 3D ThermoElastoHydroDynamic (TEHD) model for the analysis of TPJBs behaviour developed and experimentally validated in cooperation with General Electric Nuovo Pignone: the model is able to perform a nonlinear transient coupled analysis taking into account fluid dynamical, thermal and elastic effects and reaches a good compromise between the accuracy of the results and the computational efficiency.

1 Introduction

In the last years, the development trend in the turbomachinery field has pushed towards ever higher rotational speeds and loads [13], [14]. In this scenario, Tilting Pad Journal Bearings (TPJBs) have almost completely substituted the more unstable Fixed Geometry Journal Bearings. TPJBs are particular fluid dynamical bearings where the supporting action exerted on the rotor is due to the pressure field generated by the rotor rotation in a set of lubricant films interposed between the rotor and the bearings tilting pads. TPJBs, due to their intrinsic stability properties, strongly reduce the risk of fluid dynamic induced vibrations like the Oil Whirl and the Oil Whip and, thanks to their ability to dynamically follow the rotor motion, are suitable for high speed and high load applications. However, their dynamic behaviour is influenced by many different physical phenomena and hence an accurate modelling

A. Frilli, E. Meli, D. Nocciolini, S. Panconi, L. Pugi, A. Rindi
Dept. of Industrial Engineering, University of Florence, Florence, Italy, e-mail: [amedeo.frilli; enrico.meli; daniele.nocciolini; simone.panconi; luca.pugi; andrea.rindi]@unifi.it

S. Rossin
GE Oil & Gas, Florence, Italy, e-mail: stefano.rossin@ge.com

2016. Tilting pad journal bearing tehd analysis: an innovative model. In Proceedings of the IFTOMM ITALY 2016, Vicenza, Italy. A. Frilli, E. Meli, D. Nocciolini, S. Panconi, L. Pugi, A. Rindi, S. Rossin.

Extended Abstract

The 4th Joint International Conference on Multibody System Dynamics
May 29 – June 2, 2016, Montréal, Canada

A New ThermoElastoHydroDynamic Tilting Pad Journal Bearings Model

Roberto Conti[1], Amedeo Frilli[1], Enrico Meli[1], Daniele Nocciolini[1], Simone Panconi[1], Luca Pugi[1], Andrea Rindi[1] and Stefano Rossin[2]

[1] *Department of Industrial Engineering, University of Florence,*
{roberto.conti,amedeo.frilli,enrico.meli,daniele.nocciolini,simone.panconi,luca.pugi,andrea.rindi}@unifi.it
[2] *General Electric Oil & Gas, Florence, stefano.rossin@ge.com*

The turbomachinery field is constantly pushing towards higher rotational speeds and loads; this development trend has led to the overcome of Fixed Geometry Journal Bearings and to the introduction of Tilting Pad Journal Bearings (TPJBs). TPJBs are characterized by superior dynamic performances and by a greater rotordynamic stability. Their operation involves many different physical phenomena (e.g. the elastic and thermal behaviour of the pads) and hence, an accurate analysis of their behaviour is essential in order to successfully and safely design and operate them. Moreover, in order to meet the industry requirements, it is important for a TPJB model to reach a good trade-off between the accuracy of the results and the computational costs.

In this paper, the authors, in collaboration with General Electric Nuovo Pignone, present an newly developed TPJB three-dimensional model which is able to perform a coupled analysis of the main physical phenomena involved in TPJBs operations. The main goal of the model is to analyze the interactions between the thermal and fluid dynamical behavior of the lubricant with the thermal and elastic behavior of the solid components, thus obtaining a complete TEHD model (ThermoElastoHydroDynamic analysis).

Most of the models found in literature analyze the behaviour of TPJBs with a lumped parameters approach (0D and 1D models), dealing separately with the different physical phenomena and neglecting their couplings [1]. While those models are characterized by a great computational efficiency and a low accuracy, it is also possible to find fully 3D models [2], [3] but their computational loads represent a great limit for the applicability at the industry level. The proposed model aims to reach a compromise between the characteristics of the State-of-the-Art models, obtaining accurate results from a coupled analysis with a great computational efficiency.

The developed model architecture is shown in Figure 1:

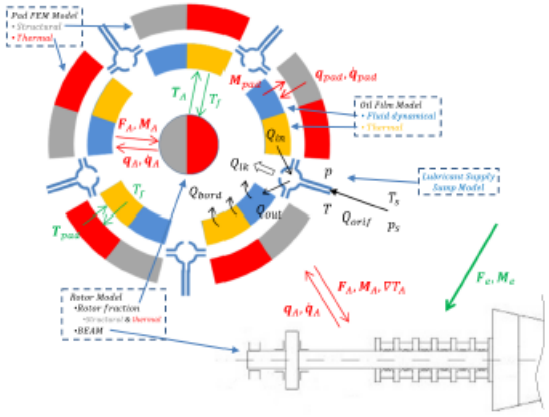

Fig. 1: General architecture of the whole model.

2016. A new thermoelastohydrodynamic tilting pad journal bearings model. In Proceedings of the IMSD CONFERENCE 2016, Montreal, Canada. R. Conti, A. Frilli, E. Meli, D. Nocciolini, S. Panconi, L. Pugi, A. Rindi, S. Rossin.

Proceedings of the ASME 2015 International Design Engineering Technical Conferences &
Computers and Information in Engineering Conference
IDETC/CIE 2015
August 2-5, 2015, Boston, USA

DETC2015/VIB-46262

A TILTING PAD JOURNAL BEARING MODEL FOR COUPLED FLUID DYNAMICAL - ROTOR DYNAMICAL ANALYSES

R. Conti, A. Frilli, E. Galardi, E. Meli,
D. Nocciolini, L. Pugi, A. Rindi
Department of Industrial Engineering (DIEF)
University of Florence
Via di Santa Marta n° 3, 50139
Florence, Italy
Email: [roberto.conti, amedeo.frilli,
emanuele.galardi, enrico.meli, daniele.nocciolini,
luca.pugi, andrea.rindi]@unifi.it

Stefano Rossin
Consulting Engineer, Ph.D.
General Electric Oil & Gas
Via Felice Matteucci n° 2, 50127
Florence, Italy
Email: stefano.rossin@ge.com

ABSTRACT

Turbomachines are continuously developing in order to reach higher levels of speed, power and efficiency and the classical Fixed Geometry Journal Bearings have been replaced by Tilting Pad Journal Bearings to avoid instability phenomena. In this paper, the authors propose an innovative quasi-3D TPJB modelling approach that allows the simultaneous and coupled analysis of the typical phenomena involved in TPJB operations. The authors focused on the accurate analysis of the interactions between the rotor and the lubricant supply plant and on the fluid dynamical effects due to the bearing that cause those couplings, aiming at reaching a good compromise between the accuracy and the numerical efficiency of the model (mandatory to analyze systems with many bearings).
The TPJB model has been developed and experimentally validated in collaboration with Nuovo Pignone General Electric S.p.a. which provided the technical data of the system and the results of experimental tests.

1 Introduction

Tilting Pad Journal Bearings (TPJB, Figure 1) are extensively used for the support of compressors, pumps and turbines because they are more reliable with respect to fixed geometry journal bearings and provide a greater stability in high speed applications, both for transient and steady state operating conditions, due to their possibility to adjust their response to the rotor motion. Consequently, due to the presence of several physical phenomena, the accurate modelling of TPJBs represents a challenging issue. Furthermore, the complexity of a turbomachinery system requires a compromise between the accuracy of the bearing model and its computational times.

The state-of-the-art models of the bearing fluid dynamical behaviour are often based on simplified approaches (i.e. lumped parameters models) [18], [32], [33]. Analogously, rotor dynamical models including TPJBs usually employ lumped spring-

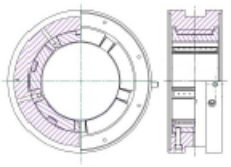

FIGURE 1. Tilting Pad Journal Bearing.

2015. A tilting pad journal bearing model for coupled fluid dynamical-rotor dynamical analyses. In Proceedings of the ASME IDETC/CIE CONFERENCE 2015, Boston, USA. R. Conti, A. Frilli, E. Galardi, E. Meli, D. Nocciolini, L. Pugi, A. Rindi, S. Rossin.

Development and Preliminary Validation of Efficient 3D Models of Tilting Pad Journal Bearings

Roberto Conti, Amedeo Frilli, Emanuele Galardi, Enrico Meli, Daniele Nocciolini, Luca Pugi, Andrea Rindi and Stefano Rossin

Abstract This paper mainly focuses on the development of efficient three-dimensional (3D) models of TPJBs, able to contemporaneously simulate both the rotor dynamics of the system and the lubricant supply plant. The proposed modelling approach tries to obtain a good compromise between the typical accuracy of standard 3D models and the high numerical efficiency of simpler and less accurate models. In this work, the whole model has been developed and validated in collaboration with *Nuovo Pignone General Electric S.p.a.* which provided the required technical and physical data. In particular, the experimental data are referred to a suitable lube oil console system, built at the GE testing center in Massa-Carrara (MS, Italy) for the verification of plant components.

R. Conti (✉) · A. Frilli · E. Galardi · E. Meli · D. Nocciolini · L. Pugi · A. Rindi · S. Rossin
Department of Industrial Engineering, University of Florence,
via di S.Marta 3, 50139 Florence, Italy
e-mail: roberto.conti@unifi.it
URL: http://www.dief.unifi.it/; http://www.ge.com/

A. Frilli
e-mail: amedeo.frilli@unifi.it

E. Galardi
e-mail: emanuele.galardi@unifi.it

E. Meli
e-mail: enrico.meli@unifi.it

D. Nocciolini
e-mail: daniele.nocciolini@unifi.it

L. Pugi
e-mail: luca.pugi@unifi.it

A. Rindi
e-mail: andrea.rindi@unifi.it

S. Rossin
e-mail: stefano.rossin@ge.com

P. Pennacchi (ed.), *Proceedings of the 9th IFToMM International Conference on Rotor Dynamics*, Mechanisms and Machine Science 21,
DOI 10.1007/978-3-319-06590-8_65

2014. Development of efficient 3d models for tilting pad journal bearings. In Proceedings of the IFTOMM CONFERENCE 2014, Milano, Italy. R. Conti, A. Frilli, E. Galardi, E. Meli, D. Nocciolini, L. Pugi, A. Rindi, S. Rossin.

Bibliography

[1] R. Barrero, J. Van Mierlo, and X. Tackoen. Enhanced Energy Storage Systems for Improved On-Board Light Rail Vehicle Efficiency. *IEEE Vehicular Technology Magazine*, pages 26–36, 2008. 1, 30

[2] W. Gunselmann. Technologies for increased energy efficiency in railway systems. *Power Electronic and Applications*, pages –. 1

[3] W.A. Kamal. Improving energy efficiency - The cost-effective way to mitigate global warming. *Energy Conversion and Management*, 38(1):39–59, 1997. 4

[4] European Environment Office. 4

[5] Association of American Railroads. 4

[6] E. Fridell et al. On-board measurements of particulate matter emissions from a passenger train. *Proceedings of the Institution of Mechanical Engineers, Part F: Journal of Rail and Rapid Transit*, 225(1):99–106, 2011. 4

[7] TSI. Technical specifications for interoperability. 6

[8] H. Douglas, C. Roberts, S. Hillmansen, and F. Schmid. An assessment of available measures to reduce traction energy use in railway networks. *Energy Conversion and Management*, 106:1149–1165, 2015. 7

[9] M. Bartłomiejczyk and M. Połom. Multiaspect measurement analysis of breaking energy recovery. *Energy Conversion and Management*, 127:35–42, 2016. 8

[10] S. Abbasi, A. Jansson, L. Olander, U. Olofsson, and U. Sellgren. A pin-on-disc study of the rate of airborne wear particle emissions from railway braking materials. *Wear*, 284:18–29, 2012. 8

[11] R. Gehrig, M. Hill, P. Lienemann, C.N. Zwicky, N. Bukowiecki, E. Weingartner, U. Baltensperger, and B. Buchmann. Contribution of railway traffic to local PM10 concentrations in Switzerland. *Atmospheric Environment*, 41(5):923–933, 2007. 8

[12] I. Salma, T. Weidinger, and W. Maenhaut. Time-resolved mass concentration, composition and sources of aerosol particles in a metropolitan underground railway station. *Atmospheric Environment*, 41(37):8391–8405, 2007. 8

[13] W.W. Marr, W.J. Walsh, and P.C. Symons. Modeling battery performance in electric vehicle applications. *Energy Conversion and Management*, 33(9):843–847, 1992. 9

[14] S. Hillmansen and C. Roberts. Energy storage devices in hybrid railway vehicles: A kinematic analysis. *Proceedings of the Institution of Mechanical Engineers, Part F: Journal of Rail and Rapid Transit*, 221:135–143, 2007. 9

[15] M. Peña-Alcaraz, A. Fernández, A. Paloma Cucala, A. Ramos, and R. R. Pecharromán. Optimal underground timetable design based on power flow for maximizing the use of regenerative-braking energy. *Proceedings of the Institution of Mechanical Engineers, Part F: Journal of Rail and Rapid Transit*, 226(4):397–408, 2012. 11

[16] et al. M.C. Falvo. Energy savings in metro-transit systems: A comparison between operational Italian and Spanish lines. *Proceedings of the Institution of Mechanical Engineers, Part F: Journal of Rail and Rapid Transit*, 230(2):345–359, 2016. 11

[17] A. González-Gil, R. Palacin, and P. Batty. Optimal energy management of urban rail systems: Key performance indicators. *Energy Conversion and Management*, 90:282–291, 2015. 11

[18] R. Barrero, X. Tackoen, and J. Van Mierlo. Stationary or onboard energy storage systems for energy consumption reduction in a metro network. *Proceedings of the Institution of Mechanical Engineers, Part F: Journal of Rail and Rapid Transit*, 224:207–225, 2010. 11

[19] R. Teymourfar, B. Asaei, H. Iman-Eini, and R. Nejati Fard. Stationary super-capacitor energy storage system to save regenerative braking energy in a metro line. *Energy Conversion and Management*, 56:206–214, 2012. 11

[20] A. González-Gil, R. Palacin, and P. Batty. Energy-efficient urban rail systems: strategies for an optimal management of regenerative braking energy. *Proceedings of the Fifth Transport Research Arena, Paris*, pages –, 2014. 11

[21] M. Steiner, M. Klohr, and S. Pagiela. Energy Storage System with UltraCaps on Board of Railway Vehicles. *Power Electronics and Applications European Conference*, pages 1–10, 2001. 12, 15

[22] Siemens. Sitras mes–mobile energy storage unit for rail vehicles, 2012. 12

[23] CAF – Construcciones y Auxiliar del Ferrocarril. Acr system, 2012. 12

[24] J.P. Moskowitz and J.L. Cohuau. STEEM: ALSTOM and RATP experience of supercapacitors in tramway operation. *Proceedings of the IEEE Vehicle Power and Propulsion Conference – VPPC 2010, Lille, France*, pages –, 2010. 12

[25] F. Lacote. Alstom – Future trends in railway transportation. *Japan Railway & Transport Review*, 42:4–9, 2005. 12

[26] M. Ogasa. Application of energy storage technologies for electric railway vehicles – examples with hybrid electric railway vehicles. *IEEJ Transactions on Electrical and Electronic Engineering*, 5:304–311, 2010. 12

[27] Railway Gazette News. Lfx-300 ameritram hybrid streetcar unveiled in charlotte, 2011. 12

[28] M. Meinert. New mobile energy storage system for rolling stock. *Proceedings of the 13th European conference on power electronics and applications – EPE09, Barcelona, Spain*, pages –, 2009. 12

[29] R. Teymourfar, R. Nejati Fard, B. Asaei, and H. Iman-Eini. Energy recovery in a metro network using stationary supercapacitors. *Power Electronics, Drive Systems and Technologies Conference (PEDSTC)*, pages –, 2011. 13

[30] M. Ceraolo and G. Lutzemberger. Stationary and on-board storage systems to enhance energy and cost efficiency of tramways. *Journal of Power Sources*, 264:128–139, 2014. 13, 36, 100, 157

[31] R. Barrero, X. Tackoen, and J. Van Mierlo. Quasi-static simulation method for evaluation of energy consumption in hybrid light rail vehicles. *IEEE Vehicle Power and Propulsion Conference*, pages 1–8, 2008. 13

[32] R. Barrero, J. Van Mierlo, and X. Tackoen. Energy savings in public transport. *IEEE Vehicular Technology Magazine*, 3(3):26–36, 2008. 13

[33] R. Barrero, X. Tackoen, and J. Van Mierlo. Analysis and configuration of supercapacitor based energy storage system on-board light rail vehicles. *IEEE Power Electronics and Motion Control Conference*, pages 1512–1517, 2008. 13

[34] J. Van Mierlo, R. Barrero, and X. Tackoen. Supercapacitors On-Board Light Rail Vehicles: Enhanced Energy Storage Systems for Improved Vehicle Efficiency. *IEEE/ASME/ASCE 2008 Joint Rail Conference*, pages –, 2008. 13

[35] A. González-Gil, R. Palacin, and P. Batty. Sustainable urban rail systems: Strategies and technologies for optimal management of regenerative braking energy. *Energy Conversion and Management*, 75:374–388, 2013. 13

[36] A. González-Gil, R. Palacin, P. Batty, and J.P. Powell. A systems approach to reduce urban rail energy consumption. *Energy Conversion and Management*, 80:509–524, 2014. 13, 16

[37] D. Iannuzzi, D. Lauria, and F. Ciccarelli. Wayside ultracapacitors storage design for light transportation systems: a multiobjective optimization approach. *International Review of Electrical Engineering*, 8(1):190–199, 2013. 13

[38] L. Mir, I. Exteberria-Otadui, I. Perez de Arenaza, I. Sarasola, and T. Nieva. A supercapacitor based light rail vehicle: system design and operations modes. *IEEE Energy Conversion Congress and Exposition*, pages –, 2009. 13

[39] Siemens. Sitras ses–stationary energy storage system for dc traction power supply, 2012. 14

[40] Bombardier. Energstor–wayside energy storage, bombardier inc, 2010. 14

[41] Adetel. Neogreen in lyon. in: Workshop on braking energy recovery systems–ticket to kyoto project, bielefeld, germany, 2011. 14

[42] ABB. Envistore–wayside energy storage system for rail transportation, 2012. 14

[43] Railway Gazette News. Supercapacitor energy storage for south island line, 2012. 14

[44] J.R. Boizumeau J.R, P. Leguay P., and E. Navarro. Braking energy recovery at the rennes metro. in: Workshop on braking energy recovery systems – ticket to kyoto project, bielefeld, germany, 2011. 14

[45] C. Tarrant. Kinetic energy storage wins acceptance, 2004. 14

[46] Vycon. Vycon wins $3.6 million contract to decrease energy consumption at los angeles metro red line westlake/macarthur park subway station. 14

[47] K. Ogura, K. Nishimura, T. Matsumura, C. Tonda C., E. Yoshiyama, and M. Andriani et al. Test results of a high capacity wayside energy storage system using Ni-MH batteries for

DC electric railway at New York City Transit. *Proceedings of the IEEE green technologies conference – GREEN 2011, Baton Rouge, USA*, pages –, 2011. 14

[48] M. Shimada, R. Oishi, D. Araki, and Y. Nakamura. Energy storage system for effective use of regenerative energy in electrified railways. *Hitachi Review*, 59:33–38, 2010. 14

[49] J. Poulin, A. Gillespie, K. Morelock, J. McDowall, and B. Inniss. Septa recycled energy optimization project with regenerative braking energy storage. septa project, 2012. 14

[50] A. Vasebi, S.M.T. Bathaee, and M. Partovibakhsh. Predicting state of charge of lead-acid batteries for hybrid electric vehicles by extended Kalman filter. *Energy Conversion and Management*, 49(1):75–82, 2008. 13

[51] K.M. Tsang, L. Sun, and W.L. Chan. Identification and modelling of Lithium ion battery. *Energy Conversion and Management*, 51(12):2857–2862, 2010. 13

[52] S. Castano, L. Gauchia, E. Voncila, and J. Sanz. Dynamical modeling procedure of a Li-ion battery pack suitable for real-time applications. *Energy Conversion and Management*, 92:396–405, 2015. 13

[53] W.H. Zhu, Y. Zhu, and B.J. Tatarchuk. A simplified equivalent circuit model for simulation of Pb-acid batteries at load for energy storage application. *Energy Conversion and Management*, 52(8):2794–2799, 2011. 13

[54] J.P. Trovão and C.H. Antunes. A comparative analysis of meta-heuristic methods for power management of a dual energy storage system for electric vehicles. *Energy Conversion and Management*, 95:281–296, 2015. 13

[55] L. Guo, K. Yedavalli, and D. Zinger. Design and modeling of power system for a fuel cell hybrid switcher locomotive. *Energy Conversion and Management*, 52(2):1406–1413, 2011. 14

[56] V. Paladini, T. Donateo, A. De Risi, and D. Laforgia. Super-capacitors fuel-cell hybrid electric vehicle optimization and control strategy development. *Energy Conversion and Management*, 48(11):3001–3008, 2007. 15

[57] Thiounn-Guermeur M. Evaluation of the hybrid locomotive PLATHEE - A Platform for Energy Efficiency and Environmentally Friendly Hybrid Trains. *Proceedings of WCRR (World Congress of Railway Research), France*, pages –, 2011. 15

[58] P. Sharma and T.S. Bhatti. A review on electrochemical double-layer capacitors. *Energy Conversion and Management*, 51(12):2901–2912, 2010. 15

[59] J. Kondoh, I. Ishii, H. Yamaguchi, A. Murata, K. Otani, K. Sakuta, N. Higuchi, S. Sekine, and M. Kamimoto. Electrical energy storage systems for energy networks. *Energy Conversion and Management*, 41(17):1863–1874, 2000. 15

[60] V. Fernão Pires, E. Romero-Cadaval, D. Vinnikov, I. Roasto, and J.F. Martins. Power converter interfaces for electrochemical energy storage systems – A review. *Energy Conversion and Management*, 86:453–475, 2014. 15

[61] L. Oliveira, M. Messagie, J. Mertens, H. Laget, T. Coosemans, and J. Van Mierlo. Environmental performance of electricity storage systems for grid applications, a life cycle approach. *Energy Conversion and Management*, 101:326–335, 2015. 15

[62] I. Grigorchenkov, D. Jhonson, and K. Pullen. Evaluation of mobile and stationary applications of energy storage for DC railways and rapid transit. *Proceedings of the RRUKA Annual Conference, London*, pages –, 2012. 26

[63] Kokam. Slpb (superior lithium polymer battery) technical specification. VI, 30, 31, 32

[64] R. Faranda, M. Gallina, and D.T. Son. A new simplified model of Double-Layer Capacitors. pages –. 33

[65] E. Tironi and V. Musolino. Supercapacitor Characterization in Power Electronic Applications: Proposal of a New Model. pages –. 33

[66] L.M. Fernandez, P. Garcia, C.A. Garcia, and F. Jurado. Hybrid electric system based on fuel cell and battery and integrating a single dc /dc converter for a tramway. *Energy Conversion and Management*, 52(5):2183–2192, 2011. 35

[67] M. Uzunoglu and M.S. Alam. Dynamic modeling, design and simulation of a PEM fuel cell /ultra-capacitor hybrid system for vehicular applications. *Energy Conversion and Management*, 48(5):1544–1553, 2007. 35

[68] M.A. Hannan, F.A. Azidin, and A. Mohamed. Multi-sources model and control algorithm of an energy management system for light electric vehicles. *Energy Conversion and Management*, 62:123–130, 2012. 35

[69] L. Pugi, R. Conti, D. Nocciolini, E. Galardi, and E. Meli. A Comprehensive Tool for the Optimization of Traction and Braking systems with respect to the Application of Energy Storage Devices. *International Journal of Railway Technology*, 4:69–93, 2015. 35

[70] R. Conti, E. Galardi, E. Meli, D. Nocciolini, L. Pugi, and A. Rindi. Energy and wear optimisation of train longitudinal dynamics and of traction and braking systems. *Vehicle System Dynamics*, pages 1–2, 2015. 35, 53

[71] R. Ramakrishnan, S.S. Hiremath, and M. Singaperumal. Dynamic Analysis and Design Otptimization of Series Hydraulic Hybrid System through Power Bond Graph Approach. *International Journal of Vehicular Technology*, pages –, 2014. 36

[72] B. Allotta and L. Pugi. *Meccatronica - Elementi di Trazione Elettrica*. Società Editrice Esculapio. 43

[73] M.J. Leigh. Brake blending. *Proceedings of the Institution of Mechanical Engineers, Part F: Journal of Rail and Rapid Transit*, 208(1):43–49, 1994. 48

[74] Nota RFI 3721. Regolamento per la circolazione dei treni. 57

[75] F. Perticaroli. *Sistemi Elettrici per i Trasporti*. CEA Editore. 72

[76] D. Zaninelli. *Sistemi elettrici per l'alta velocità ferroviaria*. Hoepli, Milano, 2011. 72

[77] D. Cornic. Efficient recovery of braking energy through a reversible dc substation. *Electrical Systems for Aircraft, Railway and Ship Propulsion*, pages –, 2010. 73

[78] UIC 544-1. Brakes, braking power, October 2014. 6th edition. VIII, XV, 93, 96, 97

[79] UIC 541-3. Brakes - disc brakes and their application - general conditions for the approval of brake pads, October 2010. 7th edition. 93

[80] EN 15734-1. Railway applications - braking systems of high speed trains part 1: Requirements and definitions. 93

[81] Official Web Site of E.R.A. 93

[82] EiF/DoA: 1/ 1/2015. Regulation 1301/2014 (1st merged ene tsi). 93

[83] EiF 13/4/2013 DoA: 1/ 1/2014. Regulation 321/2013 (2nd cr wag tsi). 93

[84] EiF/DoA: 1/ 1/2015. Regulation 1302/2014 (1st merged rst tsi). 93

[85] P. Presciani, M. Malvezzi, G.L. Bonacci, and M. Balli. Development of a braking model for speed supervision systems. *Proceedings of the WCRR 2001, World Congress on Railways Research, Köln*, pages –, 2001. 94

[86] B. Allotta, L. Pugi, M. Malvezzi, F. Bartolini, and F. Cangioli. A scaled roller test rig for high-speed vehicles. *Vehicle System Dynamics*, 48(1):3–18, 2010. 96

[87] L. Pugi, A. Rindi, A.G. Ercole, A. Palazzolo, J. Auciello, D. Fioravanti, and M. Ignesti. Preliminary studies concerning the application of different braking arrangements on Italian freight trains. *Vehicle System Dynamics*, 49(8):1339–1365, 2011. 96

[88] L. Pugi, M. Malvezzi, S. Papini, and G. Vettori. Design and preliminary validation of a tool for the simulation of train braking performance. *Journal of Modern Transportation*, 21:247–257, 2013. 96, 152

[89] E. Galardi, E. Meli, D. Nocciolini, L. Pugi, and A. Rindi. Development of efficient models of Magnetic Braking Systems of railway vehicles. *International Journal of Rail Transportation*, 3(2):97–118, 2015. 96

[90] E. Quaglietta and V. Punzo. Supporting the design of railway systems by means of a Sobol variance-based sensitivity analysis. *Transportation Research Part C: Emerging Technologies*, 34:38–54, 2013. 96

[91] S. Baccari, G. Cammeo, C. Dufour, L. Iannelli, V. Mungiguerra, M. Porzio, G. Reale, and F. Vasca. Real-Time Hardware-in-the-Loop in Railway: Simulations for Testing Control Software of Electromechanical Train Components, Railway Safety, Reliability, and Security. *Technologies and Systems Engineering*, pages 221–248, 2012. 96

[92] L. Pugi, R. Conti, D. Nocciolini, E. Galardi, A. Rindi, and S. Rossin. A Tool for the Simulation of Turbo-Machine Auxiliary Lubrication Plants. *International Journal of Fluid Power*, 15(2):87–100, 2014. 100

[93] L. Pugi, E. Galardi, C. Carcasci, A. Rindi, and N. Lucchesi. A thermo-hydraulic tool for automatic virtual hazop evaluation. *Metrology and Measurement Systems*, 21(4):631–648, 2014. 100

[94] L. Pugi, E. Galardi, C. Carcasci, A. Rindi, and N. Lucchesi. Design of a lateral and vertical semi-active suspension system for a high speed train. *Proceedings of the ECCOMAS THEMATIC CONFERENCE ON MULTIBODY DYNAMICS, Warsaw*, 29:–, 2009. 100

[95] S. Miller and J. Wendlandt. Real-Time Simulation of Physical Systems Using Simscape. *MATLAB News and Notes*, pages –, 2010. 100

[96] B.T. Kulakowski and J.F. Gardner J.L. Shearer. *Dynamic modeling and control of engineering systems*. Cambridge University Press, Cambridge, 2007. 100

[97] S. Barsali, P. Bolognesi, M. Ceraolo, M. Funaioli, and G. Lutzemberger. Cyber-physical modelling of railroad vehicle systems using Modelica simulation language. *Proceedings of*

the Second International Conference on Railway Technology: Research, Development and Maintenance, Stirlingshire, 231:1–18, 2014. 100

[98] M. Ceraolo, R. Giglioli, G. Lutzemberger, and A. Bechini. Cost effective storage for energy saving in feeding systems of tramways. *IEEE Electric Vehicle Conference (IEVC)*, pages 1–6, 2014. 100

[99] L.F. Shampine, M.W. Reichelt, and J.A. Kierzenka. Solving Index-1 DAEs in MATLAB and Simulink. *SIAM Review*, 41:538–552, 1999. 104

[100] M.E. Hosea and L.F. Shampine. Analysis and implementation of tr-bdf2. *Applied Numerical Mathematics*, 20(1):21 – 37, 1996. Method of Lines for Time-Dependent Problems. 105

[101] ESTECO. modefrontier - 2017 user guide, 2017. 106

[102] ETR1000 – Technical specifications. 108

[103] F. Gherardi and L. Vannelli. The European interoperability and the related engineering and certification challenges. *ZEV rail Glasers Annalen*, 137:188–195, 2013. 108

[104] CIFI Symposium 2015. L'evoluzione del sistema av e il frecciarossa 1000. 108, 154, 156

[105] RFI. La linea firenze-empoli-pisa: la variante signa-montelupo. IX, 114

[106] M. Ceraolo, A. Frilli, G. Lutzemberger, and L. Pugi. Regenerative braking in high speed railway applications: analysis by different simulation tools. *Proceedings of the IEEE International Conference on Environment and Electrical Engineering (EEEIC)*, pages –, 2016. 148, 149, 150, 152

[107] P. Presciani, M. Rinchi, and L. Pugi. Banchi per la certificazione del componenti frenanti. *Ingegneria Ferroviaria*, 58(3):285–294, 2003. 148

[108] UIC 541-4. Brakes - brakes with composite brake blocks - general conditions for certification of composite brake blocks, October 2010. 7th edition. 148

[109] M.J. Nieuwenhuijsen, J.E. Gomez-Perales, and R.N. Colvile. Levels of particulate air pollution, its elemental composition, determinants and health effects in metro systems. *Atmospheric Environment*, 41(37):7995–8006, 2007. 149

[110] H.G. Namgung, J.B. Kim, S.H. Woo, S. Park, M. Kim, M.S. Kim, and S.B. Kwon. Generation of Nanoparticles from Friction between Railway Brake Disks and Pads. *Environmental Science & Technology*, 50(7):3453–3461, 2016. 149, 152, 153

[111] L. Pugi, M. Malvezzi, S. Papini, and S. Tesi. Simulation of Braking Performances: the application on Ansaldobreda EMU V250. *Proceedings of the Institution of Mechanical Engineers, Part F: Journal of rail and rapid transit*, pages –, 2016. 152

[112] M. Cusack, N. Talbot, J. Ondráček, M.C. Minguillón, V. Martins, K. Klouda, and V. Ždímal. Variability of aerosols and chemical composition of PM 10, PM 2.5 and PM 1 on a platform of the Prague underground metro. *Atmospheric Environment*, 118:176–183, 2015. 152

[113] F. Braghin, F. Cheli, and G. Galli. Experimental Assessment of Structure Borne Noise Generated by a Braking Resistor. pages –. 154

[114] Microelettrica Scientifica. 157